AD NUMBER

AD446344

NEW LIMITATION CHANGE

TO

Approved for public release, distribution unlimited

FROM

Distribution authorized to U.S. Gov't. agencies and their contractors; Administrative/Operational Use; APR 1964. Other requests shall be referred to Bureau of Naval Weapons, Washington, DC 20350.

AUTHORITY

BUWEPS ltr dtd 5 Mar 1965

AD 446344

RESEARCH ON JET NOISE GENERATION AND SUPPRESSION

APRIL 1964

Prepared Under Department of the Navy,
Bureau of Naval Weapons

Contract NOw 62-0887-d
Phase I

by

W. R. Semrau

GENERAL ELECTRIC COMPANY
Flight Propulsion Division
Advanced Engine & Technology Department
Cincinnati 15, Ohio

RESEARCH ON JET NOISE GENERATION AND SUPPRESSION

APRIL 1964

Prepared Under Department of the Navy,
Bureau of Naval Weapons

Contract NOw 62-0887-d
Phase I

by

k.R. Semrau

GENERAL ELECTRIC COMPANY
Flight Propulsion Division
Advanced Engine & Technology Department
Cincinnati 15, Ohio

ABSTRACT

Experimental and analytical investigations on jet noise generation and suppression have resulted in a verification of the concept that jet noise is uniquely related to mean flow velocity distribution in the jet wake. Advances have been made in analytical techniques for calculating aerodynamic properties of free jet flow and the related acoustic properties of the flow and verification of the assumption that negligible attenuation of sound occurs during propagation through multi-element jet flows has been achieved.

Investigation of selective water injection as a jet noise suppression scheme has indicated little promise for in-flight noise reduction. Studies of noise generation by high temperature and high pressure ratio jets have extended the state-of-the-art in the area of high temperature flow noise suppression, and have resulted in a means for predicting total acoustic power beyond the limits of applicability of the Lighthill parameter.

TABLE OF CONTENTS

FOREWORD

This is the final report covering the work performed under Phase I, "Jet Noise Suppression Research", Department of the Navy, Bureau of Naval Weapons, Contract No. NOw 62-0887-d, in accordance with the Contractor's proposal entitled, "Jet Noise Suppression Research and System Studies", P61-86, dated March 1961.

The objectives of the Phase I program were: to extend the theory of jet noise suppression to high pressure ratio and high temperature flow by demonstrating the generality of the concept that jet noise is uniquely related to the flow velocity distribution in the wake; to further refine and develop analytical techniques applicable to computer solutions for jet flows and noise; to investigate significant variables influencing jet noise generation and suppressor performance; and to evaluate the feasibility of selective water injection as an in-flight suppression technique. The advanced knowledge achieved through the successful accomplishment of this research program, along with the findings of the Phase II program on operational noise problems and effects of suppression on mission performance, can be implemented toward the goal of developing a practical suppressor for military jet aircraft.

The problems dealt with in this research investigation have been divided into the five sections of this report, each of which is essentially self-contained for the convenience of the reader. However, the interrelation of the various aspects of the program is maintained by appropriate cross-references between the various sections, and by the condensation of the overall effort in the Summary.

Grateful acknowledgement is made to Commander A. Lee and Mr. R. Brown of the Bureau of Naval Weapons under whose guidance this program was carried out; to Dr. R. M. Kendall of Vidya, a Division of Itek Corporation, for his analytical contributions to the problem of jet mixing; to Mr. R. Lee, under whose technical direction this program was initiated at the Advanced Engine and Technology Department of the General Electric Company; and to Mr. D. L. Harshman, Manager of Installation Aerodynamics, Advanced Engine and Technology Department, whose guidance and encouragement contributed significantly to the accomplishment of the program objectives.

SUMMARY

Experimental and analytical investigations on jet noise generation and suppression have been carried out for the purpose of: 1) demonstrating and extending the generality of the concept that jet noise is uniquely related to jet wake mean flow velocity distributions; 2) further refining and developing analytical computer techniques for solution of jet flow and noise problems; 3) defining the effects of jet temperature and pressure ratio on noise characteristics for nozzles and nozzle suppressors; 4) determining the effect of the turbulent jet wake on the radiation of sound energy generated by multiple element suppressors; and 5) evaluating the feasibility of selective water injection as an in-flight suppression device.

The previously established technique for calculation of sound power spectra from aerodynamic properties of the jet wake is outlined in Section 1 of this report. It is demonstrated that the method is quite general, being applicable to nozzle-suppressors of various geometric designs. Furthermore, experimental evidence is presented which indicates that jet noise sound power spectra can be adequately predicted for the various nozzle configurations at flow pressure ratios up to 3.0, and flow temperatures up to 1800°R. Comparison between measured and predicted overall sound power shows that the prediction method used provides calculated levels within $\pm$ 2 db of acoustically measured levels for nearly all nozzle shapes and flow conditions tested.

In Section 2, the development of analytical techniques for jet flow field prediction is undertaken in order to provide a working tool for jet noise suppressor research. Starting from the approach suggested by the theory of Reichardt, computer programs are developed which represent an advancement of the state-of-the-art in the analysis of jet flow from complex nozzles. While it is shown that analytically derived mean flow velocity profiles for the jet mixing region in

general agrees satisfactorily with experiment, further work is required to bring computer techniques to their full state of usefullness.

In Section 3, the results of a study on jet noise generation and suppression at high flow temperatures, up to those representative of afterburning jet engine operation, are presented. Experimental data on noise generation by jets up to flow pressure ratio of 3.4 and temperature up to 3300°R has been obtained, indicating that for low pressure ratios and moderate temperatures little flow density effect exists, while over the full range of observation a temperature dependent flow density effect is found to occur. This effect is such that sound power varies with $(\rho_j/\rho_a)^n$, where n is approximately a linear function of temperature. The results of scale model experiments have been used to establish an empirical relationship between nozzle energy flux and sound power generation, applicable to concentric flows as well as simple conical nozzles. Studies of suppressor nozzle acoustical performance at high flow temperature have been carried out experimentally, with results indicating that suppression is temperature as well as pressure ratio dependent. Jet noise suppression at high flow temperatures requires further study for the purpose of deriving generalized temperature scaling laws applicable to all nozzle geometries, since the experimental results presented indicate that temperature effect on suppression may be nozzle geometry dependent. The results of the high temperature jet noise investigation point out the need for flow temperature simulation in suppressor scale model development directed toward afterburning jet engines.

Section 4 presents the results of experimental investigations on dissipation of sound, generated by a jet, in the turbulent wake of the jet itself. No evidence of sound absorption has been found, and thus no modification of the correlation of aerodynamic and acoustic jet properties is required from this consideration. The effect previously referred to by other researchers as jet noise "shielding" is shown to be the result of directivity rather than sound power change.

Selective water injection as a jet noise suppression technique has been experimentally and analytically investigated, with results presented in Section 5. Studies indicate that the desired alteration of jet mixing cannot be achieved through limited water use, and that the suppression thus accomplished is less than that expected for uniform mixing of air and water. Adverse effects of high flow temperature and velocity on noise reduction capability of water injection have been experimentally demonstrated, and indicate that this suppression scheme is not practical for in-flight noise reduction.

The knowledge gained in the successful completion of this program on jet noise suppression research can be implemented, along with other existing technology, toward the development of a jet noise suppressor for application to military aircraft in flight. Thus, noise reduction for military jet aircraft might indeed be a practical reality.

1.0 Experimental Investigation on the Relationship Between Aerodynamic Properties of the Jet Flow Field and Resultant Noise Generation

1.1 Introduction

As a result of a previous Navy sponsored General Electric research program on jet noise generation and suppression (NOas 59-6160-c) an empirical formulation was developed for relating the aerodynamic properties of a free jet to its noise characteristics (Ref. 1). The hypothesis that the sound power generated at various axial positions in the jet mixing region depends only on the mean velocity distributions at these locations led to a general quantitative relationship for determining sound power spectra for simple conical and complex suppressor nozzles. It was demonstrated that, within certain limits of flow pressure and temperature, the manner in which the flow velocity distributions vary within the jet because of nozzle geometry variation does not influence the generality of the aero-acoustic correlation.

The usefulness of the previously established correlation between aerodynamic and acoustic jet properties depends to a great extent on its applicability to realistic flow temperatures and pressures, and to various nozzle configurations. While past verification of the theory was limited to cold flow, sub-critical pressure ratios and relatively simple nozzle designs consisting of a number of identical elements, the present study considered flow temperatures up to 1800°R, pressure ratios up to 3.0, and large variety of nozzle designs, in accordance with the program work statement in Reference 2. The generality of previously established empirical constants has been re-evaluated through correlation of aerodynamic and acoustic data, indicating that the velocity profile formulation can indeed be applied to heated, high pressure ratio jets, and essentially all nozzle geometries.

1.2 Prediction of Sound Power Spectra from Flow Profile Data

The previously established relationship between aerodynamic and acoustic properties of a free jet is restated from Reference 1 :

$$P(f) = K \rho_o c_o^{-5} a_o U_o^8 \left(\frac{1}{f}\right) \int_{a_x} \left(\frac{U}{U_o}\right)^8 d\left(\frac{a}{a_o}\right) \qquad (1)$$

where:

P (f) = Sound power per cycle at frequency f.

K = Empirical constant

$\rho_o c_o^{-5} a_o U_o^8$ = Lighthill parameter

f = Frequency

u = Local mean flow velocity

a = Flow cross-section area

x = Axial location along the jet

The assumptions employed are: (1) No noise is generated within the flow potential core, and thus the integral $\int_{a_x} \left(\frac{u}{u_c}\right)^8 d\left(\frac{a}{a_o}\right)$ must be evaluated over the region a (x) external to the core flow; (2) the axial distribution of scale of turbulence within the jet is linear, that is, $L \propto X$; (3) the relationship between axial location and frequency of the sound source is given by:

$$\frac{f\, d_e}{U_o} = \left(1.25 \quad \frac{x}{d_e}\right)^{-1.22} \qquad (2)$$

where d_e, nozzle equivalent diameter, is defined by:

$$d_e = \sqrt{\frac{4}{\pi} \quad \frac{a_o}{n}} \qquad (3)$$

and n is the number of flow elements in the nozzle; (4) the total generated sound power is radiated.

Prediction of the sound power spectrum is accomplished by experimentally or analytically evaluating the integral in equation (1) at a sufficient number of x - locations along the jet so that the frequency range of interest is fully defined (Equation (2)). In this section of the report, the experimental evaluation of jet flow properties is discussed, while the analytical approach is developed in Section 2.0.

Under a previous Navy-sponsored research program (Reference 1) the validity of this method of sound power spectrum prediction was demonstrated for an eight-lobe suppressor nozzle, under cold flow and low pressure ratio conditions. For complex nozzle geometries employing elements of non-uniform size the nozzle equivalent diameter, d_e, in the sound source location equation (Eq. (2)) must be suitably defined. The definition of nozzles equivalent diameter as previously stated in Eq. (3) is a logical choice in that it is an average elemental diameter, and the total noise is generated essentially in the region where the jet flow exhibits an individual element identity. Furthermore, the jet potential core length, which is related to the location of the region of maximum noise generation, correlates with the equivalent diameter as herein defined.

The assumption that the total sound power generated is radiated into the far field is considered in Section 4.0 of this report, and it is shown that no significant dissipation of acoustic energy in the audio frequency range occurs in the turbulent jet.

In order to determine the limits of applicability and to further develop the correlation described above, experimental investigation of flow velocity profiles was carried out for seven nozzle configurations. Flow temperatures up to 1800°R and nozzle pressure ratios up to 3.0 were tested, and aerodynamic data was correlated with measured sound power spectra, as described in the following section.

1.3 Experimental Determination of Flow Velocity Profiles and Correlation with Measured Sound Power Spectra

Aerodynamic measurements were made in the free jet wake for a number of nozzle geometries and flow conditions for the purpose of defining the mean flow properties of the jet. Flow velocity distribution was determined throughout the jet wake, and acoustic properties predicted from the flow measurements were compared with measured sound power spectra.

1.3.1 Aerodynamic Measurements

Detailed flow velocity data was obtained throughout the significant noise generating regions of the jet wake for the various nozzles tested using the research facility shown in Figure 1.1. The facility consists of a burner of the type commonly employed in aircraft gas turbines, followed by a flow mixer and pressure and temperature instrumentation for accurately determining inlet conditions to the nozzle under test. Air supply capacity for the facility is up to 9 lb/sec., and flow temperatures up to 1800°R are achieved by the burner. Nozzle pressure ratios up to 3.0 were possible for the size nozzles tested (up to 13 sq. in. exit area) with heated flow. For high pressure ratio cold flow testing, an indoor facility with higher airflow capability was employed, and test instrumentation used was similar to that for hot flow measurement. The

test nozzle was mounted on the facility, shown in Figures 1.1 and 1.2, and the wake was surveyed with a combination total pressure - total temperature probe, the position of which was remotely controlled by means of probe actuators mounted from a lathe bed. During the research program, an afterburner was added to the facility (Figure 1.2) increasing flow temperature capability to 3500°R, but instrumentation difficulty precluded velocity profile measurements above 1800°R, and the addition to the facility was used for studies of noise generation at high temperature as described in Section 3 of this report.

Temperature and pressure data was recorded automatically for probe traverses at each axial location in the jet wake, and point by point calculations of flow velocity were accomplished by computer. Since the velocity in the core region of the jet is not evaluated in the prediction of sound power spectra, the problem of measuring supersonic velocities and static pressure gradients in the core region of high pressure ratio jets was bypassed. For the pressure ratios under consideration, flow velocity in the noise producing mixing region is essentially always subsonic, while the expansion region with static pressure gradients and shock structure is assigned to the jet core in which no noise is generated. Thus, the computation of flow velocity was simplified in that the assumption of static pressure equal to ambient pressure could be made.

The prediction of sound power spectra from velocity data does not require knowledge of the velocity distributions at a given axial location in the jet; only the flow velocity-flow area relationship is required (Eq. 1). Therefore, the flow velocity data was reduced to the form of equivalent velocity profiles. That is, the flow was artificially reoriented to simulate flow from a conical nozzle for the purpose of simplifying the integration process and

providing a common means of presentation for all of the flow data for the various configurations. This equivalent data is presented in the next section, having been obtained from flow velocity maps at each location in the jet, by graphically accumulating flow area in the order of decreasing flow velocity to artificially create an equivalent conical nozzle profile for each nozzle geometry tested. From the equivalent profiles, the integration required for evaluation of Equation 1 was performed graphically.

1.3.2 Acoustical Measurements

Aerodynamically predicted sound power spectra were correlated with actual noise measurements obtained for each nozzle configuration. The outdoor test facility used for flow velocity measurements was also employed for sound power evaluation. Noise measurements were made under free-field conditions. A microphone attached to a remotely controlled boom (Figure 1.3) was used to survey the sound field at a radius of 15 feet from the nozzle. The microphone a Bruel & Kjaer Type 4133, has flat frequency response to 40,000 cps. A frequency analysis of the jet noise was obtained for a number of angular locations from the jet axis utilizing the instrumentation shown in Figure 1.4. From the directivity data thus obtained, sound power spectra were computed by the process of integration of sound pressures over the radiation area. The computation procedure assumes that the ground plane is semi-absorbing so that maximum error from this source is about 1db, as the difference between assuming a totally absorbing and totally reflecting surface is 3 db. The location of the microphone at 15 feet from the jet permits measurements to a low frequency limit of 250 cps. The measurement radius was selected so as to provide far-field conditions for low frequency noise and yet not be so far from the source as to be influenced by reflections from nearby structures.

1.4 Discussion of Results

The aerodynamic and acoustical data obtained for the seven nozzle geometries tested are presented in this section, and correlation between predicted and measured sound power spectra is made.

1.4.1 Description of Nozzle Configurations

In order to determine the applicability of the aerodynamic-acoustic correlation to various nozzle geometries, a number of configurations were tested. A list of configurations and test conditions is presented in Table 1.1. The nozzles are all of approximately the same scale, with exit area ranging from 9.6 to 13 in^2. The geometric variations (as shown in Figures 1.5 thru 1.8) include simple circular exit, annular exit (plug nozzle), shrouded annular exit, multiple exit (segmented), and multiple exit with elements of unequal size. The variety of nozzle configurations provided a means of evaluating the applicability of the prediction technique to essentially all types of suppressors.

1.4.2 Correlation of Aerodynamic and Acoustic Data

From the measurements of total pressure and temperature in the jet wake for the various configurations and test points (as summarized in Table 1.1), mean flow velocities were calculated and flow velocity contours were plotted for each axial location within the jet wake. Velocity contours for the 19-tube and 18-segment nozzles are presented in Figures 1.9 and 1.10. The merging of the individual flows, which are quite distinct near the nozzle exit, can be readily observed as the flow progresses downstream. Equivalent flow profiles are derived from the velocity contours by accumulating the flow area graphically, in order of decreasing flow velocity, resulting in the profiles as shown in Figures 1.11 through 1.16. The equivalent flow profile curves enable the various

nozzles to be considered in terms of a fictitious simple circular exit geometry, but with flow profiles developing differently than for a circular exit nozzle. The normalized equivalent profiles and the curves showing the decay of maximum flow velocity as a function of axial location (Figure 1.17) provide the data required for aerodynamic prediction of sound power spectra by means of equations 1 and 2.

The spectra calculated from jet flow properties are compared with acoustically measured spectra in Figures 1.18thru 1.23. Since the levels calculated are power spectrum levels (sound power per unit bandwidth), the values which were measured in percentage bandwidths have been converted to the same constant bandwidth reference for ease of comparison. Predicted and measured total acoustic power levels for all of the nozzle configurations and flow conditions for which power spectra have been determined are compared in Figure 1.24, where the differences between measured and predicted levels are plotted against flow exit velocity.

Several observations can be made concerning the results of this investigation. The shapes of the predicted sound power spectra agree very well with measured values, and the amplitudes agree, in general, within the limits of experimental accuracy. The spectrum shape results imply that the assumed distribution of sound sources within the jet wake is adequate, and that the evaluation of nozzle equivalent diameter by Equation 3 is valid. The degree of accuracy achieved in the prediction of absolute noise levels (for spectra and total acoustic power) verifies the applicability of the fully expanded flow velocity as the significant nozzle exit velocity, and furthermore indicates that the empirical constants employed in the correlation are applicable over

the range of flow conditions tested. Although somewhat greater amplitude deviation than can be attributed to experimental error is noted for the shrouded plug nozzle geometry, it is believed that the discrepancy is due to generation of noise (other than jet noise) by the shroud. The manner in which this noise is generated has not been investigated here, but the conclusion is in agreement with the majority of past experience which shows that addition of a shroud may, under some circumstances, result in production of a number of discrete frequency noise components. The possibility that noise generated in the inner regions of a complex jet is dissipated in the surrounding turbulent flow is more fully discussed in Section 4.0 of this report. However, the applicability of the aerodynamic-acoustic correlation to the variety of suppressor configurations evaluated confirms the result of that concurrent study that no significant absorption takes place.

1.5 Conclusions and Recommendations

The results of this investigation further confirm the hypothesis presented in Reference 1, which states that the noise generated by a jet is uniquely related to the mean-flow velocity distribution within the wake. The technique for calculating sound power spectra from aerodynamic properties of the jet wake is outlined, and the generality of the technique is demonstrated for: (1) nozzle geometry variations, including circular nozzles, plug nozzles, and suppressor designs whose individual elements are not all equal in exit dimensions; (2) flow pressure ratio up to 3.0; and (3) flow temperature up to 1800°R. Jet noise spectrum shapes and levels can be adequately predicted within the limits stated.

Extension of the applicability of the jet noise suppression theory to actual afterburner temperatures (beyond the scope of the present program) is discussed in Section 3.0 of this report, and it is probable that the aerodynamic prediction technique can be applied to this condition, though possibly with some modification. Toward that goal, the analytical techniques for flow profile prediction, presented in Section 2.0, could be employed within the limits of applicability to calculate flow data for correlation with noise data at afterburning temperatures.

Finally, the equivalent mean flow velocity profiles presented for the various noise suppressor nozzles may suggest other geometric designs, more applicable to specific problems, which would generate desired profiles, and thus, low noise levels.

REFERENCES:

1. Lee, R., et. al., "Research Investigation of the Generation and Suppression of Jet Noise", General Electric Company, Flight Propulsion Division, Prepared under Bureau of Naval Weapons, Contract No. NOas 59-6160c, Jan. 1961.

2. "A Proposal for Jet Noise Suppression Research and System Studies", General Electric Company, Flight Propulsion Division, P61-86, 1961.

3. Lawrence, James C., "Intensity, Scale and Spectra of Turbulence in Mixing Region of Free Subsonic Jet", NACA Report 1292, 1956.

SYMBOLS:

a = Flow Cross-section Area

a_o = Nozzle Exit Area

d_e = Nozzle Equivalent Diameter = $\sqrt{\frac{4\, a_o}{\pi\, n}}$

f = Frequency

n = Number of Exit Elements in Suppressor Nozzle

$P(f)$ = Sound Power per Cycle

r_o = Nozzle Equivalent Radius = $1/2\ d_e$

u = Local Flow Velocity

u_o = Effective (fully expanded) Flow Velocity at Nozzle Exit

x = Axial Location, Measured from Nozzle Center Line

y = Radial Location, Measured from Nozzle Center Line

Configuration	d_e	r_o	Flow Temperature	Pressure Ratio
Conical Nozzle	4.0"	2.0"	1660°R	1.2, 1.8
"	"	"	540°R	1.2, 1.8
Plug Nozzle	3.5"	1.75"	530°R	1.6. 2.0, 2.4
Plug Nozzle with Shroud	3.5"	1.75"	530°R	1.6, 2.0, 2.4
8 Lobe Nozzle	1.41"	.71"	1800°R	1.8
"	"	"	530°R	1.8
19 Tube Nozzle	.9"	.45"	1670°R	1.8, 2.4, 3.0
"	"	"	540°R	1.2, 1.8, 2.4
18 Segment Nozzle	.825"	.413"	530°R	2.4

Table 1.1 Nozzle Configurations and Test Conditions

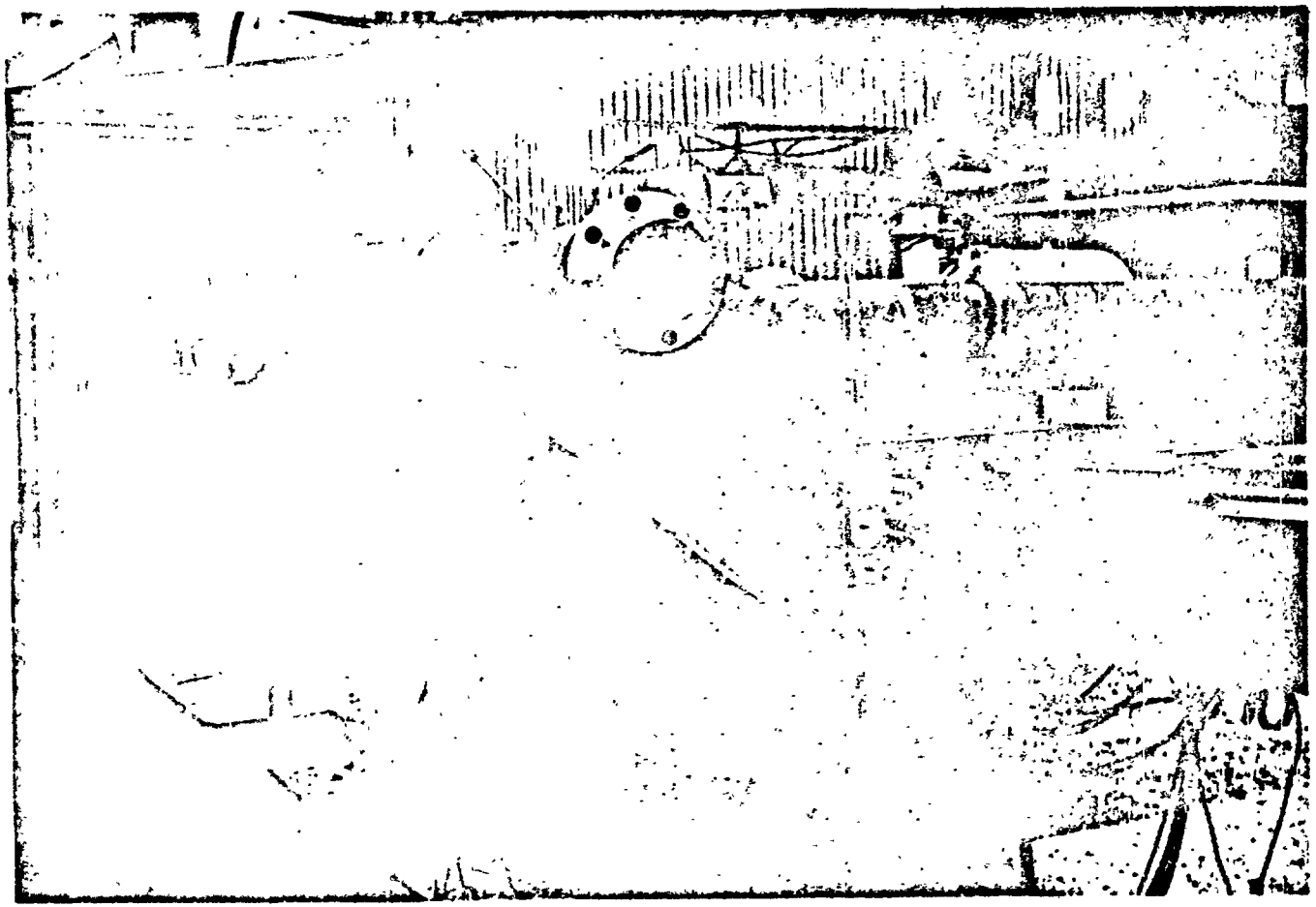

Figure 1.1 High Temperature Flow Facility for Jet Noise Research

Figure 1.2 Flow Facility with Afterburner Assembly

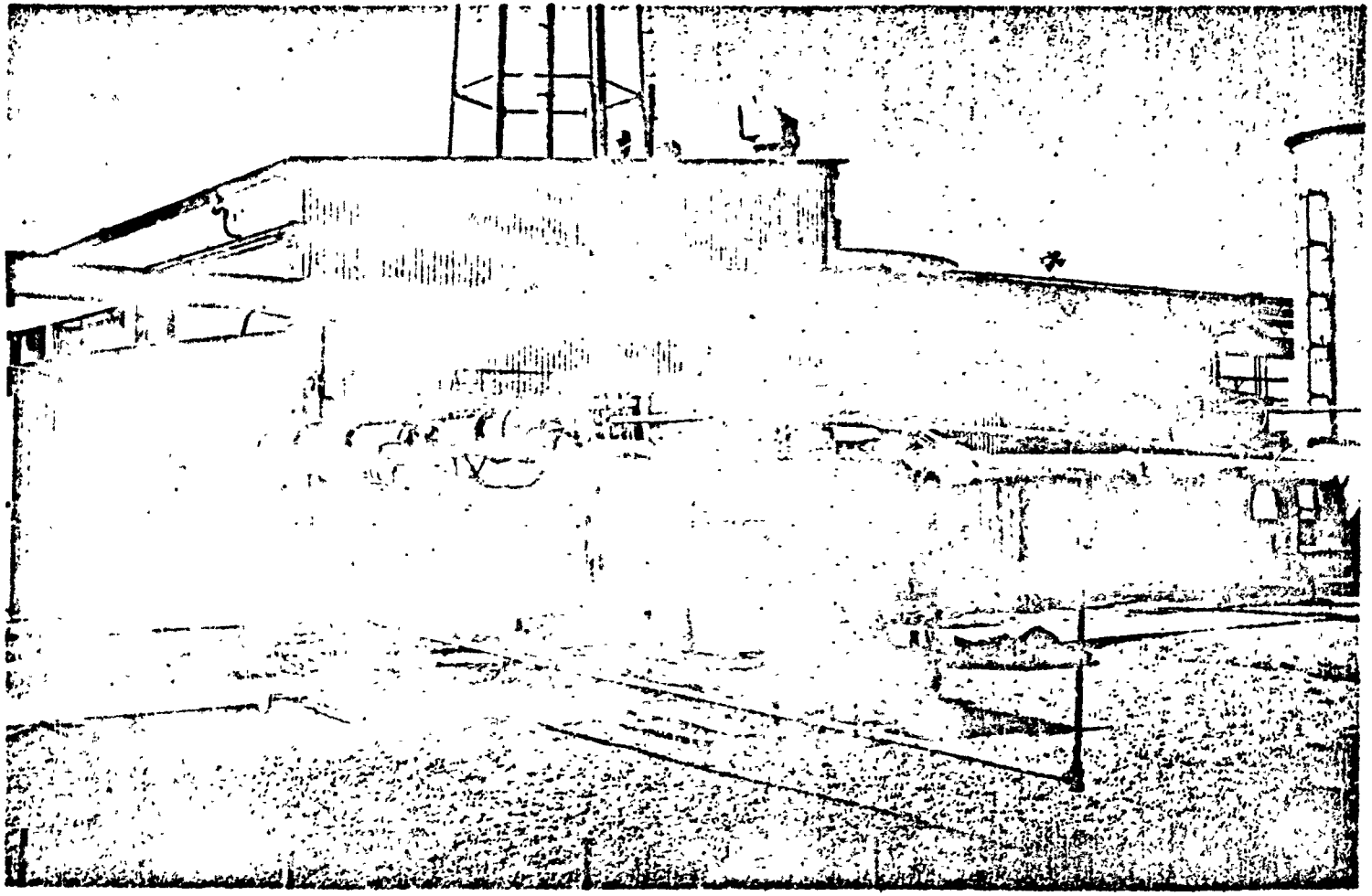

Figure 1.3 Facility for Jet Noise Research

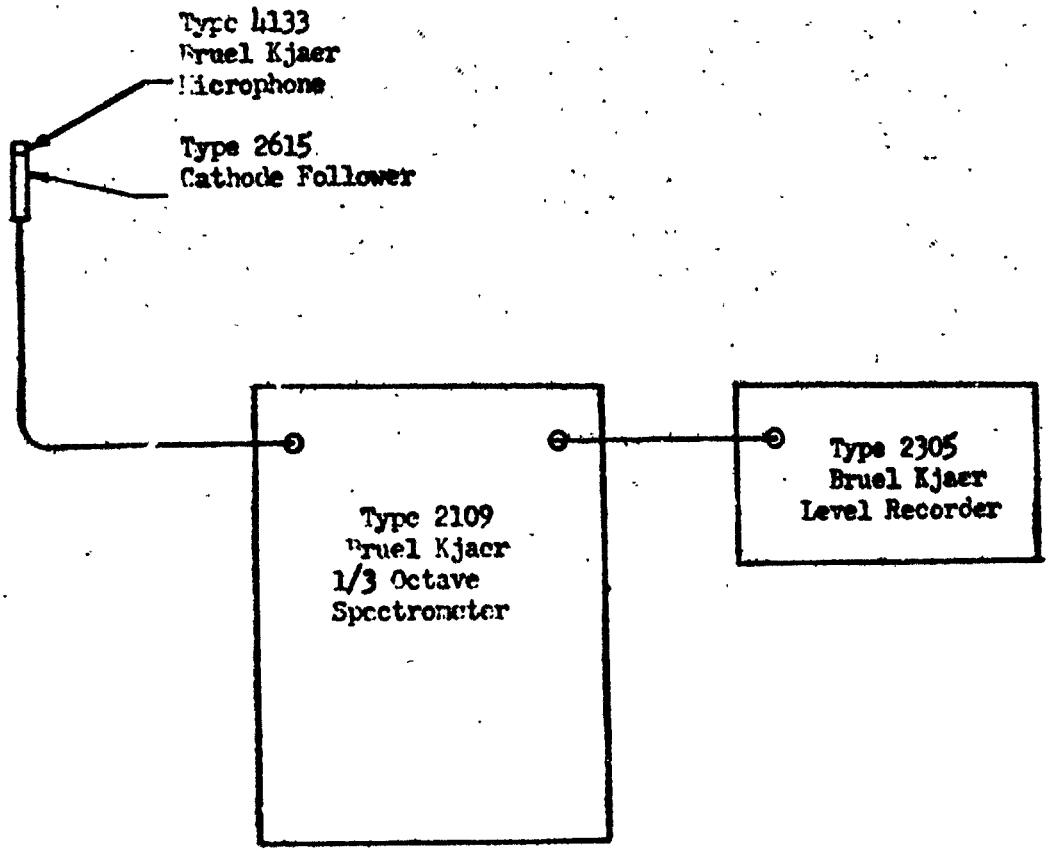

Figure 1.4 Acoustical Instrumentation

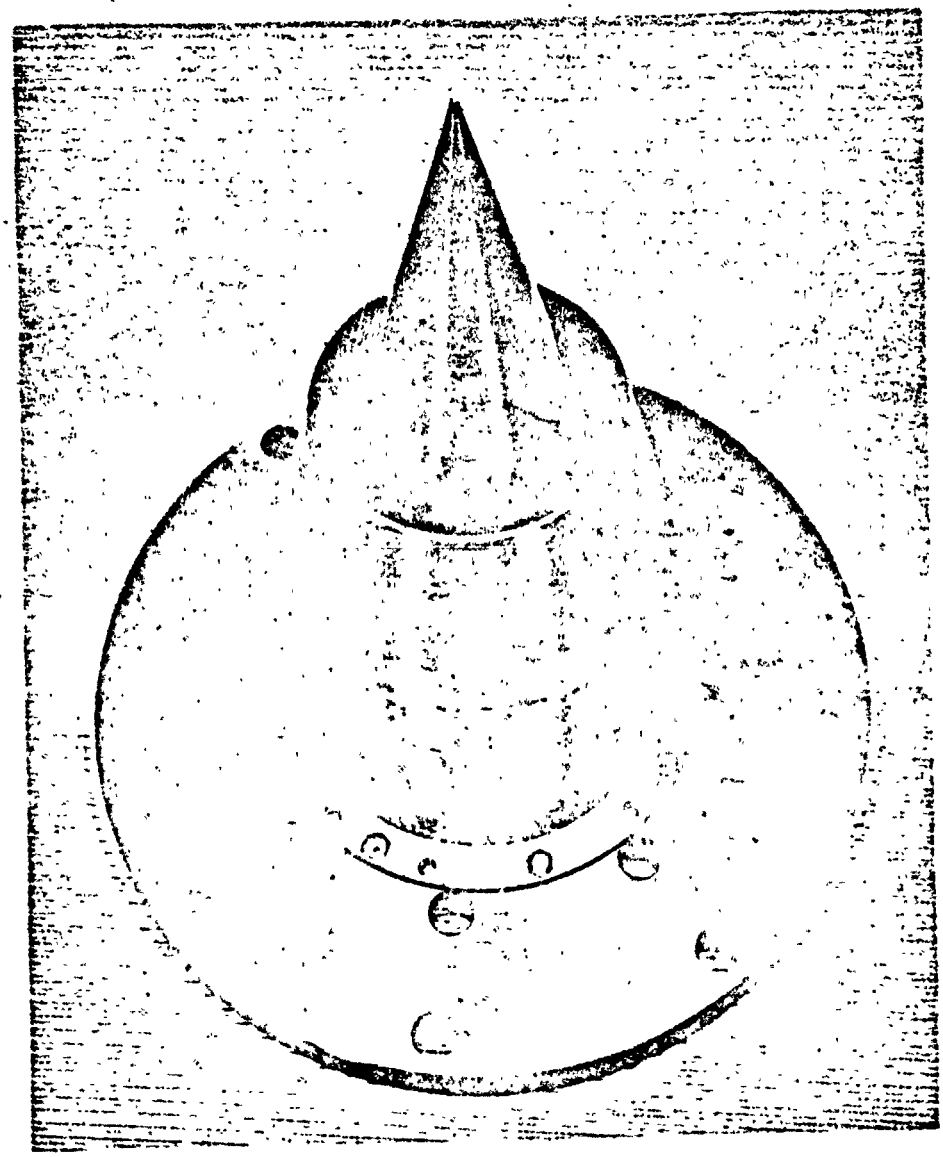

Figure 1.5a Plug Nozzle

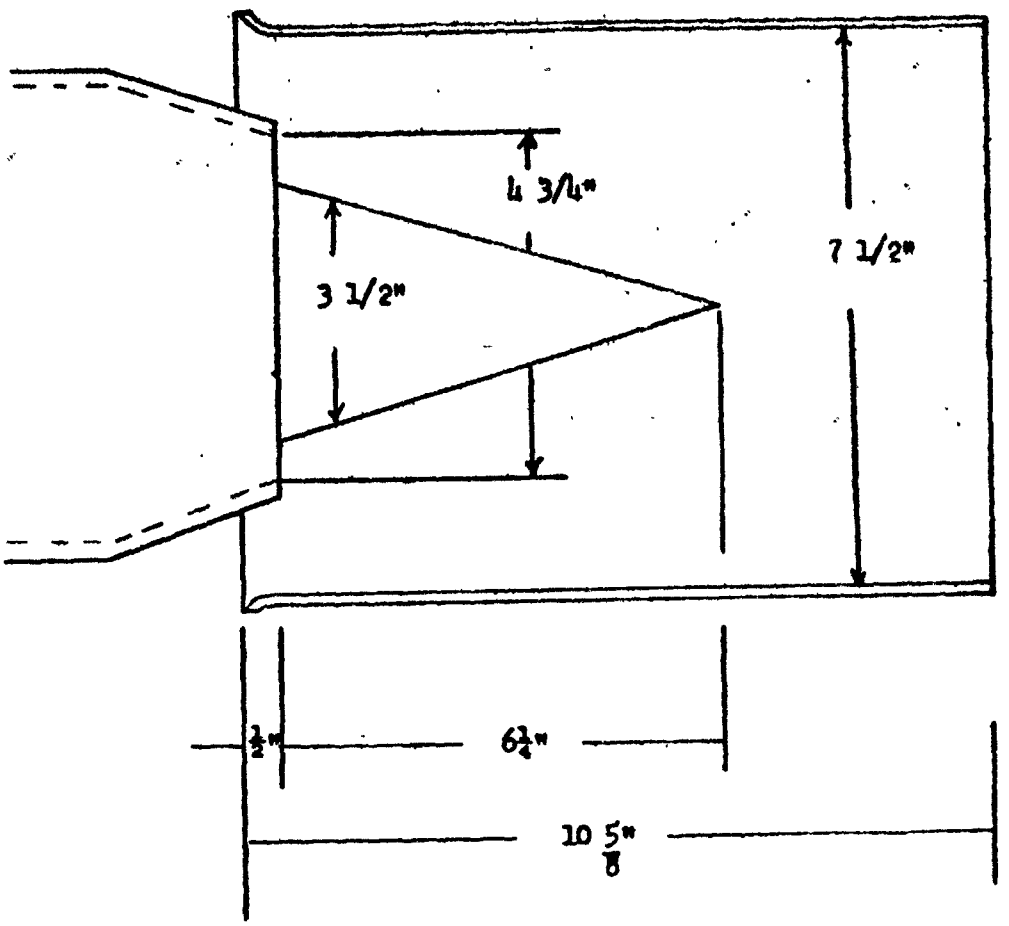

Figure 1.5b Plug Nozzle and Plug Nozzle with Shroud

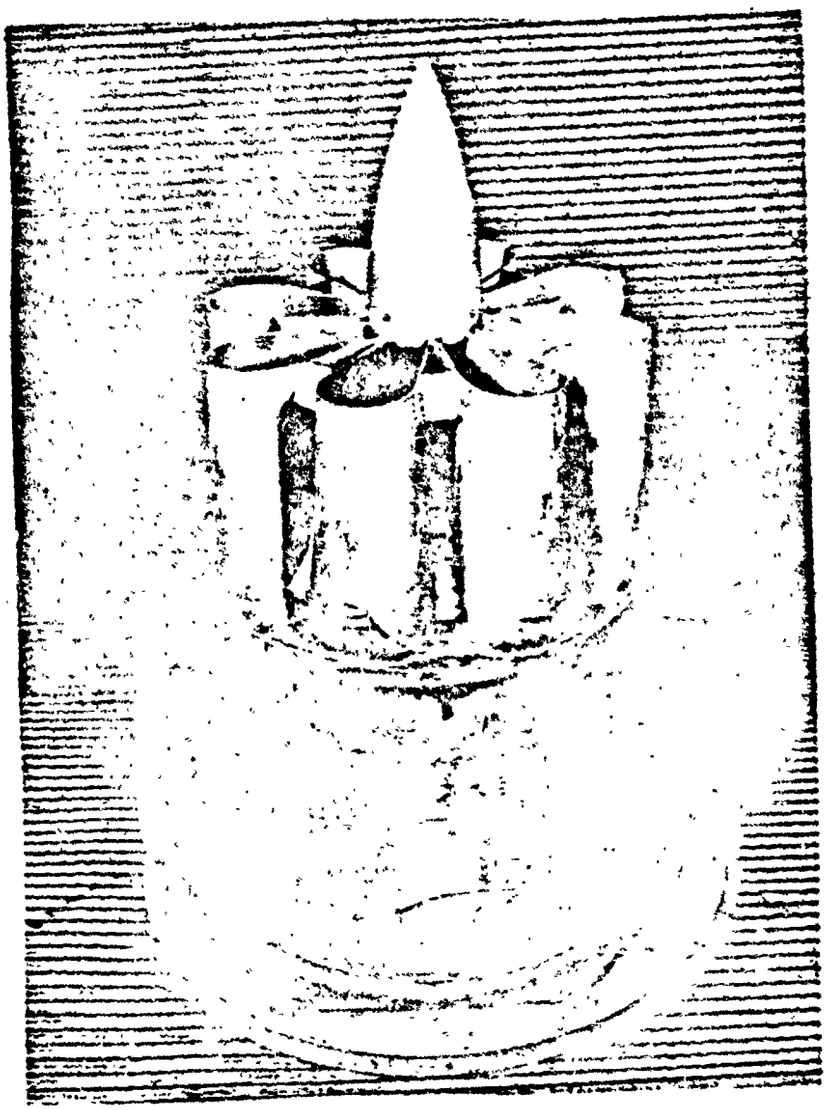

Figure 1.6a 8-Lobe Nozzle

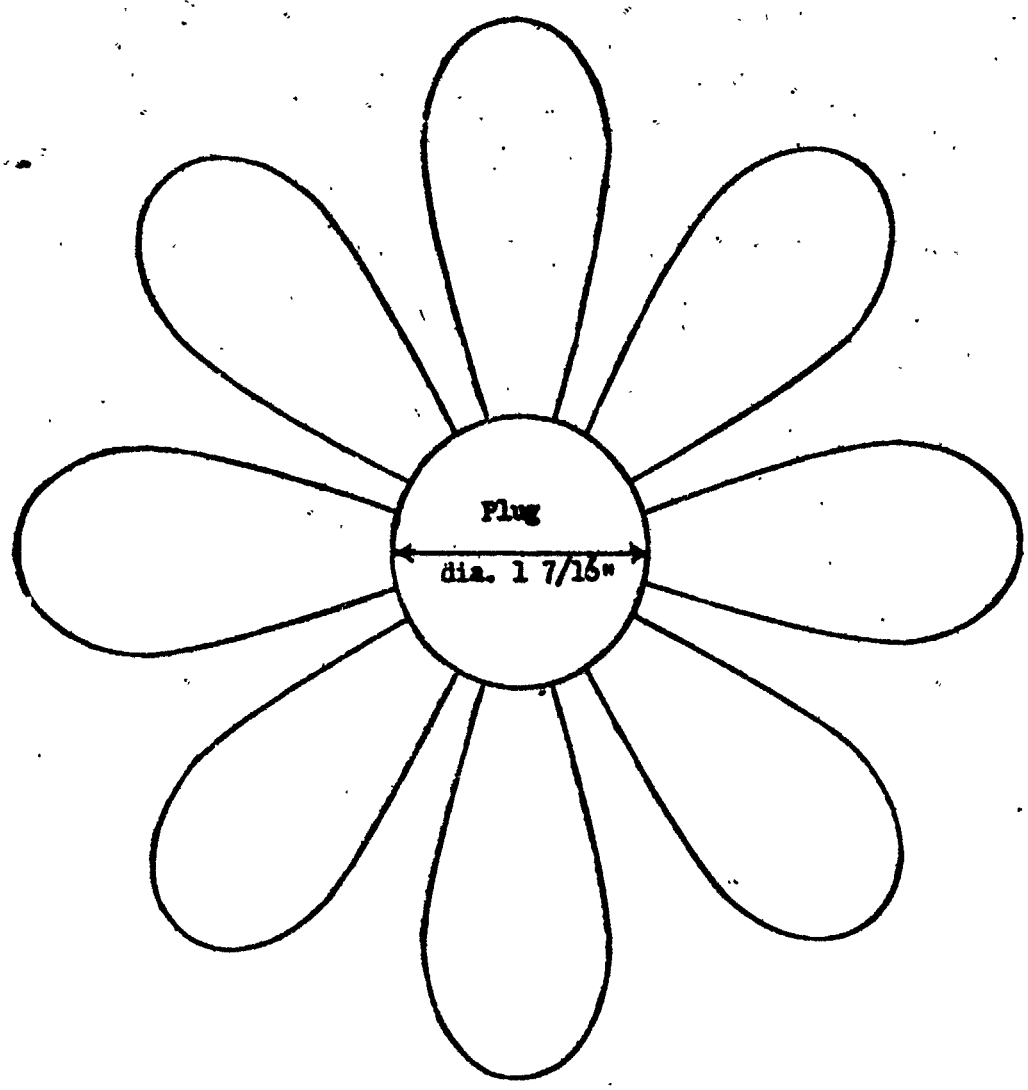

Scale : Full Size

Figure 1.6b 8 Lobe Nozzle Exit Geometry

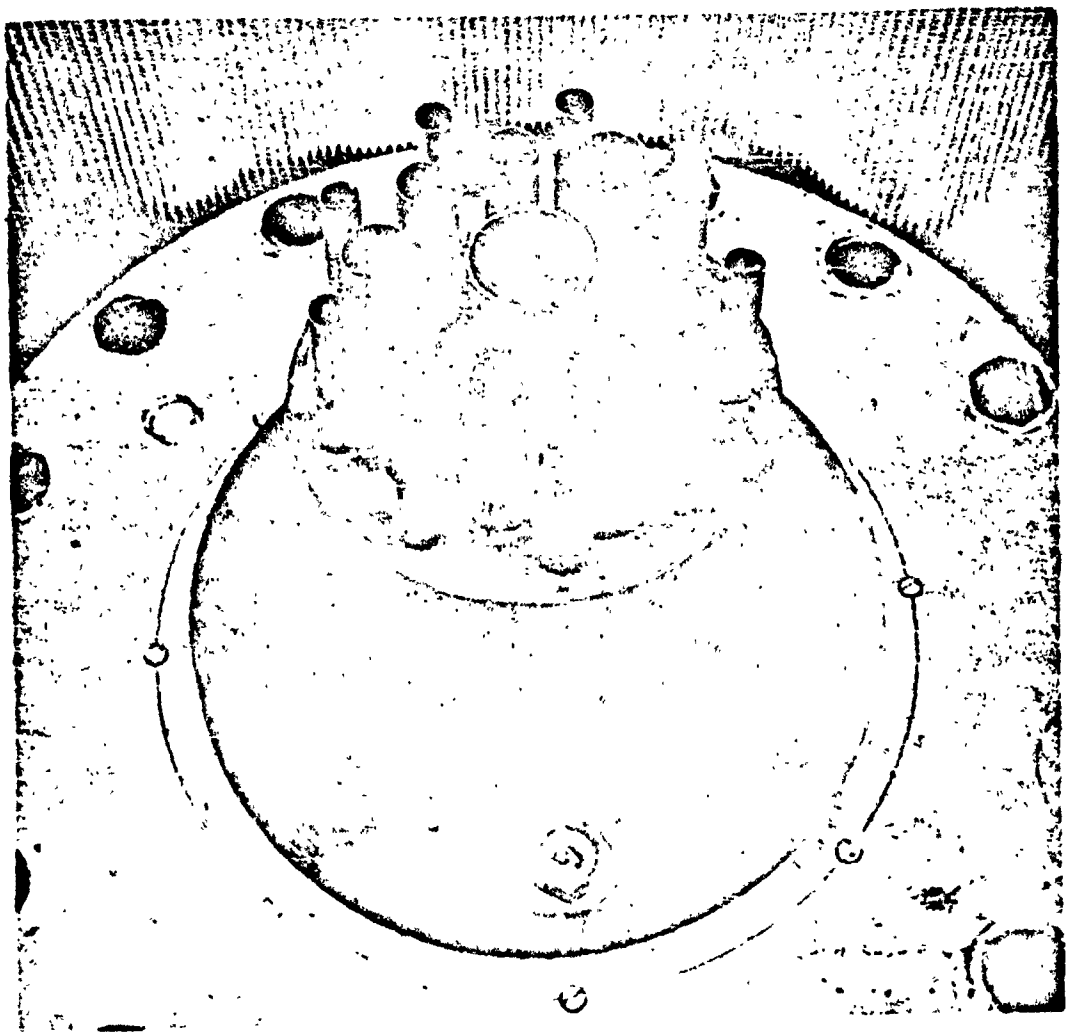

Figure 1.7a 19-Tube Nozzle

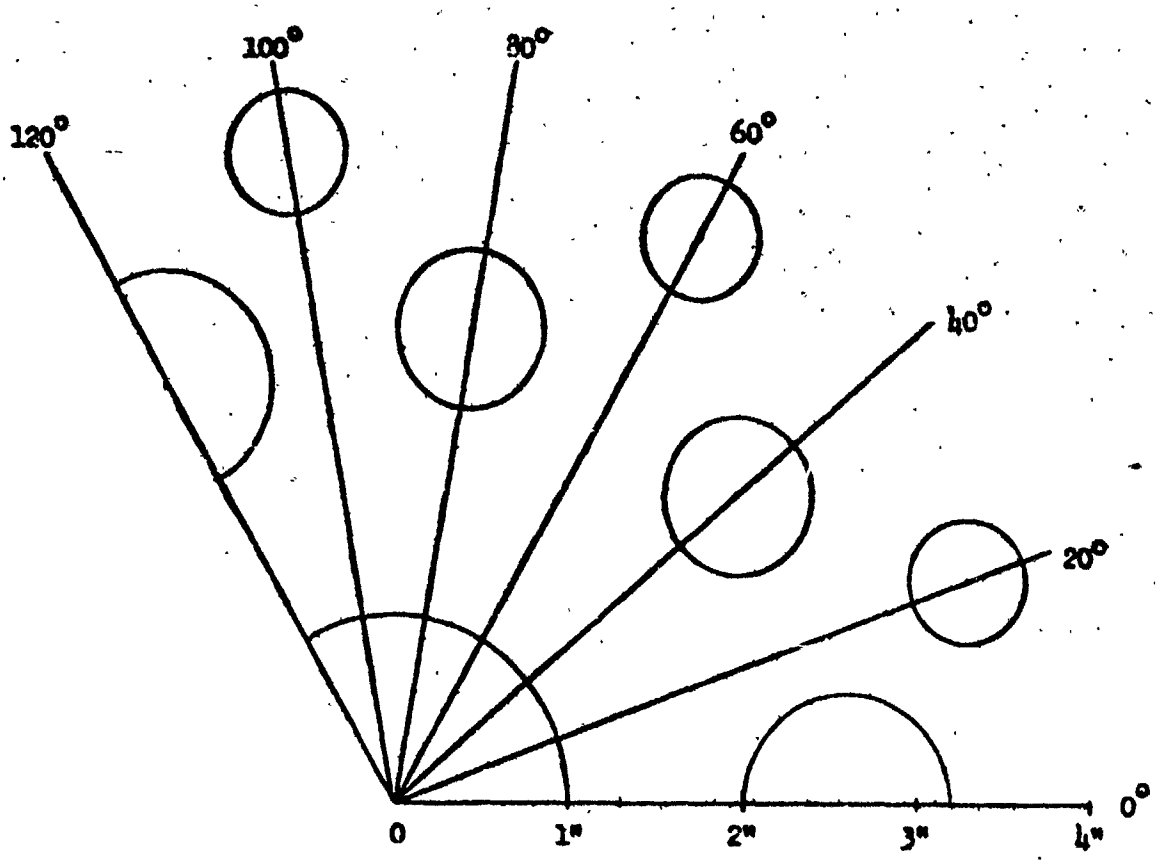

Scale : Full Size

Figure 1.7b End View of a 120° Sector of the 19-Tube Nozzle

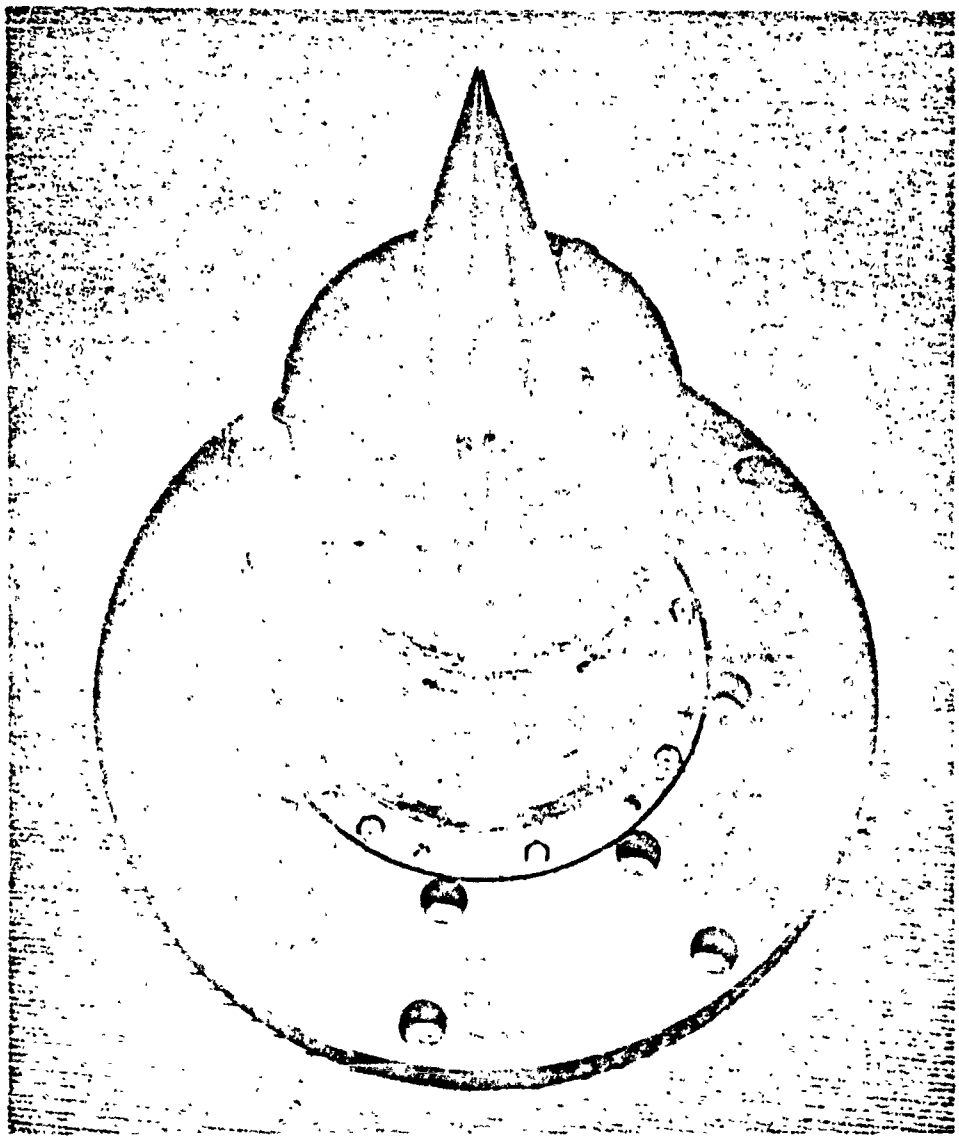

Figure 1.8a 18-Segment Nozzle

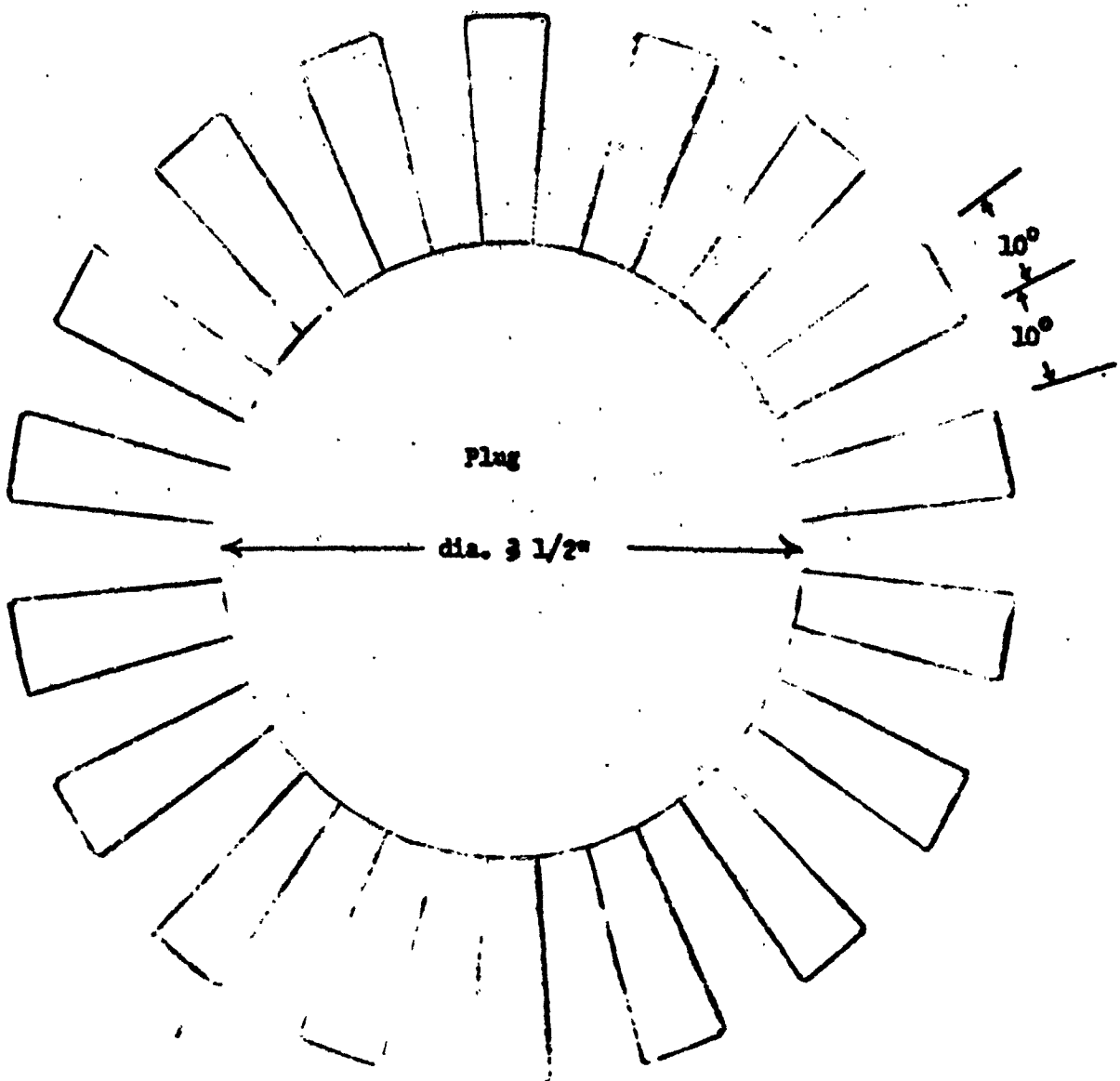

Scale : Full Size

Figure 1.8b 18 Segment Nozzle Exit Geometry

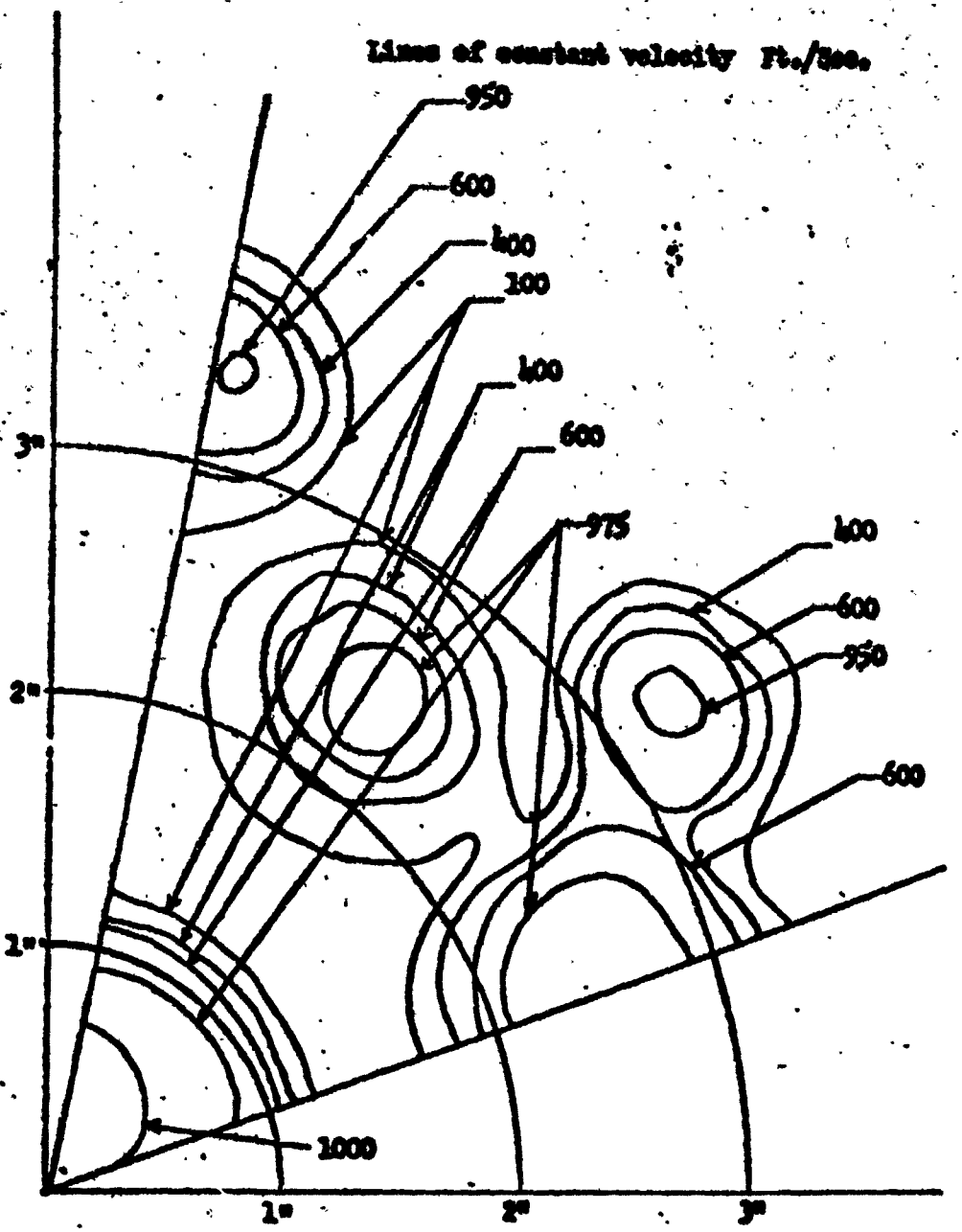

Axial Location X = 2 inches

Flow Exit Velocity = 1000 ft/sec

60° Symmetrical Section

$P_o/P = 1.8$

$T_o = 540°R$

19 Tube Nozzle

Figure 1.9a – Flow Velocity Contours.

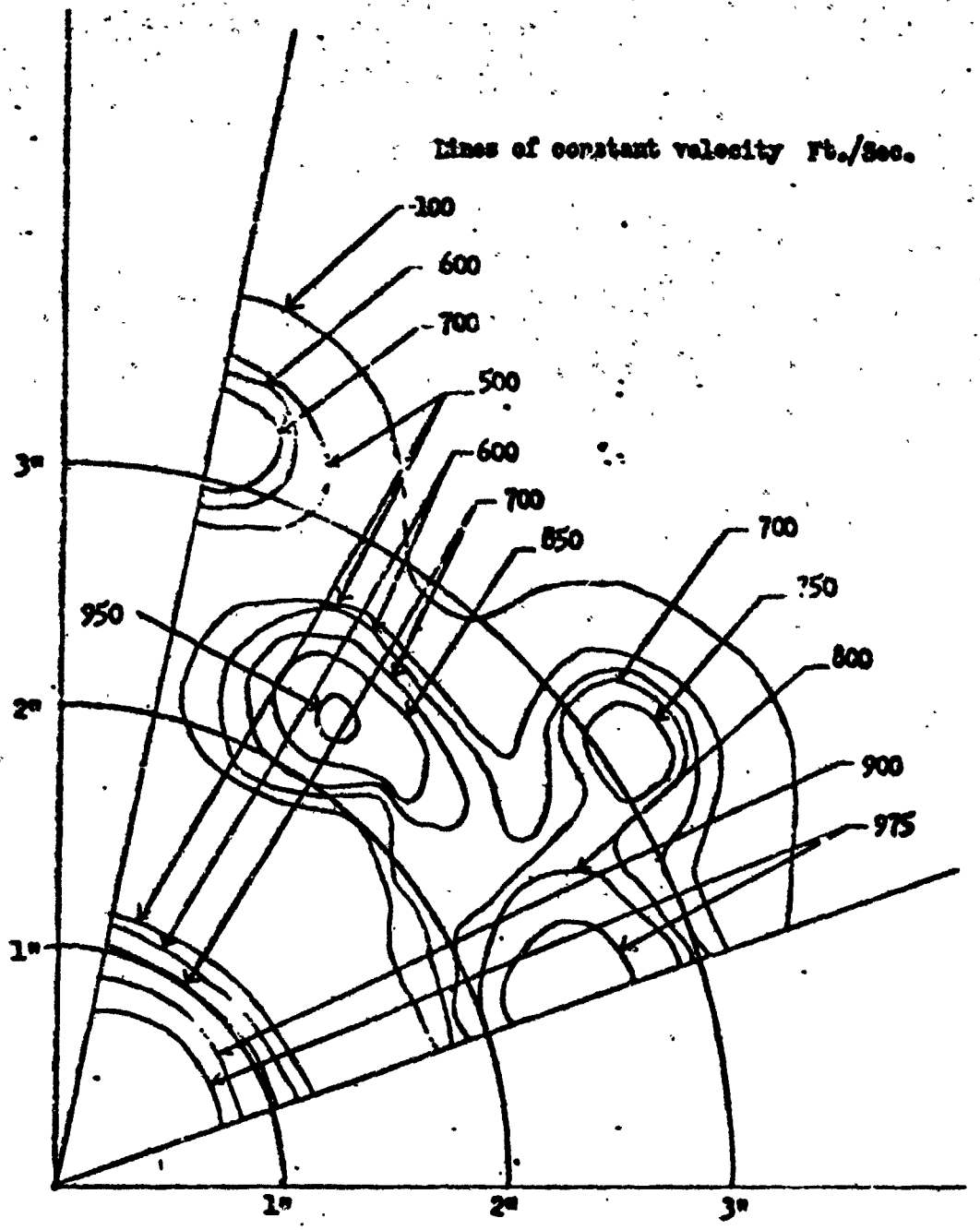

Axial Location X = 4 inches Flow Exit Velocity = 1000 ft/sec

60° Symmetrical Section $P_o/P = 1.8$, $T_o = 540^oR$

19 Tube Nozzle

Figure 1.9b- Flow Velocity Contours.

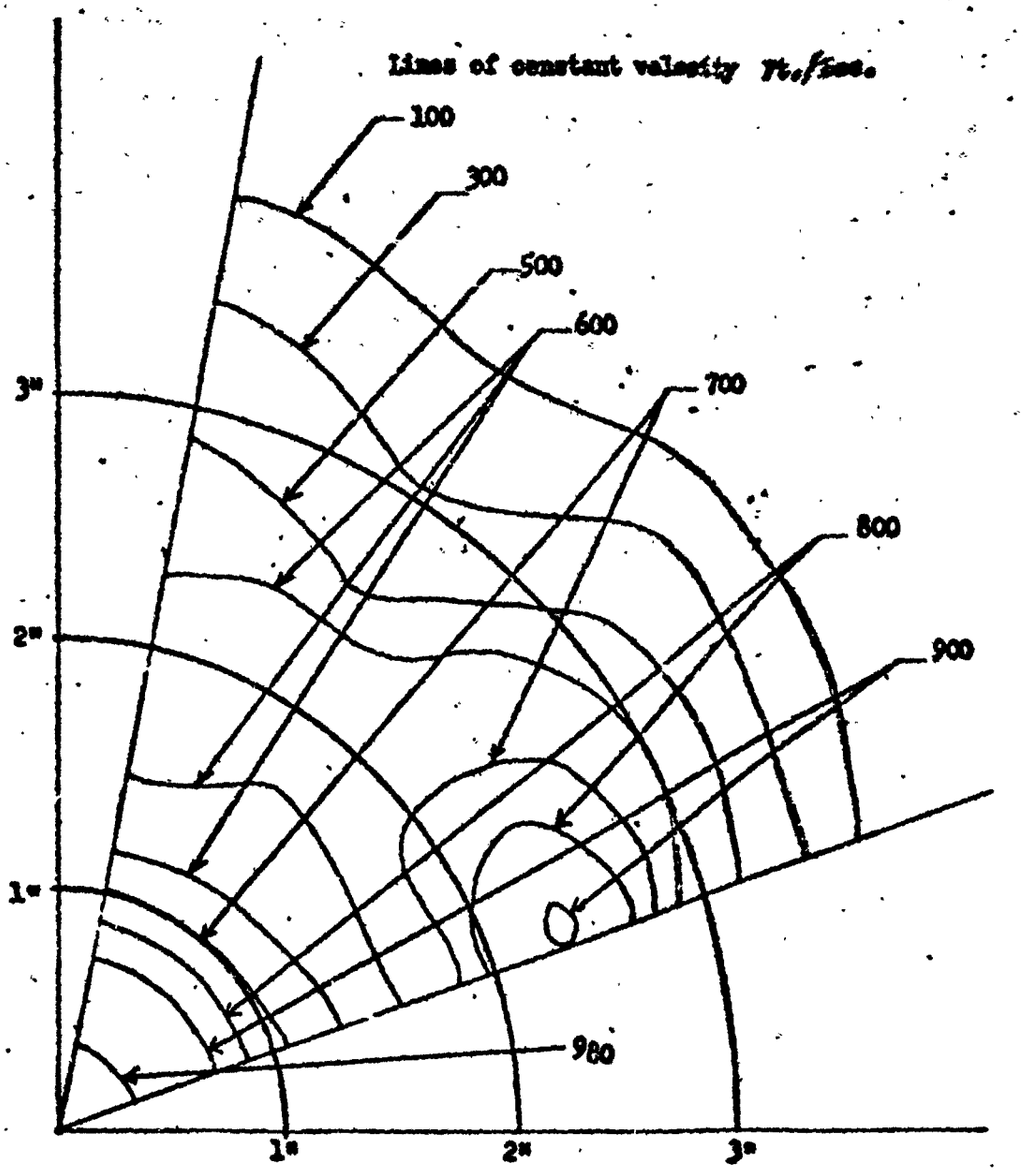

Axial Location X = 8 inches

Flow Exit Velocity = 1000 ft/sec

60° Symmetrical Section

$P_o/P = 1.8$

$T_o = 540°R$

19 Tube Nozzle

Figure 1.9c - Flow Velocity Contours.

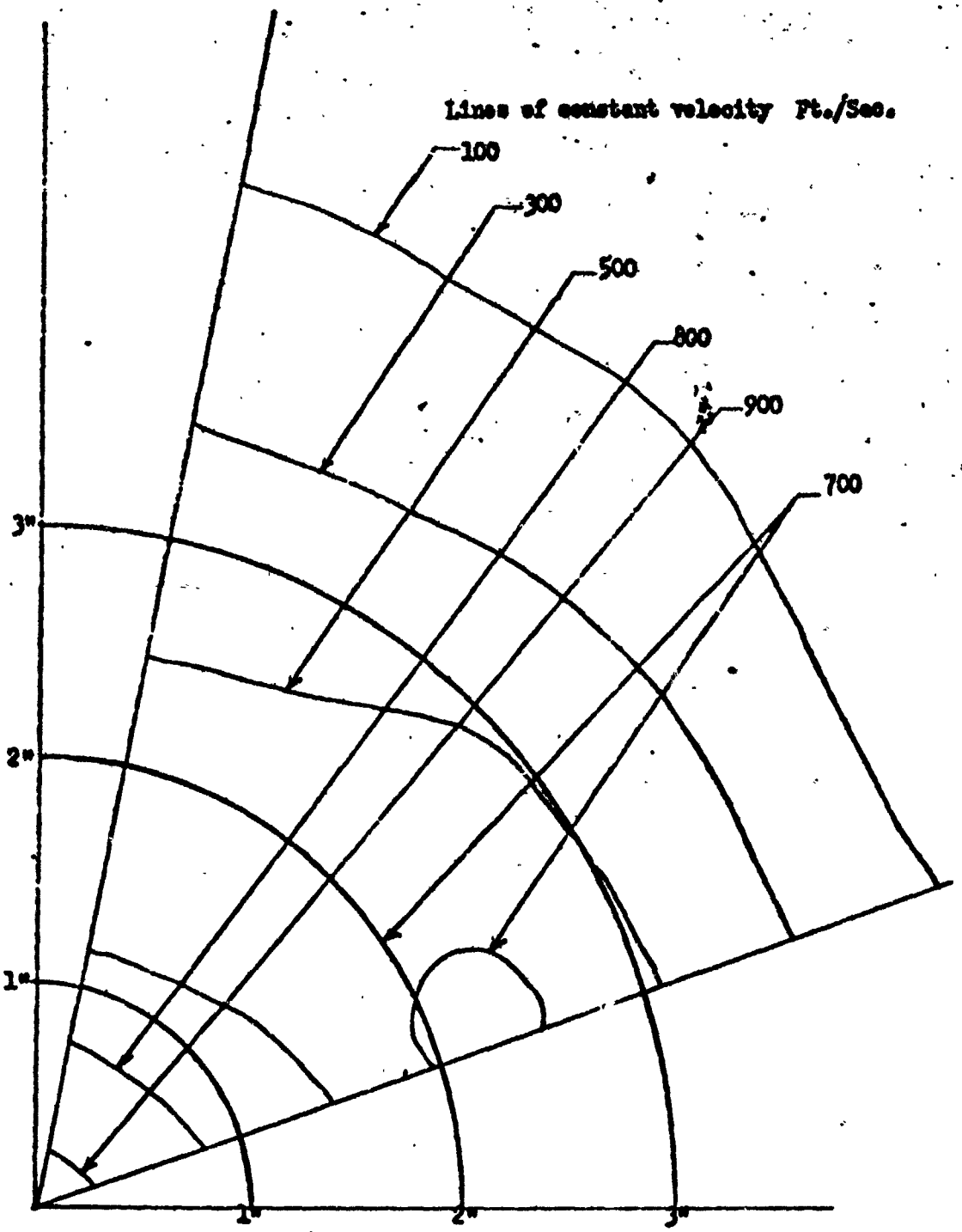

Axial Location X = 16 inches Flow Exit Velocity = 1000 ft/sec

60° Symmetrical Section $P_o/P = 1.8$

$T_o = 540°R$

19 Tube Nozzle

Figure 1.9d - Flow Velocity Contours.

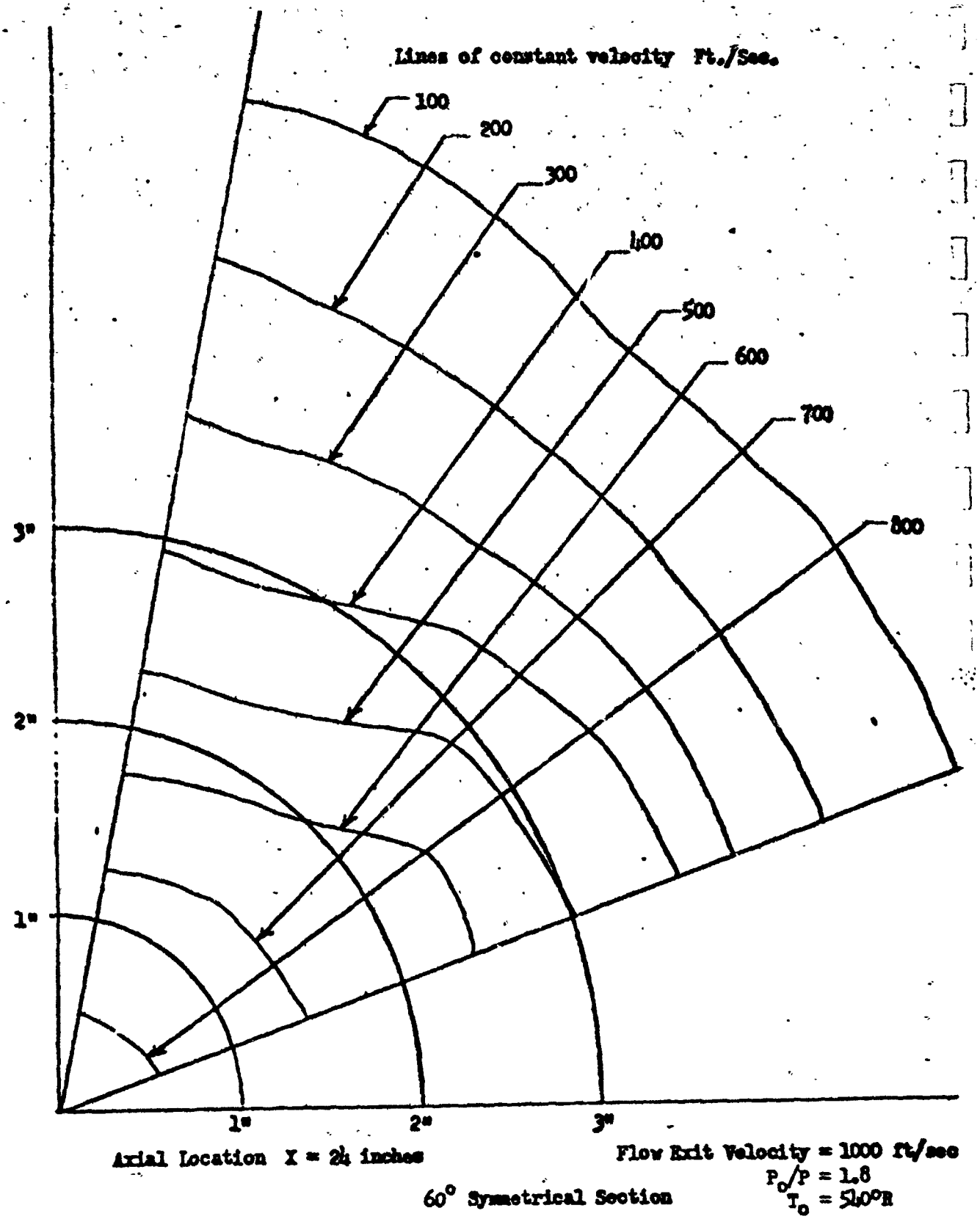

Figure 1.9e - Flow Velocity Contours.

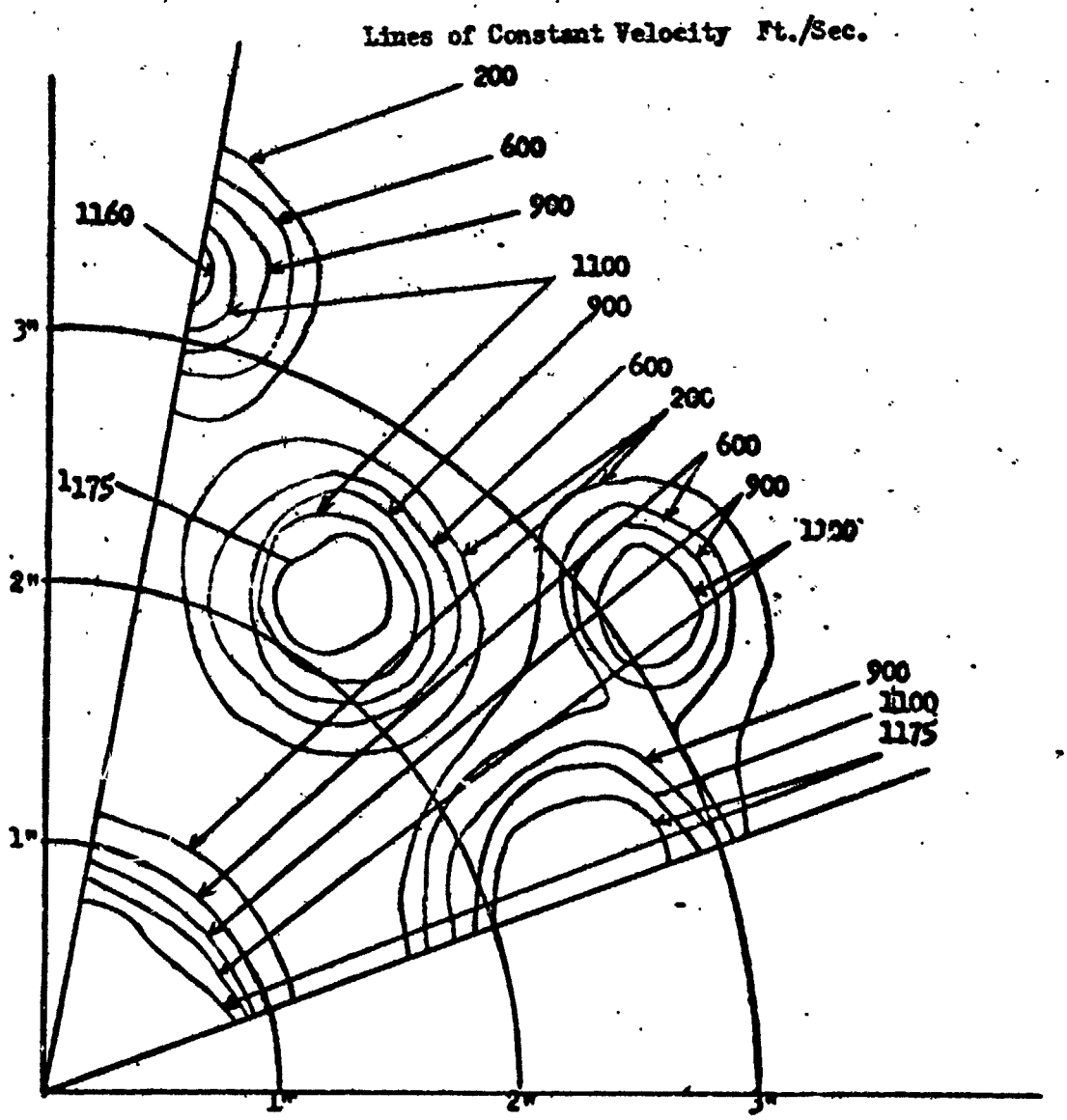

Axial Location X = 2 inches

Flow Exit Velocity = 1190 ft/sec

60° Symmetrical Section

$P_o/P = 2.4$

$T_o = 540°R$

19 Tube Nozzle

Figure 1.9f - Flow Velocity Contours.

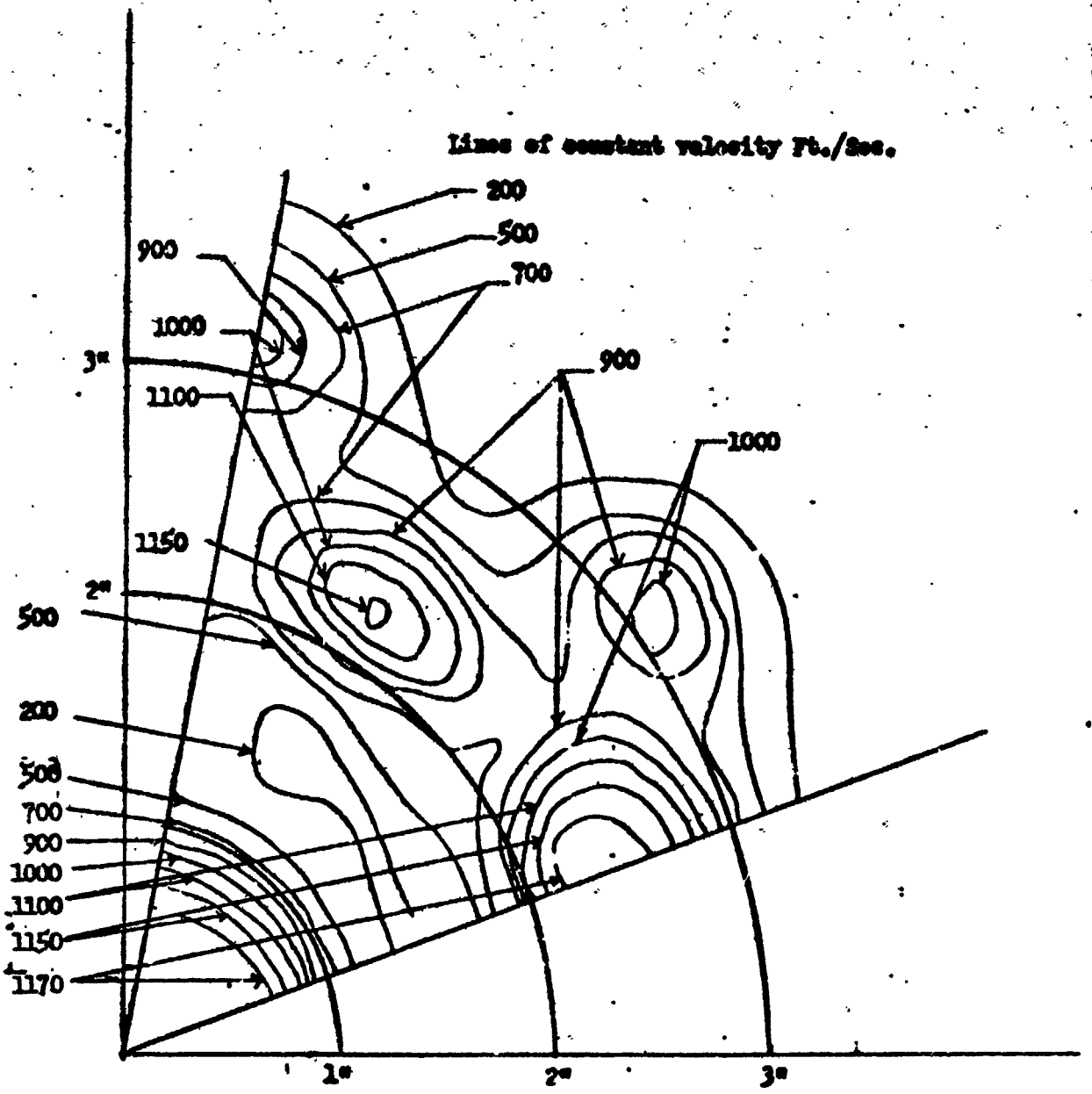

Figure 1.9g Flow Velocity Contours.

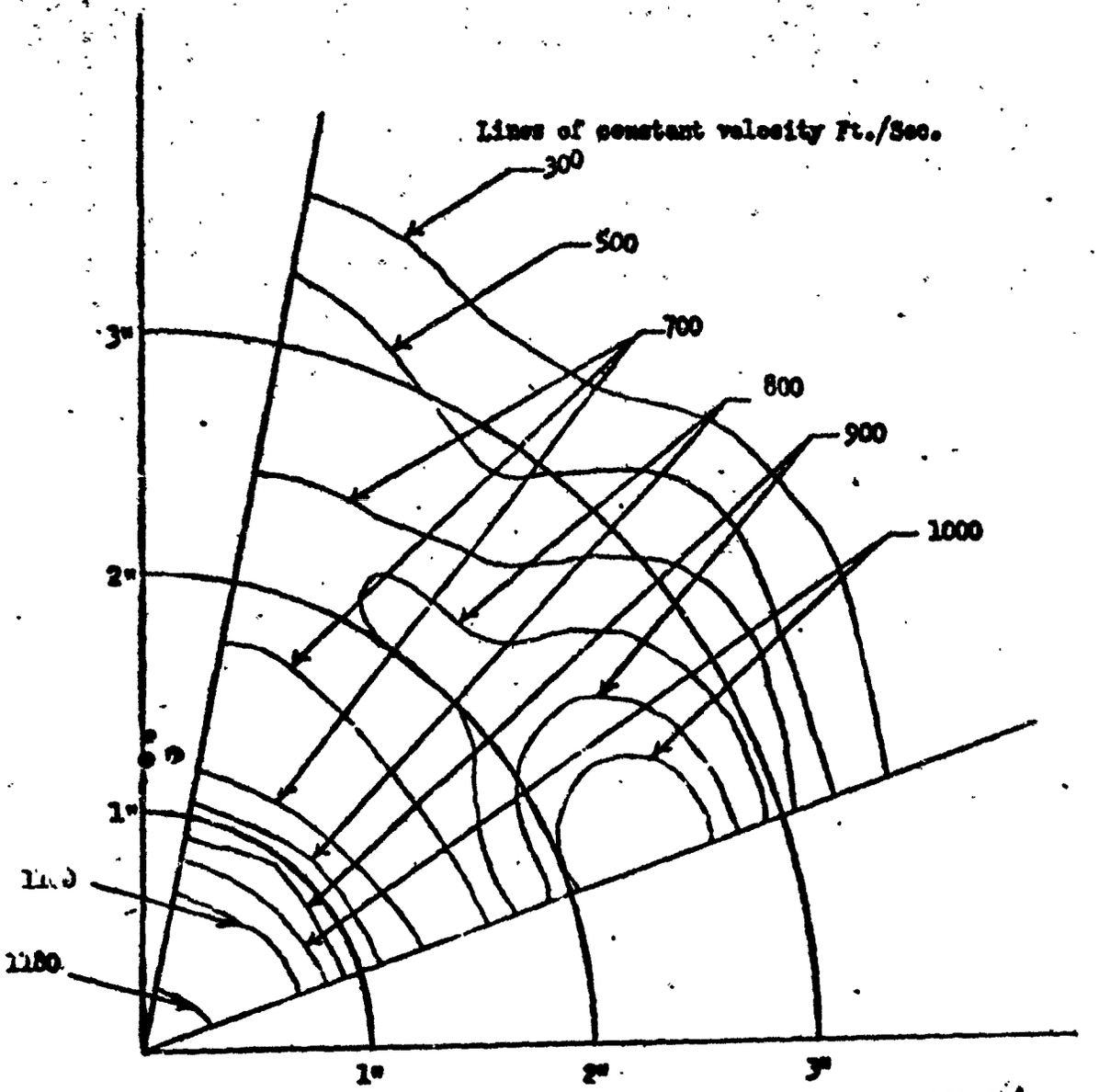

Axial Location X = 8 inches — Flow Exit Velocity = 1190 ft/sec

$P_o/P = 2.4$

60° Symmetrical Section — $T_o = 540°R$

19 Tube Nozzle

Figure 1.9h - Flow Velocity Contours.

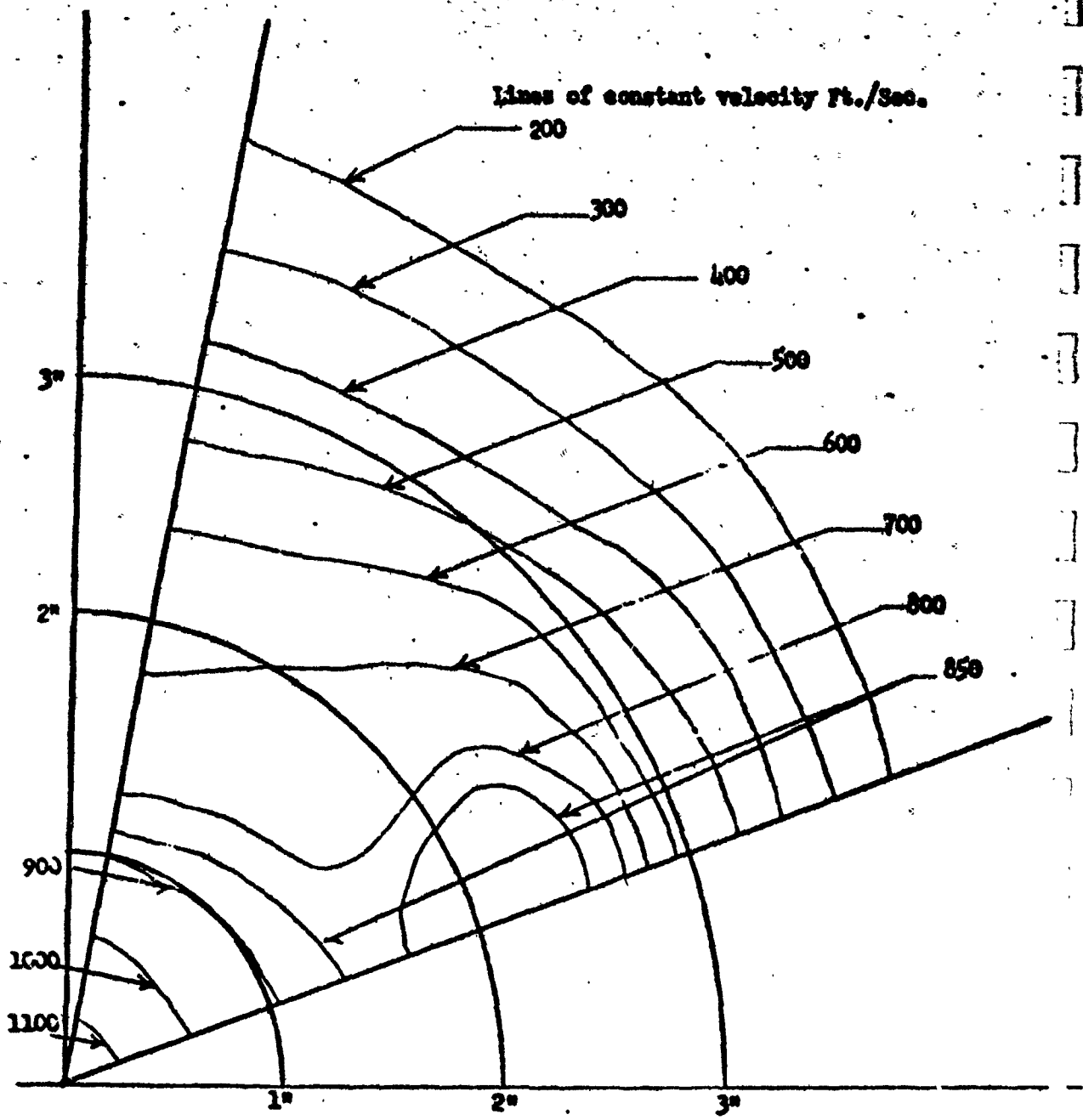

Axial Location X = 16 inches

Flow Exit Velocity = 1190 ft/sec

$P_o/P = 2.4$

60° Symmetrical Section

$T_o = 540°R$

19 Tube Nozzle

Figure 1.91 - Flow Velocity Contours.

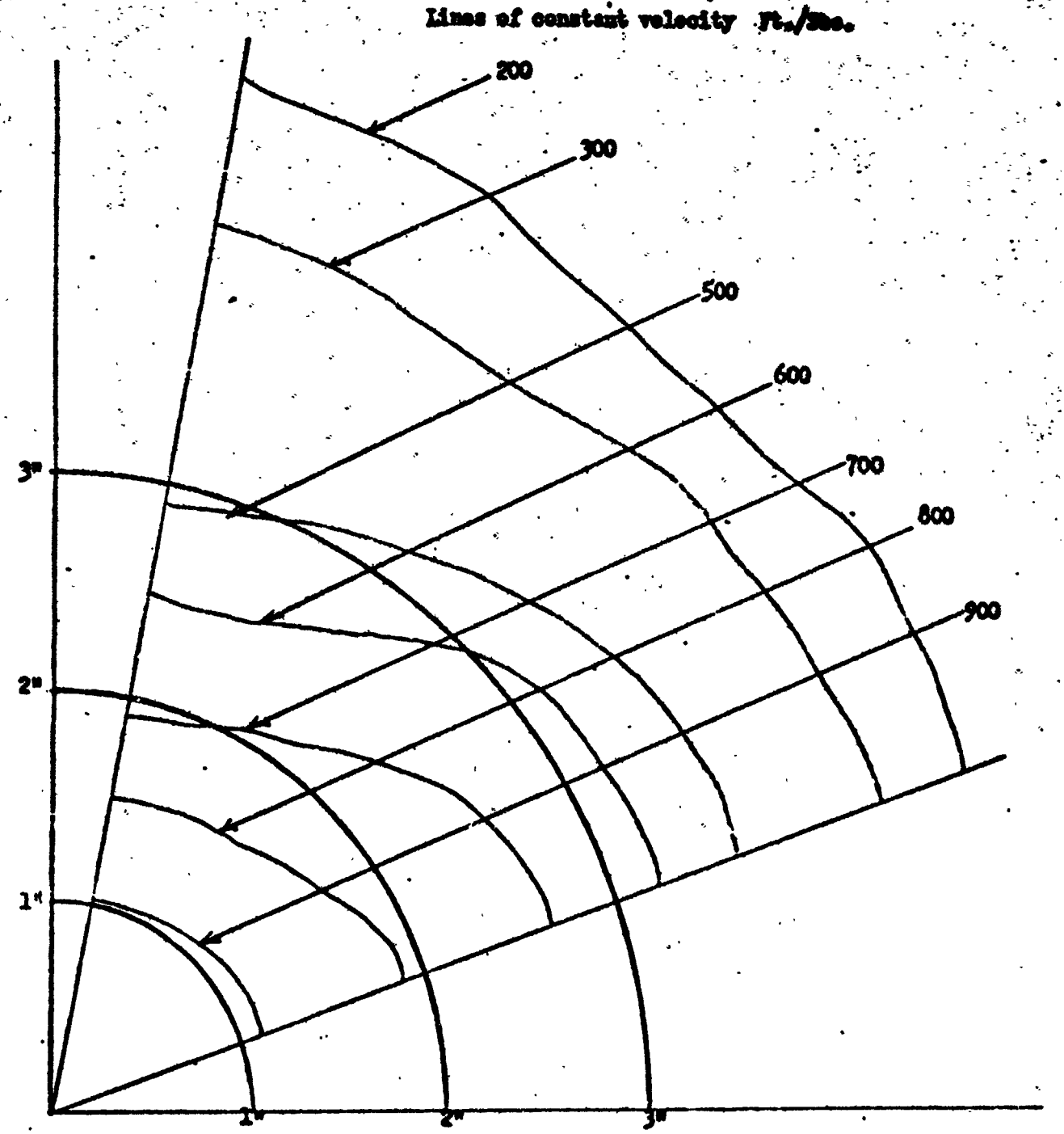

Figure 1.9j - Flow Velocity Contours.

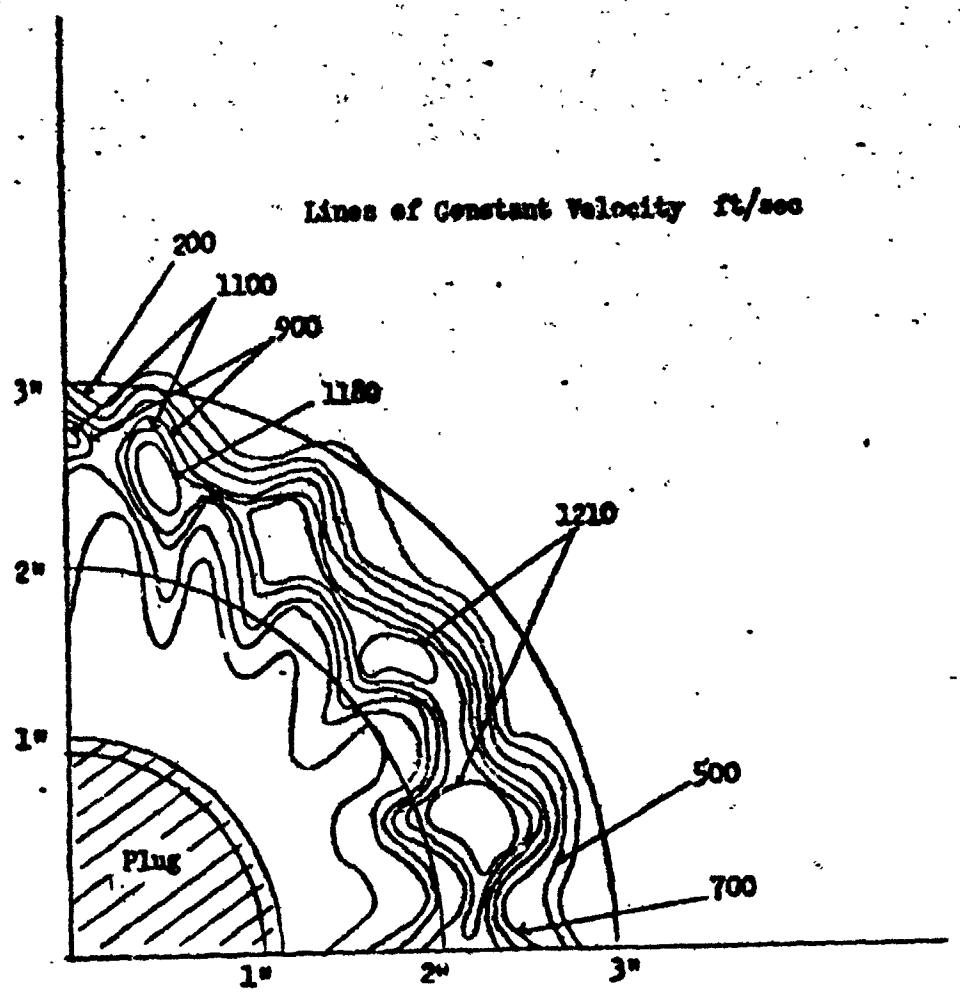

Axial Location X = 2 inches

Flow Exit Velocity = 1200 ft/sec
$P_o/P = 2.4$ $T_o = 540°R$

18 Segment Nozzle

Figure 1.10a- Flow Velocity Contours.

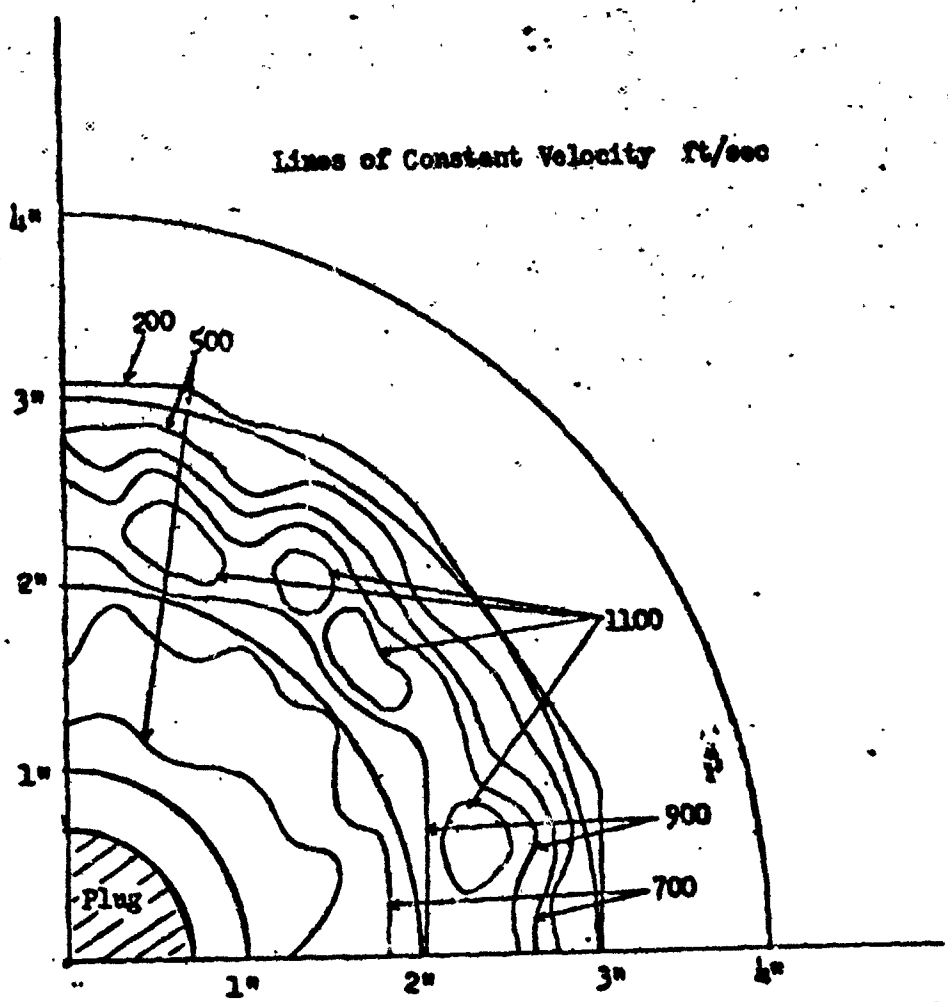

Axial Location : X = 4 inches

Flow Exit Velocity =1200 ft/sec
$P_o/P = 2.4$ $T_o = 540°R$

18 Segment Nozzle

Figure 1.10b - Flow Velocity Contours.

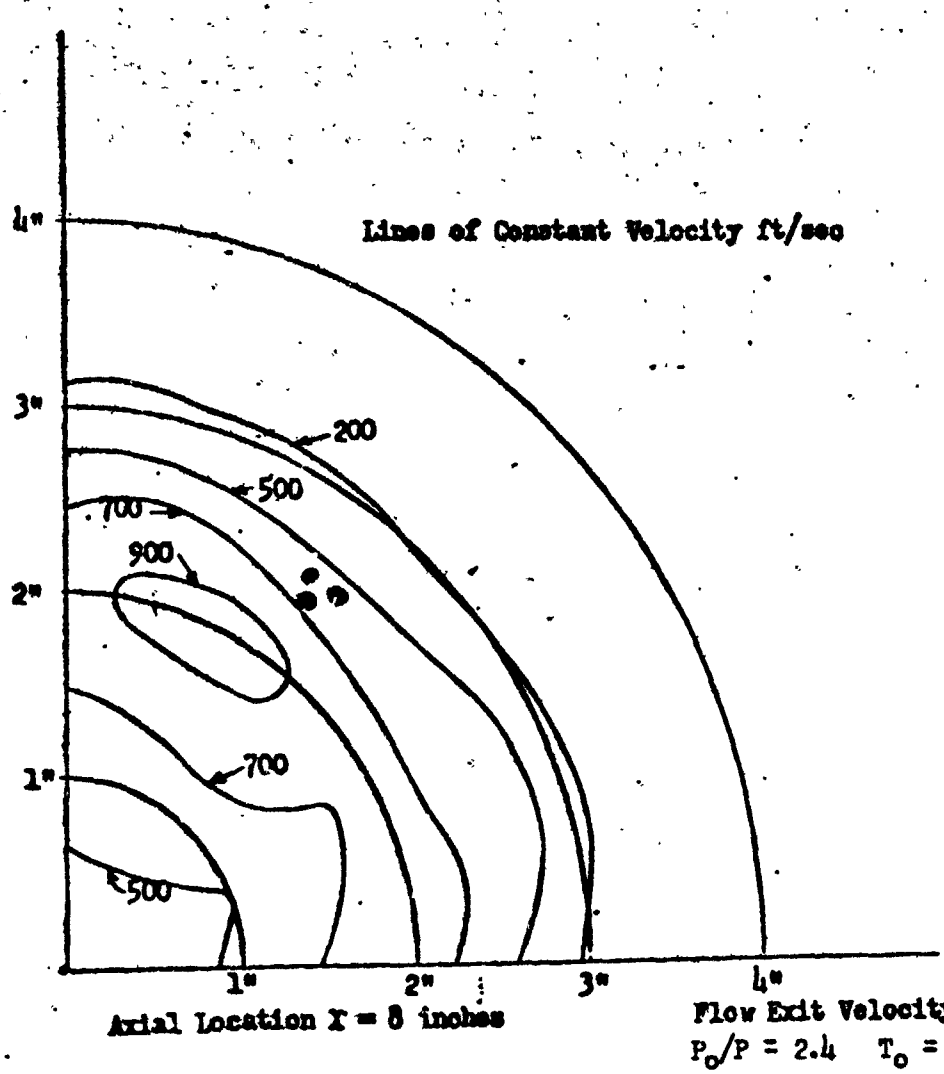

18 Segment Nozzle

Figure 1.10c - Flow Velocity Contours.

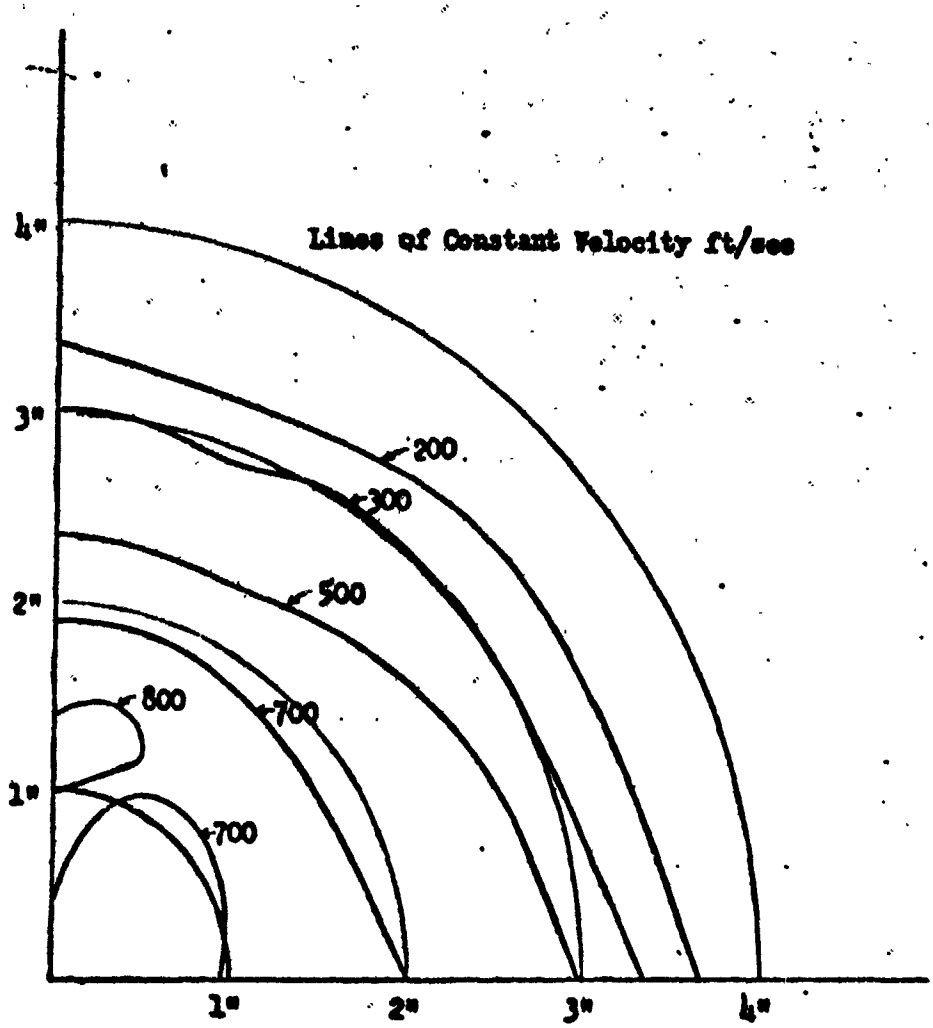

Axial Location X = 16 inches

Flow Exit Velocity = 1200 ft/sec
$P_o/P = 2.4$ $T_o = 540°R$

18 Segment Nozzle

Figure 1.10d- Flow Velocity Contours.

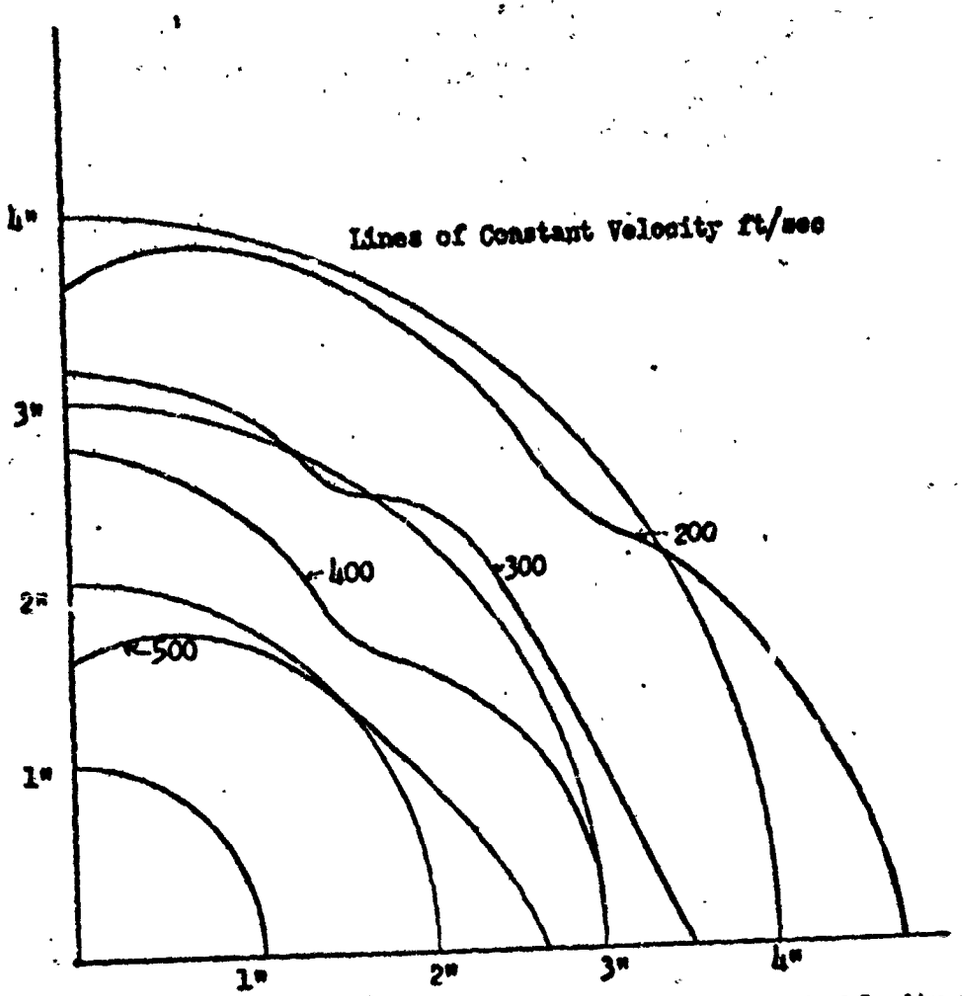

Axial Location X = 32 inches

Flow Exit Velocity = 1200 ft/sec
$P_o/P = 2.4$ $T_o = 540^oR$

18 Segment Nozzle

Figure 1.10e Flow Velocity Contours.

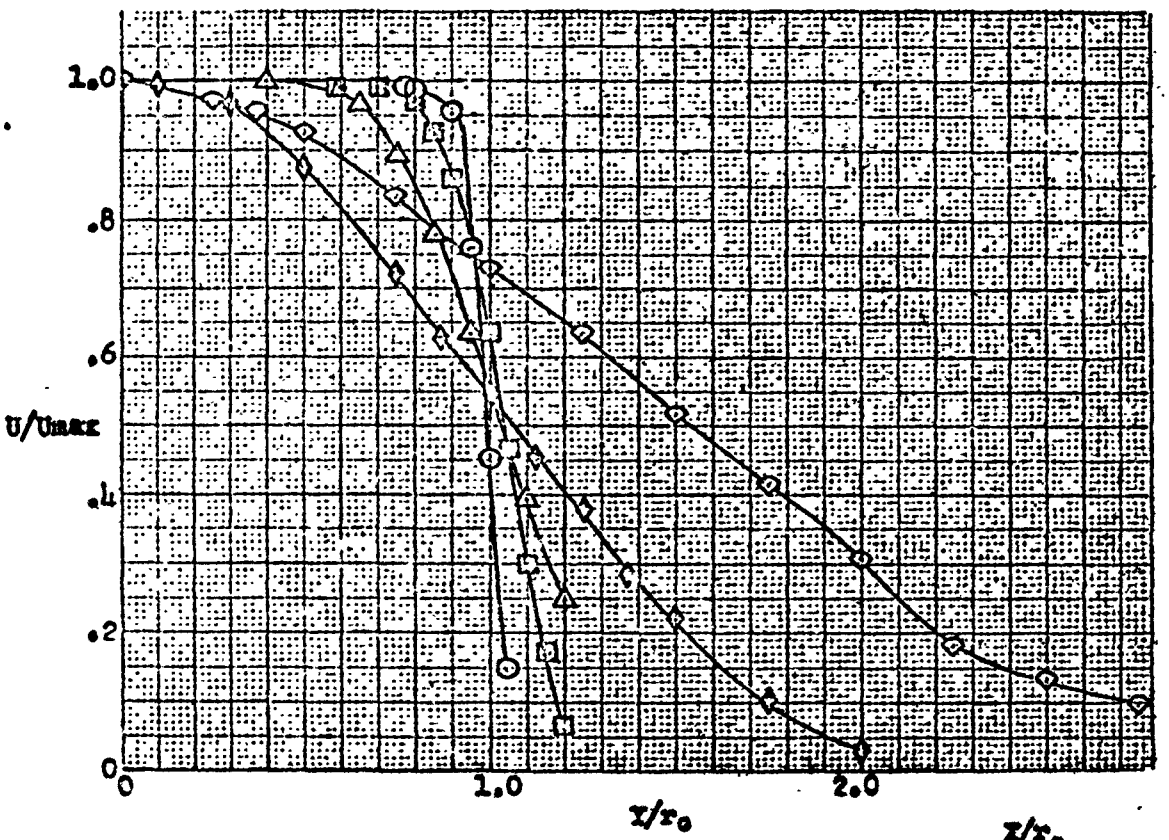

Conical Nozzle

Figure 1.11a - Normalised Equivalent Velocity Profiles

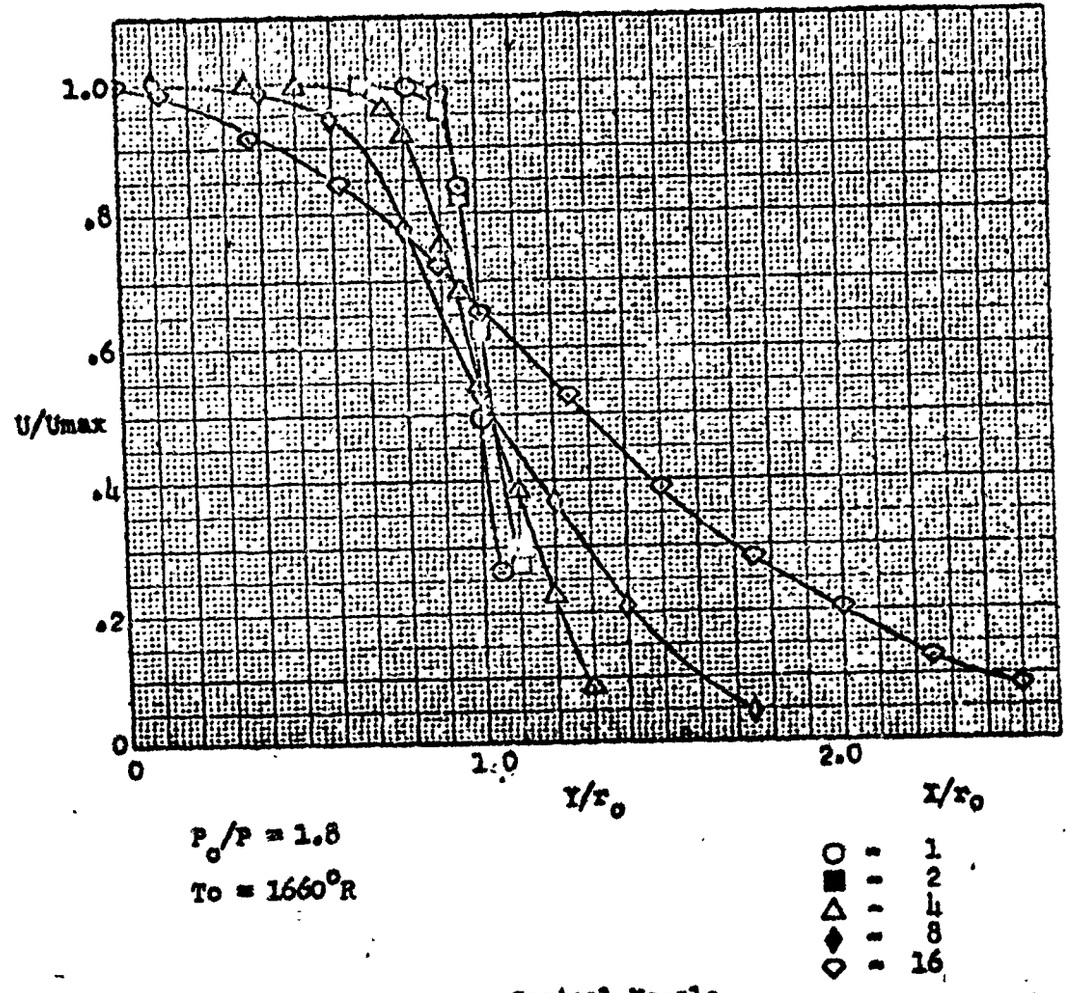

Conical Nozzle

Figure 1.11b- Normalised Equivalent Velocity Profiles

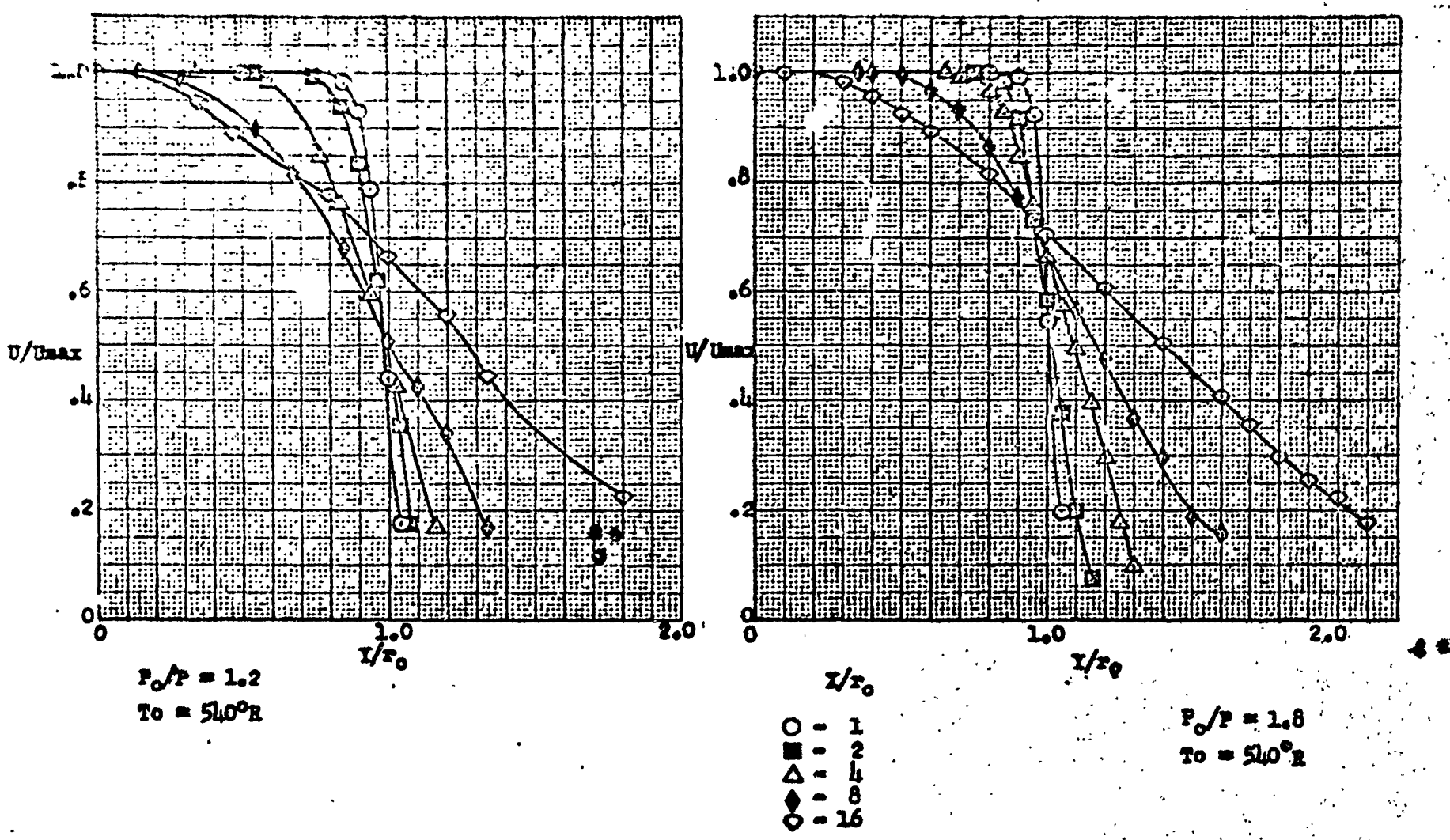

Conical Nozzle

Figure 1.11c Normalized Equivalent Velocity Profiles

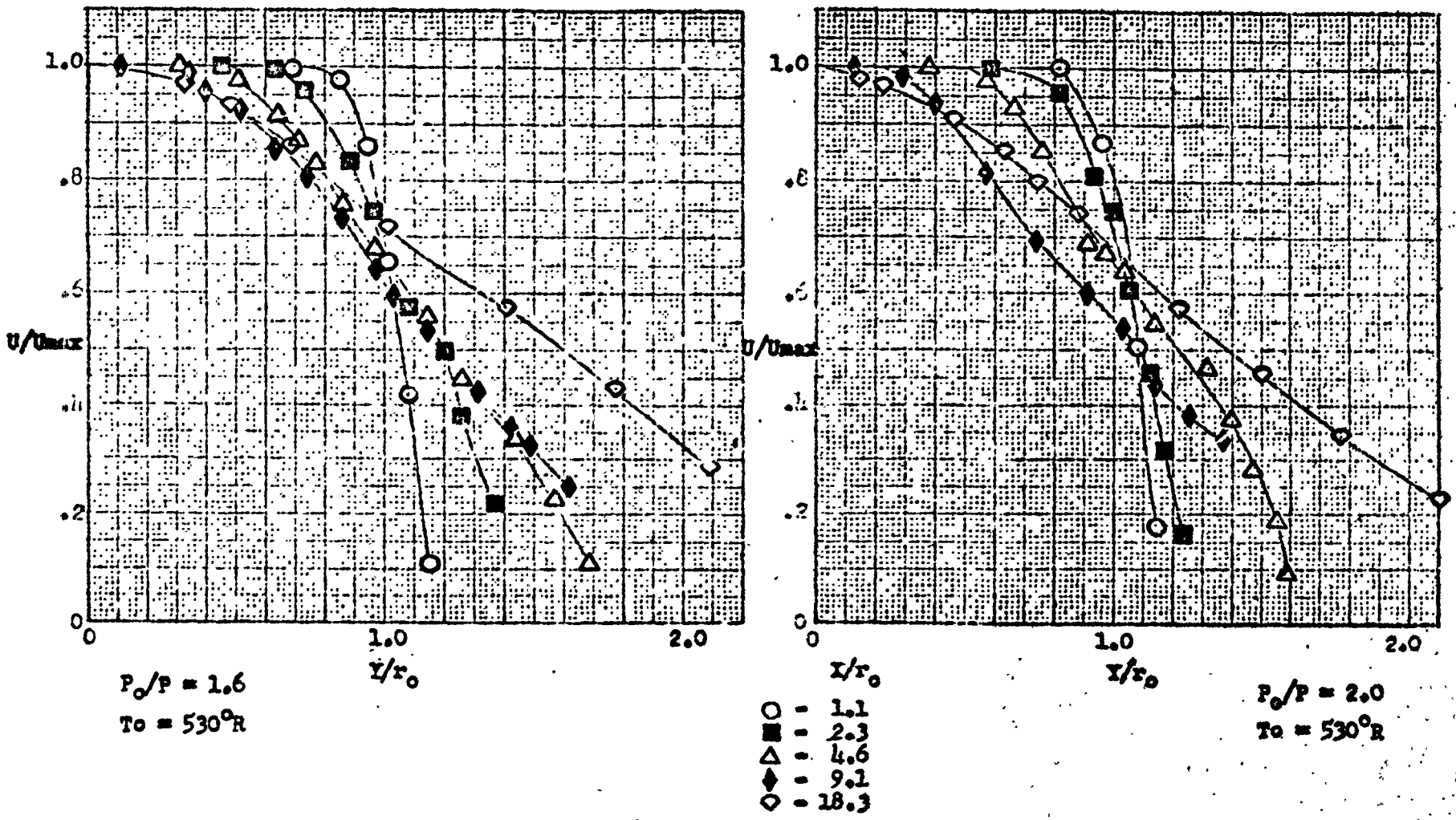

Plug Nozzle

Figure 1.12a - Normalised Equivalent Velocity Profiles

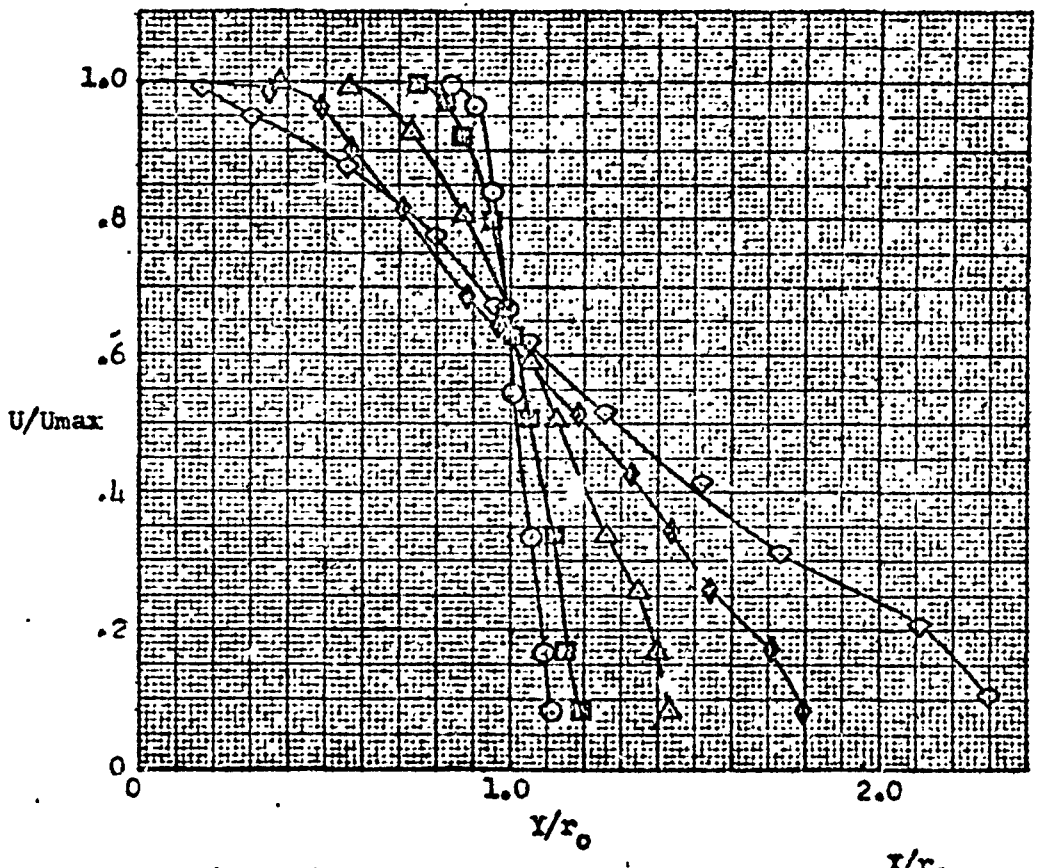

Plug Nozzle

Figure 1.12b- Normalized Equivalent Velocity Profiles

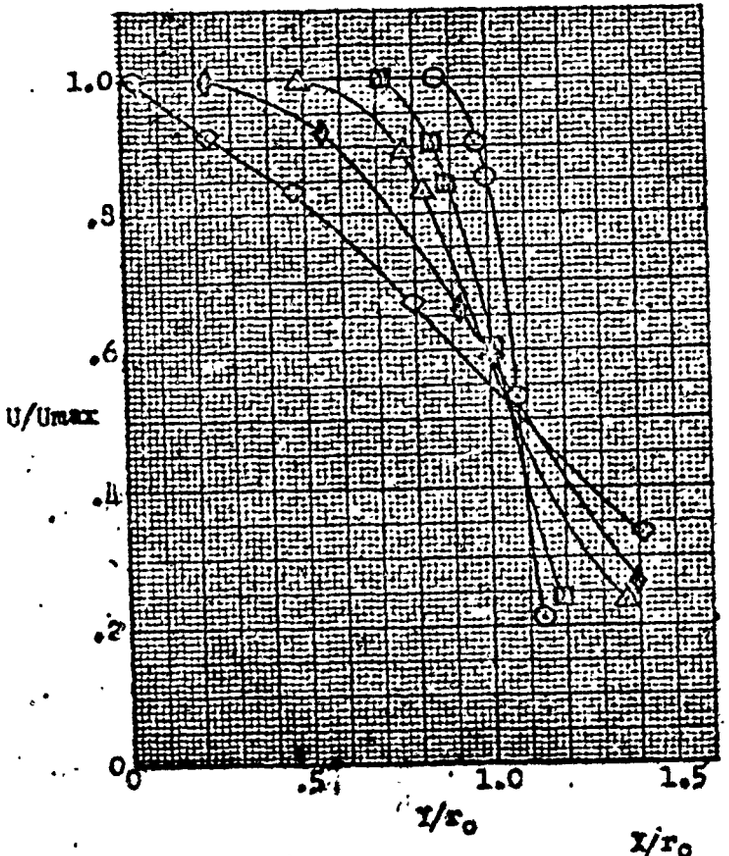

Plug Nozzle with Shroud

Figure 1.13a Normalised Equivalent Velocity Profiles

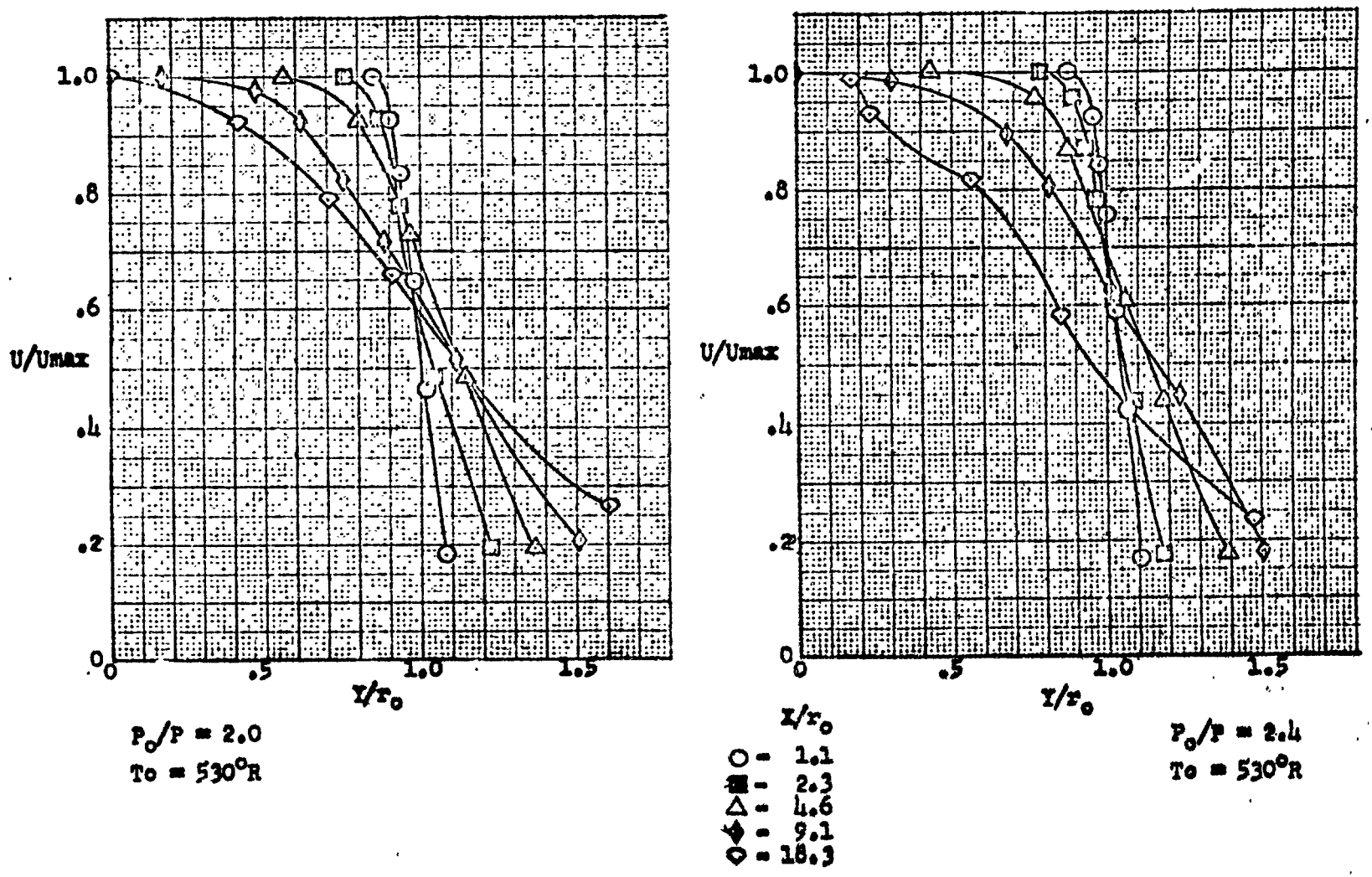

Ring Nozzle with Shroud

Figure 1.13b Normalised Equivalent Velocity Profiles

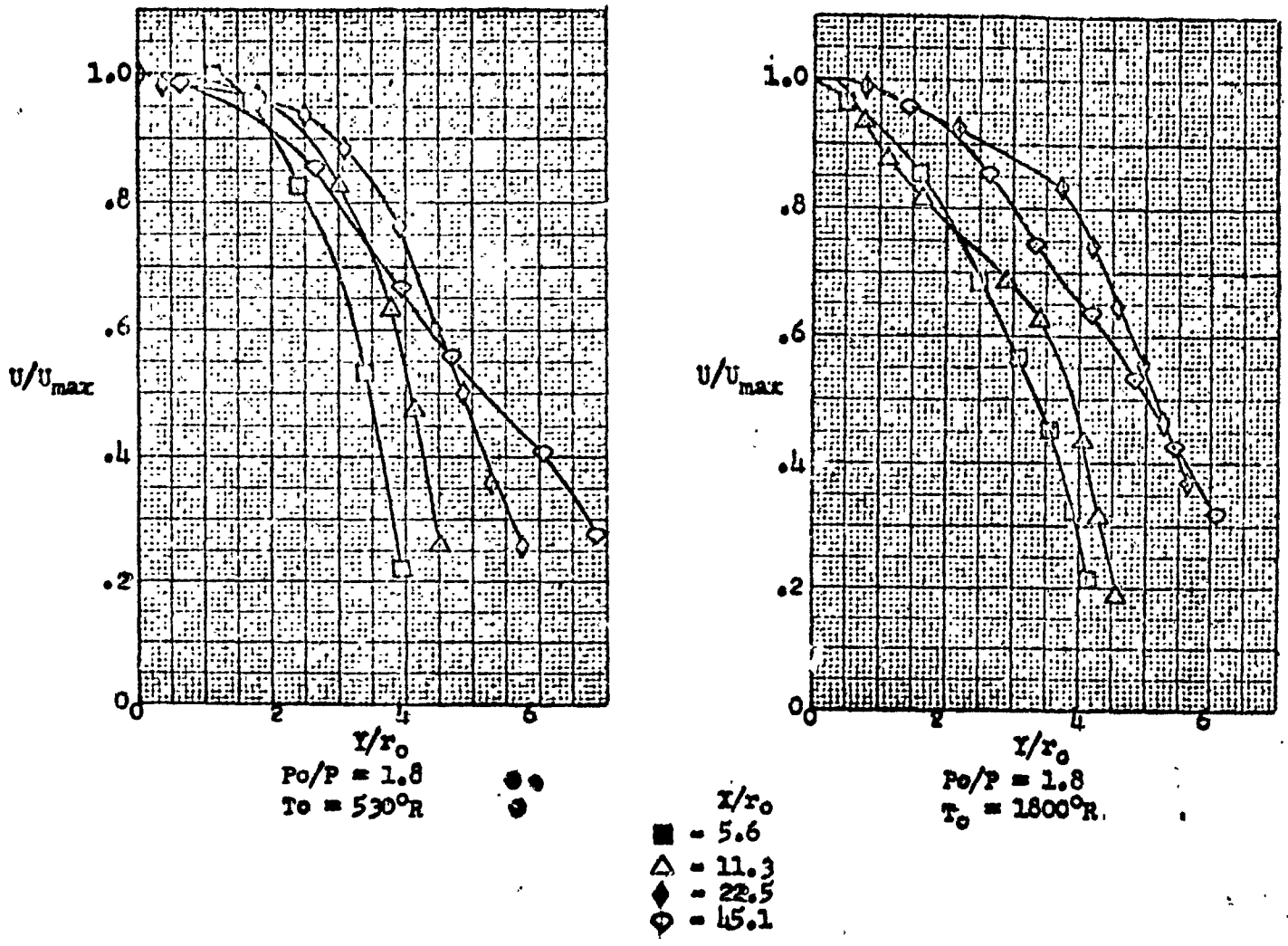

8 Lobe Nozzle

Figure 1.14 - Normalised Equivalent Velocity Profiles

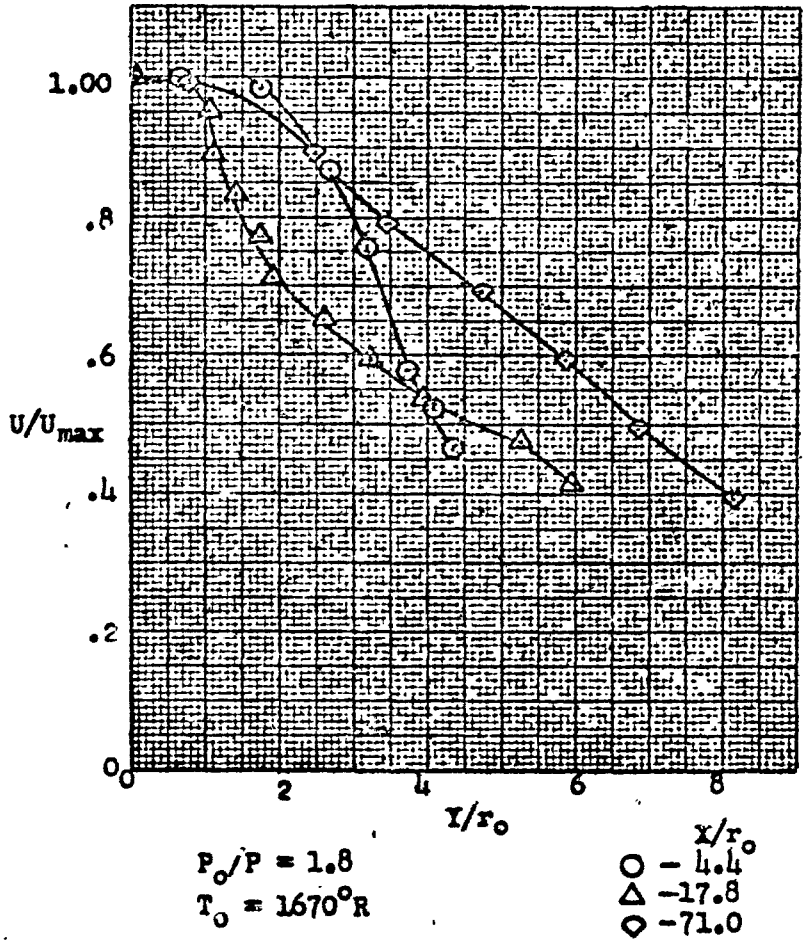

19 Tube Nozzle

Figure 1.15a- Normalized Equivalent Velocity Profiles

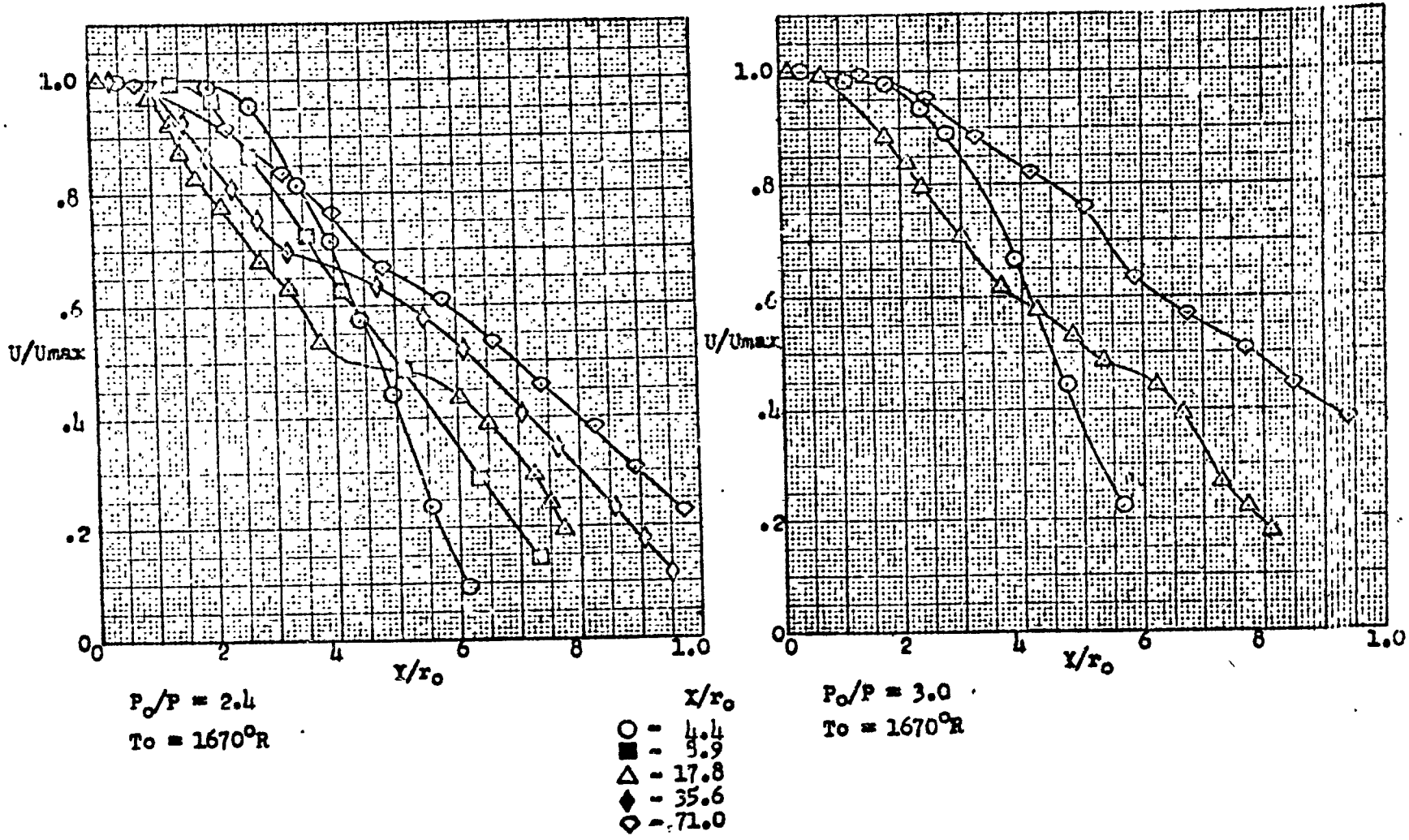

19 Tube Nozzle

Figure 1.15b - Normalized Equivalent Velocity Profiles

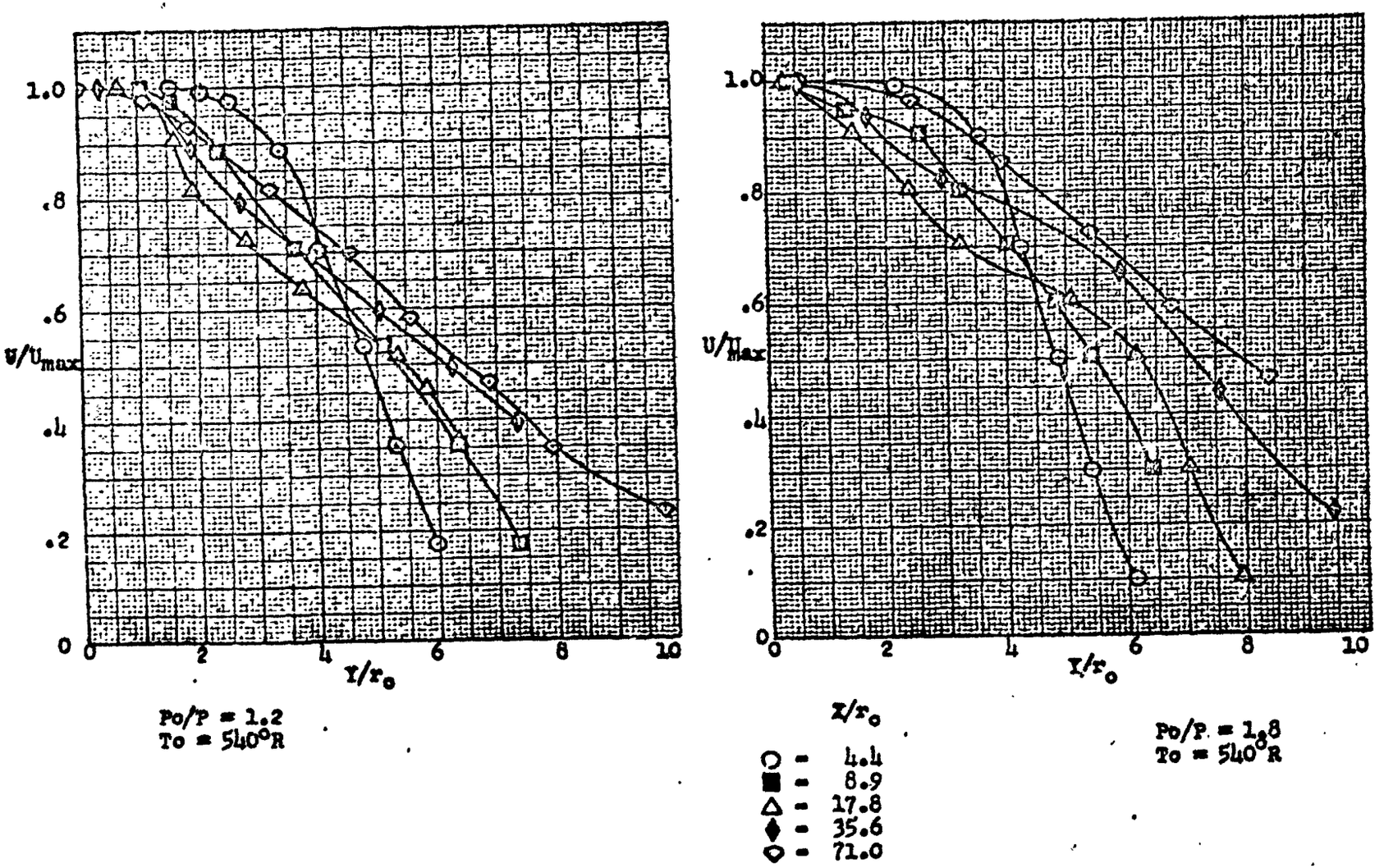

19 Tube Nozzle

Figure 1.15c- Normalised Equivalent Velocity Profiles

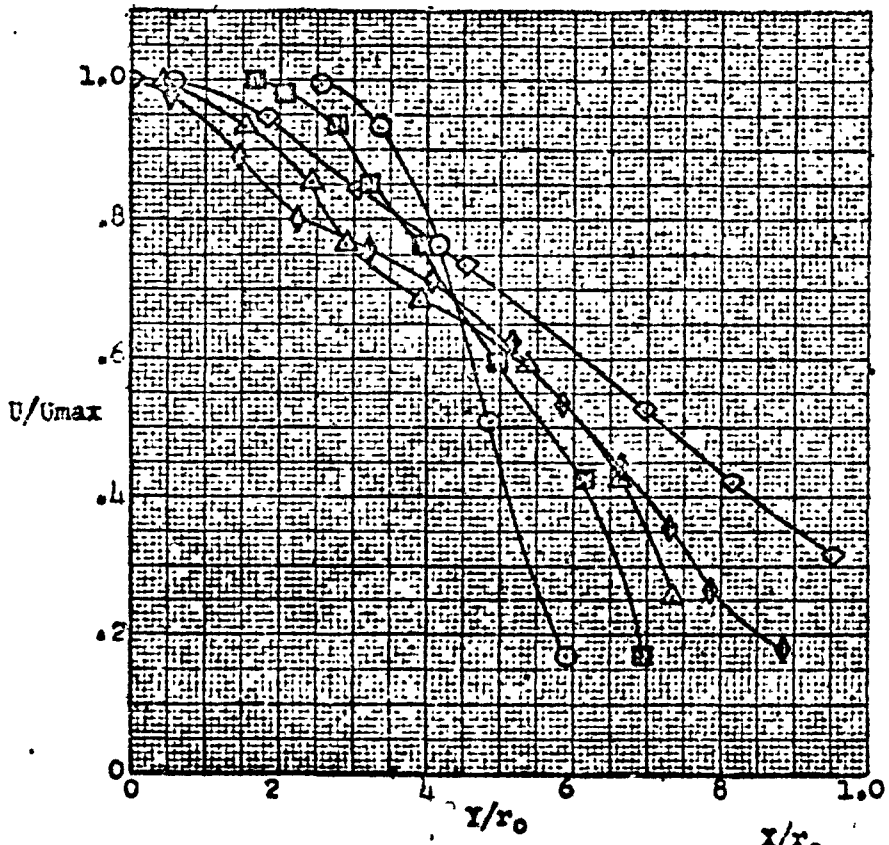

19 Tube Nozzle

Figure 1.15d Normalized Equivalent Velocity Profiles

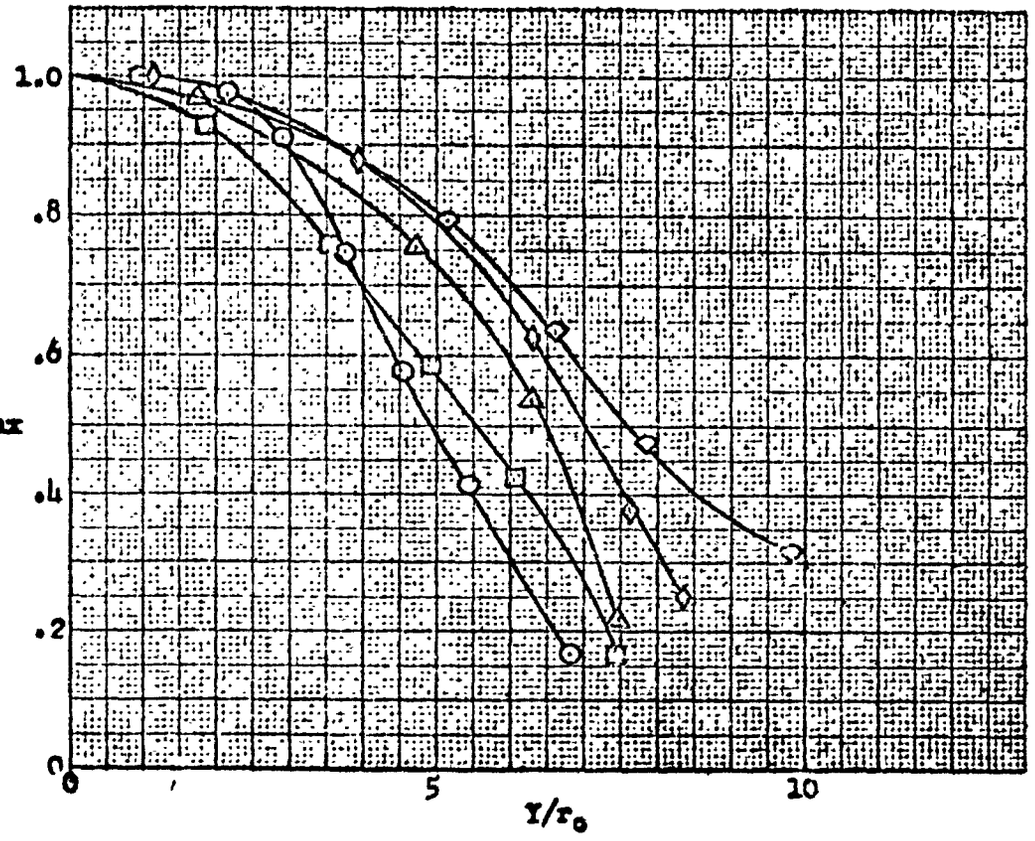

$P_o/P = 2.4$

$T_o = 530°R$

X/r_o

- ○ = 4.8
- ■ = 9.7
- △ = 19.4
- ◇ = 38.7
- ⬡ = 77.5

18 Segment Nozzle

Figure 1.16 - Normalized Equivalent Velocity Profiles

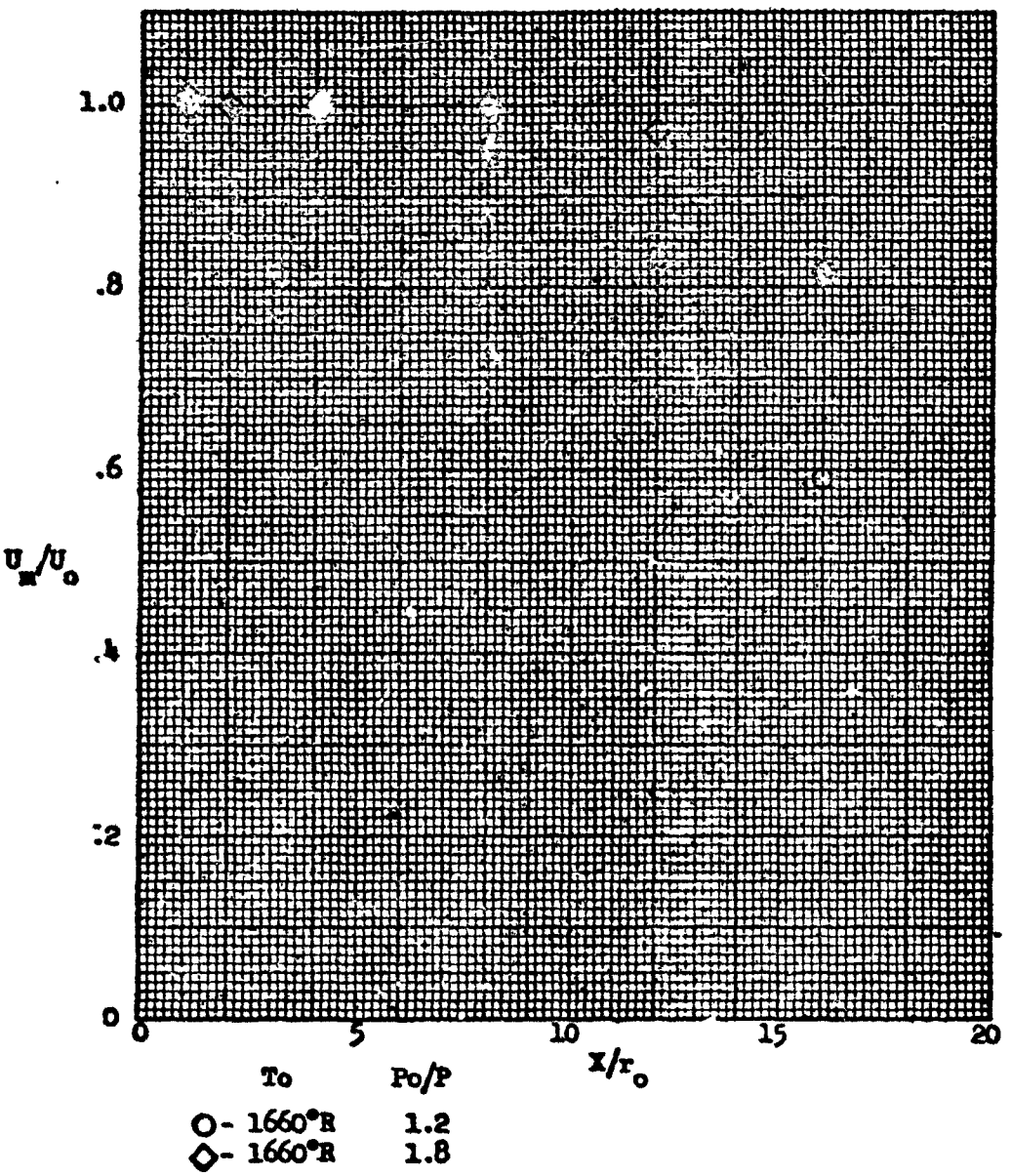

Conical Nozzle

Figure 1.17a- Maximum Velocity Decay in Axial Direction.

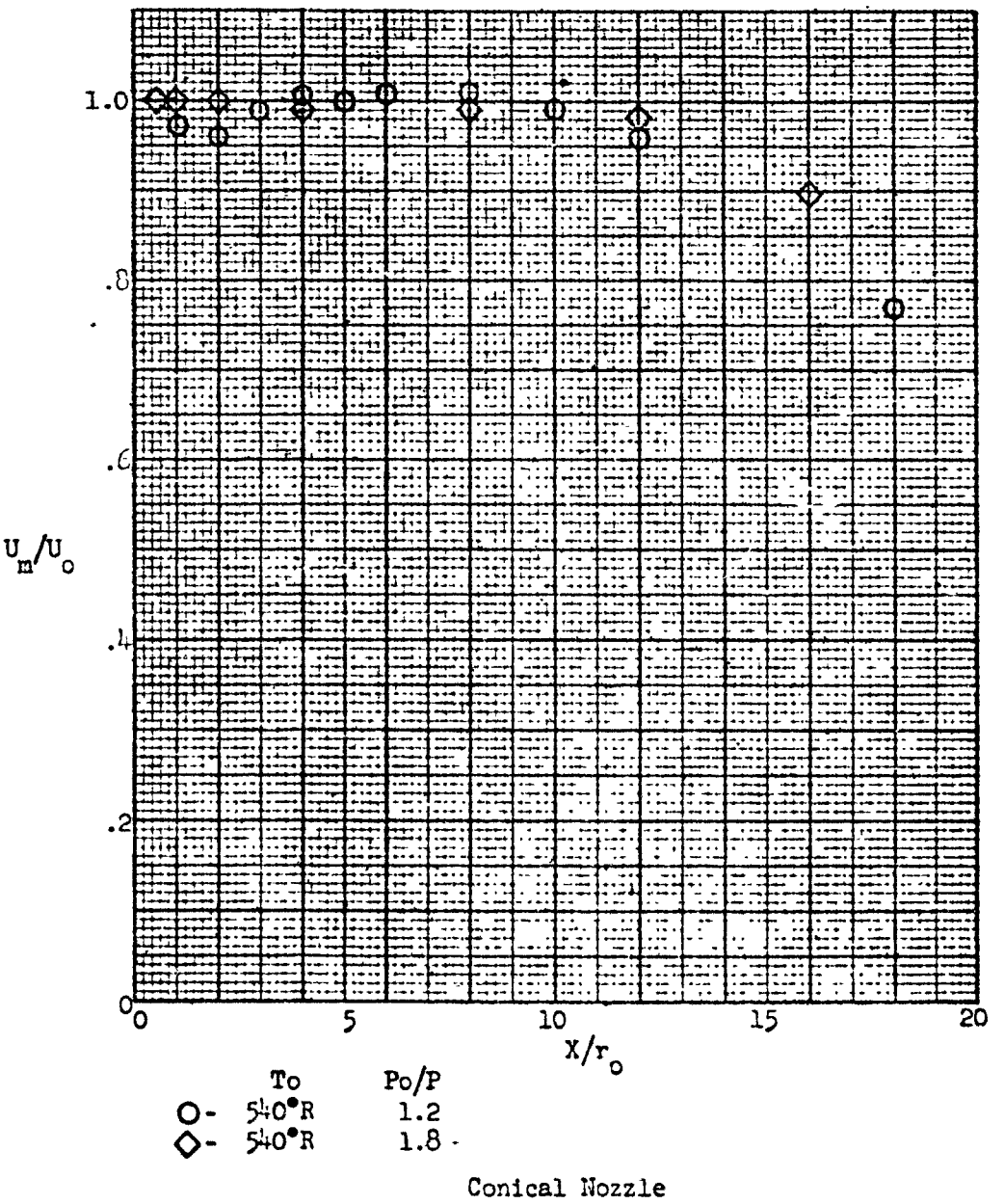

Figure 1.17b - Maximum Velocity Decay in Axial Direction.

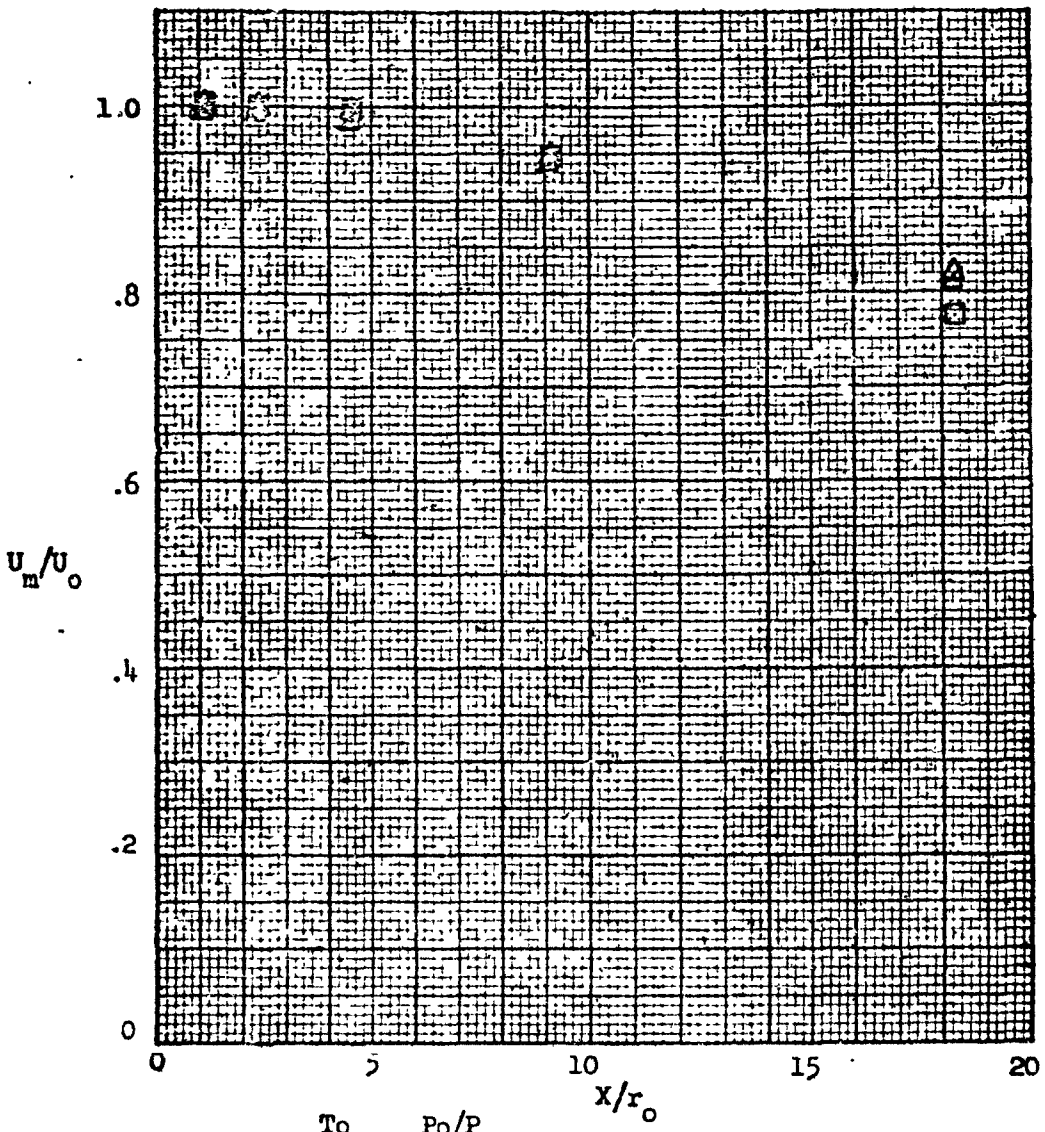

Plug Nozzle

Figure 1.17c- Maximum Velocity Decay in Axial Direction.

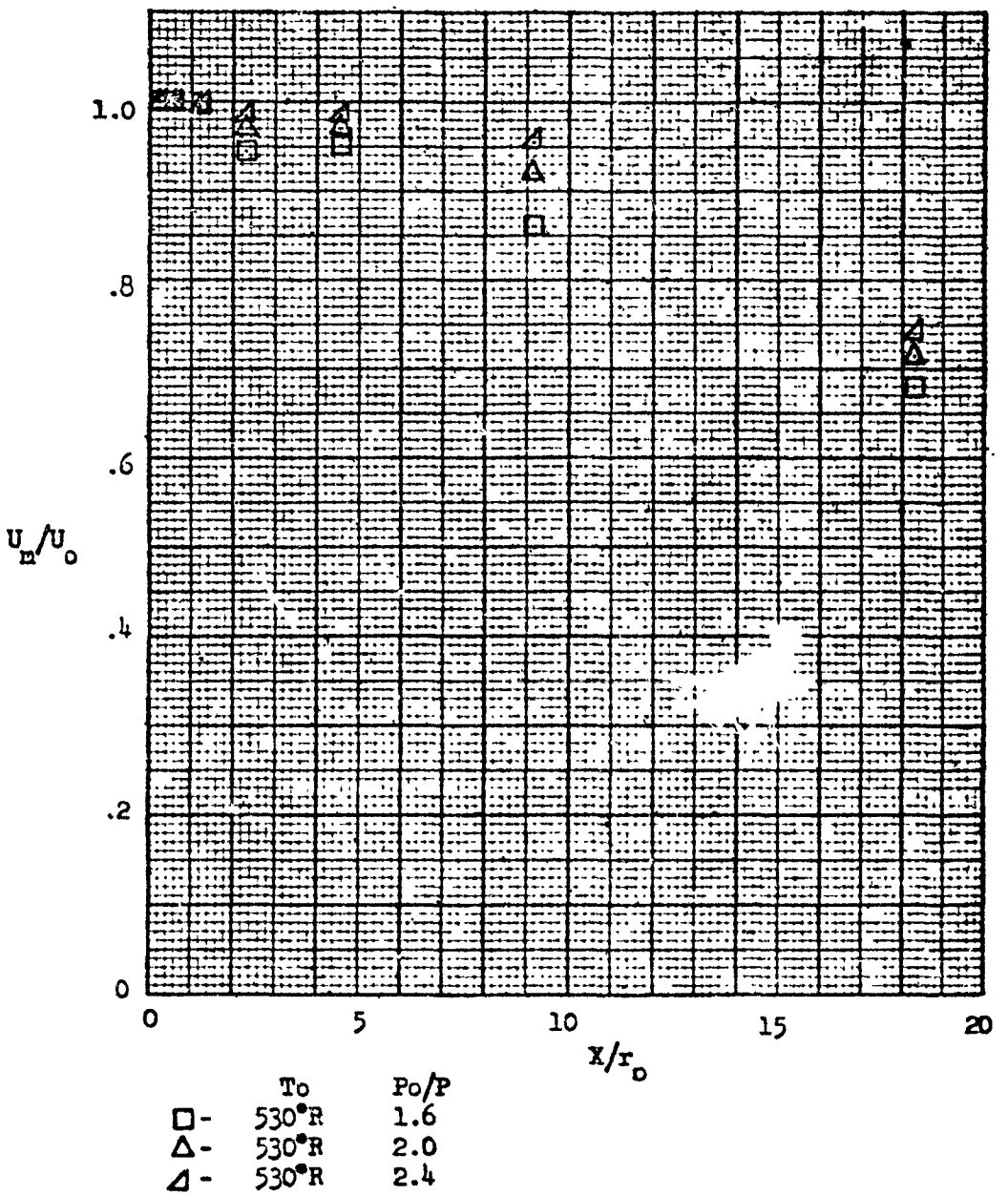

	To	Po/P
□ -	530°R	1.6
△ -	530°R	2.0
◿ -	530°R	2.4

Plug Nozzle with Shroud

Figure 1.17d - Maximum Velocity Decay in Axial Direction.

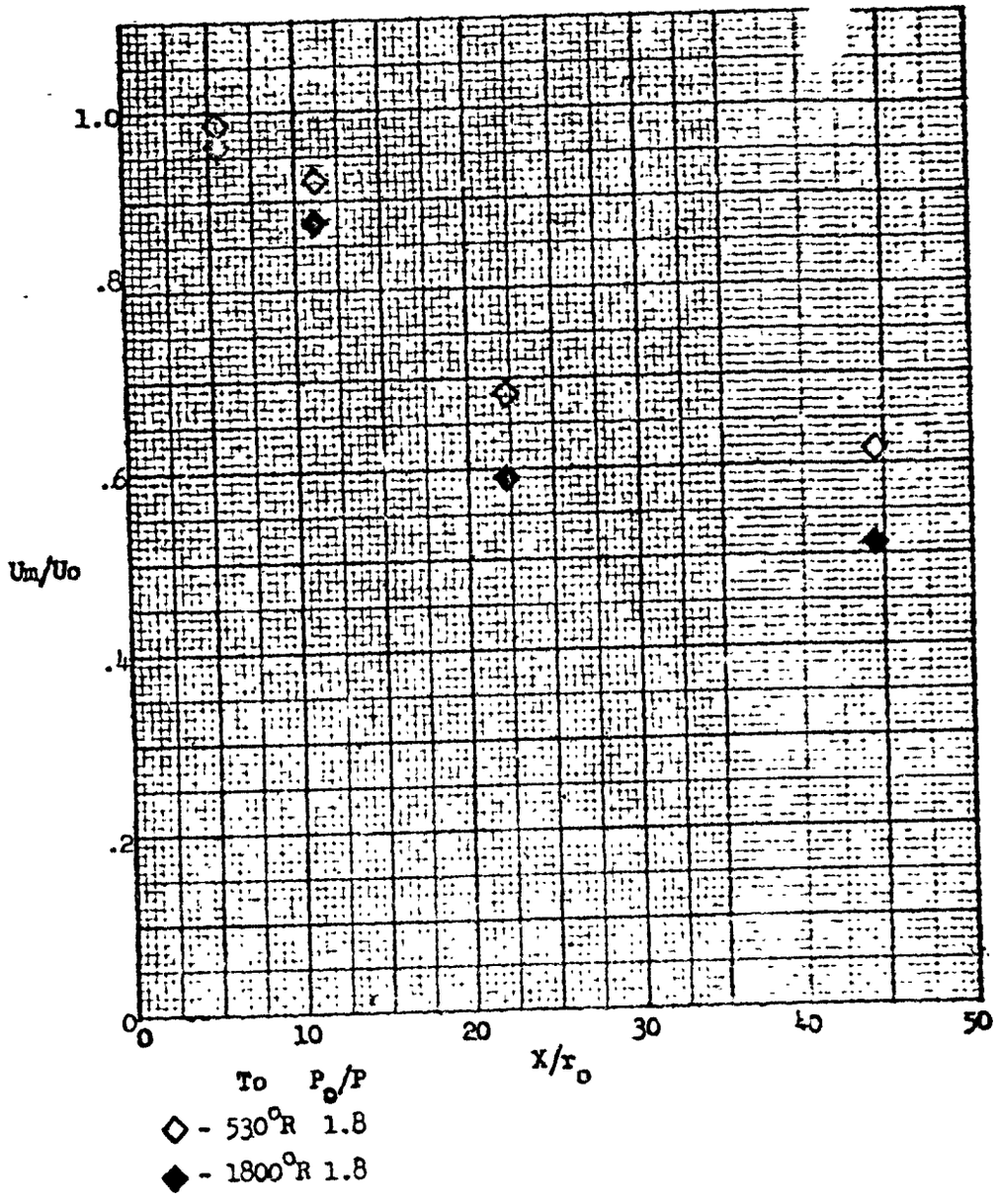

Figure 1.17e- Maximum Velocity Decay in Axial Direction.

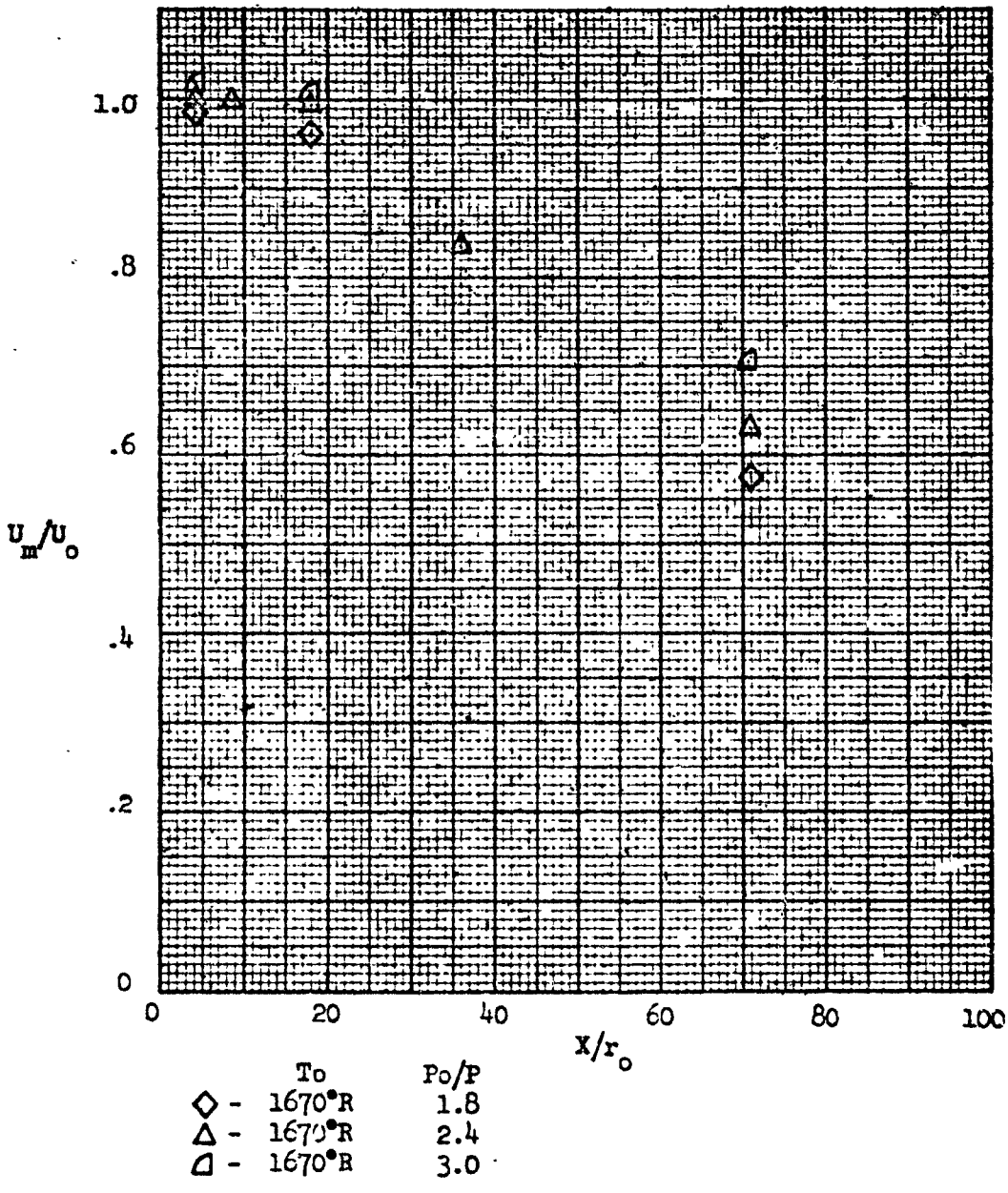

19 Tube Nozzle

Figure 1.17f - Maximum Velocity Decay in Axial Direction.

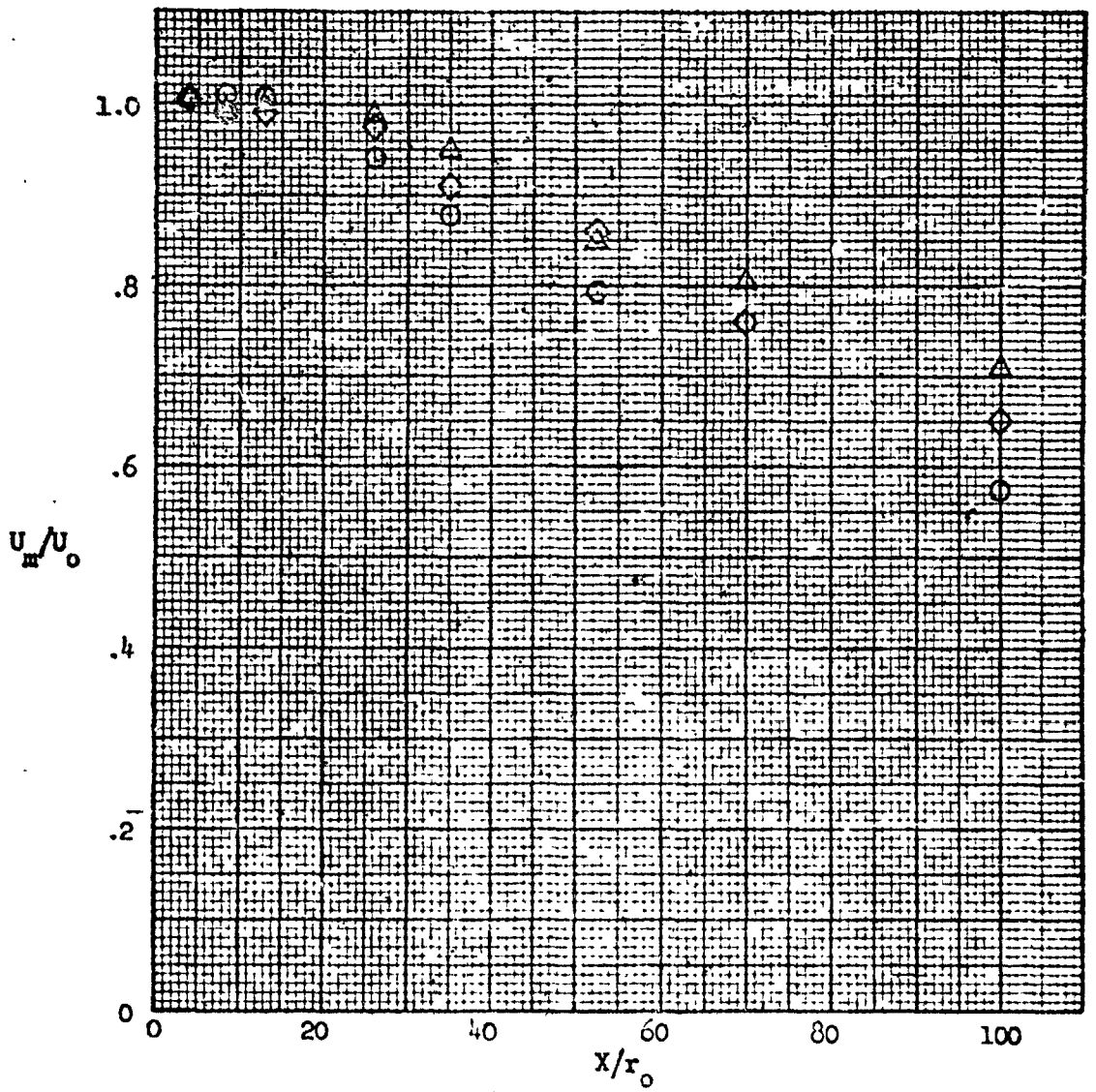

19 Tube Nozzle

Figure 1.17g- Maximum Velocity Decay in Axial Direction.

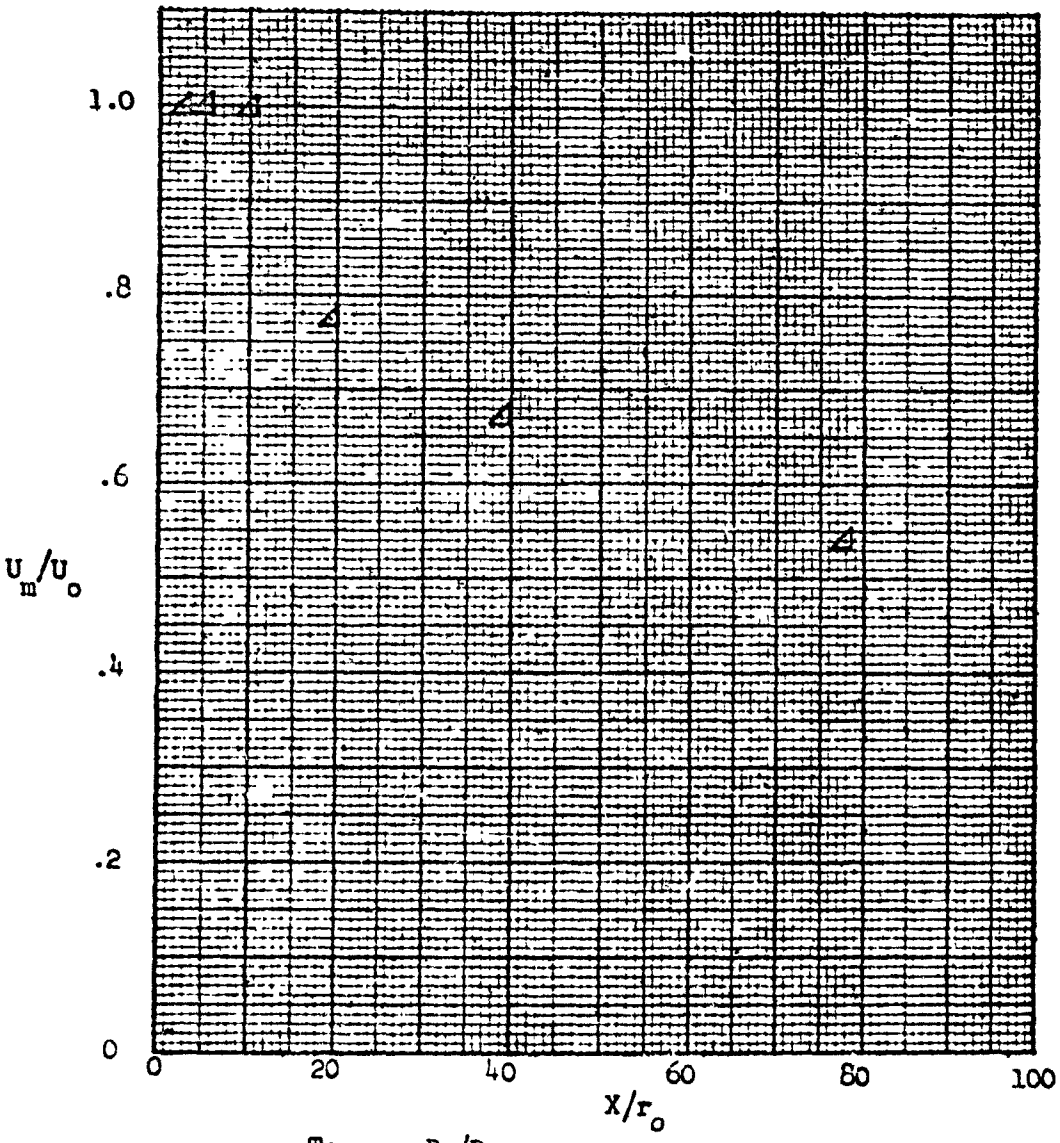

18 Segment Nozzle

Figure 1.17h - Maximum Velocity Decay in Axial Direction.

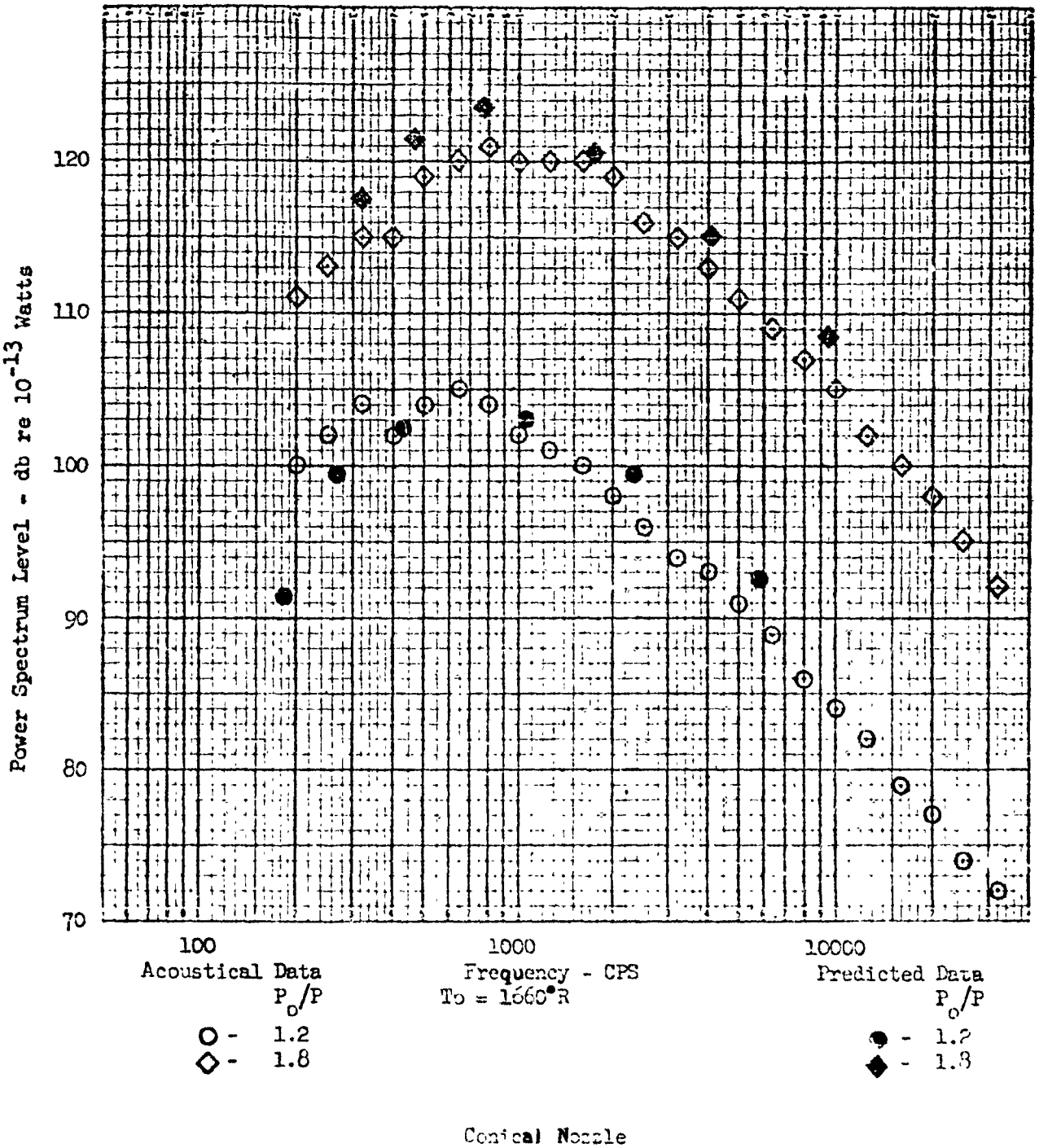

Figure 1.18a - Comparison of Predicted and Measured Sound Power Spectra.

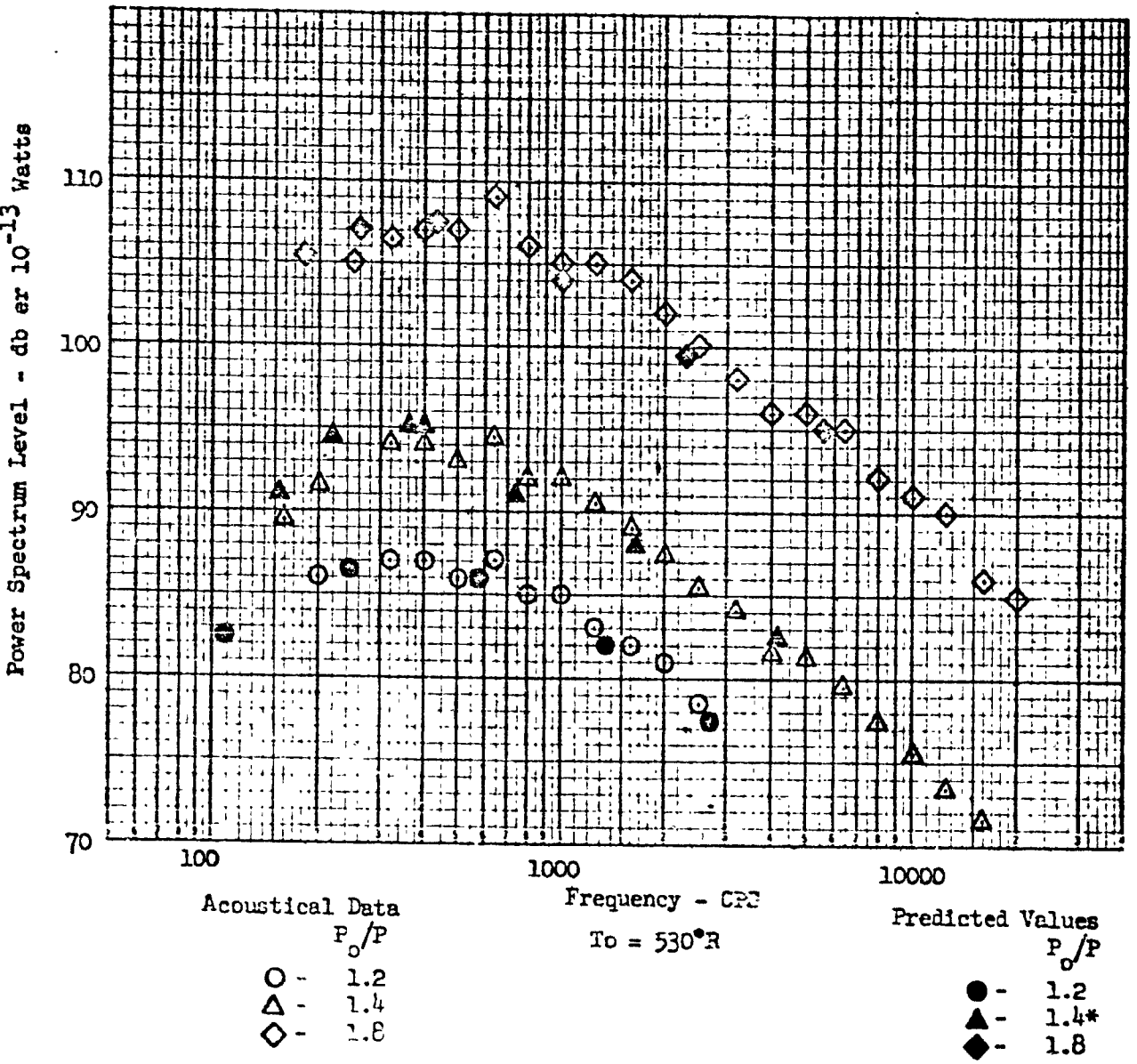

* Predicted Values Calculated from Velocity Profiles from Reference 3.

Conical Nozzle

Figure 1.18b - Comparison of Predicted and Measured Sound Power Spectra.

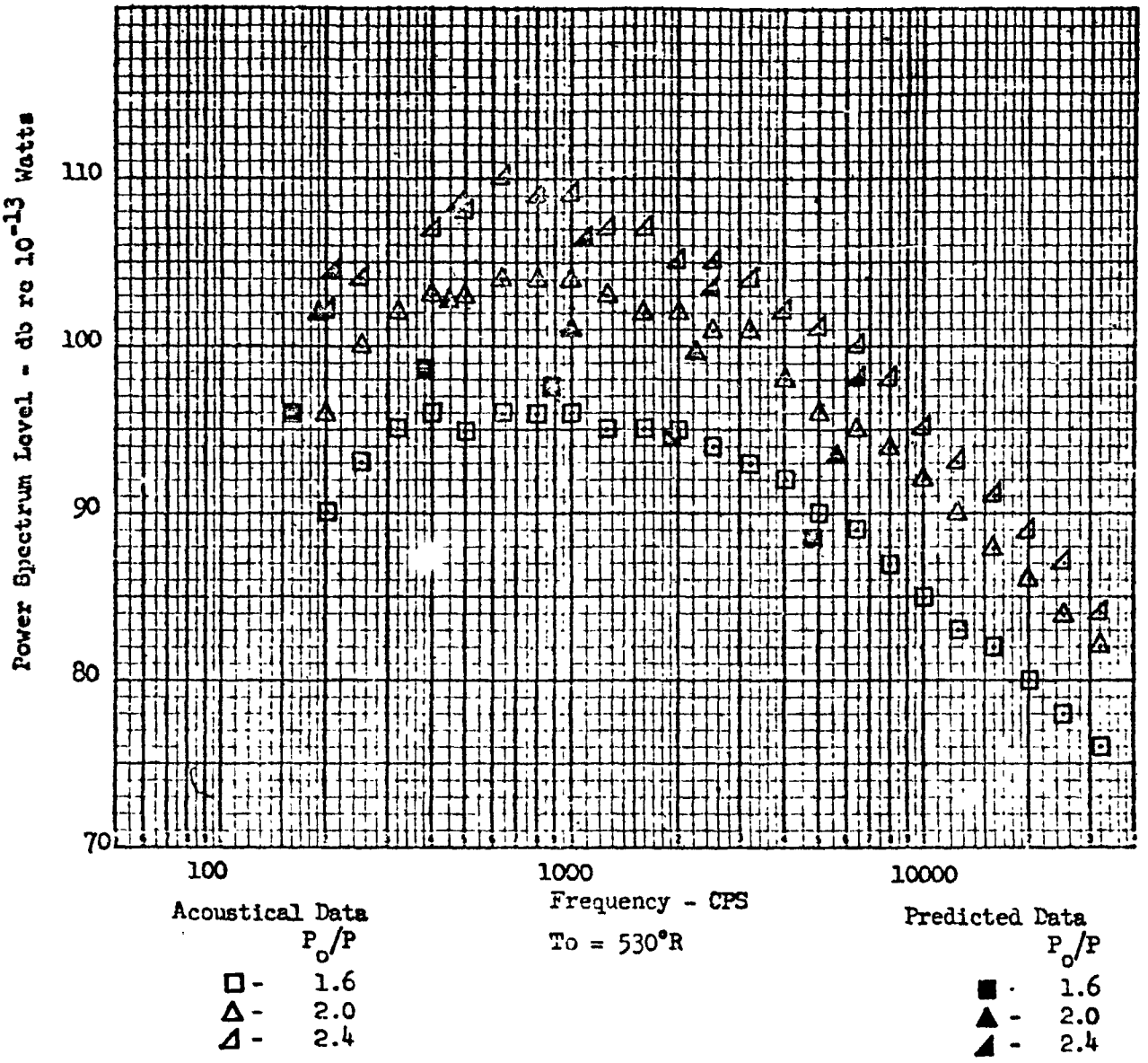

Plug Nozzle

Figure 1.19 - Comparison of Predicted and Measured Sound Power Spectra.

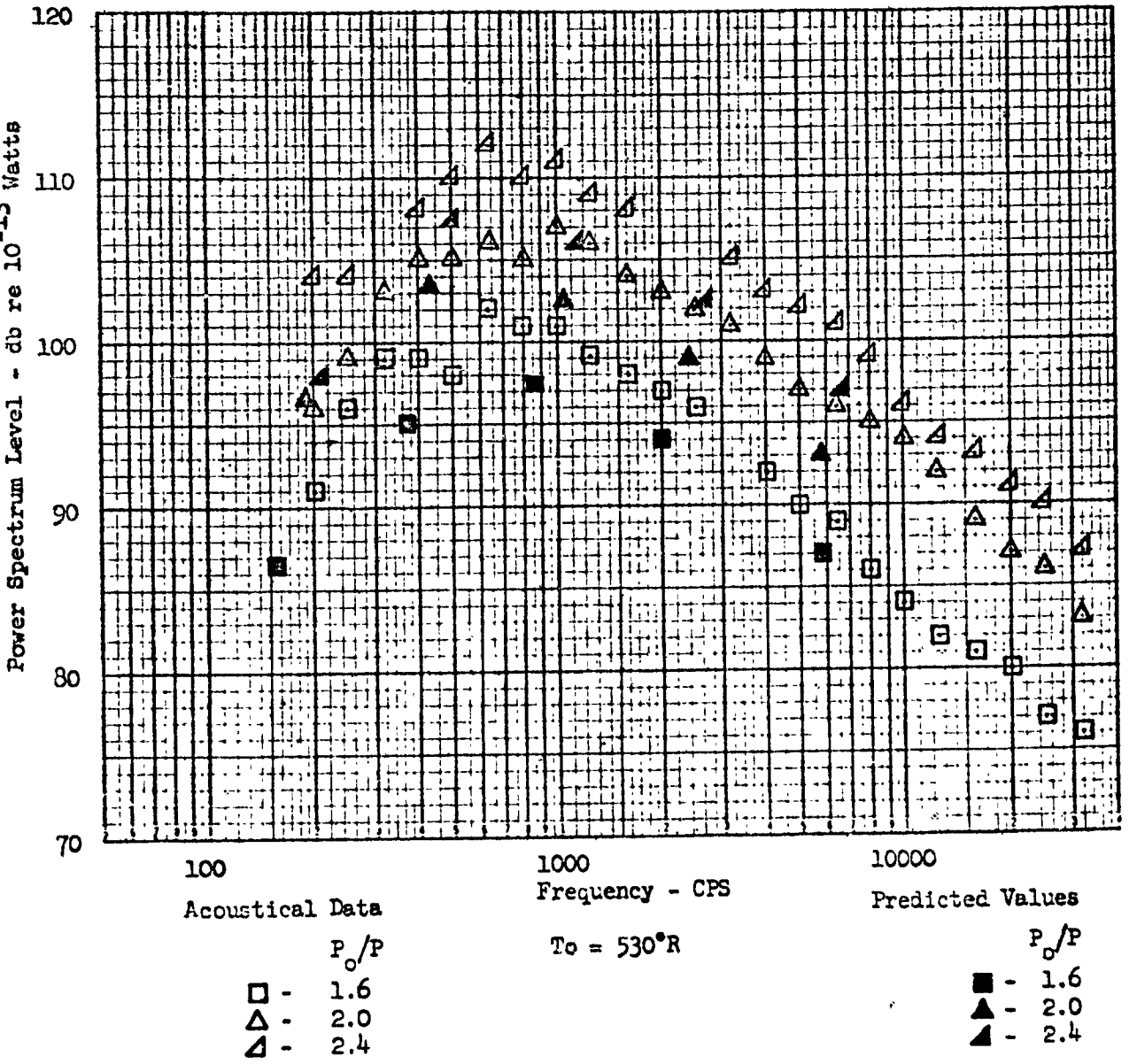

Plug Nozzle with Shroud

Figure 1.20 - Comparison of Predicted and Measured Sound Power Spectra.

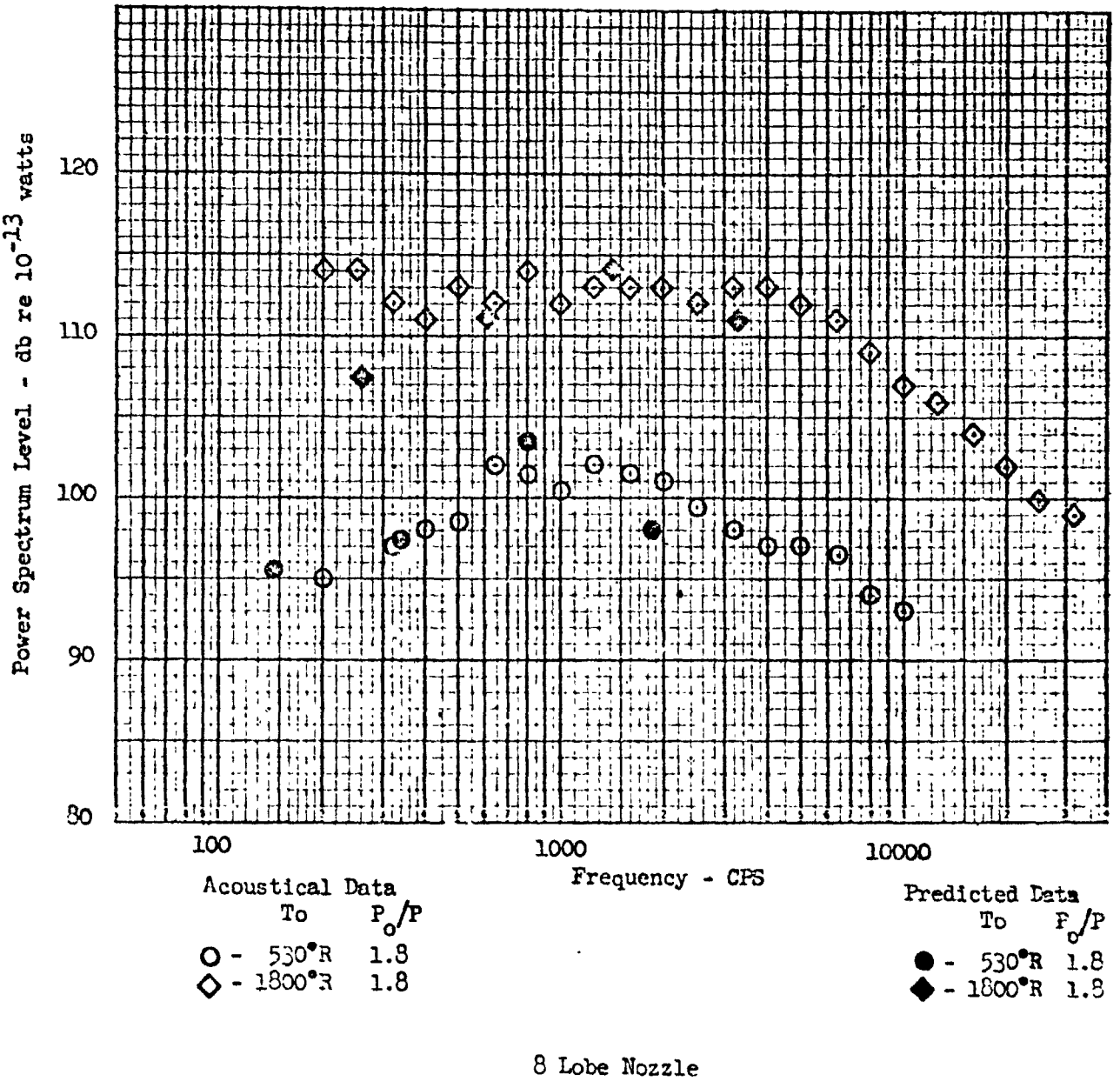

Figure 1.21 - Comparison of Predicted and Measured Sound Power Spectra.

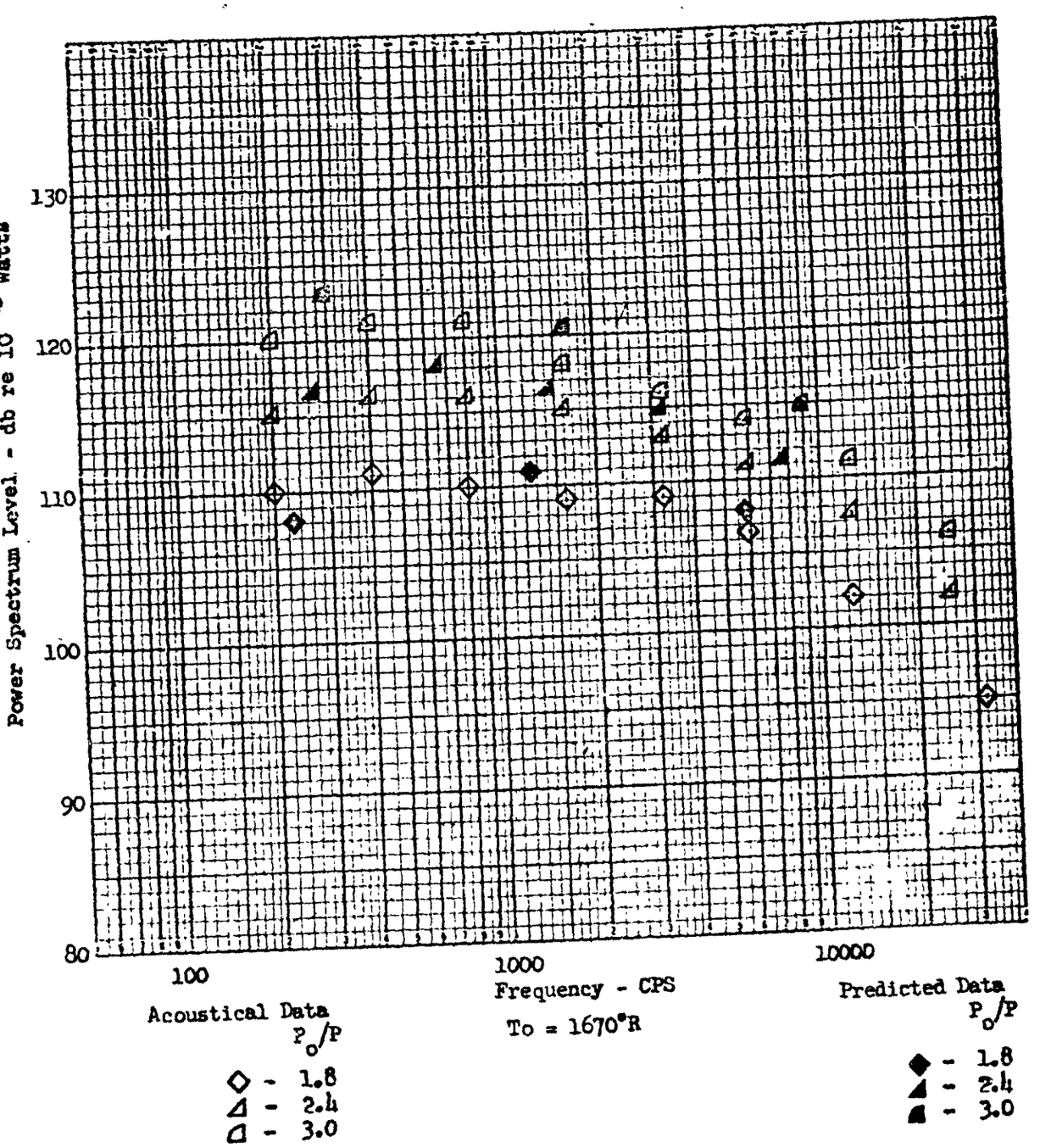

Figure 1.22a - Comparison of Predicted and Measured Sound Power Spectra.

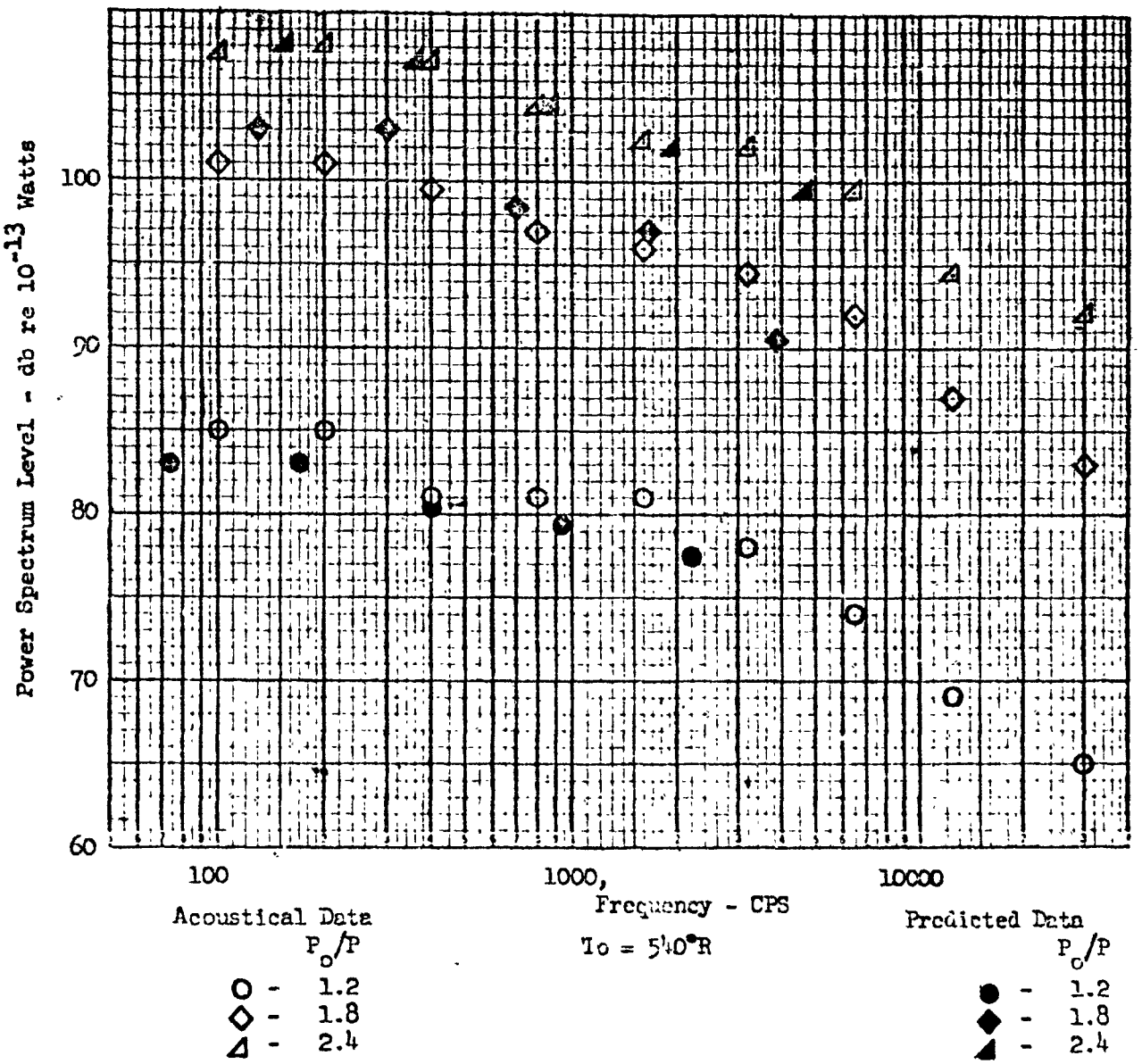

Figure 1.22b - Comparison of Predicted and Measured Sound Power Spectra.

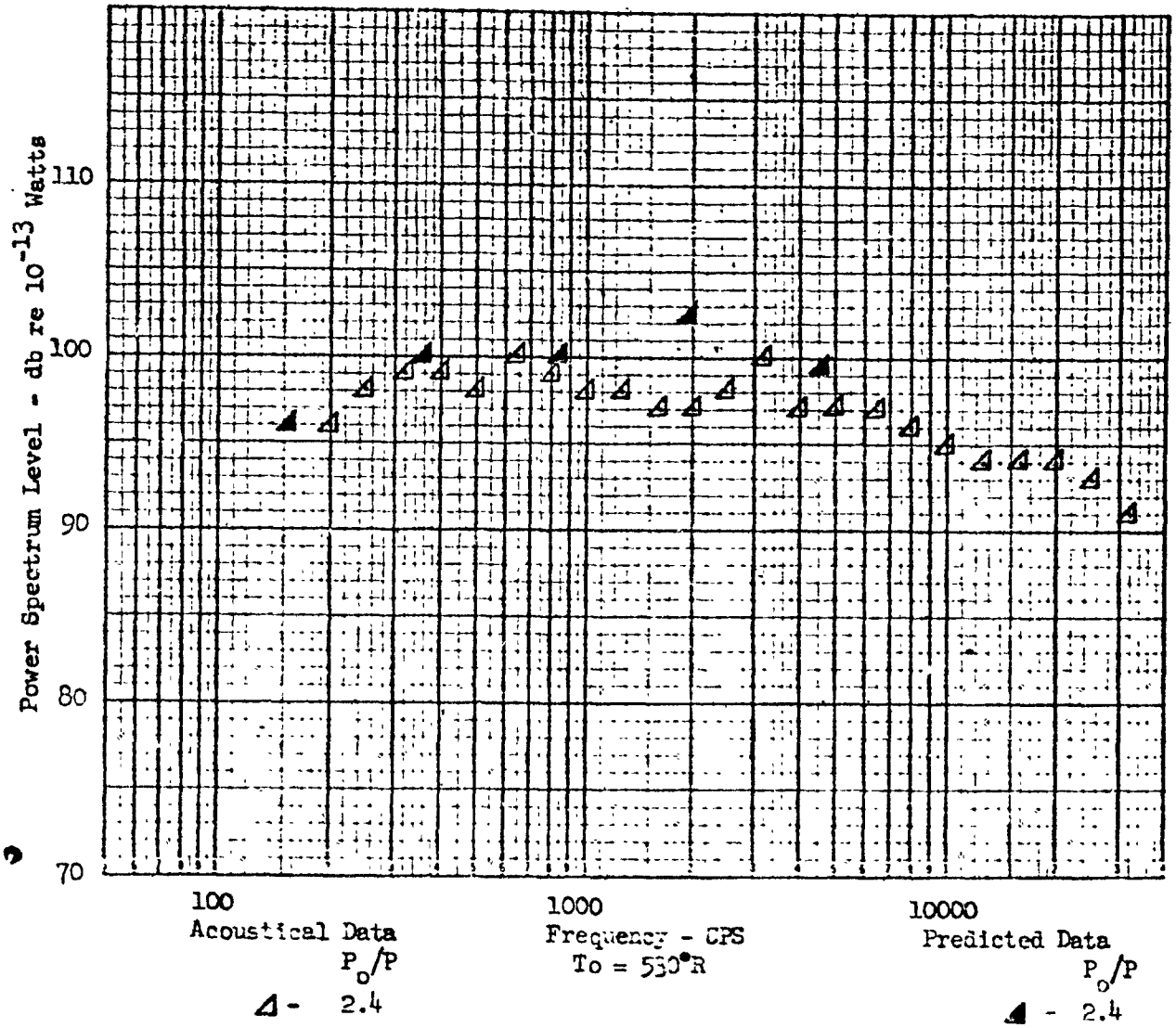

18 Segment Nozzle

Figure 1.23 - Comparison of Predicted and Measured Sound Power Spectra.

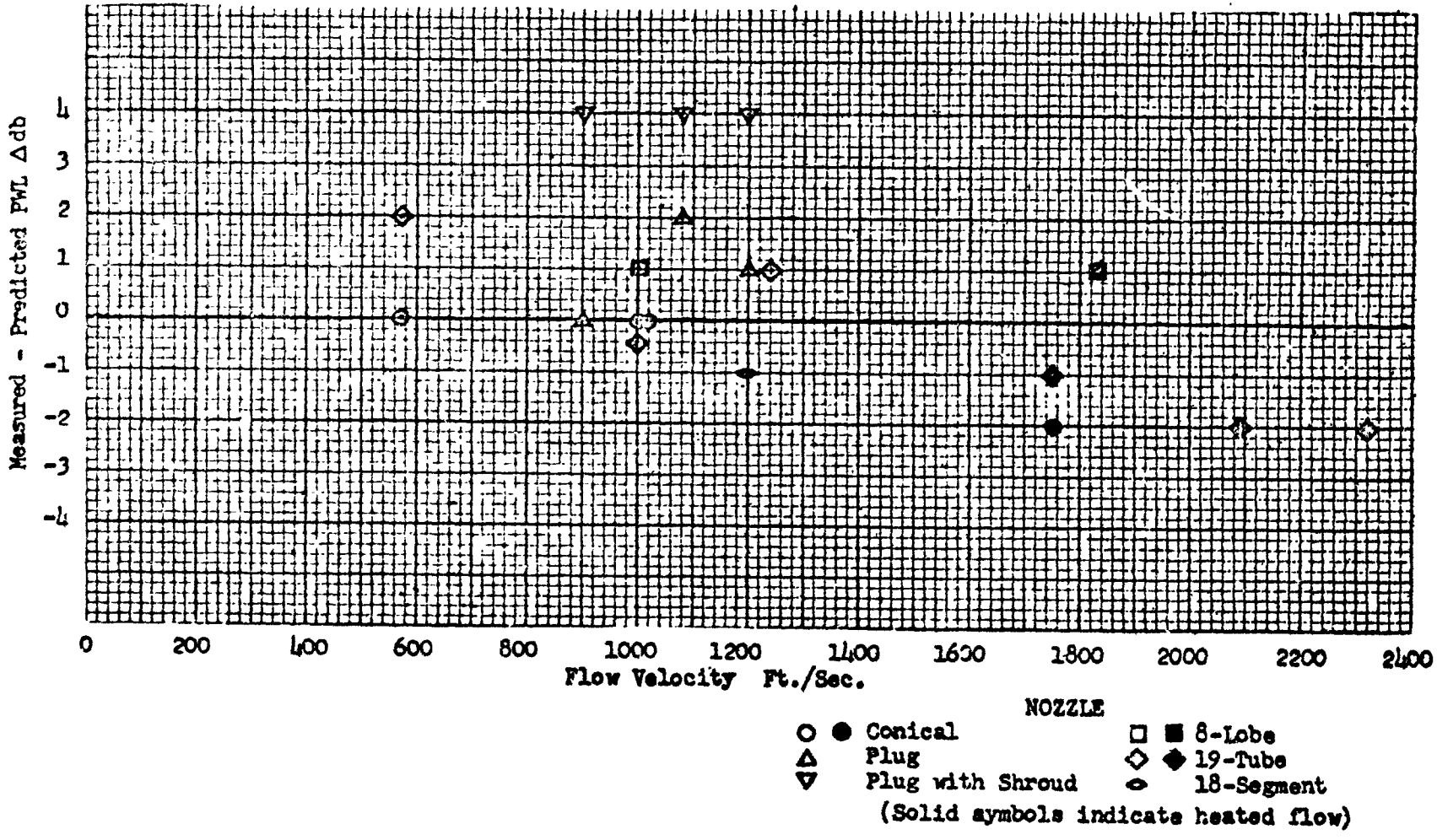

Figure 1.24 Comparison of Measured and Predicted Total Acoustic Power Levels.

2.0 ANALYTICAL STUDY ON THE PREDICTION OF AERODYANMIC PROPERTIES OF FREE JET FLOWS

2.1 Introduction

In the preceding section of this report, as well as in Reference 1, the unique relationship between aerodynamic noise generation and jet flow field properties has been demonstrated. Thus, from knowledge of the flow field the jet noise sound power spectrum can be determined by analytical means. In order to relate jet noise to nozzle geometric parameters by the previously developed acoustical theory, a means is first required for prediction of the flow field.

The subject of free jet mixing and resultant noise generation has been the object of extensive experimental and analytical research for a number of years. In the field of free jets, the most complicated practical problem is found in the analysis of the free jet flow emanating from sound suppressor configurations. It has been found through research that good sound suppression performance requires a significant amount of geometric complexity. The analysis of the complicated jet flows produced by such configurations must depend heavily upon a very simple theory to be at all manageable. Such a theory is the approach suggested and used by Reichardt, and is the one the authors have demonstrated to be of practical usefulness to the analysis of the flow fields from jet suppressors.

In this study the development of analytical techniques for jet flow field prediction is undertaken in order to provide a working tool for suppressor research. The theory is applied to the problem of predicting aerodynamic properties of jet flows from suppressor nozzles through the use of a computer program. This section presents the analysis and computer programs that have

been developed around these theories toward the goal of analytically predicting the jet flow fields for complex nozzle geometries, from which the jet acoustical properties can be determined using existing techniques.

2.2 Theoretical Analysis and Computer Program Development

The analytical theory and method presented in this report are extensions of the theory and method originally developed in Reference 1. The original work produced satisfactory results in the prediction of the flow field and noise produced by elemental jet types (i.e., jets from circular and rectangular exits). That work was culminated by a computer program which provided the means for evaluating the theory for complicated jet flows. It is in the prediction of complicated jet flows (such as from the nozzle geometry shown in Figure 2.1 that the original work has been found to be marginally satisfactory. Predicted and experimentally determined profiles for the nozzle shown in Figure 2.1 are compared at a number of flow cross sections in Figure 2.2. It is the task of the study reported here to improve the original work in order that deficiencies can be removed.

2.2.1 Theoretical Analysis of the Jet Flow Field

This section of the report presents the analysis of an arbitrary jet flow field in which the solutions for velocity, shear stress, and other properties of the jet flow are considered for the most general case. The formal and detailed derivation of the equations, which supports the broad treatment given the analysis in this section, are presented in Section 2.6.

The principle problem area of this study has been the description of the manner in which jets that have different properties (i.e., velocity,

density, etc.) intermix. More specifically, the problem has been the proper analytical formulation for the rate of jet spreading (or mixing) under conditions of relative flow. Once the mixing process is accurately described, the determination of such properties as velocity, shear stress, and density is easily accomplished.

The original treatment of the jet flow problem (Ref. 1) used the Reichardt hypothesis which states that the spreading property of free jet mixing is dependent only on the downstream distance (i.e., the x-coordinate). This hypothesis was used in the Reference 1 analysis even for complicated flows such as those emanating from sound suppressors. There is an extensive body of literature in existence, some of which is referenced in this report, which supports the theory that relative velocities determine the rate at which mixing regions spread. Physically, one may think of the mixing region as one composed of large eddies (of size comparable to the mixing region itself) which cause the transport of momentum, energy, and concentration. The size of these eddies is a function of the shear forces forming it and the time per unit distance available for their formation (convective effect). The first effect is often described by an expression involving the jet Mach number such as the one below:

$$\frac{dx}{db_m} = C_{b1} \left(1 + C_{b2} M_c\right) \tag{1a}$$

This expression shows that, the higher the jet Mach number, the smaller the eddy size at a given station (Refs. 57 and 58).

Research at Stanford has shown that the velocity profiles for simple relative jet flows can be predicted by using a simple empirical

differential equation relating the growth rate to the relative velocity difference (Ref. 2). In this research activity, it has been found that the relative or convective velocity effect on mixing is well approximated by the equation given below:

$$\frac{dx}{db_m} \sim \frac{U_1 + U_2}{U_1 - U_2} \tag{1b}$$

During the time when the work of this report was in progress, no information was available as to the manner in which these two effects were interrelated. As a consequence, for the purposes of this study, the two effects were geometrically superimposed to give the following equation:

$$\frac{dx}{db_m} = C_{b1} \left(1 + C_{b2} M_c\right) \frac{(U_1 + U_2)}{(U_1 - U_2)} \tag{2}$$

Previous researchers have also found this relative velocity effect. In particular, Willis and Glassman (Ref. 3) found a strong relative velocity effect; however, they were not able to derive an empirical equation describing the effects they found. Similarly, Marshall and Bailey, and Weinstein (Refs. 4 and 5) report a relative velocity effect on the spread of the mixing region but again do not develop equations describing this effect. Kendall (Ref. 1) found that the centerline velocity distribution, using the Reichardt method, was well described using the rate of spread given by Equation (1) for the case of zero external flow velocity.

Section 2.2.3 gives the results of this analysis using the linearly superimposed solution (Eq. (2)) in a comparison of theory and data.

For simple jets, the relative flow velocity (or density) effect produces no difficulty so far as the theory of Reichardt is concerned. It is only when more than two simultaneous flows are concerned (such as might occur in a triple annulus of three different flows or in multi-element jet exit shapes) that difficulty with the Reichardt method is found. Before delving into a detailed discussion of this difficulty, it is perhaps well to give an example showing the practical significance of the problem. The most obvious example occurs in the superimposition technique for nozzle suppressors that is used in the Reichardt method itself. Consider the suppressor element shown in the sketch below surrounded in part by induced flow resulting from the mixing action of the jet:

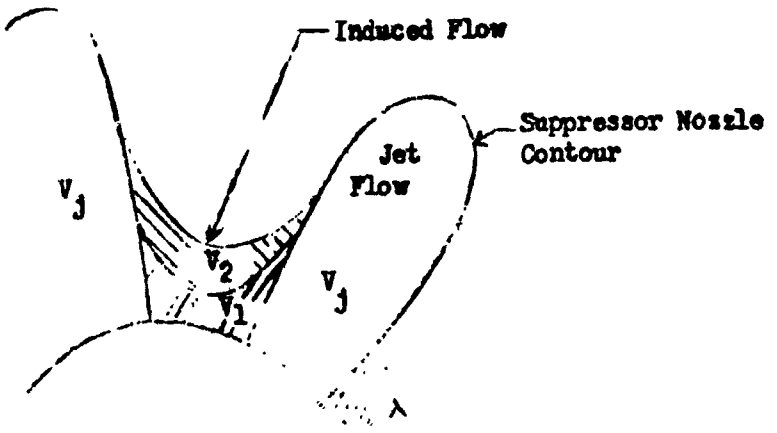

Sketch (a). - Suppressor Flow Approximation.

In the approximation technique used with the present theory (to be explained in subsequent sections), the induced flow is conveniently broken up into arbitrary fictitious jet flows, each having a unique velocity and other properties. The relative velocity results suggest that all three flows (V_j, V_1, V_2) spread at different rates as they contact one another.

In the multitube type of suppressor, a similar situation arises as the mixing regions of each of the individual tubes interact. Since the interaction is not uniform, the convective velocity and hence the rate of mixing vary in all dimensions.

Another example is a multi-element suppressor having both primary jet flow and a sound suppressing low-energy secondary flow, all embedded in a finite external flow field. Such cases as these cause difficulty in the Reichardt method which in all other respects has proven to be extremely successful in dealing with the complicated flow fields fround in suppressor nozzle configurations.

In his study of jet flows, Reichardt found that the simplified constant pressure axial momentum equation for turbulent flow

$$\frac{\partial \overline{\rho u}^2}{\partial x} + \frac{1}{r}\frac{\partial}{\partial r}\left(r\,\overline{\rho uv}\right) = 0 \tag{3a}$$

could be satisfied by an elemental exponential equation (as ascertained from analyzing experimental data of conical free jet mixing).

$$\overline{\rho u}^2 \sim \frac{1}{b_m^2}\, e^{-r^2/b_m^2} \tag{3b}$$

if certain arbitrary conditions were satisfied, specifically,

$$\overline{\rho uv} = -\frac{b_m}{2}\frac{db_m}{dx}\frac{\partial \overline{\rho u}^2}{\partial r} \tag{3c}$$

In this elemental relation, there appears the variable b_m upon which the rate of spread of the mixing region depends. It can be shown that the differential

equation for axial momentum (Eq. (3a)) is satisfied by Equation (3b) if, and only if, the parameter b_m is solely dependent upon the x-coordinate. Here the variable b_m is the same as that appearing in Equations (1a), (1b), and (2). That the variation of b_m in the other coordinate planes does lead to fallacious results can be readily shown as illustrated below:

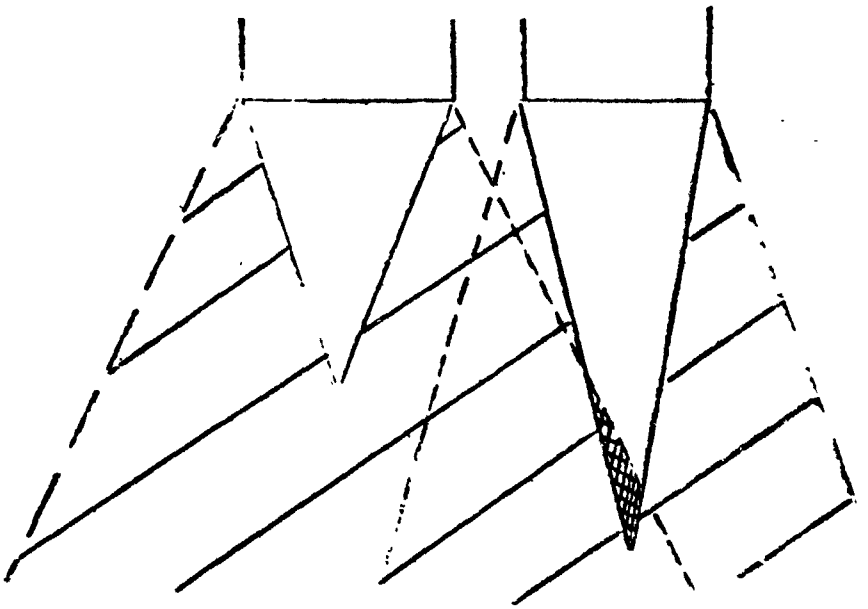

Sketch (b).- Y dependent b_m conflict.

Consider the intermixing of two, two-dimensional jets, each spreading at a different rate (Sketch (b)). According to the superposition theory, which results from the linearization of the differential Equation (3a), the momentum in the mixing region, shown cross-hatched, is given by the sum of the momentum of the individual jets (which spread according to Equation (3b). In the potential core of the jet undergoing the least spread, there is found momentum flux from the other jet which is spreading faster. This region is shown by the double cross-hatching in Sketch (b). Thus it is found in this particular region that the momentum flux is the sum of the momentum flux of the potential core of

the first jet plus the momentum flux spread from the second jet - and this sum is greater than the momentum flux from the first jet alone. Such a result yields velocities in the potential core of the first jet (i.e., the jet that is spreading the least) which are greater than those found at the exit plane, a result contrary to physical reality. This discrepancy represents a limiting condition of prediction for jets having significant core interference.

The method used is an implicit solution for the x-coordinate using the spreading parameter b_m as a dummy-dependent variable as suggested in the original work by Kendall in Reference 1. In this technique, the properties of the jet are determined for various b_m planes, and the x-coordinate, which is now spacially dependent in the b_m planes, is determined using Equation (2) above. In the b_m planes, the momentum and energy equations are uniquely satisfied, and the contradiction demonstrated in Sketch (b) (which cannot occur in the b_m planes) is necessarily avoided but the continuity of the x-plane is not guaranteed. Even if the x-plane is continuous, the satisfaction of momentum and energy conservation principles in a plane of constant x is not necessarily guaranteed.

This particular problem area is a subtle one and perhaps not too important to the general class of free jet flows; and yet it is of utmost importance to the successful analysis of the acoustic suppression phenomena found in suppressor nozzles.

A closely related subject to the foregoing is the relative rate of spread of momentum and energy. Experiments of previous years led to the well-known result that energy spreads faster than momentum in free jet turbulent

mixing. The turbulent Prandtl number which relates the momentum transport to energy transport is commonly given the value of 0.7 to describe this phenomenon. The rate of spread of energy can be analytically specified in a manner quite analogous to the spread of momentum. Reference 15 shows that the Reichardt technique linearizes the energy and concentration equations in the same manner as the momentum equation. The analysis of concentration spreading, in this study is limited to concentration spreading at the same rate as energy (i.e., turbulent Lewis number of unity). There is a spreading parameter b_h associated with the energy spreading as there is a b_m in momentum spreading. In this study, the analysis was extended to relate b_h to b_m through Prandtl number. This was accomplished using the definition of Prandtl number and the equations for shear stress, etc., that are derived from the Reichardt method. Several approximations regarding shear stress derivatives must be made to achieve the stated result which has a simplicity in keeping with the state-of-the-art in spreading property knowledge. The approximate derivation is presented in Section 2.6.1 of this report, and the result is shown to be that the spreading parameters are related by the square root of Prandtl number:

$$\frac{b_m}{b_h} \simeq \sqrt{Pr} \tag{4}$$

This result has been programmed into the computer solutions contained in the report.

The solution for the properties of the jet flow downstream of the exit plane has been extended in generality from what was developed in Reference 1. The basic technique involved is the summation of momentum, energy,

and concentration flux using the same integral form as that developed in Reference 1. Only the general method of development will be presented here as the details of the derivation are presented in Section 2.6.2.

Using the superposition technique, the momentum, energy, and concentration flux at any point in space downstream of a jet exit contour(s) can be written as integrals having the form shown below in Equations (5), (6), and (7):

$$M_f = \frac{1}{2\pi} \sum_{\text{contours}} (\overline{\rho u^2})_e \int_\theta (1 - e^{-r^2/b_m^2}) \, d\theta \tag{5}$$

$$H = \frac{1}{2\pi} \sum_{\text{contours}} (\overline{\rho u h_r})_e \int_\theta (1 - e^{-r^2/b_h^2}) \, d\theta \tag{6}$$

$$K_i = \frac{1}{2\pi} \sum_{\text{contours}} (\overline{\rho u \zeta_i})_e \int_\theta (1 - e^{-r^2/b_h^2}) \, d\theta \tag{7}$$

By means of the energy equation, the velocity can be expressed in terms of these quantities as shown in Section 2.6.2. The resulting expression for velocity is a quadratic in which only the positive root has significance. The equation is given below.

$$\frac{}{u} = \frac{H}{2\mathcal{E}} + \left(\frac{H^2}{4\mathcal{E}^2} + \frac{M_f \, c_{p_o} \, T_o^o}{\mathcal{E}} \right)^{1/2} \tag{8a}$$

where

$$\mathcal{E} = \frac{M_f}{2} + \frac{c_{p_m} \, p}{R_g} \tag{8b}$$

Once the velocity is known, the other properties of the jet such as temperature, density, enthalpy, etc., can be immediately obtained. The solution for the velocity and other jet properties has been generalized to the point of handling n number of different gases, each having its own molecular weight and specific heat relationship. This means that the solution is applicable to the study of hot turbojet exhausts in the analysis of sound suppressors. The only restriction that is made on the thermodynamics of the solution is that the jet flows at the exit be chemically frozen.

In Reference 1, it was found necessary to include two-dimensional effects in the equation for shear stress in order to obtain analytical results comparable with experimentation. At that time, the amended shear-stress equations were not included in the computer solution. This condition has been rectified and the equation for shear stress, in the course of this inclusion, has been refined. The exact derivation of the shear-stress equations stated below is given in Section 2.6.3. For the radial shear:

$$\tau_r = \sum_{\text{contours}} \frac{\overline{(\rho u^2)}_e}{\pi} \frac{db_m}{dx} \int \cos\theta \left[\sqrt{\pi}\,\mathrm{erf}\,(r/b_m) - \frac{\sqrt{\pi}}{2}\,\mathrm{erf}\left(\frac{r}{b_m\sqrt{2}}\right) - \frac{r}{b_m} e^{-(r/b_m)^2} \right] d\theta \qquad (9)$$

and a similar relation for the circumferential shear stress with sin θ replacing cos θ. The total shear at any flow-field point is given simply by the square root of the sum of the two component shears squared. A brief discussion of the results and comparison with the test data is given in Section 2.3. It is pertinent to note here that the computer programs can be used as research tools

in this area as well as in the spreading coefficient problem previously mentioned. Here the effect of density on shear stress can be analyzed and the correctness of the present formulation for shear stress determined.

2.2.2 Analysis of Jet Flow Acoustical Properties

In this section, extensions to the acoustic theory presented in Reference 1 are considered. The refinement of the formulation for the generation of aerodynamic sound power proceeds from the point in Reference 1 where equation (A.36) is presented. The more involved derivations are presented in Section 2.6 of this report.

In the present work, more dependence is placed on the Reynolds shear stress parameter. This is a favorable development in that a suppressor is likely to have a bigger effect on the variation of shear stress than on any other aerodynamic parameter in the jet flow. The development is given in Section 2.6.4 where the result is shown to be

$$\frac{d\,P_a}{d\,\ln f} = \frac{C_a\,U_c\,\alpha}{\left(\frac{d\,(\ln U_c)}{d\,(\ln x)} - 1\right)\rho_o a_o^5} \int_A (\tau^7\,\rho^{-3})^{1/2}\,dA \qquad (10)$$

The analyses of this report show that the maximum power is generated at the terminus of the potential core in agreement with results of the majority of experimental researchers in this field.

The largest deficiency of analytical techniques for the prediction of jet acoustic power is the inability to accurately predict the reduction in acoustic power which is experimentally found with the multiple-exit or

contoured exit nozzles. This acoustic attenuation has been found to depend on both geometric and aerodynamic properties of the jet flow. Tests have shown that sound reduction can be produced even with simple jets by placing two simple exits, such as rectangles, in proximity to each other.

As a backup method, in case the refined aerodynamic techniques described above do not suffice to give the proper attenuation, an attenuation mechanism and an analytical method have been established in this study. The most obvious mechanism is the well-established attenuation of sound energy through viscous dissipation and is the one used here. In the case of a jet flow, the attenuation is presumed to occur in the mixing region where the apparent turbulent viscosity is the greatest. Such a mechanism has intuitively satisfying characteristics which explain several of the experimentally observed effects. These are:

(a) Sound suppressors which seem to work best are those having inner jet flows (e.g., the multi-tube suppressor). By the above notion, the sound energy produced by the inner jets is absorbed by the mixing regions surrounding these jets.

(b) As the jet velocity increases, more of the acoustic energy is passed through the mixing region by refraction. This plus the greater turbulent viscosity produces increased attentuation with increasing Mach number.

(c) Attentuation of sound energy produced by suppressors is known to be frequency dependent. The formulation that is

developed in this study is found to have frequency entering to the second power.

However, the theory of the viscous damping mechanism suffers in two areas. The first and most important is that the phenomenon is not in agreement with experimental evidence. Secondly, the mechanism does not lend itself to mathematical formulation since an exact analysis would detail the history of the wave front from each equivalent source in three-dimensional space. Because of the first deficiency, such an exact solution is not justified.

The development of the attenuation phenomenon presented herein is based on the Kirchhoff equation for plane waves (Ref. 6). In the Kirchhoff development used in this report, the viscous coefficient is replaced by the eddy viscosity, and the eddy Prandtl number is substituted into the equation. Further, a measure of the length over which the attenuation takes place is estimated using the mixing region width parameter, b_m. To account for the fact that more of the attenuation would seem to occur in the innermost portions of the jet (a logical consequence of the theory), a porosity factor is applied to the attenuation; this porosity factor relates the attenuation of each source in the acoustic integration to its location within the jet flow purely on a geometric basis. The developments of this theory and the equations below are given in Section 2.6.4. These equations are

(a) The attenuation formula is:

$$\alpha = e^{-\alpha_k X_e} \qquad \text{(11a)}$$

where

$$\alpha_k \sim \frac{\overline{\eta}_e f^2}{\rho_o a_o^3} \left(\frac{4}{3} + \frac{\gamma - 1}{Pr} \right) \tag{11b}$$

(b) The mean length:

$$X_e = C_x b_m E_f M_c \tag{12}$$

(c) The porosity:

$$E_f = \frac{R' A_n}{R_c A_c} \tag{13}$$

The above set of Equations, (10) to (13), plus Equation (2), contain five arbitrary constants, the determination of which is discussed in Section 2.3. Some preliminary results obtained using these formulas in the circular exit solution program are given in Section 2.3 of this report.

2.2.3 Computer Program

The equations of the foregoing section, along with many subordinate equations, have been written into two separate programs in the process of the development of the solution. The need for two programs has a historic background which can be briefly outlined at this point. The formulation of the equations was performed early in the study contract and it was at that time obvious that the determination of the five arbitrary coefficients involved in the solution could be obtained only through a trial-and-error procedure using a computer solution. Rather than modify the original program at this point, it was decided to create a small program which would fulfill the following three goals:

(a) Provide an economical means for obtaining the values for the five arbitrary coefficients.

(b) Provide means for ascertaining the correctness of the relative velocity effect on sound attenuation.

(c) Provide program logic for insertion into the main program during its revision.

It became obvious, however, as the programming of the "simple program" commenced that the problem had become complicated to the point where even a simple circular exit solution required sophisticated and extensive programming, especially if it was to be used in the revised main program. When it became obvious, moreover, that the simple solution was too large for the 1620 computer, several of the first goals were compromised and reliance, instead, was placed upon the use of the final major program. The circular exit program, then, as it has turned out, has had the function of performing (a) and part of (b) noted above. It has yielded preliminary values for the five arbitrary coefficients, and major portions of the program are being used in the main program itself.

The simple circular exit program cannot be used for multiple-exit configurations, that is, double annuli, but it can be used to evaluate the acoustic attenuation observed when a secondary flow of large expanse (compared to that of the jet itself) surrounds the circular jet. This encompasses by far the majority of the experimental data available on jet flows including those data available on mixing and the spread of mixing regions in jets surrounded by finite external flow fields.

In the following sections, the philosophy of the two programs, some of the programming methods used, and the broad physical features of the programs will be discussed. In Section 2.6.5, a more detailed description of the programs is given.

Preliminary Computer Program

The solution technique of the simple circular-exit program is, in general, parallel to that of the main program, and for this reason it will be discussed only briefly. In the simple circular-exit program, the inverse procedure is used wherein the solution is first performed for various b_m planes and then x is explicitly calculated using Equation (2). This technique offers the advantage that the flux integrations (which are b_m dependent) need be performed but once for any exit configuration (in this case the exit radius); then the results of these integrations are used for all subsequent running of that exit configuration. Such a technique offers a factor of four saving in computer time compared to doing the integrations each time the program is run. In the main program a similar technique is used. The velocity is obtained through an iteration procedure as it is in the main program, and the sound power calculation is performed explicitly after the x's (and therefore frequency) have been determined.

Main Computer Program

In this section is presented the philosophy underlying the computer programming of this project and an outline description of the program. This program combines the geometric generality of the previous computer program reported in Reference 1 with aerodynamic generality and sophistication established in this study. The aerodynamic generality stems from the fact that the

program can handle any number of gases having different compositions and heat capacities. At present, its only thermodynamic limitation is that the gas flows at the nozzle exit must be chemically frozen. Except for the "moderate compressibility limitation" on the development of the shear-stress equation, and the inherent thermodynamic limitations placed on the differential equation solution (i.e., the original simplified differential equation due to Reichardt), the program makes no restrictions as to the density, temperature, and the Mach number of the cases it can handle. Specifically, the program as it now stands should be capable of providing reasonably accurate solutions to actual turbojet suppressor problems. The only aerodynamic restriction that is placed on the solution is that the overpressure ratio of the jet at the exit plane be nearly unity. Actually, the program can be used in certain circumstances for the overpressure case and for providing approximate solutions to the ejector flow problem through clever input to the program. These techniques are discussed in Section 2.4.

The biggest stumbling block to the program development has been, as mentioned previously, the technique for the relative velocity effect. Another problem has been the development of a method for dividing the flow field so that the integrations in the sound-power calculation will have good accuracy. The program now integrates 200 points (approximately) in a typical quadrant of symmetry. For most suppressor configurations, this fineness is not sufficient to provide accurate sound-power integrations for frequencies higher than those found at the terminus of the elemental potential cores. For example, a typical multi-tube suppressor would require about an order-of-magnitude increase in the number of mesh points to obtain accurate acoustic integrations at the higher

frequencies. Such an increase is impossible to attain in the present program because of the memory storage limitations. It is thought, however, that the 200-point solution will provide sufficient accuracy to at least determine the maximum power output of these sound suppressors.

The program calculates flow properties and acoustic properties for a number of b_m planes, the number depending upon the length ratio and the acoustic bandwidth specified in the input. For example, if data are desired from the exit plane to a point downstream corresponding to $x/R_{c,e}$ of about 30 and the acoustic spectrum is to be in one-third octave bandwidths, then about 19 b_m planes (exponentially spaced) will be used. This technique will assure a high probability of calculating an acoustic point for each acoustic band.

The program makes a "pass" through the 200 points of each b_m plane three times. On the first pass, it calculates the flow-field velocity and other properties such as density, temperature, etc., places the velocity values into memory storage, and then puts it and other property values on the output tape. On the second pass (currently bypassed) the program interrogates the magnitude of the velocity of neighboring mesh points (surrounding the point in question) to determine whether or not to subdivide the existing mesh into much finer increments to provide a more accurate solution in a way which avoids the machine memory-capacity problem. The main mesh can be divided in one of three ways: a horizontal division by eight, a vertical division by eight, or a combined horizontal and vertical division by eight to provide 64 points within the existing mesh. The size of this inner mesh is increased as the program proceeds to calculate b_m planes further downstream. For example, at an $x/R_{c,e}$ of approximately eight, the program divides the major meshes into 16 points

instead of 64, the general idea being, of course, that the mixing regions at this point are so large that 16 points provide as much accuracy as 64 points provide near the exit plane. There is also a practical reason for this decrease in mesh size. As the program proceeds to b_m planes located further downstream, the number of meshes increases and would soon exceed the capacity of the 7094 memory. By increasing the mesh size, the mesh solutions can actually be nested in the machine logic. Figure 2.3 shows a b_m plane and some typical major mesh points having inner mesh divisions at several physical locations in the b_m plane, and shows how these inner meshes are nested to conserve memory storage.

On the third pass, the program interrogates the velocity points, which are stored in memory, within "the cone of influence" from the point in question. This cone of influence has a physical size approximately equal to twice the size of the typical mixing region at that point in space. Figure 2.4 shows the cone of influence interrogation on a figurative basis. The program determines the relative maximum and minimum of the velocity points in the b_m plane within the cone base circle and uses these relative maximum and minimum in a calculation of spreading properties of the jet flow and the acoustic properties. From these properties, a unique value of x and frequency is obtained for each of the major mesh points.

At each point, the sound power which is calculated is assigned a frequency index which is related to the frequency calculated at that point. This sound-power calculation (which at this time is in terms of energy) is added to all other energy calculations in the b_m plane in question having like frequency indices. These frequency indices have a bandwidth tolerance of one-tenth octave. At the termination of a b_m plane, the sound-power calculations

are ordered in decreasing levels of sound power and those sound-power sums having frequency indices within one-third of an octave of each other are added and the frequency of this sum is normalized. Figure 2.5 presents a basic flow chart for the program, outlining the discussion just presented. It in no way represents the entire logic of the program which is far more extensive. This flow chart is keyed to the program listing in the more complete discussion of the program in Section 2.6.5.

2.3 Discussion of Results

This section will discuss the results that have been achieved in this study program. Included in this discussion are the evaluation of the coefficients, comparison of theoretical velocity profiles with the data, comparison of theoretical shear stresses with data, and comparison of the theoretical sound-power production with data.

Evaluation of Constants

The analytical theory developed in this study involves five arbitrary constants which must be determined from the data existing in the literature. Two of these coefficients are in the equation which relates the rate of spread of the mixing region to the axial coordinate and the convective Mach number (Eq. (3)) and one of each are in the equations for sound-power generation, attenuation, and frequency. In the evaluation that has been conducted thus far, the constants have been found to be coupled so they cannot be determined independently, thus increasing the difficulty of obtaining values for the constants.

The constants for the rate of spread equation have been determined largely from the work of Lawrence (Ref. 7) following the work originally done in this area (Ref. 1). Kendall based the value of the coefficients in Equation (1) upon the spreading of the flux on the jet centerline where the cylindrical solution is completely analytic. In the present study, the velocity profiles for all space have been compared with the data of Lawrence and the best fit of the velocity profiles has yielded the coefficient value. It has been found that the coefficients are only slightly different from the values presented in Ref. (1). These values are:

$$C_{b1} = 13.5 \tag{14a}$$

$$C_{b2} = 1.5 \tag{14b}$$

The above constant values produced reasonably good predictions of the velocity profile data at all points in the flow field for the two cases that were run (refer to Section 2.3). The acoustic prediction at Mach 0.7 is extremely good concurrently. However, the acoustic prediction at Mach 1.05 was found to be 2db lower than the data (Fig. 2.6). This result is directly attributable to the reduction in mixing predicted by Equation (3) for the higher jet Mach number. With C_{b2} set equal to zero, the prediction of jet noise is seen to be much better.

The work done by researchers in the field of acoustics has generally supported the contention that the frequency of the sound produced at a given x location is proportional to the eddy velocity. On this basis, the value of the coefficient would be expected to have a value of 2.0. Using the

sound-power profiles such as Figure 4-11 in Reference 1 and the results of the circular solution, the value of the coefficient has been found to be

$$C_f \cong 4.5 \tag{15}$$

These same data have yielded values for the sound-power coefficient and the attenuation coefficient of

$$C_a = 1410 \tag{16}$$

$$C_x = 250 \tag{17}$$

If the analysis were precisely correct, these values for the coefficients would apply for all manner of configurations and conditions. However, since the analysis is at best approximate, it may be found in the course of running other configurations that minor changes in the value of these coefficients will yield better overall results.

Velocity Profiles

Figures 2.7(a) through 2.7(e) present the results of the theoretically predicted velocity profiles determined with the theory presented herein as compared with the data of Reference 7. It is seen that the theory indicates less spread of momentum flux at both high and low values of the axial distance. Since the theory conserves momentum, the shape of the velocity profile suggests that the data are in error since the data definitely do not satisfy the conservation of momentum condition at axial distances near the exit.

Shear Stress

The comparison of theoretical and experimental determination of the shear stress found in simple flows is made in Figure 2.8. It is seen that the theoretical prediction is in reasonable agreement with the data (in keeping with the prediction of Ref. 1).

Sound-Power Prediction

Figure 2.6 presents the acoustic predictions obtained with the theory and the values of the constants given previously. At Mach 0.7, the prediction is by all standards excellent. The premature dropoff in sound power at the low frequencies found previously has been eliminated. At Mach 1.0, the results have not been quite as satisfactory for reasons suggested before. Note that the difference between theory and data is quite uniform and that here again the theory seems to be predicting the correct profile and frequency shift.

2.4 Additional Approximations for Ejector, Overpressure, and Induced Flow

Ejector Approximation

Because of the problem encountered in the mixing rate difficulty discussed in Section 2.1, the extension of the analysis to encompass ejector (i.e., shrouded nozzle configurations) was not performed in this study. However, sufficient work was done to establish an approximate procedure that can be used with the existing program to determine the flow-handling characteristics of ejector-type sound suppressors. The method is approximate because the theory behind it assumes constant pressure mixing and because it uses a fictitious geometry surrounding the primary flow. This pseudo-geometry is shown in Figure 2.9, wherein a hexagonal outer nozzle surrounds the primary nozzle, the

hexagonal configuration replacing the actual circular ejector, (such a configuration is of little use in those sound suppressors utilizing an ejector surrounding a complicated exit configuration such as the petal suppressor shown in Sketch (a). The hexagonal configuration is necessary to deceive the program into generating reflected velocity profiles at the hexagonal boundaries which then approximate a shearless wall velocity profile. Such a solution for simple ejector geometries should produce qualitative flow-rate ratios for those ejector configurations in which the secondary shroud length is quite short.

Overpressure Approximation

The overpressure approximation that can be used is again restricted to simple configurations such as a multitube suppressor and/or to low overpressure ratios. The criterion is the degree of flow interaction and the attendant shock structure strength in the downstream flow field. Such shock structures obviously cannot be handled by the existing program. The approximation that can be made for these simplified cases is to increase the exit area to one corresponding to the exit Mach number based upon one-dimensional expansion of the exhaust gases to the ambient static pressure. The modified area coordinates are then substituted for the physical exit coordinates in the input to the program.

Induced-Flow Approximation

A possible cause of the suppression of jet noise found with complicated jet exit configurations is the inducement of a flow in the mixing regions. Such flow inducement theoretically reduces the shear stress and thereby the noise level. To duplicate this effect analytically, it is necessary to input to the computer program a fictitious exit shape, modifying the actual

suppressor exit shape. In the modified shape, estimated velocity values are used to produce the induced flow. Referring to Sketch (a), which is a partial view of a petal-type suppressor exit, the fictitious exit shape that is added is shown by the dashed lines and the approximate flow in this portion is shown by the cross hatching. Such a technique allows the computer to consider the added jet flow as the entrained flow. This technique remains to be verified using the new computer solution of this study.

2.5 Detailed Analyses and Computer Programs

2.5.1 Derivation of Prandtl Relation

The Prandtl number relates the transport of energy to the transport of momentum. By definition, the turbulent Prandtl number is given by the following equation:

$$Pr = \frac{c_p \eta_e}{k_e} \tag{18}$$

The definition of the eddy viscosity and heat-conduction coefficients in this equation are as follows:

$$\eta_e = - \frac{\tau}{\partial \bar{u}/\partial r} \tag{19}$$

$$k_e = - \frac{\overline{\rho c_p}\ \overline{v' h^{o}{}'}}{\partial \bar{h}^{o}/\partial r} \tag{20}$$

Now as shown in Section 2.5.3, the shear stress is given by

$$\tau = \left(\frac{b_m}{2}\right)\left(\frac{d\, b_m}{dx}\right)\left(\frac{\partial(\overline{\rho_u{}^2})}{\partial r}\right) \tag{21}$$

Substitution into Equation (19) yields

$$\eta_e = \frac{\frac{b_m}{2}\left(\frac{d\, b_m}{dx}\right)\left[\frac{\partial(\overline{\rho_u{}^2})}{\partial r}\right]}{\partial \bar{u}/\partial r} \tag{22}$$

To put the expression for k_e in a similar form, it is necessary to make the following approximation:

$$\overline{\rho v' h^o} \approx \overline{\rho v' h^o} \tag{23}$$

which will hold reasonably well for moderately incompressible mixing. By analogy to the linearization of momentum flux (which leads to (21), one can show that

$$\overline{\rho v' h^o} = -\frac{b_h}{2}\left(\frac{d\, b_h}{dx}\right)\left[\frac{\partial(\overline{\rho u h^o})}{\partial r}\right] \tag{24}$$

where the use of the enthalpy spreading parameter b_h can be noted. Substitution into (20) produces the following equation:

$$k_e = \frac{c_p \frac{b_h}{2}\left(\frac{d\, b_h}{dx}\right)\left[\frac{\partial(\rho u h^o)}{\partial x}\right]}{\frac{\partial \bar{h}^o}{\partial r}} \tag{25}$$

Substituting the relations for the transport of momentum and energy (22) and (25) into (18) yields the following equation:

$$Pr = \frac{b_m\left(\frac{d\, b_m}{dx}\right)\left[\frac{\partial(\overline{\rho u^2})}{\partial r}\right] \Big/ \left(\frac{\partial \bar{u}}{\partial r}\right)}{b_h \frac{d\, b_h}{dx}\left[\frac{\partial(\overline{\rho u h^o})}{\partial r}\right] \Big/ \left(\frac{\partial \bar{h}^o}{\partial r}\right)} \tag{26}$$

Equation (2) shows that db_m/dx is approximately constant, at least up to the end of the potential core. The presumption made here is that the b_h derivative will behave similarly. If such is the case, the derivative ratio is proportional to the ratio of the spreading parameters. With this approximation and further expanding the derivatives in (26) (neglecting radial gradients of density), the following result obtains:

$$Pr \simeq \frac{b_m^2}{b_h^2} \left(\frac{2\bar{u}}{\bar{u} + \bar{h}^\bullet \frac{\partial \bar{u}}{\partial \bar{h}^\bullet}} \right) \tag{27}$$

This expression relates the square of the spreading parameter ratio to the Prandtl number and another term containing derivatives of velocity and enthalpy. This latter term can be written in terms of logarithmic derivatives

$$\left(\frac{b_h}{b_m} \right)^2 = \frac{1}{Pr} \left[\frac{2}{1 + \frac{\partial(\ln \bar{u})}{\partial(\ln \bar{h}^\bullet)}} \right] \tag{28}$$

The approximation which is made at this juncture is that the logarithmic derivative ratio is approximately unity. This approximation leads to the final result that the spreading coefficients are related to the square root of the Prandtl number.

$$\frac{b_m}{b_h} \simeq \sqrt{Pr} \tag{29}$$

The validity of the above approximation would seem to be most open to question under isoenergetic mixing conditions where theoretically there is no gradient in stagnation enthalpy.

2.5.2 Derivation of Velocity and Related Expressions

At any point in the jet flow field the flux of momentum, energy, and gas concentration are known as a consequence of the theory used in this study (see Eqs. (5), (6), and (7)). These three flux quantities will be termed M_f, H, and K in the subsequent development. It can be shown that the mean of the product of the unsteady quantities in these flux functions, namely,

$$M_f = \overline{\rho u^2} \tag{30}$$

$$H = \overline{\rho u h_r} \tag{31}$$

$$K_i = \overline{\rho u k_i} \tag{32}$$

can be well approximated by the product of the means. The error is generally less than 10 percent. Reference 15 presents an exact treatment of this problem and it will not be considered further here. Also, the concentration expression commonly used for the mixing of two dissimilar gases is extended in this analysis to an indefinite number of gases without the benefit of a formal proof. Thus

$$k_o = 1 - \sum k_i \tag{33}$$

where k_o is the total concentration of ambient gases at a point and the sum represents the calculated total concentration of jet gases.

From the energy equation, using the Crocco relative enthalpy for boundary condition satisfaction, one obtains

$$h_r^o = h - h_o^o + \frac{u^2}{2} \tag{34}$$

Now using the concentration expression given above, the local specific heat for an arbitrary gas mixture is given by

$$c_p = c_{p_i} k_i + \left(1 - \sum k_i\right) c_{p_o} \tag{35}$$

As will be seen, it is convenient to define a mean specific heat in the derivation of the velocity expression such as

$$\overline{c_{p_m}} = \int_{T_1}^{T_2} c_p \, dt \Big/ (T_2 - T_1) \tag{36}$$

If the specific heat is related to temperature through a series expansion of the type

$$c_p = \lambda_1 + \lambda_2 T_2 \tag{37}$$

then by (35) there results

$$c_p = k_i \left(\lambda_{i,1} + \lambda_{i,2} T \right) + \left(1 - \sum k_i\right) c_{p_o} \tag{38}$$

and substitution into Equation (36) yields the following equation for the mean specific heat:

$$c_{p_m} = \frac{k_i \lambda_{i,1} (T_2 - T_1) + k_i \lambda_{i,2} (T_2^2 - T_1^2) / 2}{T_2 - T_1} + \frac{\left(1 - \sum k_i\right)\left[\lambda_{o,1} (T_2 - T_1) + \lambda_{o,2} (T_2^2 - T_1^2) / 2\right]}{T_2 - T_1} \tag{39}$$

Taking the base enthalpy point at absolute zero reduces the above equation to the one used in this study

$$c_{p_m} = \frac{k_i \lambda_{i,1} + k_i \lambda_{i,2} T}{2} + \left(1 - \sum k_i\right)\left(\frac{\lambda_{o,1} + \lambda_{o,2} T_2}{2}\right) \tag{40}$$

Substitution of this mean specific heat into the energy equation produces

$$\bar{\rho}\bar{u}\,\overline{h_r^o} = \bar{\rho}\bar{v}\left(\frac{c_{p_m}T - c_{p_o}T^o + \overline{u^2}}{2}\right) = H \tag{41}$$

The following algebraic manipulations and substitutions can be performed to produce a quadratic expression in the desired velocity variable:

$$\rho = \frac{H - \bar{u}\,c_{p_m}\,P/Rg(k)}{u^3/2 - \bar{u}\,c_{p_o}\,T_o^{\,o}} \tag{42}$$

$$\rho\bar{u}^2 = \bar{u}^2\left(\frac{H - \bar{u}\,c_{p_m}\,P/Rg}{u^3/2 - \bar{u}\,c_{p_o}\,T_o^{\,o}}\right) = M_f \tag{43}$$

$$\bar{u}^2\left(H - \frac{\bar{u}\,c_{p_m}\,P}{R_g}\right) = M_f\left(\frac{\bar{u}^3}{2} - \bar{u}\,c_{p_o}\,T_o^{\,o}\right) \tag{44}$$

$$\left(\frac{M_f}{2} + \frac{c_{p_m}\,P}{R_g}\right)\bar{u}^2 - H\bar{u} - M_f\,c_{p_o}\,T_o^{\,o} = 0 \tag{45}$$

In this quadratic, only positive roots have physical significance and the final equation for the velocity is

$$\bar{u} = \frac{H}{2\xi} + \left(\frac{H^2}{4\xi^2} + \frac{M_f\,c_{p_o}\,T_o^{\,o}}{\xi}\right)^{1/2} \tag{46}$$

where:

$$\xi = \frac{M_f}{2} + \frac{c_{p_m}\,P}{R_g} \tag{47}$$

For the general case involving gas mixtures of different molecular weights and specific heat coefficients, the solution is iterative around the variables, c_{p_m} and R_g. This is done through the solution for concentration

$$k_i = \frac{K_i}{\rho \bar{u}} \tag{48}$$

the gas constant

$$R_g = R_{g_i} k_i + (1 - \sum k_i) R_{g_o} \tag{49}$$

and Equation (40) for the mean specific heat, c_{p_m}. When the molecular weight and specific heat are constant and equal for all the gases entering into the problem, then the solution does not involve iteration. In running the programs, the convergence of the velocity solution has been rapid.

2.5.3 Shear-Stress Derivation

The derivation has as its basis, the representation of shear stress by the well-known equation for Reynolds stress

$$\tau_{ij} = \rho \overline{u'v'} \tag{50}$$

Now it can readily be shown that the mean of the fluctuating quantities in (1) can be replaced with differences of mean quantities. Thus,

$$\overline{u'v'} = \overline{uv} - \bar{u}\,\bar{v} \tag{51}$$

If the presumption of moderate incompressibility made in Reference 1 is made again here, then the results of (51) substituted into (50) yields the fundamental

relation used for the shear stress in the derivation

$$\tau = \tau_{ij} = \overline{\rho uv} - \overline{\rho}\,\bar{u}\,\bar{v} \tag{52}$$

Reichardt found a relationship between the first term of (52) and the radial gradient of momentum flux in his mixing solution. For an elemental jet, this relation is

$$\overline{\rho uv} = -\frac{b_m}{2}\left(\frac{db_m}{dx}\right)\left[\frac{\partial(\overline{\rho u^2})}{\partial r}\right] \tag{53}$$

The momentum flux at any point in space for an elemental jet from the Reichardt solution is given by

$$\overline{\rho u^2} = \overline{(\rho u^2)}_e A_e e^{-r^2/b_m^2} \Big/ \pi b_m^2 \tag{54}$$

and the derivative of (54) with respect to r yields the following relation:

$$\frac{\partial(\rho u^2)}{\partial r} = -2\,\overline{(\rho u^2)}_e A_e\, r\, e^{-r^2/b_m^2} \Big/ \pi b_m^4 \tag{55}$$

Substitution of this result into (3) gives a relation for the first term in quantities which can be evaluated through a computer integration.

The second term is reduced by applying the continuity equation to the flow field of the elemental jet. In polar coordinates, this expression is

$$\frac{\rho v}{r} + \frac{\partial(\rho \bar{v})}{\partial r} + \frac{\partial \rho \bar{u}}{\partial x} = 0 \tag{56}$$

At a given x-plane, the gradient of mass flux with respect to x can be considered to be a function of r only. Thus, the above differential equation becomes a simple first-order differential equation in one unknown, having as its solution

$$\rho \bar{v} = \frac{1}{r} \int_0^r \frac{\partial(\rho \bar{u})}{\partial x} \, r' dr' \tag{57}$$

where the constant of integration is zero. Multiplication through by $\bar{u}$ leads to the result

$$\rho \bar{v} \bar{u} = \frac{\bar{u}}{r} \int_0^r \frac{\partial(\rho \bar{u})}{\partial r} \, r' dr' \tag{58}$$

Using again the elemental jet momentum flux relation (54) and taking the differentiation outside of the integration, the following sequence of equations can be written:

$$\rho \bar{u} \bar{v} = \frac{\bar{u}}{r} \frac{\partial}{\partial x} \left(\int_0^{\pi} \frac{\rho \bar{u}^2}{u} \, r' \, dr' \right) \tag{59}$$

$$\rho \bar{u} \bar{v} = \frac{\bar{u}}{r'} \frac{(\rho \bar{u}^2)_{A_e}}{\pi} \frac{\partial}{\partial x} \left(\int_0^{r'} \frac{e^{-r'^2/b_m^2}}{\bar{u}} \, r' dr' \right) \tag{60}$$

Introducing (54) (with the mean of the product assumed equal to the product of the means) $\bar{u}$ can be eliminated, namely,

$$\overline{\rho}\,\overline{u}\,\overline{v} = \frac{e^{-r^2/2b^2}\,(\overline{\rho u^2})_e A_e}{\sqrt{\rho}\; b_m\, r\, \pi}\; \frac{\partial}{\partial x}\left[\left(\frac{1}{b_m}\int_0^r \frac{e^{-r'^2/b^2}\, r'\, dr'}{e^{-r'^2/2b_m^2}/\sqrt{\rho}}\right)\right] \tag{61}$$

Presuming that the x-directed gradient of density is nearly zero justifies the insertion of the density square root into the derivative. The density expression may be removed altogether if it is presumed that the local density is approximately equal to the mean density over the integration. Such simplification reduces Equation (61) to the following (after integration):

$$\overline{\rho}\,\overline{u}\,\overline{v} \simeq \frac{e^{-r^2/2b_m^2}\,(\overline{\rho u^2})_e A_e}{\pi\, b_m\, r}\left\{\frac{\partial}{\partial x}\left[b_m\left(1 - e^{-r^2/2b_m^2}\right)\right]\right\} \tag{62}$$

Performing the indicated partial differentiation and combining terms leads to the following final expression for the second term of the shear-stress equation for an elemental jet in terms of quantities which can be evaluated:

$$\overline{\rho}\,\overline{u}\,\overline{v} = \frac{(\overline{\rho u^2})_e A_e}{\pi\, b_m\, r}\left(\frac{d\, b_m}{dx}\right)\left[e^{-r^2/2b^2} - \left(\frac{r^2}{b_m^2} + 1\right) e^{-r^2/b_m^2}\right] \tag{63}$$

Addition of the two terms produces this result for the elemental jet shear stress:

$$\tau = \frac{(\overline{\rho u^2})_e A_e}{\pi\, b_m\, r}\left(\frac{d\, b_m}{dx}\right) e^{-r^2/b_m^2}\left(1 + 2\,\frac{r^2}{b_m^2} - e^{r^2/2b_m^2}\right) \tag{64}$$

The shear stress at a point in the flow field of a finite jet is obtained by the linear super position of the solutions obtained for the elemental jet. (The exit is decomposed into a matrix of elemental jets.) In the computer program, the super position is replaced by an integration. The radial and tangential components of the shear stress are obtained by multiplying the integral relation by the cosine or sine of the angle between lines connecting the point in question to the origin and to the elemental jets being integrated. (See Fig. 2.10).

Again utilizing the superimposable nature of the equations, integration over the exit plane produces the total shear in the two coordinate directions (s and ϕ):

$$\tau_s = \int_{A_e} \frac{\overline{(\rho u^2)}_e}{\pi b\, r'} \frac{d\, b_m}{dx} e^{-r^2/b_m^2} \cos\theta \left[\frac{r'^2}{b_m^2} - e^{r'^2/2b_m^2} + \left(\frac{r'^2}{b_m^2} + 1 \right) \right] dA_e \qquad (65)$$

Integrating in polar coordinates ($dA = r'dr'd\theta$) with respect to r' yields

$$\tau_s = \sum_{\text{contours}} \frac{\overline{(\rho u^2)}_e}{\pi} \frac{d\, b_m}{dx} \int \cos\theta \left[\sqrt{\pi}\, \text{erf}\ (r/b_m) - \sqrt{\frac{\pi}{2}}\, \text{erf}\left(\frac{r}{b_m \sqrt{2}} \right) - \frac{r}{b_m} e^{-(r/b_m)^2} \right] d\theta \qquad (66)$$

and a similar expression for ϕ with sin θ replacing cos θ.

2.5.4 Sound-Power Derivation

In Reference 1, the following equation was derived from the theory of Lighthill:

$$P_a(x) \sim \left(\overline{\Delta V}\ f_e^4 \int_V \tau^2\, dV \right) / \rho_o a_o^5 \qquad (67)$$

This equation relates the sound power produced within a volume, $\overline{\Delta V}$, about a point in the flow field to the eddy oscillation frequency and the shear stress generating the eddy. The volume at the point is, as in Reference 1, assumed to have as its characteristic dimension, the mean size of the eddy, σ. Utilizing the relation below (again from Ref. 1) yields the following equation for the volume in question. The frequency equation derived in Reference 1 is also used here.

$$\overline{\Delta V} \sim \sigma^3 \qquad (68)$$

$$f_e \sim \frac{1}{\sigma} \left(\frac{\tau}{\rho} \right)^{1/2} \qquad (69)$$

The product of these two quantities is then:

$$\overline{\Delta V}\ f_e^4 \sim \frac{U_c}{x} \left(\frac{\tau}{\rho} \right)^{3/2} \qquad (70)$$

By placing the shear stress and density variables into the integrals of (67) and simplifying, there results

$$P_a(x) \sim \frac{U_c}{\rho_o a_o^5} \int_V \frac{(\tau^7 e^{-3})^{1/2}}{x}\, dV \qquad (71)$$

This volume integral can be replaced with an area integral by considering the sound power to be produced in unit length.

$$\frac{dP}{d \ln x} \sim \frac{U_c}{\rho_o a_o^5} \int_A \left(\tau^7 e^{-3}\right)^{1/2} dA \qquad (72)$$

From the frequency relation

$$f \sim U_c/x \qquad (73)$$

the following useful equation can be derived:

$$\frac{d \ln f}{d \ln x} \sim \frac{d \ln U_c}{d \ln x} - 1 \qquad (74)$$

Substitution of the last relation into Equation (72) yields the sound power per cycle of frequency (or bandwidth). Introducing the attenuation coefficient and the arbitrary constant into the equation produces the equation for sound-power production used in this study

$$\frac{dP}{d \ln f} = \frac{C_a U_c \alpha}{\left(\frac{d \ln U_c}{d \ln x} - 1\right) \rho_o a_o^5} \int_A \left(\tau^7 p^{-3}\right)^{1/2} dA \qquad (75)$$

The acoustic power developed by free jets (sound suppressors in particular) has two characteristics: (1) a Mach number effect and (2) a shielding effect wherein the sound produced by eddies internal to the overall jet structure are apparently masked, shielded, or attenuated in some manner by the surrounding flow field. An exact solution would describe the attenuation, refraction, and convection effects of the sound produced at each point in the

flow field. To avoid the difficulties of performing such a solution, two parameters will be artificially introduced into the standard viscous dissipation formula, which (it is hoped) will provide the desired effects. These are: (1) the jet porosity which simply relates the point to the jet flow field in a geometric fashion and (2) an extent effect which should provide a measure of the time the acoustic energy is under the influence of the viscous dissipation.

Forming an attenuation coefficient

$$\alpha = e^{-\alpha_k X_e} \tag{76}$$

where X_e is given by

$$X_e \sim b_m E_f M_c \tag{77}$$

and where α_k is obtained from the Kirchhoff viscous dissipation equation

$$\alpha_k \frac{\overline{\eta}_c f^2}{\rho_o a_o^3} \left(\frac{4}{3} + \frac{\gamma - 1}{Pr} \right) \tag{78}$$

This equation is slightly different from the form usually found. Here the eddy viscosity replaces the kinematic viscosity and has been factored out of the expression through the use of the Prandtl relation. The eddy viscosity in Equation (78) is taken to be some mean viscosity over the mixing region. To obtain this effect, the following arbitrary equation has been formed.

$$\overline{\eta}_e \sim \frac{\partial}{\partial x} (\eta_e) \frac{X_e}{2} + \eta_e \tag{78}$$

The local eddy viscosity is given by the standard definition

$$\eta_e = \tau / (\partial \bar{u} / \partial r) \tag{80}$$

and using the approximate relation for the shear stress neglecting density effects produces

$$\eta_e = \frac{\rho U_c b_m}{2} \frac{d b_m}{dx} \tag{81}$$

It should be noted that the above relation for the eddy viscosity is an approximation for the elemental jet and not for the general flow field which would involve integration of such quantities (as in Section 2.6.2).

In light of the preceding approximations in the attenuation development, such an integration is not warranted.

Finally, the arbitrary equation for the porosity effect that has been tentatively used in this study is given below:

$$E_f \sim 1 - \frac{R' A_n}{R_c A_c} \tag{82}$$

In effect, this equation arbitrarily de-emphasizes the sound energy produced by mixing regions close to the jet axis.

Clearly, the use of such arbitrary expressions reflects the complete lack of experimental knowledge in this area which could direct such analytical efforts and, moreover, the complexity of the situation, which discourages a more detailed and fundamental treatment.

2.5.5 Computer Program Description

This section of the report presents the description of the two programs that were developed in the course of the study contract. Of the two programs, the second or main program will receive the most attention since it is the one having the most significance to the analysis of suppressors and, indeed, is the desired product of the study. These programs are presented in this section and the reader is asked to refer to these sections during the descriptions which follow. As part of the program description typical input and output for the two programs and the manner in which the programs are used will be discussed.

Single Circular Exit Program

The single circular exit program and its two companion sub-routines are presented in this section. The first of these sub-routines (Sub-routine Flux) is used once for a given exit radius and the second subroutine is used thereafter. The exception to this procedure is if different bandwidths in the acoustic spectrum are desired or if a different starting point in the b_m dummy coordinate is desired. These cases require that the longer, first-mentioned subroutine be used (again for the first run only). The running time for the program using the second subroutine is a factor of four less, so that there is a considerable advantage to using it. A typical running time for the program using the second subroutine is about 1 hour on the 1620 computer (evaluating 19 b_m planes). The second subroutine (Subroutine Short Run) is used in conjunction with the output from the first subroutine (the output used is a part of the input).

The following brief paragraphs give a functional resume of the major portions of the program.

Preceding the exit-conditions calculation, input, and normal program preliminaries, is the sound-power function which is the main equation for the noise prediction. It is basically the same as Equation (10). In the exit-conditions calculation, the properties at the exit plane such as velocity, temperature, and the fluxes of mass momentum and energy are determined. The flux values are necessary, of course, in determining properties in the jet flow.

The determination of initial conditions is primarily for the various integrations which take place later in the program. Of particular note is the frequency initialization procedure. Here the frequency bands are specified and the sound power in them cleared to zero.

Next follows the determination of the number of b_m planes which will be calculated and the specification of limits for the various loops in program logic.

Entering into the radius loop (wherein the points along a radial ray are calculated) the flux calculation loop is first found and it is at this point that either of the two subroutines to the program are called. From the flux calculation, the velocity is determined.

The calculation of the local aerothermal acoustic properties is followed sequentially by the calculation of sound power. The sound-power calculation procedure is more complex than need be for this program since, in the case of a simple circular exit, there is only one mixing region and hence

only one characteristic frequency in each b_m plane. The procedure shown is used in the main program where more than one characteristic frequency is found.

The radius loop is concluded with the integration of the momentum energy and mass flux in the b_m plane. These integrations are used primarily to check the program's accuracy since energy and momentum are theoretically conserved. The radius loop is terminated when the velocity difference (jet minus free stream) approaches zero and the program is completed with the calculation of sound power in decibels and the final output.

Because the program is quite simple, the only procedure that might require a little explanation is the manner in which the two subroutines are used. The program also has an idiosyncrasy in the subroutine transfer which also bears some explanation.

Presume that the program has been run once with the first subroutine and it is now desired to run it with the short flux subroutine. It is necessary, then, to take the output cards from the first running and remove all acoustic output data. This is easily accomplished since these data are readily distinguished blocks of output. The modified output should then consist of a sequence of two output data cards followed by a blank card etc., from beginning to end. In this form, it can be considered input for the short-flux subroutine running of the program. Figure 2.11 shows the respective positions of the input as it would be loaded in the course of running the program. Notice that the modified output-input follows the regular input to the program.

A peculiarity may be found in running the short flux program. Since the output does not have the significant figure accuracy carried in the

machine, the termination of the radius loop previously mentioned does not occur for precisely the same radius with the second subroutine because of a minor difference in velocity values. This naturally destroys the correct sequence of operation if the machine overruns on a b_m plane calculation. The machine continually checks the sequence so that such an error automatically halts the machine. To correct this situation (which is found to occur only for the last few b_m plane calculations), it is only necessary to set (artificially) the flux value in the output to zero on the last card of the particular troublesome b_m plane output. (In Figure 2.13 of the typical output, these quantities are circled).

Figure 2.12 shows some typical input to the program, which, for the most part, is largely self-explanatory. The units are in ft-lbs-seconds for all quantities including those for specific heat and the gas constant. As the program now stands, the proper value for the characteristic radius is the same as the radius itself. The output is presented in Table I which again is largely self-explanatory. The program has been modified so that the decibel calculation is performed for as many bandwidths as in the output to the b_m planes (19 in the case shown in Figure 2.13).

Main Program

The Compressible Flow Mixing Profile and Acoustics Program and its subroutines (presented in this Section) is a greatly expanded version of the original computer program developed in the study reported in Reference 1. The major contributor to this expansion has been the logic required by the routine for the determination of the spreading characteristics of the jet flow under relative conditions, and the routines required to avoid exceeding the memory-storage capacity of the machine. Much of the flux integration logic for complicated exit shapes that was developed in the original program has been retained and can be recognized in the major subroutine to the program - Subroutine FLUX. It was originally thought that computational time could be significantly reduced by integrating the flux from simple exits with simplified methods such as used in the Single Circular Exit program. In particular, the intent was to calculate circular and rectangular exit shapes in this fashion. It has turned out though that only the circular exit can be so treated, due to the complexity of integrating the shear equations for the rectangular exit in closed form. Subroutine CFLUX is this routine. It is somewhat different than the subroutine used for the Single Circular Exit program, in that the former recognizes the circular exit as a point source at sufficient removed distances from the exit (which again increases the speed of the program). For this reason, subroutine CFLUX will provide greatly reduced computational times for suppressor exit shapes such as the multiple tube nozzle.

The following discussion will consider first the main program and its self-contained subroutine and then the principle subroutines to the program itself. As in the preceding program discussion, the emphasis will be

placed on the functional aspects of each of the major portions of the program and little or no mention will be made of the programming logic involved.

Skipping past the two inner subroutines for the moment, the first section of technical importance are the exit area and exit conditions calculation procedures. In the first, the total exit area of the nozzle configuration under consideration is calculated. In addition, the area of each of the elements making up the nozzle (as in a multiple tube-type suppressor nozzle) is stored for later use in the flux integral checks. In the conditions calculation procedure, there are two techniques and one iteration involved. The iteration is necessary because in this program only the exit stagnation pressure and temperature are specified, and all properties are obtained from these two properties. In the case where variable gamma is being considered, an iteration on the energy equation is required to determine the exit static conditions. In the first method (constant and identical gamma and molecular weight for all gases of the system), the iteration procedure is not required since the exit static properties can be obtained from the standard one-dimensional Mach number relations.

As in the previous program, certain initial calculations and zero settings must be performed and these are found next in this program as well. The frequency initialization is much the same as before. The velocity is set equal to the free-stream value to assure correct interrogation results.

The determination of the indices on the major loops in the program logic follow the initial condition determinations, and this in turn is followed by the major loop of the program which determines the set of b_m planes

in which the values for the acoustic and aerodynamic properties of the jet flow are calculated.

It is at this point, that the control for the b_m plane pass is found. The program makes three passes in each b_m plane as discussed in Section 2.2.3. The pass is controlled by the value of a special program signal term - in this case the coded word is IBPAS. In every pass, the program logic proceeds to the flow-field matrix which determines the two-dimensional point matrix in the flow-field b_m planes. These points are determined by means of radius and angle loops which specify points approximately at the corners of rectangles (refer to the flow chart, Fig. 2.5).

The Section entitled "No Mesh Set on NMDOM" is artificially included in the program on a temporary basis to insure that the second pass of the program is bypassed. As noted previously, this section must be bypassed because the companion subroutine to the matrix subdivision has not yet been completed.

The flux loop procedure follows next, and it is at this point that the subroutines are called into the main program. The various fluxes are summed over the number of individual elements that exist in the suppressor configuration. Several bypasses are included in the flux calculation to reduce the program running time. The first of these, entitled "X zero shear and iteration bypass", is used at the first b_m plane calculation which is coplanar with the exit of the suppressor nozzle and which is used to associate the exit velocity with corresponding mesh points in the first b_m plane. The second bypass is on the shear and velocity iteration calculations which are not needed for those matrix points lying within the potential core of the jet efflux.

The velocity iteration which follows is the same as that used in the preceding program with the addition of a CP and PGC (perfect gas constant) loop which provides a solution for gases of different molecular weight and variable specific heat. Two coefficients are used to describe the functional relationship between specific heat and temperature.

The next major section of importance is the interrogation loop wherein those points lying within a circle whose radii are twice the width of the mixing region are compared to determine the relative maximum and minimum of this set of points. Since the major mesh points are not subdivided in the present program the inner mesh points cannot be interrogated, and for this reason this portion of the program is now bypassed as indicated in the listing. Once the relative maximum and minimum velocities in a given mixing region are known, then properties such as the convective velocity, the local value of the x-coordinate, the eddy viscosity, and the acoustic properties can be determined. The attenuation calculation procedure is identical to that used in the preceding program, and only slight modifications have been made to the x determination and the eddy viscosity calculation procedures.

The matrix subdivision section of the program, which is by-passed for reasons previously discussed, contains three separate routines depending upon the manner in which the major mesh points are subdivided.

The first two sections beginning with statements numbered 167 and 168, respectively, divide the major matrix either circumferentially or radially, and the section beginning with statement 169 performs the division both ways. In all three cases the actual subdivision is carried out by one of

the self-contained subroutines (subroutine mods). This subroutine tells the main program what the mesh size is in the subdivision - for b_m planes near the exit this division is 8 by 8; for b_m planes near the end of the potential core the division is by 4; and downstream of this point the division is by 2. For b_m planes three diameters downstream of the nozzle exit plane there are no inner mesh sub-divisions.

Following this calculation procedure, are the ratio calculations for the output, sound-power calculations (which are similar to those in the preceding program), the mass momentum and energy integrations, and the termination of the mesh point angle and radius loops. Next is found the acoustic search and addition routine which is another major portion of the program logic and the one which uses the other internal subroutine for the program - subroutine orders. It is here that the program searches through the frequency indices that have been determined at a given b_m plane (one frequency index being associated with each mixing region having different relative maximum and minimum velocities). Those sound-power values having frequency indices less than one-third octave apart are added together to form the acoustic output of the program. The band assignment and shift routine on the following page is currently not used in this program due to memory limitations. In it, the machine compensates for the fact that the sound power is being calculated at discrete points and not integrated throughout the whole flow field. In the band assignment and shift routine, the program searches through the bands that have been specified in the output after the final b_m plane has been calculated to make sure that each major frequency (i.e., the major mixing regions) contribute to each bandwidth once and only once after they appear and before they

disappear. Finally, all the sound power from the various mixing regions are added at each bandwidth to give the total sound power generated. At present, since the band assignment and shift is not operational, this function will have to be performed by hand, using the output from the acoustic bandsearch and addition routine.

Following the main program listing, is the listing for subroutine FLMA and its subordinate subroutines. This subroutine is a complicated bit of programming logic which is necessary to avoid exceeding 7090 machine memory storage. It also serves to keep the cost of running the program down to a reasonable level. In this subroutine, the geometric integrations that are performed for each matrix point are stored along an axial ray so that for each position in space the geometric integrations need to be performed but once. Since there are approximately 19 b_m plane calculations, this technique alone presents a 19 to 1 saving in computational time. This subroutine also stores the value of the flux integrations themselves so that subsequent runs with this particular geometry can be made without re-doing the time-consuming integrations which (as in the preceding program) will result in a considerable time reduction.

Despite its complexity, the main program is easier to use than the first. Any number of cases can be considered at the same time, since the program uses the correct subroutines automatically. Thus, any sequence of nozzle configurations and aerodynamic cases for each configuration can be handled in any sequence desired. It is important that a correct case number for each configuration be included since it is the case number which tells the machine which subroutine it is to use. For instance, case No. 1 is reserved for the first-run integrations which are stored on a master tape. This master tape must be used for all subsequent running of this configuration.

2.6 Conclusions

In the course of conducting this study, several significant areas worthy of further analytical and experimental research were uncovered. These areas, of course, are refinements to the existing knowledge and, as a consequence, will be less rewarding for the same amount of work than has been experienced in the past. This is particularly true in the one area that has caused the most concern in the present study - the relative velocity effect on the rate of spread of jet mixing.

The conclusions of this study are as follows:

(1) Reichardt's mixing theory is not adequate in fully describing the relative rate of mixing in complicated flow situations.

(2) The jet Mach number effect observed primarily in the data of Reference 10, are in contradiction to the observed acoustic results from Reference 1. (Presuming the present acoustic theory is essentially the correct one). As a consequence, the value for the second rate of spread coefficient (constant C_{b2}) is found to be zero at transonic jet Mach numbers.

(3) Experimental evidence indicates that the rate of spread in the mixing region is to some degree x dependent. This effect is not included in the present analysis, and the acoustic predictions for circular exits indicate that such a dependence is desirable for a more accurate prediction.

(4) The modified shear-stress equations successfully predict experimentally measured shear stresses.

(5) The analytical velocity profiles, in general, satisfactorily agree with experiment. In this regard, it is noted that the experimental data of Reference 7 seem to have a deficiency in that the data are at odds with the conservation of momentum principle.

(6) In general, the computer programs presented herein are an advancement in the state-of-the-art in the prediction of fluid dynamic and acoustic properties of interacting free jets. Further work is required, however, to bring these programs to their full state of usefulness.

COMPUTER PROGRAM LISTINGS

SINGLE CIRCULAR EXIT PROGRAM LISTING

```
C      SINGLE CIRCULAR EXIT  AERO-ACOUSTIC SOLUTION     RDG6-8-3  8380.01
C
C       FORMAT AND DIMENSION STATEMENTS
C
       DIMENSION RAD(100),
      1         EVIS(100) ,DSPL(25),FREQ(25),DB(25),REMAX(2),REMIN(2),GAM
      2AE(2),RGE(2),CPE(2),TPE(2),          TTE(2),AVELE(2),UE(2),RHOE(2),
      3TNLPE(2),EMOM(2),EMAS(2)
   70:  FORMAT (8F10.5)
   703  FORMAT (I10,6F10.5)
   705 FORMAT(4F10.4, E10.3,3I10)
   710  FORMAT (2F10.4,2I10,2E10.3 /1H  )
   711  FORMAT (8F10.4/  5F10.4,2I10/1H  )
   712 FORMAT  ( 4F10.4,I10,2E10.3/  ( 40X,I10,2E10.3))
   713  FORMAT  (I10,2E10.3,F10.4)
       COMMON NK,NS,PI,     CL,BMTIL
C
C      FUNCTION
C
       DSPF (A,B,C) = A*CA*UCONN*  ATTN*SQRTF((SHEAR**7.)/(RHO**3.))*RADJ
      1*DERAD/(B*(C**5.)*(1.0-DLNUC))
C
C       INPUT
C
   571  READ  703, NMNOZ,CDIM,RADC,REMAX(1),REMAX(2),REMIN(1),REMIN(2)
   572 READ 701, PRADL,CX,CA,CFREQ,CB1,CB2,P,BMOR,BMINT,(GAMAE(L),RGE(L),
      1CPE(L),TPE(L),TTE(L),L= 1,2)
       FREQ = 0.
       PI = 3.14159
       TPI = 6.28318
       AREAC = PI*RADC*RADC
       RADL = RADC
       SEMAS = 0.
       SEMOM = 0.
       SENLP = 0.
       EANOZ = 0.
C
C      EXIT CONDITIONS CALCULATION
C
       NKP =  NMNOZ + 1
       DO 601 K= 1, NKP
       GAMEX = (GAMAE(K) - 1.)/GAMAE(K)
       EMACH =        2.*(((TPE(K)/P)**GAMEX) -1.)/(GAMAE(K)-1.)
       TE = TTE(K) / (1. + (GAMAE(K) - 1. ) * EMACH/ 2.)
       AVELE(K) = SQRTF ( GAMAE(K) * RGE(K) * TE)
       EMACH = SQRTF (EMACH)
       UE(K) = EMACH * AVELE(K)
       RHOE(K)  = P / (RGE(K) * TE )
       TNLPE(K) = CPE(K) * TTE(K)  -CPE(NKP) * TTE(NKP)
       EMAS (K) = RHOE(K) *UE(K)
       EMOM(K) = EMAS(K) *UE(K)
       EXTA =  PI *(REMAX(K) *REMAX(K) - REMIN(K) *REMIN(K))
       SEMOM = EMOM(K) * EXTA +SEMOM
       SEMAS = EMAS(K)*EXTA +SEMAS
       SENLP = EMAS(K) *TNLPE(K)       *EXTA + SENLP  + .00001
         UDIV = UE(1)
         TDIV = TTE(1)
```

```
        RHODV = RHOE(1)
      SHDIV = RHOE(1)    * UE(1)   *UE(1)
  601 EANOZ = EANOZ + EXTA
C
C     END EXIT CALCULATION
C
      UMAX = UE(1)
      UMIN = UE(NKP)
      AVELC = AVELE(1)
      URAT = (UMAX +UMIN)/2.0
      UCONV = URAT
      BM = BMINT
      BMOLD = 0.0
      DRADI = RADC / 20.
C
C     INITIAL CONDITIONS LOOP
C
      RAD(1) = 0.
      DO 610 KJP= 1,99
      KJ  = KJP +1
      RAD(KJ   ) = RAD (KJP) + DRADI
  610 EVIS(KJ) =0.
      EVIS(1)=0.
      XOLD = 0.
      DUCNV = 0.0
      NSC = 0
C
C     END INITIAL CONDITIONS LOOP
C
C     FREQUENCY NEST INITIALIZATION LOOP
C
      DSPL(1) = 0.
      DB(1) = 0.
      FREQI(1) = 125.
      NOCT = 24
      FREQJ = 1.259921
      DO 560 JFREQ = 2,NOCT
      FREQI(JFREQ) = FREQI(JFREQ - 1) * FREQJ
      DB(JFREQ) = 0.
  560 DSPL (JFREQ)  = 0.
C
C     END FREQUENCY INITIALIZATION
C
C
      DSL = 0.
      BMRAT  = BMOR *RADC/BMINT
      NMBM=   3. * LOGF (BMRAT ) / 0.69315
C
C     BM LOOP
C
      DO 540 I= 1,NMBM
C
C     CONVECTIVE VELOCITY CALCULATION
C
      UCONN = (UMAX + UMIN ) / 2.0 + DUCNV*  (BM-BMOLD)
      CMACH = UCONN / AVELC
C
```

```
C      SPREADING COEFFICIENT CALCULATION
C
       DXBM = (CB1 * (1.0 + CB2*( 1.0 - EXPF (- BM/(0.2*RADC)))*
      1CMACH)*(UMAX + UMIN))/(UMAX - UMIN)
       IF (I- 1) 100,591,592
  591  DXBMO = DXBM
  592  X= XOLD +(DXBM + DXBMO )*(BM -BMOLD) / 2.
       BH = BM     /SQRTF(PRADL)
       XRA = X / (XOLD + 0.0001 )
       UCONR = UCONN/UCONV
       DLNUC=LOGF(UCONR)/LOGF(XRA)
        DUCNV     = (UCONN - UCONV    )/ (X - XOLD)
       UCONV = UCONN
       ISETI = BM/(RADC*0.15)
       NMDOJ = 2  **ISETI
       IF (NMDOJ - 8) 593,594,594
  594  NMDOJ = 4
  593  DOJ = NMDOJ
       DERAD = DRADI * DOJ
       NMJMX = (RADC + 2.5*BM ) / DRADI      +3.
       TMIT = 0.
       TMAST = 0.
       TNTPT = 0.
       FNSS = 1.
       TYPE 705,X,AVELE(1),UE(1),BM, TNLPE(1)  ,NMBM,  NMJMX,NMDOJ
C
C      RADIUS LOOP
C
       DO 510 J=1, NMJMX,NMDOJ
       DLI = CDIM
       RADJ= RAD(J)
C
C       END COEFFICIENT CALCULATION
C
C      FLUX CALCULATION LOOP
C
       CL = RADJ/ REMAX(1)
       BMTIL = BH /REMAX (1)
       SJ = -1.
       CALL FLUX (SHK,SJ)
       BMTIL = BM     / REMAX (1)
       SJ = 0.
       CALL FLUX (SF,SJ)
       IF (SF-0.001) 522,522,523
  523  TM = EMOM(1)*SF
       H = EMAS(1)*TNLPE(1)*SHK
       SHEAR =      EMOM(1)*SJ /DXBM
C
C      VELOCITY ITERATION
C
       RG = 1700.
       U3 = 500.
       U2 = 0.
       U1 = 100000.
       GO TO 97
   91  AP = TM /2.0 + CP * P/RG
       UN    = H/( 2.0 * AP) + SQRTF ( H *H/(4.0 * AP* AP ) + ( TM * CPE(N
```

```
     1KP)*TTE(NKP)/AP ))
      UD = UN     - U3
      IF ( ABSF (UD) -  1.  ) 96, 96, 92
   92 U2 = (U2*U3 -U1*UN    )/(U2 +U3 -U1-UN)
   95 U1 = U3
      U3 = U2
      U2 = UN
      GOTO 98
   97 RHO = TM /(U3*U3)
       GO TO 99
   98 RHO = TM /(UN*UN)
   99 T=  P/(RG * RHO   )
   82 RG = RGE(1)
      CP = CPE(1)
      GO TO 91
C
C     LOCAL PROPERTIES
C
  522 TMASI = 0.
      TMI = 0.
      TNTPI = 0.
      RADJR = RADJ/RADC
      SHERR = 0.
      URAT = 0.
      VMACH = 0.
      GO TO 505
   96 GAMMA= CP / (CP - RG)
      TNTLP = H /(RHO * UN)
      TT =(TNTLP + CPE(NKP) * TTE(NKP))/CP
      AVEL     = SQRTF ( GAMMA * RG * T)
      VMACH= UN /AVEL
C
C      EDDY VISCOSITY AND DERIVATIVE CALCULATION
C
      EVISN = RHO * UCONN * BM          /(2.0  *DXBM )
      DEVIS = (EVISN - EVIS(J))/(X-XOLD)
      EVIS(J) = EVISN
C
C     RATIO CALCULATIONS
C
        RADJR=RADJ/RADC
        XR=X/RADC
        SHERR = SHEAR/SHDIV
        RHOR = RHO/ RHODV
        TTR = TT/TDIV
        URAT =UN   / UDIV
      BMR=BM    /X
        UCONR = UCONN/UDIV
C
C     ATTENUATION CALCULATIONS
C
       IF (RADL - RADJ) 1, 1, 3
    1 RADP = RADL
       GO TO 2
    3 RADP = RADJ
    2 EFUNC = 1.0 - RADP * EANOZ / (RADL * AREAC)
      XEFEC = CX * BM     * EFUNC * CMACH
```

```
      EVISM = EVIS(J)+DEVIS*XEFEC/2.0
      FREQO=FREQ
      FREQ = CFREQ * UCONN / X
C
C     FREQUENCY NEST INDEX
      IFREQ = 3.  * LOGF (FREQ / 125.  ) /.69315 + 1.
C
C     SOUND POWER CALCULATION
      ATKRK=FREQ*FREQ*EVISM*(4./3.+(GAMMA-1. )/PRADL)/(RHOE(NKP)*AVELE(N
     1KP)**3.)
      ATTN = EXPF (- ATKRK *XEFEC)
      IF(I-1) 100,487,494
  487 IF (J-1) 100,493,494
  493 IFREQ = IFREQ
      GO TO 5
  494 FRED = IFREQ - IFREQ
      IF ( ABSF(FRED) - 0.05) 6,6,5
    6 GO TO (7,7,7,7,8),NSC
    7 SC = 1.
      NSC = NSC + 1
      DDSPL = DSPF(SC, RHOE(NKP),AVELE(NKP))
      DSL = DSL + DDSPL
      GO TO 521
    8 SC = 0.5
      DDSPL = DSPF(SC, RHOE(NKP),AVELE(NKP))
      DSL = DSL - 0.5 *DSPLO
      DSPLO= - 0.5 *DDSPL
      DSL = DSL + DDSPL
       GO TO 521
    5 DSPL (IFREQ) = DSPL (IFREQ) + DSL
      PUNCH  710, XR, RADJR, IFREQ,NSC,DSPL(IFREQ),FREQO
      SC = 1.
      DDSPL = DSPF( SC,RHOE(NKP), AVELE(NKP))
      DSPLO = DDSPL
      DSL = DDSPL
       NSC = 2
      IFREQ = IFREQ
C
C      MASS MOMENTUM AND ENERGY INTE GRATIONS
C
  521 TMASI = TPI * RADJ*FNSS * RHO * UN
      TMI = TPI * RADJ*FNSS*TM
      TNTPI = TPI * RADJ*FNSS * RHO * UN     * TNTLP
      TMAST = TMAST + TMASI
      TMIT = TMIT + TMI
      TNTPT = TNTPT + TNTPI
      IF (J-1)100,483,484
  483 UMAX = UN
      AVELC = AVEL
      FNSS = 2.
  484 FNSS = 6.- FNSS
      GO TO 510
C
C     TERMINATION OF RADIUS LOOP
C
  505 RADL = RADJ
       XOLD = X
```

```
      TMIT = (TMIT -    TMI/2.   )*DERAD /3.
      TMAST = (TMAST -    TMASI/2.   )*DERAD /3.
      TNTPT  = (TNTPT -      TNTPI/2.   )*DERAD / 3.
C
C     INTEGRAL CHECKS
C
      FEMOM = (SEMOM -  TMIT ) /SEMOM
      FEMAS = (SEMAS -  TMAST) / SEMAS
      ENRG = (SENLP - TNTPT ) /SENLP
      PUNCH 711,XR,RADJR,URAT,SHERR,SHK,VMACH,SF,SJ,DLI,UCONR,BMR,DXBM,T
     1TR,NS,NK
      PUNCH 712,XR,FEMOM,ENRG ,SJ  ,(KJP,FREQI(KJP),DSPL(KJP), KJP =1,NO
     1CT)
      GO TO 520
  510 PUNCH 711,XR,RADJR,URAT,SHERR,SHK,VMACH,SF,SJ,DLI,UCONR,BMR,DXBM,T
     1TR,NS,NK
C
C     END RADIUS LOOP
C
  520 BMOLD = BM
      DXBMO = DXBM
  540 BM = 1.259921*BM
      DSPL(IFREQ) = DSPL(IFREQ) + DSL
      DO 530  KJ = 1,NOCT
      DRAT = DSPL(KJ) /0.0000000000001   +1.
  530 DB (KJ    ) = 10. *LOGF(DRAT) * 0.434
      PUNCH 713,(K  ,FREQI(K  ),DSPL( K),DB( K),K  =1,NOCT)
C
C     END K LOOP
C
  803 IF (SENSE SWITCH 2)  801,802
  801   GO TO 571
  802   GO TO 572
C
  100  PAUSE
       GO TO 803
       END
```

```
C   SUBROUTINE FLUX CALCULATION PROCEDURE
C
      SUBROUTINE FLUX ( PSI, TAU)
      COMMON NK,NS,PI,DLI,CL,BMTIL,          PNS,XSQ,EXPOC,TPSI
       IF  (TAU) 205, 201,201
  205 NSGO = 2
      GO TO 202
  201 NSGO = 1
      TAU = 0.
  202 XSQ = 1.0/(BMTIL *BMTIL)
      EXPOC = (1.-CL)*(1.-CL)*XSQ
      PNS = 4.
      PSIP = 0.
      PSI = 0.
      TPSI = 0.
      TTAU = 0.
      DL = 0.
      IF(CL-1.)203,204,204
  204 VL=CL-1.
      NS = 1. / DLI + 0.99999
      VN=NS
      DL = 1./(   VN )
      GO TO 206
  203 IF(EXPOC -20.)222,221,221
  221 PSIP = 1.
      GO TO  208
  222 PSIP= 1. - EXPF(-EXPOC)
  208 NS=CL/DLI+.99999
      IF(NS) 231,231,224
  224 VN=NS
      DL = CL /(   VN)
       VL = 1. - CL
      PSIP= PI*VL*(1.-PSIP)*0.66666*XSQ*DL + PSIP
  206 NS=2*NS
      DO 212 IS= 1, NS
      NK = IS
  233 VL = VL + DL
      TARG =      (CL/VL + VL/CL - 1./(VL*CL)) /2.
      PHI = ATANF(SQRTF(1. - TARG*TARG )/TARG)
      IF (PHI) 214,215,215
  214 PHI= PI + PHI
  215 EXPAR = VL*VL*XSQ
      IF(25.-EXPAR) 231,231,216
  216 PSI = PNS*EXPF(-EXPAR)*PHI*VL
      GO TO (217,218),NSGO
  217 TAU = PNS*EXPF(-EXPAR)*(1.+2.*EXPAR -EXPF(EXPAR/2.))*SINF(PHI)
  218 TPSI = TPSI + PSI
      TTAU = TTAU + TAU
      PNS = 6. - PNS
  212 CONTINUE
  231 PSI = PSIP +     (TPSI*2.-PSI    )*XSQ*DL/(3.*PI)
      GO TO ( 219,220) , NSGO
  219 TAU = ABSF((TTAU-    TAU/2.)*DL/(3.*PI*BMTIL))
  220 RETURN
      END
```

```
C       SHORT RUN SUBROUTINE
        SUBROUTINE FLUX ( PSI,TAU)
        COMMON NK,NS,PI,     CL,BMTIL
  220 FORMAT (5F10.6)
        NS = 0
        NK = 0
        RADI = 0.
        BMD = 0.
        IF (TAU) 213,206,206
  213 READ 220, XR,RADJR, SF,SJ,SHK
        RADI = RADJR - CL
        IF (ABSF(RADI) - 0.01 ) 205,205,202
  206 BMD =      XR - BMTIL
        IF(ABSF(BMD) - 0.005) 201,201,202
  202 PAUSE
        TYPE 220,RADI,BMD,XR,RADJR,CL
        PSI = 1.0
        TAU = 0.0
        GO TO  210
  201 PSI = SF
        TAU= SJ
        GO TO 210
  205 PSI = SHK
        TAU = -1.
  210 RETURN
        END
```

MAIN PROGRAM LISTING

```
*       COMPRESSIBLE FLOW MIXING PROFILE AND ACOUSTICS PROGRAM - VIDYA-63-4
C
C
      SUBROUTINE ORDERS(N,V,IPH)
      DIMENSION V(100),IPH(100)
      LN = N
      DO 1 I=1,LN
    1 IPH(I) = I
    2 K = 0
      DO 4 J=2,LN
      IF (V(J-1)-V(J)) 3,4,4
    3 VT = V(J-1)
      V(J-1) = V(J)
      V(J) = VT
      IT = IPH(J-1)
      IPH(J-1) = IPH(J)
      IPH(J) = IT
      K = 1
    4 CONTINUE
      IF (K) 6,6,2
    6 RETURN
      END
*     LIST
*     LABEL
C
C
C     MATRIX INDEX AND MODULAR OVERRIDE SUBROUTINE
C
      SUBROUTINE MODS(MFRST)
      COMMON PI,PI2,PRADL,PRASQ,FREQJ,IMH,BM,XE,NEST,NUM,LEAV,PHI,ALPO,R
     1A,SIG,CDIM,ISAP,BMINT,RADC,SF,SH,SJR,SJC,MODSG,NMDOM,MODP
      MODP=(MODSG-1)/25
      MFRST = 1
      IF (MODP-(NMDOM-1 ))218,218,217
  217 NMDOM=NMDOM*2
  218 MFRST=MFRST + MODP
      MODX=MODSG-25*MODP
      RETURN
      END
      LIST
C
C
*     LABEL
*     LIST
*     XEQ
*     CARDS COLUMN
*     LIST
      DIMENSION                    XE(50), ALPO(50), LEAV(50), NUM(50), KN
     1(50),ISAP(50),XITA(50),GMW(50),PTE(50),TTE(50),ENTLP(50),PGCE(50),
     2CPE(50),GAMK(50),RHOE(50),EM(50),UE(50),ACK(50),EMAS(50),EH(50),SF
     3(50),SH(50),SJR(50),SJC(50),GK(50),GKON(50),SPL(25),DB(25),FREQ(2
     45),ISSM(20),NREJ(  ),KAFP(25),ISPL(85),DSPS(85),ETA(2,50),UN(20,20
     5),IFEX(20,20),UZ(20,20),DXBMO(20,20),UCONV(20,20),EVIS(20,20),DSFL
     6(20,20),XOLD(20,20),UN1(  ,  ),UZ1(  ,  ),UN2(  ,  ),UZ2(
     7  ,  ),DSPL(25,25,25)
      COMMON PI,PI2,PRADL,PRASQ,FREQJ,IMH,BM,XE,NEST,NUM,LEAV,PHI,ALPO,R
     1A,SIG,CDIM,ISAP,BMINT,RADC,SF,SH,SJR,SJC,MODSG,NMDOM,MODP
```

```
    1 FORMAT(6I10,2F10.4)
    2 FORMAT (2F10.4)
    3 FORMAT (2F10.4,3I10)
    4 FORMAT(        80H1                                                  COMPRESSI
     1BLE FLOW MIXING PROFILE PROGRAM///65H
     2                              INPUT DATA///)
    5 FORMAT(18H                     OPF8.5,17H                    1PE11.5,14H
     1              OPI11.5,15H                    1PE11.4///)
    6 FORMAT(19H0                  NC1=I3,13H          NCF=I3,12H        LPH1=
     1I3,12H        1SYM=I2,14H          NEST=I3,13H         INDX=I3  //19H
     2              RADC=F6.3,9H     CDIM=F6.3,8H
    8 FORMAT(13H0          XE(I2,2H)=F8.2,                                  7H  ALPO
     1(I2,2H)=F7.4,     7H  LEAV(I2,2H)=I3, 7H   NUM(I2,2H)=I3,7H     KN(I
     22,2H)=I3,7H  1SAP(I2,2H)=I3)
    9 FORMAT(23H0                    DALP(I2,1H,I2,2H)=F7.4,7H    RA(I2,1H,
     1I2,2H)=F7.4,7H  DALP(I2,1H,I2,2H)=F7.4,7H    RA(I2,1H,I2,2H)=F7.4)
   10 FORMAT(76H1                                      OPERATING CONDITIONS FOR
     1 CASE NUMBER  I4
   11 FORMAT(    61H1                                                  EXIT CO
     1NDITIONS///  95H                CONTOUR        STATIC          VELO
     2CITY        MACH        MOMENTUM       ENTHALPY/ 93H
     3              TEMPERATURE                        NUMBER        FLUX
     4       FLUX// 95H                                  DEG RANKINE        FT
     5/SEC                    LB/SQ FT       LB/SQ FT///19H
     6     I2,11H            OPF8.2,7H        F8.2, 6H       F6.3, 5H      1P
     7E9.3, 6H       1PE9.3))
   12 FORMAT(110H0            RADIUS       ANGLE     VELOCITY     TEMP     MO
     1MENTUM     ENTHALPY      RADIAL      TANGENTIAL     TOTAL  /110H
     2                                                  FLUX          FLUX
     3        SHEAR         SHEAR         SHEAR  /110H                FT
     4RADIANS     FT/SEC     DEG R     LB/SQ FT     LB/FT SEC     LB/SQ FT
     5 LB/SQ FT     LB/SQ FT///)
   13 FORMAT( 9H          1PE10.3,5H      0PF5.3,5H    F6.1,4H     F6.1,1P
     15E12.3/)
   14 FORMAT(57H                                                        ASR
     1=1PE11.4///)
   15 FORMAT(612 )
   16 FORMAT(5F10.4 )
   17 FORMAT (69H0                                              EXIT AREA OF C
     1ONTOUR NUMBER I2,2H = F10.4  )
   18 FORMAT (94H0                    CONTOUR                          TOTAL T
     1EMPERATURE                    TOTAL PRESSURE/ 91H
     2                             DEGREES RANKINE                        LB
     3/SQ FT//(18H                    I2, 30H
     4 F8.2, 24H                         F8.2/))
   19 FORMAT ( 89H1                    CONTOUR          MOLECULAR WEIGHT
     1    LAMBDA ONE           LAMBDA TWO  /89H
     2                        FT2/S2-DEGR          (FT/S-DEGR)SQ//20X13,16
     3XF6.3,12X1PE10.3,10XE10.3  )
   20 FORMAT  (9XF10.3,5XF5.3,5XF6.4,4XF6.4,1P5E12.3  )
   23 FORMAT (40H                    SOUND POWER SPECTRUM  ///29X     M F
     1REQUENCY       FREQUENCY    SOUND POWER                    /       K
     2   H INDEX                    DB REF 10-13W        ///////
     3   I3           1PE10.3         0PF10.5  )
  300 FORMAT (40H1 PSUEUDO AXIAL LOCATION-S SUB M=F9.5,25H FT           C
     1ASE NUMBER- I3  ///)
  302 FORMAT (1H )
```

```
  303 FORMAT(76H1                                                    SOUND POWER
     1 INDEX AND MASS FLUX// 115H      PSUEDO AXIAL LOCATION          S
     2OUND POWER LEVEL INDEX        MASS FLUX       VELOCITY TO THE 8TH
     2OUND POWER LEVEL INDEX     FREQUENCY INDEX    VELOCITY TO THE 8TH
     3- INTEGRAL/106H                    FEET                    (FT LB/SQ
     4 SEC)SQ                                  FT**10/SEC**8///)
  304 FORMAT  (  76H1                                        COMPRESSIBLE FLO
     1W MIXING PROFILE PROGRAM//
     234H                        CASE NUMBER-I2/
     3                             40H                  PSUEDO AXIAL LOCAT
     4ION = F9.5,3H FT//  79H                          RADIUS
     5  ANGLE                TOTAL PRESSURE/  80H
     6 FEET                RADIANS                INCHES HG GAUGE)
  305 FORMAT(23H                          F9.3,  13H              F6.3,  19H
     1                    F7.3)
  307 FORMAT(2I3,3F10.5,4F10.2 )
  309 FORMAT(6H    X(I2,2H)=F8.5, 9H    SPL(I2,2H)=1PE11.4,8H     FM(I2
     1,2H)=1PE11.4,  8H    U8(I2,2H)=1PE11.4//)
  329 FORMAT (10X,F10.2,F10.2)
  330 FORMAT (I10)
      DSPF(A,B) = A * B          *SQRTF(TU2RO*TU2RO*TU2RO*TAU)
      PI=3.1415927
      PI2=6.2831853
      NT2 = 2
C
C     INPUT DATA READIN AND PRINTOUT
C
      READ INPUT TAPE NT2 ,15,NT3,NT4,NT5,NT6,NT7,NT8
      READ INPUT TAPE NT2,1,NCI,NCF,INDX,NEST,LPHI,ISYM,RADC,CDIM
      READ INPUT TAPE NT2,3,(XE(K),ALPO(K) ,ISAP(K),LEAV(K),NUM(K),KN(K)
     1,K=1,NEST)
      FLPHI=LPHI
      WRITE OUTPUT TAPE NT3,4
      WRITE OUTPUT TAPE NT3,5,NCI,NCF,LPHI,ISYM,NEST,INDX,RADC,CDIM
      SEMAS=0.
      SEMOM=0.
      SENLP=0.00001
      AREAC=PI*RADC*RADC
      EANOZ=0.
      DO 319 K=2,NEST
      NUMK= NUM(K)
      READ INPUT TAPE NT2,2,(DALP(N,K),RA(N,K),N=1,NUMK)
      ISAPE=ISAP(K)
      FLEAV = LEAV(K)
      WRITE OUTPUT TAPE NT3,8,K,XE(K), K,ALPO(K),K,LEAV(K),K,NUM(K)
     1,K,KN(K),K,ISAP(K)
      NUMK=NUM(K)
      WRITE OUTPUT TAPE NT3,9,(N,K,DALP(N,K),N,K,RA(N,K),N=1,NUMK)
C
C                          EXIT AREA CALCULATION
C
      GO TO (315,316,317),ISAPE
  315 XITA(K)  = .25*(RA(1,K) + RA(NUMK,K))*DALP(1,K)
      DO 313 N  = 2, NUMK
  313 XITA(K )=XITA(K )+ .25*(RA(N,K) + RA(N-1,K))*DALP(N,K)
      XITA (K) = XITA(K)*FLEAV
      GO TO 319
```

```
  316 XITA(K)=PI*RA(1,K)*RA(1,K)
      GO TO 319
  317 S1 = RA(3,K) *RA(3,K) +RA(1,K)*RA(1,K) -2.*RA(1,K)*RA(3,K)*COSF(DA
     1LP(1,K))
      S2 = RA(1,K)*RA(1,K) +RA(2,K)*RA(2,K)-2.*RA(1,K) *RA(2,K)*COSF(DAL
     1P(2,K))
      XITA(K)=S1*S2
      WRITE OUTPUT TAPE NT3,17,K,XITA(K)
  319 EANOZ=EANOZ + XITA(K )
C
C                              EXIT CONDITIONS
      DO 999   NC = NC1,NCF
      READ INPUT TAPE NT2,307,OCTD,NOCT,XINT,XOR,PRADL,FREQB,CMW,PS,CP
      READ INPUT TAPE NT2,16,(PTE(K),GMW(K),TTE(K),ETA(K,1),ETA(K,2),K=
     11,NEST)
      WRITE OUTPUT TAPE NT3,10,NC,OCTD,NOCT,XINT,XOR,PRADL,FREQB,PS,CMW,
     1CP
      DO 119 K=1,NEST
  119 WRITE OUTPUT TAPE NT3,18,K,PTE(K),TTE(K)
      IF(ETA(1,1))120,120,121
  121 DO 120 K= 1,NEST
      WRITE OUTPUT TAPE NT3,19,K,GMW(K),ETA(K,1),ETA(K,2)
  120 CONTINUE
      ENTLO = (ETA(1,1)+ETA(1,2)/2.*TTE(1))*TTE(1)
      LBPAS=1
      DO 113 K=1,NEST
      IF(ETA(1,1))111,111,112
  112 ENTLP(K) = (ETA(K,1)+ETA(K,2)/2.*TTE(K))*TTE(K)
      PGCE(K)=49690./GMW(K)
      PGC = PGCE(K)
      IF(PTE(K)-PS) 321,321,322
  322 TEK=TTE(K)*(PS/PTE(K))**0.286
  115 CPE(K)=ETA(K,1)+ETA(K,2)*TEK
      CP = CPE(K)
      STEN1=(ETA(K,1)+ETA(K,2)/2.*TEK)*TEK
      LBPAS=2
      GO TO 378
  111 PGC = 49690./ CMW
      PGCE(1)=PGC
      ENTLP(K)= TTE(K)*CP
      CPM=CP
      ENTLO = CP*TTE(1)
  378 GAM = 1./(1.-PGC/CP)
      GAMK(K)=GAM
      ACH2 = 2.*((PTE(K  )/PS)**(1. -1./GAM)-1.)/(GAM - 1.)
      GO TO (407,408),LBPAS
  407 TEK = TTE(K) / (1.+ (GAM-1.)*ACH2/2.)
  408 RHOE(K)=PS/(PGC*TEK)
      SV2 = GAM * PGC * TEK
      GO TO (116,381),LBPAS
  381 STEN2=ENTLP(K)/(1.+ACH2/2.*GAM/RHOE(K)*PS
      DSTEN=STEN2-STEN1
      TEK=DSTEN/CPE(K)+TEK
      IF (ABSF(DSTEN-10.) 116,116,115
  321 CPE(K) = ETA(K,1)+ETA(K,2)*TTE(K)
      CP = CPE(K)
      LBPAS= 1
```

```
      GO TO 378
  116 EM(K) = ACH2 * GAM * PS
      UE(K)     = SQRTF(ACH2 * SV2)
      SVE(K) = SQRTF(SV2)
      ACH(K) = UE(K)/SVE(K)
      EMAS(K) = RHOE(K)*UE(K)
      ENTLP(K)=ENTLP(K) -ENTL0
  113 EH(K) = EMAS(K)*ENTLP(K)
      GAM = GAMK(1)
      PGC=PGCE(1)
      ASR= PS *GAM *GAM *PGC *SQRTF(GAM *PGC * TE(1)    )*TE(1)
      UDIV = UE(INDX)
      TDIV = TTE(INDX)
      RHODV=RHOE(INDX)
      SHDIV = RHOE(INDX) * UE(INDX) + UE(INDX)
      WRITE OUTPUT TAPE NT3,11, (K,TEK      , UE(K)    , ACH(K),EM(K),EH(K
     1),K= 1,NEST)
      WRITE OUTPUT NT3    ,14,ASR
      DO 122 K=2,NEST
      REMAS=RHOE(K)*(UE(K)-UE(1))
      SEMAS=SEMAS +REMAS*XITA(K)
      SEMOM=SEMOM+REMAS*XITA(K)*(UE(K)-UE(1))
      SENLP=SENLP+REMAS*ENTLP(K)*XITA(K)
C
C                          END EXIT CALCULATION
C
C                 FREQUENCY NEST INITIALIZATION LOOP
C
      IF (NOCT) 513,513,514
  513 NOCT = 10
  514 IF(OCTD) 515,515,516
  515 OCTD = 1
  516 SPL(1)=0
      DB(1) = 0
      FREQ1(1)= FREQ8
      NOCFD = 10* NOCT
      OCT = NOCT
      NOCT = OCT*OCTD
      FREQJ=EXPF(0.69315/OCTD)
      DO 561 JFREQ=2,NOCT
      FREQ1(JFREQ)=FREQ1(JFREQ-1)*FREQJ
      DB(JFREQ)=0.
  561 SPL(JFREQ) = 0.0
C                    Not Operational
C               SOUND POWER INITIALIZATION
C
      DO 151 N=1,NOCT
      DO 151 K=2,NMBM
      DO 151 M=1,MIXT
  151 DSPL(N,K,M) = -1.
C
C                 VELOCITY INITIALIZATION LOOP
C
      DO 511 M=1,20
      DO 511 I=1,40
  511 UN(I,M) = 0.
C
```

```
C                    INITIAL CONDITIONS
C
C
      IFIL = 44 /17* LPHI) + 1
      IFINI=0
      IFINP=0
      INPEJ=0
      SET1=1.
      SET2=1.
      ISET = 0
      NMJOJ=1
      ISET1 = 0
      DEL = 1.
      MRADL = 0
      NMJMX = 11
      DFL=0.
      MAT = 1
      SET1 = 0.
      FREQ = 0.01
      XOLD = 0.
      DUCNV = 0.
      STMP = 0.
      X=0.
      RADL=RADC
C
C                          INDEX REGISTER DETERMINATION
C
      IF (XINT) 94.94.95
   94 XINT = CDIM / 4.  + 0.01
   95 IF(XOR) 517.517.518
  517 XOR = 10.
  518 BMRAT = XOR * RADC / XINT
      NMBM = OCTD * LOGF (BMRAT) /0.69315    + 2.
      BMINT = 0.075 * XINT
      BM = 0.
      DSIGZ=RADC / 10.
C
C                                  B M LOOP
C
      DO 185 KA=1.NMBM
      IBPAS = 1
      IF (KA-1) 99.99.100
  100 MBPAS = 1
      GO TO 118
   99 MBPAS=2
  118 RACO = 2.*BM
      DSIG=DSIGZ*SET2
      DO 727 II=1.NOCFD
  727 DSPS(II)=0.
      DSIGP = DSIG/8.0
      IMAST = 0.
      IMIT = 0.
      INIPT = 0.
      IFINL=1
      UBI=0.
      MI=-0
      WRITE OUTPUT TAPE NT3.300.BM.NC
      WRITE OUTPUT TAPE NT6.300.BM.NC
```

```
      WRITE OUTPUT TAPE NT7,300,BM,NC
      LINE3=8
      LINE6=8
      LINE7=8
      WRITE OUTPUT TAPE NT3
      WRITE OUTPUT TAPE NT6,12
      WRITE OUTPUT TAPE NT7,
C
C                        FLOW FIELD MATRIX
C
  998 SIG=0.001*DSIG
      IBPAS = IBPAS+1
      BUG = SIG
C
C     RADIUS LOOP
C
      DO 286 M=1,NMJMX
      DPHI = PI2/FLOATF (LPHI*IS)
      DPHI =           DPHI *SET2
      ISSY = IPIL*(M-1) + 1 - ISYM
      ISSM(M) = ISSY
      DPHIP=DPHI/8.0
      PHI=0.
C
C                        ANGLE LOOP
C
      DO 152 I=1,ISSY
      IM=0
      MM=0
      MAT = 1
      IFEX = 0
      NVPAS = 1
      DERAD = DSIG
      DEPHI = DPHI
C
C           NO MESH SET ON NMDOM
C
      NMDOM = 8
C
C           BYPASS REGISTER -FLUX SUMMATION
C
      GO TO (153,205,505) ,IBPAS
  505 GO TO (204,288),MBPAS
C
C                        FLUX LOOP
C
  153 SFT = 0.
      SHEAR = 0.
      SHEAC = 0.
      SHEAT = 0.
      TM = EM(1)
      H = EH(1)
      CALL FLMA(NC,I,M,KA)
      DO 971K=2,NEST
      K=2+NEST-IK
      IF (SF(K) - .999) 411,411,412
  412 KNK = 1
```

```
      GO TO 413
  411 KNK = KN(K)
  413 TM = TM + (EM(K) - EM(KNK))*SF(K)
      H =  H + (EH(K) - EH(KNK))* SH(K)
      GK(K)=EMAS(K) * SH(K)
C
C          X ZERO SHEAR AND ITERATION BYPASS
C
      GO TO (328,349),MBPAS
  328 SHEAR = SHEAR +(EM(K) - EM(KNK)) * SJR (K)
      SHEAC = SHEAC +  (EM(K) - EM(KNK)) * SJC(K)
      SHERT = SQRTF(SHEAR * SHEAR + SHEAC * SHEAC)
  349 IF(SF(K)-0.999)97,97,324
   97 SFT=SFT+SF(K)
      K = 1
  324 IF(SFT-0.001)272,523,523
C
C          POTENTIAL CORE BYPASS
C
  272 UN(I,M)=UE(K)
      TNTLP=ENTLP(K)
      RHO = RHOE(K)
      GAM = GAMK(K)
      SHEAR = 0.
      SHEAC = 0.
      SHEAT = 0.
      TS = TTE(K)/(1. +(GAM-1.)/2.*ACHM*ACHM)
      ACHM = ACH(K)
      GO TO 382
  523 GO TO (102,334),MBPAS
C
C               END  BYPASS
C
C
C
C                       VELOCITY ITERATION
C
  334 U3 = 500
      IFEX(I,M)=1
      GO TO 98
  102 U3 = UN(I,M)
   98 U2 = 0.
      U1 = 100000.
      GO TO 103
  104 AP=TM/2.0+CPM*PS/PGC
      UN(I,M) H/(2.0*AP) + SQRTF (H*H/(4.0*AP*AP; + (TM*ENTLO /AP))
      UD = UN(I,M) - U3
         (ABSF(UD-1.) 105,105,107
  107 U2 = (U2*U3-U1*UN(I,M)/(U2+U3-U1-UN(I,M))
      U1 = U3
      U3 = U2
      U2 = UN(I,M)
      GO TO 108
  103 RHO = TM/(U3 * U3)
      TS = PS/(1700.*RHO)
      GO TO 109
  108 RHO = TM / (UN(I,M) * UN(I,M))
      TS = PS/(PGC * RHO)
```

```
  109 IF(ETA(1,1)) 104,104,114
C
C                    CP AND PGC LOOP
C
  114 TOTLK = 0.
      CPM=0.
      CP=0.
      PGC = 0.
      DO 521 NK = 2, NEST
      GKON (NK) = GK(NK)/(RHO*UN(I,M))
      PGC = PGCE(NK)*GKON(NK)+PGC
      CP = GKON (NK) * (ETA(NK,1) + ETA(NK, 2)*TS + ETA (NK, 3)/(TS*
     1TS)) + CP
      CPM=GKON(NK)*(ETA(NK,1)+ETA(NK,2)/2.*TS)  +CPM
  521 TOTLK = TOTLK + GKON (NK)
      PGC = PGC + (1. - TOTLK) * PGCE (1)
      CP = CP + (1. - TOTLK) * (ETA(1,1) + ETA (1,2) * TS
      CPM = CPM + (1. -TOTLK)*(ETA(1,1) + ETA(1,2)*TS)
      GO TO 104
C
C                       LOCAL PROPERTIES
C
  105 GAM = CP / (CP-PGC)
      TNTLP = H/(RHO*UN(I,M))
      SV = SQRTF (GAM * PGC * TS)
      TT=TNTLP/CP
      ACHM = UN(I,M) / SV
  382 TPG= PS*(1.+(GAM-1.)/2.*ACHM * ACHM) ** (GAM/(GAM-1.))-PS
      TP = TPG + PS
      HGIN = TPG/70.727
      WRITE OUTPUT TAPE NT6,13,SIG,PHI,UN(I,M,TS,TM,H,SHEAR,SHEAC,SHERT
      IF(SENSE SWITCH 5) 213,214
  213 WRITE OUTPUT TAPE NT6,305,SIG,PHI,HGIN
  214 GO TO (414,415),MBPAS
  415 UZ(I,M) = UN(I,M)
```

```
C
C                    X BYPASS AND MESH BYPASS
C
  414 GO TO (562,172,206,207), MAT
C
C                    INTERROGATION LOOP
C
  204 MXPLN = 1
      UMAX =0.
  255 UMIN = UN (I,M)
      MDM = RACO/DSIG + 1.
      IDI = RACO / ( SIG*DPHI) +1.
      MMIN = MAXOF (M-MDM,1)
      MMAX = MINOF (M+MDM,MRADL)
      IMIN = MAXOF(I-IDI,1)
      IMAX = MINOF (I+IDI,ISSY)
      DO 181 MP = MMIN, MMAX
      I1 =((IMIN -1)*(MP-1))/(M-1) +1
      I2 =((IMAX -1)*(MP-1))/(M-1) + 1
      DO 181 IP = I1,I2
      GO TO (883,882),MXPLN
  882 UMAX = MAX1F(UZ(IP,MP),UMAX)
      UMIN = MIN1F(UZ(IP,MP),UMIN)
      GO TO 881
  883 UMAX = MAX1F (UN(IP,MP),UMAX)
      UMIN = MIN1F (UN(IP,MP),UMIN)
  881 IF (NMDOM-8) 333,181,181
C                    This section now bypassed
C                    INNER MESH INTERROGATION
C
  333 IFX = (IFEXO(MP,IP)  )/100 + 1
      INDI = IFEXO(MP,IP)
      GO TO (187,192,193,194),IFX
  192 MODSG = INDI
      CALL MOD(MFRST)
      DO 195 MPP=MFRST,8,NMDOM
      GO TO (884,885),MXPLN
  885 UMAX = MAX1F(UZ1(MODX,IP,MPP),UMAX)
      UMIN= MIN1F(UZ1(MODX,IP,MPP),UMIN)
      GO TO 195
  884 UMAX = MAX1F(UN1(MODX          ,IP,MPP),UMAX)
      UMIN = MIN1F(UN1(MODX          ,IP,MPP,UMIN)
  195 CONTINUE
      GO TO 181
  193 MODSG = INDI
      CALL MOD(MFRST)
      DO 196 IPP=MFRST,8,NMDOM
      GO TO (886,887),MXPLN
  887 UMAX = MAX1F(UZ1(MODX,IPP,MP),UMAX)
      UMIN = MIN1F(UZ1(MODX,IPP,MP),UMIN)
      GO TO 196
  886 UMAX = MAX1F (UN1(MODX          ,IPP,MP),UMAX)
      UMIN=MIN1F(UN1(MODX          ,IPP,MP ),UMIN)
  196 CONTINUE
      GO TO 181
  194 MODSG = INDI
      CALL MOD(MFRST)
```

```
      DO 198 MPP=MFRST,8,NMDOM
      DO 198 IPP= MFRST + 8, NMDOM
      GO TO (888,889),MXPLN
  889 UMAX = MAX1F(UZ2(MODX,IPP,MPP),UMAX)
      UMIN= MIN1F(UZ2(MODX,IPP,MPP),UMIN)
      GOTO 198
  888 UMAX = MAX1F (UN2(MODX           ,IPP,MPP),UMAX
      UMIN = MIN1F (UN2(MODXMODX       ,IPP,MPP),UMIN)
  198 CONTINUE
  181 CONTINUE
C
C                     CONVECTIVE VELOCITY CALCULATION
C
  187 GO TO (281,282),MXPLN
  281 UCONN = (UMAX + UMIN) /2.0
      CMACH = UCONN/SVE(1)
      DXBM=(CB1*(1.+CB2*(1.-EXPF(-XOLD/(2.*RADC)))*CMACH)*(UMAX+UMIN))/
     1 (UMAX-UMIN)
      IF (KA-3) 875,873,873
  873 IF (XOLD) 874,874,875
  874 MXPLN = 2
      GO TO 255
  282 UCONP= (UMAX + UMIN)/2.
      CMAP= UCONP/SVE(1)
      DXBMO( I,M) = (CB1*(UMAX+UMIN))/(UMAX-UMIN)
C
C                     X DETERMINATION
C
      X = (DXBM  +DXBMO(I, M))/2.*BM
      GO TO 876
  875 X=XOLD(I,M)+(DXBMO(I,M)+DXBM)    /2.0*(BM-BMOLD)
  876 TAU=SHERT(I,M)/DXBM
      DXBMO(I,M) = DXBM
C
C                     EDDY VISCOSITY AND CONVECTIVE CALCULATIONS
C
      XRA = X/(XOLD+0.0001)
      IF(KA-2) 345,345,346
  345 UCONV(I,M) = UCONN
  346 UCOVR = UCONN / UCONV(I,M)
      DLNUC = LOGF (UCOVR)/LOGF(XRA)
      UCONV(I,M) = UCONN
      EVISN = RHO * UCONN * BM /(2.0*DXBM)
      DEVIS = (EVISN - EVIS(I,M)) / (X-XOLD)
      EVIS (I,M) = EVISN
C
C                     ATTENUATION CALCULATION
C
      IF(RADL - SIG) 199,199,201
  199 RADP = RADL
      GO TO 202
  201 RADP = SIG
  202 EFUNC = 1.0 - RADP*EANOZ / (RADL * AREAC)
      XEFEC = CX * BM * EFUNC * CMACH
      EVISM = EVISN + DEVIS   XEFEC.*2.0
      FREQO = FREQ
      FREQ = CFREQ * UCONN / X
```

```
      ATKRK = FREQ * FREQ * EVISM * (4./3.+(GAM-1.)/PRADL) /(RHOE(1)*SVE
     1(1)**3.0)
      ATTN=EXPF(-ATKRK*XEFEC)
C
C                     FREQUENCY NEST INDECES
C
      IFREQ = OCTD * LOGF (FREQ / FREQB) / 0.69315 + 1.0
      NFREQ = 10 * LOGF (FREQ/FREQB)/0.69315+1.0
      NFREQ = 10 * LOGF (FREQ/FREQB  )     /0.69315 +1.0
      GO TO 562
      GO TO 215
C                                        This section now bypassed
C                       MATRIX SUBDIVISION
C
  205 IF (NMDOM -8) 355,355,125
  356 IF(IFEX(I,M) -200) 352,352,125
  352 IF (IFEX(I,M)) 354,354,353
  353 INREJ = INREJ + 1
      NREJ(INREJ) = MODF(IFEX(I,M)-1,100) +1
  354 IF (M-1) 125,125,129
  129 IF (I-1) 125,125,133
  133 INDI = 1
      II= ((I-1)*(M-2))/(M-1)+1
      SFSGR = SFT(I,M)-SFT(II,M-1)
      IF(ABSF(SFSGR)-0.1) 152,152,135
  135 INDI = INDI +1
  152 SFSGP = SFT(I,M)-SFT(I-1,M)
      IF(ABSF(SFSGP)-0.1)125,125,158
  158 INDI = INDI +2
      NVPAS = 2
      GO TO 125
  337 GO TO (125,167,168,169),INDI
  167 IFIN1 = IFIN1+1
      IFEX (I,M) = IFIN1
      MODSG = IFIN1
      SIG = SIG+(SET1-7.5)*DSIGP
      MAT = 2
      DERAD = DSIGP   *DEL
      CALL MODS(MFRST)
      IF (NMDOM-8) 336,562,562
  336 DO 203 MM=MFRST,8,NMDOM
      GO TO 153
  172 UN1(MODX,I,MM)=UN(I,M)
      GO TO (416,417),MBPAS
  417 UZ1(MODX,I,MM) = UN(I,M )
  416 SIG = SIG + DERAD
      GO TO 125
  203 CONTINUE
      GO TO 562
  168 IFIN = IFIN + 1
      IFEX(I,M)=IFIN+100
      MODSG=IFIN1
      PHI=PHI +(SET1-7.5)*DPHIP
      DEPHI = DPHIP *DEL
      MAT = 3
      CALL MODS(MFRST)
      IF(NMDOM-8) 229,562,562
```

```
  229 DO 209 IM=MFRST ,8,NMDOM
      GO TO 153
  206 UN1(MODX,IM,M)=UN(I,M)
      GO TO (418,419),MBPAS
  419 UZ1(MODX,IM,M)=UN(I,M)
  418 PHI = PHI + DEPHI
      GO TO 125
  209 CONTINUE
      GO TO 562
  169 IFIN2=IFIN2+1
      IFEX(I,M)=IFIN2+200
      MODSG=IFIN2
      SIG = SIG + (SETI-7.5)*DSIGP
      PHI = PHI +(SETI-7.5)*DPHIP
      DERAD = DSIGP *DEL
      DEPHI = DPHIP *DEL
      MAT=4
      CALL MODS(MFRST)
      IF(NMDOM-8) 223,562,562
  223 DO 211 MM=MFRST,8,NMDOM
      DO 212 IM=MFRST,8,NMDOM
      GO TO 153
  207 UN2(MODF(MODX      ,IM,MM) = UN(I,M)
      GO TO (501,502),MBPAS
  502 UZ2(MODX,IM,MM)=UN(I,M)
  501 PHI = PHI + DEPHI
      GO TO 125
  212 CONTINUE
      SIG = SIG + DERAD
  211 CONTINUE
      MAT = 1
      GO TO 562
C
C           SOUND POWER FACTOR
C
  125 TU2RO=TAU/RHO*TAU
      DSFL(I,M)= DSFL(I,M) + DSPF(DERAD,DEPHI)
      GO TO (562,344), NVPAS
C
C                          RATIO CALCULATIONS
C
  562 RR = SIG/RADC
      SR1=SHEAR/SHDIV
      SR2 = SHEAC/SHDIV
      SR3= SHEAT/SHDIV
      RHOR = RHO/RHODV
      URAT = UN(I,M)/UDIV
      TTR=TT/TDIV
      TR=TS/TDIV
      BMR  =  BM/X
      WRITE OUTPUT TAPE NT3,20,RR,PHI,RHOR,URAT,TR,TTR,SR1,SR2,SR3
C
C             INTERMEDIATE BYPAS REGISTER
C
      GO TO (152,541,215),IBPAS
  541 GO TO (344,152) ,NVPAS
C
```

```
C                    SOUND POWER CALCULATION
C
C
  215 FRED = NFREQ - NFREQ
      IF(ABSF(FRED)226,226,357
  357 MIX=MIX +1
      FR= FREQ(KA,MIX)*UCONV(I,M)/UCONN*X/XOLD(I,M)
      IFR= 10.*LOGF(FREQ/FREQ1(IFREQ))/.69315 +1.
      IDIF = IFR-NFREQ
      IF(IDIF) 358,362,358
  358 IF(DSPL(NFREQ,KA,MIX+1) 362,362,363
      IF(MIX-20)363,364,364
  363 MIX = MIX +1
      GO TO 357
  362 DSPL(NFREQ,KA,MIX)=DSPL(NFREQ,KA,MIX)+DSL*CA/P12*FLPH1/A5R
  364 DSPS(NFREQ)=DSPS(NFREQ)+DSL*CA/P12*FLPH1/A5R
      DSL=0.
      GO TO (356,506),LFINL
  356 DDSPL = DSFL(I,M)*DXBM**-7/(1.-DLNUC)*UCONN*ATTN
      NFREQ = NFREQ
  226 DDSPL = DSFL(I,M)*DXBM**-7/(1.-DLNUC)*UCONN*ATTN
      IF(I-1) 273,273,276
  275 IF(I-ISSY) 276,273,273
  273 DDSPL=DDSPL/2.
  276 DSL = DSL+DDSPL
      U8=UN(I,M)**8
      U81=U81+U8*DEPH1*DESIG
      WRITE OUTPUT TAPE NTB,20,RR,PHI,TAU,DXDB,ATTN,DLNUC,DDSPL,FREQ,X
      GO TO 166
C
C                MASS MOMENTUM AND ENERGY INTEGRATIONS
C
C
  344 TMAS1=SIG*RHO*UN(I,M) *DESIG*DEPH1
      TM1=TMAS1*UN(I,M)
      TNTP1=TNTLP*TMAS1
      GO TO (284,278),NVPAS
  284 IF(I-1) 277,277,283
  283 IF(I-ISSY) 278,277,277
  277 TMAS1=TMAS1/2.
      TM1=TM1/2.
      TNTP1=TNTP1/2.
  278 TMAST = TMAST + TMAS1
      TMIT = TMIT + TM1
      TNTPT = TNTPT + TNTP1
      IX=X/CDIM*2.
  233 GO TO (166,203,209,212),MAT
C                    TERMINATION OF ANGLE LOOP
C
  166 XOLD(I,M) = X
      LINE3=LINE3+1
      LINE6=LINE6+1
      LINE7=LINE7+1
      IF(LINE3-40) 241,241,244
  241 WRITE OUTPUT TAPE NT3,300,BM,NC
  244 IF(LINE6-40) 242,242,245
  242 WRITE OUTPUT TAPE NT6,300,BM,NC
  245 IF (LINE7-40) 243,243,152
```

```
  243 WRITE OUTPUT TAPE NT7,300,BM,NC
  152 PHI=PHI+DPHI
C
                        TERMINATION OF RADIUS LOOP
      SIG=SIG+DSIG-BUG
  286 BUG=0.
      GO TO (998,998,288),IBPAS
  288 RADL = SIG
      MRADL = M
      BMOLD = BM
      GO TO (326,325),MBPAS
  325 BM = BMINT
      GO TO 327
  326 BM=-FREQJ * BM
      LFINL=2
      GO TO 357
C
C                               ACOUSTIC BAND SEARCH AND ADDITION
C
      CALL ORDERS (NOCFD,DSPS,ISPL)
      JK=1
      JMI=1
      JEND=0
      JDFSG=10/OCTD
      NOJ=NOCFD-1
      NOJP=NOCFD
  459 DO 453 JM=JMI,NOJ
      IF(DSPS(JM) 453,453,458
  458 JP=JM+1
      DO 451 J=JP,NOJP
      GO TO (457,455),JK
  457 IF(DSPS(J)) 454,454,455
  454 NFSIG=NOJP
      GO TO 456
  455 ISPLD=ISPL(J)-ISPL(JM)
      IF(ABSF(ISPLD)-JDFSG) 452,452,451
  452 DSPS(JM)=DSPS(JM)+DSPS(J)
      ISPL(JM)=(DSPS(J)*FLOATF(ISPL(J))+DSPS(JM)*FLOATF(ISPL(JM)))/(DSPS
     1(JM)+DSPS(J))
      ISPL(J)=-99
      DSPS(J)=-1.
      JEND=1
  451 CONTINUE
      JSIG=JMI
      IF(JEND) 374,374,453
  453 CONTINUE
      GO TO 374
  456 NOJ=NFSIG-1
      NOJP=NFSIG
      JMI=2
      JK=2
      GO TO 459
  374
C                           INNER INDEX DETERMINATION
C
  327 NMJMX=(20.*BM/RADC+10.)/SET2 +1.
      IF(NMJMX-20 ) 600,600,601
```

```
  601 SET2 = SET2*2.
      ISET = ISET + 1
      MRADL=(MRADL+1)/2
      NMDOJ = SET2
      GO TO 327
      NMDOJ = 2 ** ISET
  600 ISETI = LOGF ( BM/(CDIM * 0.15))
      SETI2=2**ISETI
      IF (NMDOM-8) 531,532,532
  531 NMDOM= SETI2
  532 DEL = NMDOM
      SETI=ISETI
                        TERMINATION OF BM LOOP
C
      WRITE OUTPUT TAPE NT3,303
      DO 141 IFREQ=1,NOCT
      WRITE OUTPUT TAPE  NT3,5,BM,SPS(IFREQ),IFREQ,U81
  141 CONTINUE
  185 CONTINUE
```

This section not operational

```
C                       BAND ASSIGNMENT AND SHIFT
C
  383 DO 386 IF=1,NOCT
       KSIG = 0
      MIXT=20
      DO 386 M= 1,MIXT
      CALL          ORDERS (NMBM,DSPL,KAPP)
      DO 386 KA= 2,NMBMP
      MIXT=MIXM(M)
      NDRAT = 1
      IF (DSPL(IF,KA,M) 391,395,395
  391 IF(IF-1) 395,395,665
  665 IF(DSPL(IF-1,KA,M) 393,394,394
  393 IF(IF-2) 395,395,666
  666 IF(DSPL(IF-2,KA,M) 395,396,396
  396 NDRAT=2
  394 IF (IF-(NOCT-1)) 667,395,395
  667 IF(DSPL(IF+1,KA,M) 397,398,398
  397 IF(IF-(NOCT-2)) 668,395,395
  668 IF(DSPL(IF+2,KA,M) 395,399,399
  395 GO TO 392
  398 GO TO (661,662), NDRAT
  661 DSPL(IF,KA,M) = (DSPL(IF-1,KA,M) + DSPL(IF +1,KA,M))/2.
  662 DSPL(IF,KA,M) = (DSPL(IF-2,KA,M) + DSPL(IF+1 ,KA,M))/2.
  399 GO TO (663,664), NDRAT
  663 DSPL(IF,KA,M) = (DSPL(IF-1,KA,M) +DSPL(IF+2,KA,M))/2.
  664 DSPL(IF,KA,M) = (DSPL(IF-2,KA,M) + DSPL(IF+2,KA,M))/2.
      KAD = KAFP(KA+1)-KAFP(KA)
      IF (ABSF (KAD)-1) 385,385,386
  385 KAPP = KAFP(KA+1)
      KSIG = 1
      IF (DSPL(IF+1,KAPP,M)) 387,387,388
  387 DSPL(IF+1,KAPP,M)  = DSPL(IF,KAPP,M)
  388 IF(DSPL(IF-1,KAPP,M) 389,389,391
  389 DSPL(IF-1,KAPP,M)  = DSPL(IF,KAPP -1,M)
  392 DSPL(IF,KAPP,-1,M) = (DSPL(IF,KAPP-1,M) + DSPL(IF,KAPP,1))/2.
  386 CONTINUE
```

```
      IF(KSIG-1) 390,383,383
  390 DO 384 IF=1,NOCT
      DO  384 M=1,20
      DO  384 KA=2,NMBM
      SPL (IF)= DSPL(IF,KA,M) +SPL(IF)
      SAFD  =SPL(IF)/0.000000000000!        +1.
      DB(IF)=10*LOGF(SAFD)//0.268
  384 WRITE OUTPUT TAPE NT3,23,IF,FRE1(IF),DB(IF)
      CALL COPY(NT6,1)
      CALL COPY(NT7,1)
      CALL COPY (NT8,1)
      END FILE NT4
  999 CONTINUE
      REWIND NT4
      CALL EXIT
      END
```

```
      SUBROUTINE FLMA(NC,I,M,KA)
      COMMON  PI,PI2,PRADL,PRASQ,FREQJ,IMH,BM,XE,NEST,NUM,LEAV,PHI,ALPO,
     1RA,SIG,CDIM,ISAP,BMINT,RADC,SF,SH,SJR,SJC
      DIMENSION MML(8),KAL(8),SF(30),SH(30),SJR(30),SJC(30),SFP(  ,  ),S
     1HP(  ,  ),SJCP(  ,  ),SJRP(  ,  )
      IF(NC-1)99,20,50
   20 IF(I-1) 99,21,25
   21 IF(M-1) 99,22,28
   22 IAL=1
      IF(KA-1)99,23,27
   23 FRLO=LOGF(FREQJ)
      RABI=RADC/BMINT
      SET2=1.
      MML(1)=1
      IFG=1
      MAXM=0
      MIT=1
   24 KAL(MIT)=LOGF(RABI*(SET2-.5)/FRLO+1.9999
      IF(KAL(MIT)-NMBM)25,40,26
   25 MIT=MIT+1
      SET2=SET2+SET2
      GO TO 24
   26 KAL(MIT)=NMBM
      GO TO 40
   27 REWIND NT5
      IJU=NMDOJ
      MLO=1
      GO TO 34
   28 MIT = (M-1)*NMDOJ
      IF(MIT-MAXM) 30,30,29
   29 MAXM=MIT
      MML(ISET)=M
      IFC=1
      GO TO 40
   30 MLO=MLO+MJU
      IF(MLO-MML(IAL) 32, 32,31
   31 IJU=MJU/2
      MLO=MLO-IJU*(M-1)
      MJU=IJU*(3-M)+(MML(IAL)-1)/2
      IAL=IAL+1
   32 MIT=MJU-1
      CALL FILE(NT5,MIT)
   34 MJU=IJU
      IFC=0
      GO TO 38
   35 IF(IFC)99,36
   36 DO 37 MAT=2,IJU
   37 READ TAPE NT5, MIT
   38 READ TAPE NT5,MIT,MAT,((SFP(KAP,K),SHP(KAP,K),SJCP(KAP,K),SJRP(KAP
     1,K),KAP=MIT,MAT),K=2,NEST )
   33 DO 39 K=2,NEST
      SF(K)=SFP(KA,K)
      SJR(K)=SJRP(KA,K)
      SJC(K)=SJCP(KA,K)
   39 SH(K)=SHP(KA,K)
      WRITE TAPE NT4, (SF(K),SH(K),SJR(K),SJC(K),K=2,NEST)
      RETURN
```

```
   40 M2=N
      I2=I
      IL=ISET
   41 IF(MODF(M2,2) 99,42,44
   42 IF(MODF(I2,2) 99,43,44
   43 IL=IL+1
      M2=M2/2
      I2=I2/2
      GO TO 41
   44 KALI=KAL(IL)
      MIT=KALI-KA+1
      CALL FLUX (MIT),SFP,SHP,SJCP,SJRP
      WRITE TAPE NT5,KA,KALI,((SFP(KAP,K),SHP(KAP,K),SJCP(KAP,K),SJRP(KA
     1P,K),KAP=KA,KALI),K=2,NEST)
      IF(I-ISSY) 33,49,99
   49 END FILE NT5
      GO TO 33
   50 READ TAPE NT4,(SF(K),SH(K),SJR(K),SJC(K),K=2,NEST)
      RETURN
   99 HALT
      END
C
C
      SUBROUTINE FLUX(MIT,SFP,SHP,SJCP,SJRP)
      COMMON  PI,PI2,PRADL,PRASQ,FREQJ,IMH,BM,XE,NEST,NUM,LEAV,PHI,ALPO,
     1RA,SIG,CDIM,ISAP
      DIMENSION SIC(  ),SIR(  ),VI(  ),TI(  ),CMX(  ),VAO(  ),TAO(  ),SA
     1RO(  ),SACO(  ),XE(30),NUM(30),LEAV(30),ISAP(30),ALPO(30),DALP(80,
     230),RA(80,30),SFP(  ,30),SHP(  ,30),SJCP(  ,30),SJRP(  ,30)
      DO 193 K=2,NEST
      NODE = 2
      BO=BM
      DO 201 IB=1,MIT
      SIC(IB)=0.0
      SIR(IB)=0.0
      VI(IB)=0.0
      TI(IB)=0.0
      CMX(IB)=BO+XE(K)
  201 BO=BO*FREQJ
      NUMK= NUM(K)
      LEAF=LEAV(K)
      ISAPE=ISAP(K)
   30 PHAL=PHI-ALPO(K)
   31 ABPA=ABSF(PHAL)
      IF(ABPA-PI)34,34,32
   32 PHAL=PHAL-SIGNF(PI2,PHAL)
   33 GO TO 31
   34 COSPA=COSF(ABPA)
      RADO=SQRTF((RA(NUMK,K)-SIG)*(RA(NUMK,K)-SIG)+2.*RA(NUMK,K)*SIG*
     1(1.-COSPA))
      IF (RADO-0.0005 * CDIM) 35,35,36
      RADO=0.0
   35 NODE = 1
      GO TO (44,36,44),ISAPE
   36 COSTO=(SIG-RA(NUMK,K)*COSPA)/RADO
      IF(ABSF(COSTO)-1.0)38,37,37
   37 TNO=(PI-SIGNF(PI,COSTO))/2.
```

```
      SINTO= 0.0
      GO TO 39
   38 SINTO = SIGNF (SQRTF (1. -COSTO*COSTO),PHAL)
   40 THO=ATANF(SINTO/COSTO)
      IF(COSTO) 151,152,152
  151 THO=THO+PI
      GO TO 154
  152 IF(THO) 153,154,154
  153 THO=THO+PI2
  154 GO TO (39,143,39),ISAPE
      CL=RADO/RA(1,K)
      CRA=RA(1,K)
      CALL CFLUX(MIT,VI,TI,SIC,CL,CRA)
      DO 210,IB=1,MIT
      SIR(IB)=SIC(IB)*COSTO
      SIC(IB)=SIC(IB)*SINTO
      SIC(IB)=SIR(IB)*SINTO
      SIR(IB)=SIR(IB)*COSTO
      GO TO 143
   39 DO 203 IB=1,MIT
      RADX = RADO/CMX(IB)
      VAO(IB)=1.-EXPF (-RADX*RADX)
      GO TO (41,42),IMH
   41 TAO(IB)=1.-EXPF(-(RADX*PRADL)*(RADX*PRADL))
   42 SA     =(0.88623*ERRORF(RADX) + RADX * (VAO(IB)-1.0))*CM
      SARO(IB)=SA     *COSTO
      SACO(IB)=SA     *SINTO
  203 CONTINUE
C
C     LEAF INTEGRATION
C
   44 DO 134 J=1,LEAF
      DO 134 N=1,NUMK
   46 PHAL = PHAL - DALP(N,K)
   47 ABPA = ABSF (PHAL)
      IF (ABPA - PI) 50,50,48
   48 PHAL = PHAL - SIGNF(PI2,PHAL)
   49 GO TO 47
   50 COSPA = COSF(ABPA)
      RAD = SQRTF((RA(N,K)-SIG)*(RA(N,K)-SIG)+2.*RA(N,K)*SIG*(1.-
     1COSPA))
      IF (RAD -0.0005 * SIG) 51, 51, 52
   51 NODE = 1
      GO TO 132
   52 COST = (SIG-RA(N,K)*COSPA)/RAD
      IF(ABSF(COST )-1.0)54,53,53
   53 TH =(PI-SIGNF(PI,COST ))/2.
      SINT = 0.0
      GO TO 62
   54 SINT = SIGNF(SQRTF(1. -COST * COST),PHAL)
   56 TH=ATANF(SINT/COST)
      IF(COST)   161,162,162
  161 TH=TH+PI
      GO TO 59
  162 IF(TH) 163,59,59
  163 TH=TH+PI2
   59 GO TO (60,62),NODE
```

```
   60 NODE = 2
      DTH = 0.0
      GO TO 121
   62 DTH = TH - THO
   63 ABDTH = ABSF(DTH)
      IF(ABDTH - DTHM)121,121,65
   65 IF(ABDTH - PI)66,66,101
C
C     0 - 360 CORRECTION
C
  101 THO = THO + SIGNF(PI2,DTH)
  106 GO TO 62
C
C     INITIATION OF AUXILIARY INTEGRATION
C
   66 LQ=ABDTH/DTHM+1.
      Q = LQ
   68 DTH=DTH/Q
      RCRC = RADO*COSTO - RAD*COST
      RCRC = RCRC + SIGNF(0.00000001, RCRC)
   70 ABLE=(RADO*SINTO-RAD*SINT)/RCRC
   71 BKR=RADO*SINTO-ABLE*RADO*COSTO
C
C     AUXILIARY INTEGRATION
C
   75 DO 92 L=1,LQ
   76 TH=THO + DTH
   77 COST = COSF(TH)
   79 SINT=SINF(TH)
   80 RAD=BKR/(SINT-ABLE*COST)
      DO 204 IB=1,MIT
      RADX=RAD/CMX(IB)
   81 VA = 1. - EXPF (-RADX * RADX)
   83 SA =(0.88623 * ERRORF(RADX) + RADX * (VA-1.0))*CM
   84 SAR = SA * COST
      SAC = SA * SINT
   86 VI(IB)=VI(IB)+(VA+VAO(IB))*DTH
   89 SIC(IB)=SIC(IB)+(SAC+SACO(IB))*DTH
   88 SIR(IB)=SIR(IB)+(SAR+SARO(IB))*DTH
      GO TO (90,91),IMH
   90 TA=-EXPF(-RADX*PRADL)*(RADX*PRADL))+1.
      TI(IB)=TI(IB)+(TA+TAO(IB))*DTH
      TAO(IB)=TA
   91 VAO(IB)=VA
      SACO(IB)=SAC
      SARO(IB)=SAR
  204 CONTINUE
   92 THO  = TH
   93 GO TO 132
C
C     MAIN LINE INTEGRATION
C
  121 DO 205 IB=1,MIT
      RADX=RAD/CMX(IB)
      VA =-EXPF (-RADX * RADX) + 1.
  122 SA =(0.88623 * ERRORF(RADX) + RADX * (VA-1.0))
      SAR = SA * COST
```

```
  124 SAC = SA * SINT
      VI(IB)=VI(IB)+(VA+VAO(IB))*DTH
  126 SIR(IB)=SIR(IB)+(SAR+SARO(IB))*DTH
      SIC(IB)=SIC(IB)+(SAC+SACO(IB))*DTH
      GO TO (127,128),IMH
  127 TA=-EXPF(-(RADX*PRADL)*(RADX*PRADL))+1.0
      TI(IB)=TI(IB)+(TA+TAO(IB))*DTH
      TAO(IB)=TA
  128 VAO(IB)=VA
      SACO(IB)=SAC
      SARO(IB)=SAR
  205 CONTINUE
      THO = TH
  132 RADO = RAD
      COSTO = COST
  134 SINTO = SINT
  143 SFP(IB,K)=VI(IB)
      GO TO (191,192) IMH
  192 TI(IB)=VI(IB)
  191 SHP(IB,K)=TI(IB)
      SJCP(IB,K)=SIC(IB)
  193 SJRP(IB,K)=SIR(IB)
      RETURN
      END
C
C
      SUBROUTINE CFLUX (MIT,VS,TS,SSC,CL
      COMMON  PI,PI2,PRADL,PRASQ,FREQJ,IMH,IM,XE
      DIMENSION ARR(40),VS(30),TS(30),SSC(3)), XE(20),SFL(40)
      ISJ=1
      DL1=20.
      DL2=4.
      EXPOC=(1.-CL)*(1.-CL)
      CL1=1./CL
      CL2=CL+CL1
      CL1=CL-CL1
      VL=ABSF(CL-1.)
      DL=MAX1F(CL/DL1,(CL-1.)/DL2)
      VLO=VL
      B=0.16666667
      A=0.33333333
      SFO=0.
      SFL(1)=0.
C     INCREMENTS AND AREAS
      IF(CL-1.) 203,204,204
  204 NS=1./DL+.9999
      VN=NS
      DL=1./VN
      ARR(1)=0.
      GO TO 206
  203 NS=CL/DL+.99999
      IF(NS) 231,231,224
  224 VN=NS
      DL=CL/VN
      ARR(1)=PI*EXPOC
  206 NS=NS+NS+1
      DO 215  IS=2,NS
```

```
      VL=VL+DL
      VLS=VL*VL
      CPHI2=CL1/VL+VL/CL
      SPHI2=SQRTF(4.-CPHI2*CPHI2)
      PHI=ATANF(SPHI2/CPHI2)
      IF(PHI) 214,215,215
  214 PHI=PHI+PI
      CTHE2=CL2-VLS/CL
      THE=ATANF(SQRTF(4.-CTHE2*CTHE2)/CTHE2)
      IF(THE) 217,275,275
  217 THE=THE+PI
  275 SFL(IS)=(B*SFO+A*SPHI2)*DL       +SFL(IS-1)
      SFO=SPHI2
      C=A
      A=B
      B=C
  215 ARR(IS)=VLS*PHI+THE-VL/CL3*SPHI2
C     FLUX INTEGRATIONS AT SEQUENTIAL B PLANES
      BO=BM
      DO 233 IB=1,MIT
      VI=0.
      TI=0.
      SIC=0.
      BD=BO+XE(K)
      IF(BD) 280,280,281
  280 XSQ=1000000.
      GO TO 296
  281 XSQ=CRA /BD
      XSQ=XSQ*XSQ
  201 BO=BO*FREQJ
      IS=ISJ+1
      ISO=1
      DLJ=DL*FLOATF(ISJ)
      VL=ABSF(CL-1.)
      VL=VL+DLJ/2
  272 VLS=VL*VL
      EXPAR=VLS*XSQ
      EXPV2=EXPF(-EXPAR/2.)
      EXPV=EXPV2*EXPV2
      ARD=ARR(IS)-ARR(ISO)
      VI=VI+ARD*EXPV
      GO TO (270,271),IMH
  270 TI=TI+ARD*EXPF(-EXPAR*PRASQ)
  271 SIC     =SIC     +EXPV*(1.+EXPAR+EXPAR-EXPV2)*(SFL(IS)-SFL(ISO))
      ISO=IS
      VL=VL+DLJ
      IS=XMINOF(IS+ISJ,NS)
      IF(ISO-NS) 272,296,296
  296 VS(IB)=VI/PI*XSQ
      TS(IB)=TI/PI*XSQ
      SSC(IB)=SIC/PI*XSQ
      IF(ARR(1)) 233,233,298
  298 VS(IB)=1.-EXPF(-EXPOC*XSQ     )+VS(IB)
      GO TO (299,295),IMH
  295 TS(IB)=VS(IB)
      GO TO 233
  299 TS(IB) = 1.-EXPF(-EXPOC*XSQ     *PRASQ)+TS(IB)
```

```
233 CONTINUE
    RETURN
    END
```

LIST OF SYMBOLS

A	area
A_c	area of circle having a radius equal to $R_{c,e}$
A_n	nozzle exit area
C_a	acoustic constant
C_{b1}, C_{b2}	constants
C_f	frequency constant
C_x	length constant
E_f	porosity parameter for attenuation
H	enthalpy flux function (Eq. (7))
K	concentration flux function (Eq. (7))
M	Mach number
M_c	convective Mach number
M_f	momentum flux function (Eq. (5))
P	pressure (static)
P_a	acoustic power
Pr	Prandtl number
R	geometric radius (circular nozzle exit radius)
R'	flow-field coordinate
R_c	largest radius of the mixed flow field
R_g	gas constant
T	temperature

U	bounding velocity
U_c	convective velocity
V	volume
X_e	attenuation length measure
a	acoustic velocity
b_m	momentum spreading parameter
b_h	enthalpy spreading parameter
c	coefficient
c_p	specific heat
c_{p_m}	mean specific heat
f	frequency
f_m	frequency at point of maximum noise production
f_s	frequency determined by Strouhal relation
h	enthalpy
h_r	relative enthalpy (Eq. (A.17))
k	local concentration
k_e	eddy heat-condution coefficient (Eq. (A.3))
r	radial coordinate (polar) (for elemental jet flows) (Fig. 10)
r'	variable of integration (Fig. 10)
s	polar coordinate (radial) (Fig. 10)
t	temperature (variable of integration)
$\bar{u}$	local mean velocity, (x-directed)
u'	fluctuating component of the x-directed velocity
$\bar{v}$	local mean velocity (r-directed)

v'	fluctuating component of the r-directed velocity
w	watts
x	axial coordinate
$\overline{\Delta v}$	space correlated mean eddy volume
α	attenuation energy ratio, coordinate angle (Fig. 10)
α_K	Kirchhoff attenuation parameter
γ	ratio of specific heats
λ	specific heat coefficients
η_e	eddy viscosity coefficients
ρ	density
τ	shear stress
θ	angle coordinate (Fig. 10)
ξ	velocity parameter (Eq. (8b))
σ	eddy characteristic dimension

Subscripts

1, 2	adjacent gas flows
e	exit
i	gas (concentration) index
i,j	tensor components
o	ambient
m	maximum
n	exit element index
r	relative (enthalpy) (Eq. (A.17))
s, ϕ	vector directions

Superscripts

o	stagnation
—	mean

REFERENCES

1. Lee, R., Kendall, R. M., et al.: Research Investigation of the Generation and Suppression of Jet Noise. General Electric Co., Rept. under Contract Noas-59-61610-c, January 1961, ASTIA Doc. AD-251-887.

2. Sabin, C. M.: An Analytical and Experimental Study of the Plain, Incompressible Turbulent Free Shear Layer with Arbitrary Velocity Ratio and Pressure Gradient. MD-9, Dept. of Mechanical Engineering, Stanford University, 1963.

3. Willis, D. Roger, Glassman, Irvin: The Mixing of Unbounded Co-Axial Compressible Streams, Project Squid, Technical Report PR-70-P, Princeton University, Princeton, New Jersey, November 1957.

4. Marshall, L. A., Bailey, R. N.: Turbulent Mixing of Parallel Streams in Enclosed Passages, Aircraft Gas Turbine Division, General Electric Company, Cincinnati 15, Ohio, January 1958.

5. Weinstein, Alvin S.: Diffusion of Momentum From Free and Confined Slot Jets Into Moving Secondary Streams, Carnegie Institute of Technology, Department of Mechanical Engineering, Pittsburgh, Pennsylvania, Scientific Report No. 2, under Contract No. AF 18(600)-969, Supplemental Agreement 2(54-925), May 4, 1955, AFCRC-TN-55-476.

6. American Institute of Physics Handbook, pp. 3 - 49, 1957.

7. Laurence, James C.: Intensity, Scale, and Spectra of Turbulence in Mixing Region of Free Subsonic Jet, National Advisory Committee for Aeronautics, Report 1292, 1956.

8. Korst, H. H., Chow, W. L., and Zumwalt, G. W.: Research on Transonic and Supersonic Flow of a Real Fluid at Abrupt Increases in Cross Section. Final Report, M. E. Tech. Rept. 392-5, Univ. of Illinois, Urbana, Illinois, Dec. 1959.

9. Korst, H. H.: A Theory for Base Pressure in Transonic and Supersonic Flow. Jour. of Applied Mechanics, vol. 23, 1956, pp. 593-600.

10. Ragsdale, W. C.: An Experimental Study of Supersonic Mixing. NASA X62-11367, June 15, 1962.

11. Marshall, L. A. and Bailey, R. N.: Turbulent Mixing of Parallel Streams in Enclosed Passages. AGT - Tech. Information Series R58AGT44, Aircraft Gas Turbine Div., General Electric Co., January 1958.

12. Uchida, Shigeo: On Turbulent Free Mixing of Parallel Streams of Two Different Gases. Polytechnic Inst. of Brooklyn, N. Y., ASTIA Doc. AD 260 302, June 1961.

13. Constant Area Mixing of Non-Isoenergetic Co-Axial Compressible Streams. Rept. No. AEDC-TR-61-18, January 1962.

14. Reichardt, H.: New Theory of Free Turbulence. Aeit. Ang. Math. and Mech., vol. 21, 1941, p. 21, Roy. Aero. Soc. Jour., vol. 47, 1943, p. 167.

15. Alexander, Lloyd G., Baron, Thomas and Comings, Edward W.: Transport of Momentum, Mass, and Heat in Turbulent Jets, University of Illinois Engineering Experiment Station, Bulletin Series No. 413.

16. Johannesen, N. H.: Further Results on the Mixing of Free Axially Symmetrical Jets of Mach Number 1.40, Aeronautical Research Council. May 6, 1959, 'A.1' Report.

17. Napolitano, Luigi G.: Two-Dimensional Plane Mixing of Homogeneous and Non-Homogeneous Streams, Polytechnic Institute of Brooklyn, Department of Aeronautical Engineering and Applied Mechanics, November 1957, PIBAL Report No. 400. AFOSR TN-57-756, AD 136 745.

18. Ting, Lu: On the Mixing of Two Parallel Streams, Polytechnic Institute of Brooklyn, Department of Aeronautical Engineering and Applied Mechanics, July 1958, PIBAL Report No. 441. AFOSR TN 58-628, AD 162 158. See also: J. Math. & Phys., vol. 38, no. 3, p. 153, Oct. 1959.

19. Napolitano, Luigi G.: High Speed Machine Solutions for Plane Turbulent Homogeneous and Non-Homogeneous Mixing, Polytechnic Institute of Brooklyn, Department of Aeronautical Engineering and Applied Mechanics, October 1957, PIBAL Report No. 399, AFOSR TN-57-755, AD 136 744.

20. Laurence, James C., and Stickney, Trumen M.: Further Measurements of Intensity, Scale, and Spectra of Turbulence in a Subsonic Jet, Lewis Flight Propulsion Laboratory, Cleveland, Ohio, National Advisory Committee for Aeronautics, Technical Note 3576, October 1956.

21. Laurence, James C.: Turbulence Studies of a Rectangular Slotted Noise-Suppressor Nozzle, Lewis Research Center, Cleveland, Ohio, Technical Note D-294, NASA, Sept. 1960.

22. Mixing of Compressible Fluid Streams, United Aircraft Corporation, Research Department, East Hartford, Conn., Report R-12006-02, Reported by: K. K. Klingensmith, Approved by: Reeves Morrison, February 17, 1948, Copy No. 34.

23. Horst, H. H., and Chow, W. L.: Compressible Non-Isoenergetic Two-Dimensional Turbulent ($P_{r_t} = 1$) Jet Mixing at Constant Pressure - Auxiliary Integrals Heat Transfer and Friction Coefficients for Fully Developed Mixing Profiles, Mechanical Engineering Department, Engineering Experiment Station, University of Illinois, Urbana, Illinois, MD Technical Note 392-4, January 1959.

24. Rosensweig, Ronald E.: Measurement and Characterization of Turbulent Mixing, Fuels Research Laboratory, Department of Chemical Engineering, Massachusetts Institute of Technology, May 18, 1959.

25. Landis, Fred and Shapiro, Ascher H.: The Turbulent Mixing of Co-Axial Gas Jets, September 1950.

26. Corrsin, Stanley and Uberoi, Mahinder S.: Further Experiments on the Flow and Heat Transfer in a Heated Turbulent Air Jet, Report 998, California Institute of Technology.

27. Hoge, Harold J.: On the Theory of Mixing of Fluid Streams, Headquarters, Quartermaster Research & Engineering Command, US Army Quartermaster Research & Engineering Center, Natick, Massachusetts, Pioneering Research Division, Technical Report PR-2, Project Reference: 7-99-01-001, February 1959.

28. Torda, T. P., and Stillwell, H. S.: Analytical and Experimental Investigations of Incompressible and Compressible Mixing of Streams and Jets, WADC Technical Report 55-347, University of Illinois, March 1956, Wright Air Development Center.

29. Bailey, Harry E., and Kuethe, Arnold M.: Supersonic Mixing of Jets and Turbulent Boundary Layers, Department of Aeronautical Engineering, University of Michigan, June 1957, Wright Air Development Center, WADC Technical Report 57-402, ASTIA Document No. AD 150992.

30. Johannesen, N. H.: The Mixing of Free Axially Symmetrical Jets of Mach Number 1.40, Aeronautical Research Council, Department of the Mechanics of Fluids, University of Manchester, Communicated by D.G.S.R.(A), Ministry of Supply, January 14, 1957, A 1 Report, 18 967 FM 2490.

31. Richards, E. J.: Note on the Effect of Velocity Profile on Jet Noise, Aeronautical Research Council, December 8, 1958, 'A.3' Report. A.R.C.20,606, N.59, E.A.659, A.C.538.

32. Franklin, R.E., and Foxwell, J.H.: Pressure Fluctuations Near a Cold, Small-Scale Air Jet (Measurement of Space Correlations), Department of Aeronautical Engineering, University of Southampton, Ministry of Aviation, Aeronautical Research Council Reports and Memoranda, London: Her Majesty's Stationery Office, 1960. R. & M. N°. 3162.

33. Appleton, J.P., and Davies, H. J.: Theoretical Investigation of the Sound Field Produced Downstream of a Choked Two-Dimensional Channel Due to Unsteady Upstream Entropy Fluctuations, Department of Aeronautical Engineering, University of Southampton, Ministry of Supply, Aeronautical Research Council Current Papers, London: Her Majesty's Stationery Office, 1959, C.P. No. 461.

34. Research in Acoustics and Hydrodynamics at Eight British Universities and Technical Colleges, Office of Naval Research, London, Technical Report ONRL-47-57, American Embassy, London, England, April 23, 1957.

35. Mayes, William H., Lanford, Wade E., and Hubbard, Harvey H.: Near-Field and Far-Field Noise Surveys ofSolid-Fuel Rocket Engines for a Range of Nozzle Exit Pressures, Technical Note D-21, Langley Research Center, Langley Field, Va., August 1959.

36. Cheng, Sin-I: On the Aerodynamic Noise of a Jet, General Applied Science Laboratories, Inc., Westbury, L. I., New York, GASL Technical Report No. 148, Contract No. AF 49(638)-194, April 1959. AFOSR TN-59-1308.

37. Lee, R. and Wenzelberger J.: Correlation Between the Sound Power Spectrum of a Free Jet and Its Aerodynamic Characteristics, IAS Paper No. 59-106, Presented at the IAS National Summer Meeting, Los Angeles, California, June 16-19, 1959. General Electric Company.

38. Moretti, Gino and Slutsky, Simon: The Noise Field of a Subsonic Jet, General Applied Science Laboratories, Inc., Westbury, L. I., New York, GASL Technical Report No. 150, Contract No. AF 49(638)-194, November 1959. AFOSR TN-59-1310.

39. Smith, E. B.: Noise Reduction by Interfering Jets, Flight Propulsion Laboratory Department, Aircraft Gas Turbine Division, General Electric Company, Cincinnati 15, Ohio. November 1958. R58AGT876.

40. Lassiter, Leslie W., and Hubbard, Harvey H.: The Near Noise Field of Static Jets and Some Model Studies of Devices For Noise Reduction, National Advisory Committee for Aeronautics, Report 1261. 1956.

41. Howes, Walton L., Callahan, Edmund E., Coles, Willard D., Mull, Harold R.: Near Noise Field of a Jet-Engine Exhaust, National Advisory Committee for Aeronautics, Report 1338, 1957.

42. Ribner, H. A.: The Sound Generated by Interaction of a Single Vortex With a Shock Wave, Institute of Aerophysics, University of Toronto, June 1959, UTIA Report No. 61.

43. Howes, Walton L.: Similarity of Near Noise Fields of Subsonic Jets, Lewis Research Center, Cleveland, Ohio, Technical Report R-94, NASA, 1961.

44. Howes, Walton L.: Similarity of Far Noise Fields of Jets, National Aeronautics and Space Administration, Technical Report R-52, 1960.

45. Mawardi, O. K.: Aero-Thermoacoustics (The Generation of Sound by Turbulence and by Heat Processes), Massachusetts Institute of Technology, Cambridge, Mass.

46. Soehngen, E. E., and Holman, J. P.: Experimental Studies on the Interaction of Strong Sound Fields With Free Convection Boundary Layers, ARL Technical Report 60-323, Aeronautical Research Laboratory Air Force Research Division, October 1960.

47. Ribner, H. S.: A Theory of the Sound from Jets and Other Flows in Terms of Simple Sources, Institute of Aerophysics University of Toronto, UTIA Report No. 67, AFOSR TN 60-950; July 1960.

48. Ribner, H. S.: On the Strength Distribution of Noise Sources Along a Jet, Institute of Aerophysics University of Toronto, UTIA Report No. 51, April 1958.

49. Eckhaus, Wiktor: Some Remarks on the Theory of Noise Generation by Turbulent Shear-Flows, ASRL Technical Report No. 92-2, Massachusetts Institute of Technology, NASA, December 1960.

50. Fitzpatrick, H. M., and Lee, Robert: Measurements of Noise Radiated by Subsonic Air Jets.

51. Fakan, John C., and Mull, Harold R.: Effect of Forward Velocity on Sound-Pressure Level in the Near Noise Field of a Moving Jet, Lewis Research Center, Cleveland, Ohio, Technical Note D-61, NASA, October 1959.

52. Gerrard, J. H.: An Investigation of the Noise Produced by a Subsonic Air Jet, Fluid Motion Laboratory, University of Manchester, Aeronautical Research Council, Communicated by Mr. P. R. Owen, June 30, 1955, A2 Report. 17724, FM 2270.

53. North, Warren J., Callaghan, Edmund E., and Lanzo, Chester D.: Investigation of Noise Field and Velocity Profiles of an Afterburning Engine, Research Memorandum, Lewis Flight Propulsion Laboratory, Cleveland, Ohio, NASA, September 24, 1954, RM E54G07.

54. Lighthill, M. J.: On Sound Generated Aerodynamically. I.- General Theory, Department of Mathematics, The University of Manchester, Communicated by M. H. A. Newman, F.R.S. - Received November 13, 1951.

55. Cole, J. N., Von Gierke, H. E., Kyrazis, D. T., 1/Lt, USAF, Eldred, K. M., Humphrey, A. J., 1/Lt, USAF: Noise Radiation From Fourteen Types of Rockets in the 1,000 to 130,000 Pounds Thrust Range, WADC Technical Report 57-354, AD 130794, Aero Medical Laboratory, Wright Air Development Center, December 1957.

56. Mayes, William H., Lanford, Wade E., Hubbard, Harvey H.: Near-Field and Far-Field Noise Surveys of Solid-Fuel Rocket Engines for a Range of Nozzle Exit Pressures, Technical Note D-21, Langley Research Center, Langley Field, Virginia, NASA, August 1959.

57. Vasiliu, J.: Turbulent Mixing of a Rocket Exhaust Jet With a Supersonic Stream Including Chemical Reactions, J. of the Aerospace Sci., 29, (1), 1962, 19-28.

58. Korst, H. H., Page, R. H., and Childs, M. E.: A Theory for Base Pressures in Transonic and Supersonic Flow, ME TN 392-2, OSR RN 55 39, Univ. of Illinois, Eng. Exp. Station, 1955.

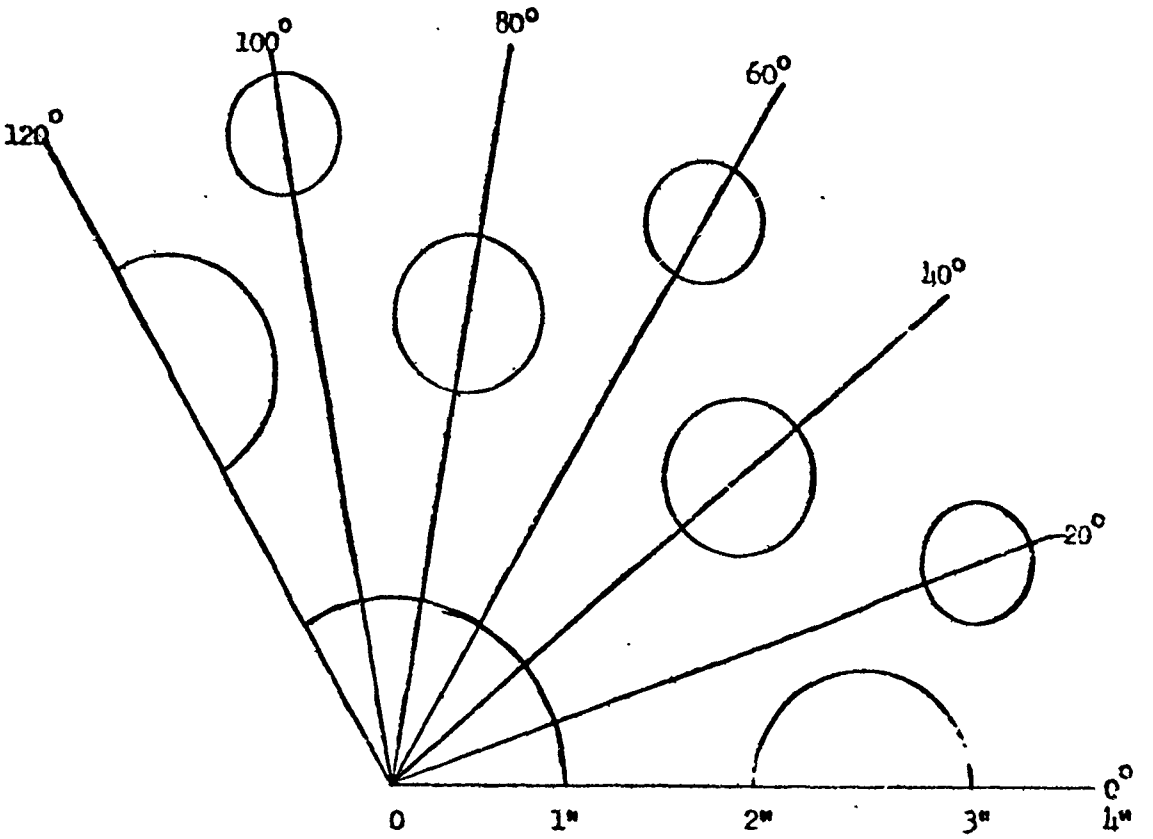

Figure 2.1 - End View of a 120° Sector of the 19 Tube Nozzle

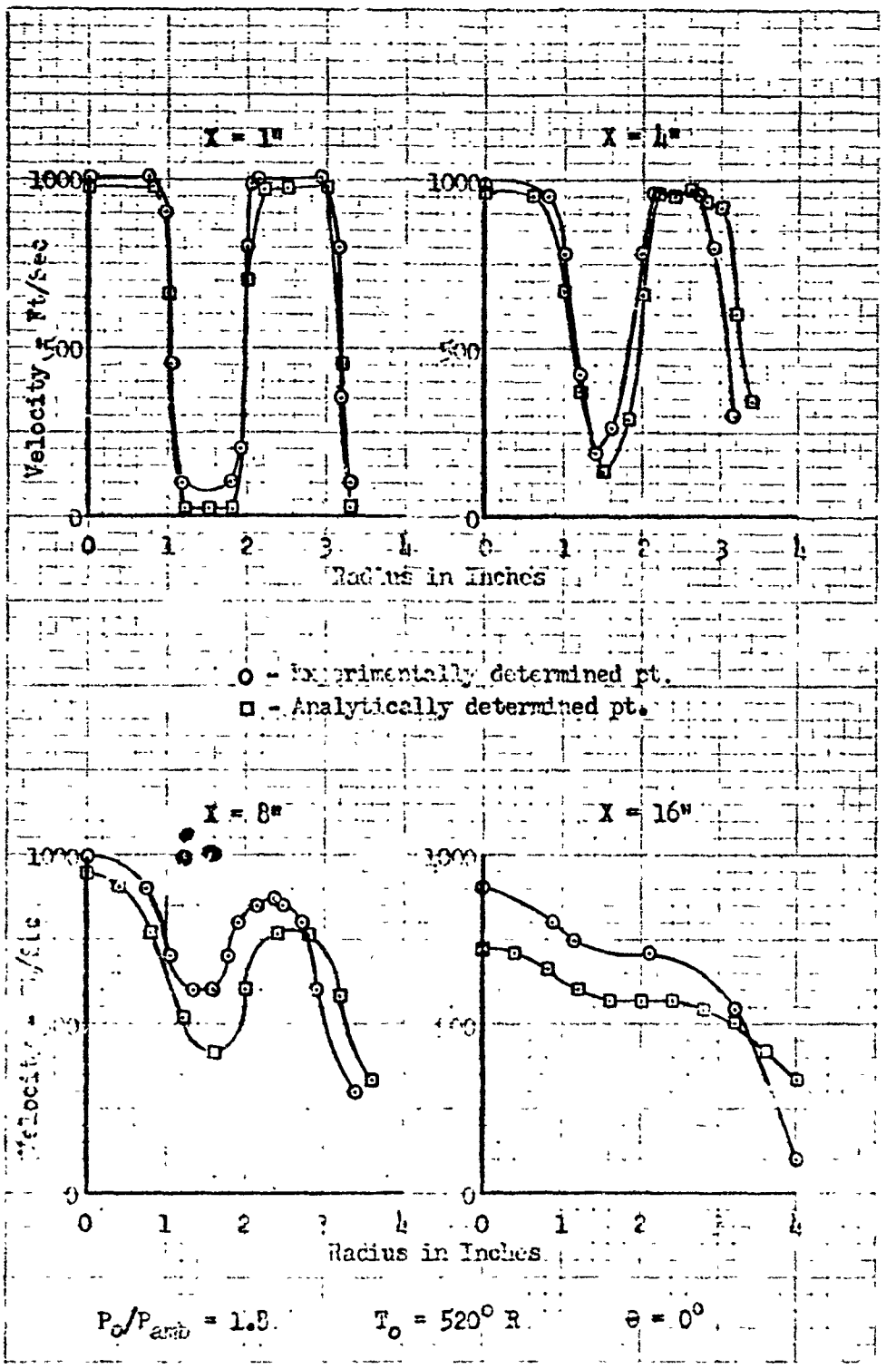

Figure 2.2(a) - Mean Velocity Profiles for the 19 Tube Nozzle

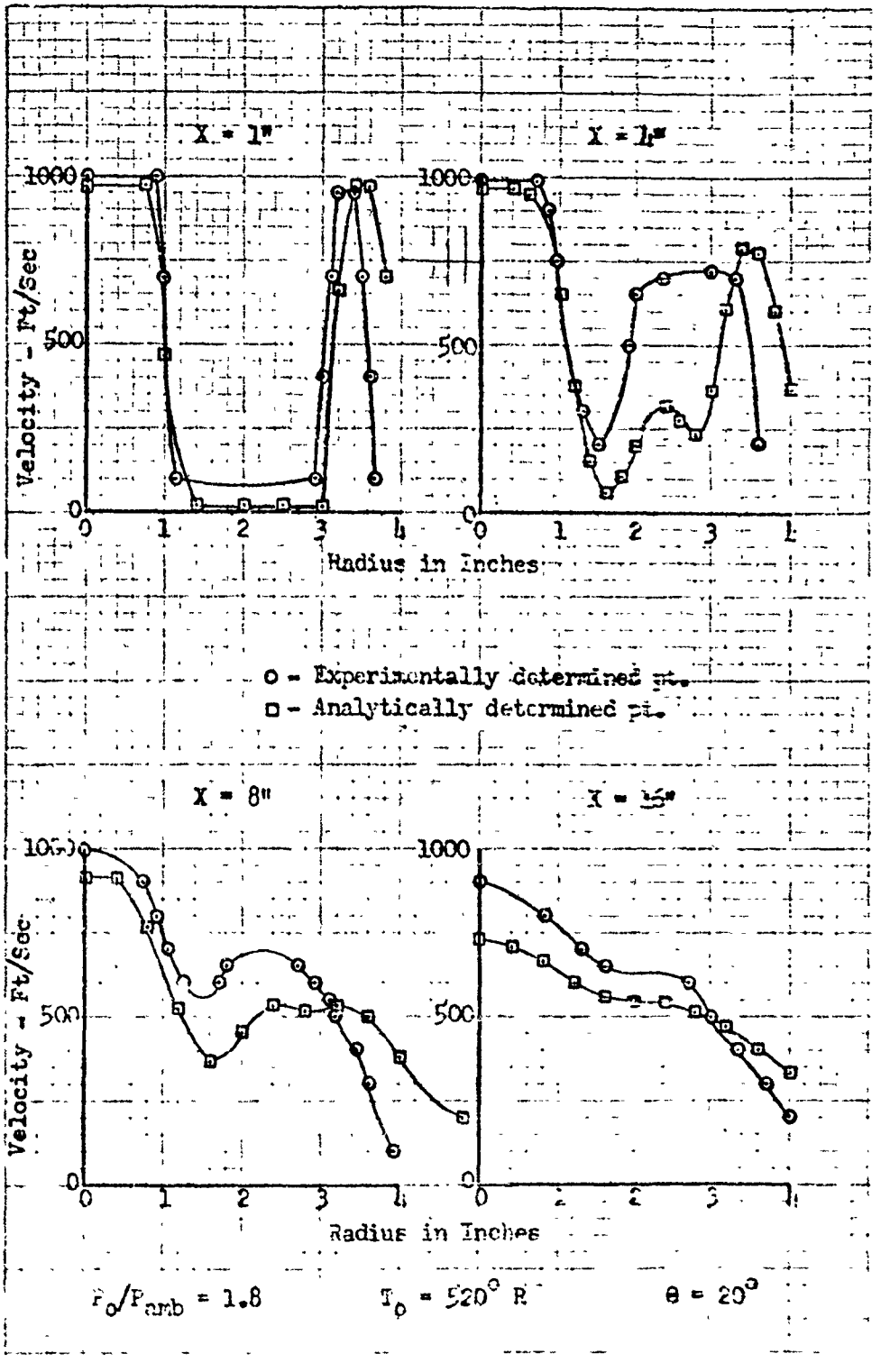

Figure 2.2(b) - Mean Velocity Profiles for the 20° Inlet Nozzle

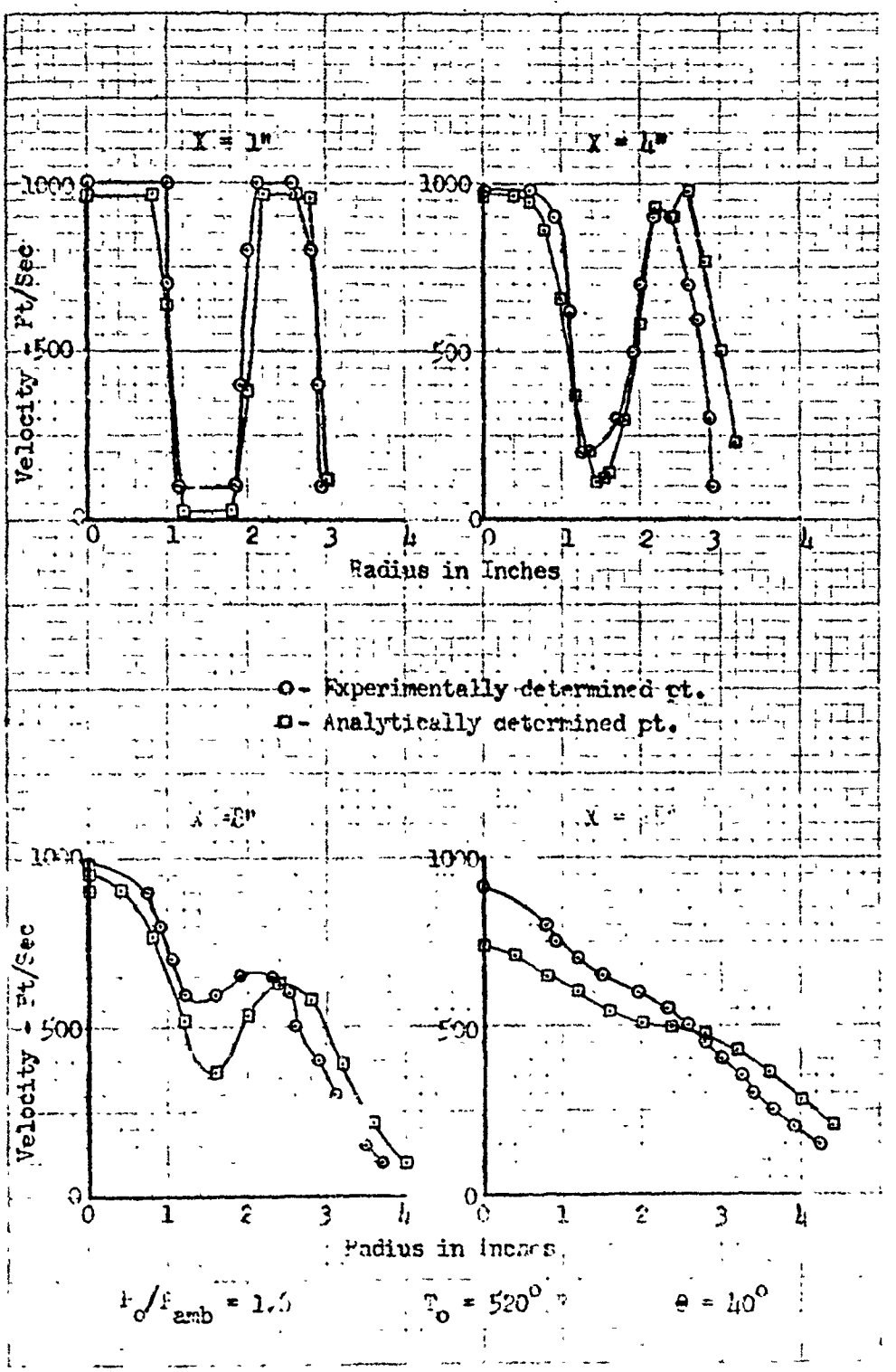

Figure 2.2(c) - Mean Velocity Profiles for the 1/ Tube Nozzle

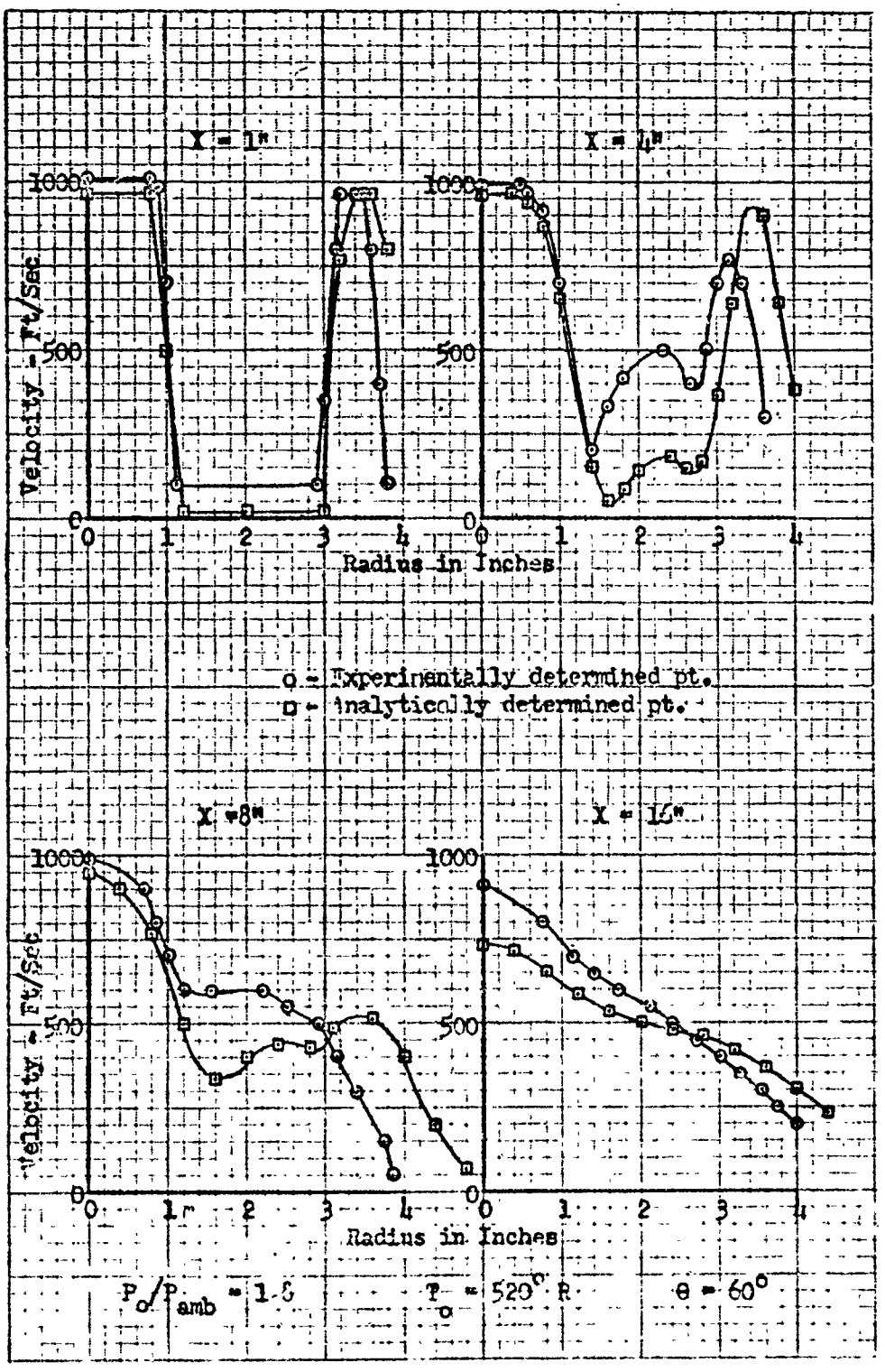

Figure 2.2 (d) - Mean Velocity Profiles for the 19 Tube Nozzle

1. Vertical division by four.
2. 4 by 4 division
3. Nesting of two 4 by 4 division in memory storage.
4. Horizontal division by four.
5. No division

① ② ③ ④ Points interrogated for the 4 by 4 inner mesh subdivision.

Note: Cross hatching indicates area of integration.

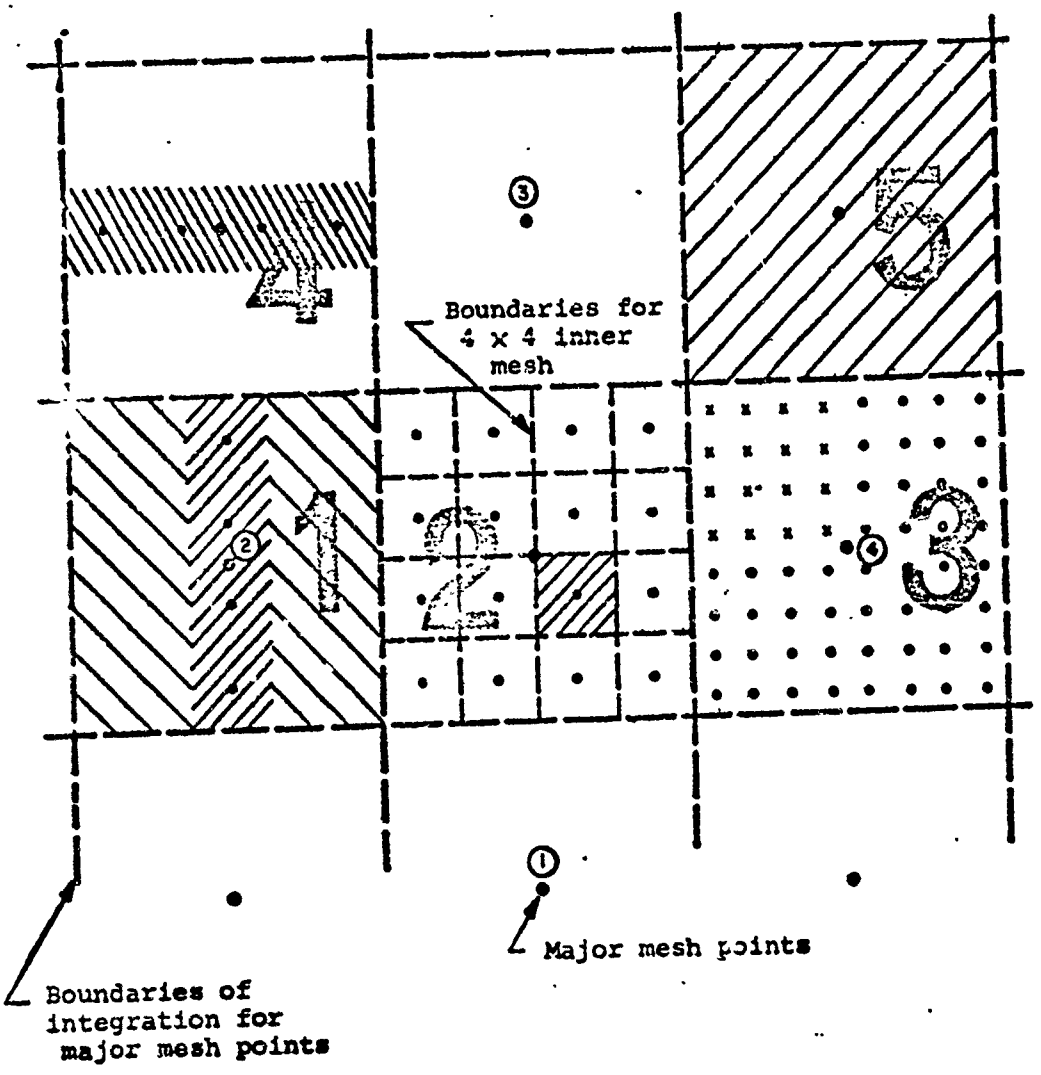

Figure 2.3 - Matrix division, integration, and superposition for b_x plane.

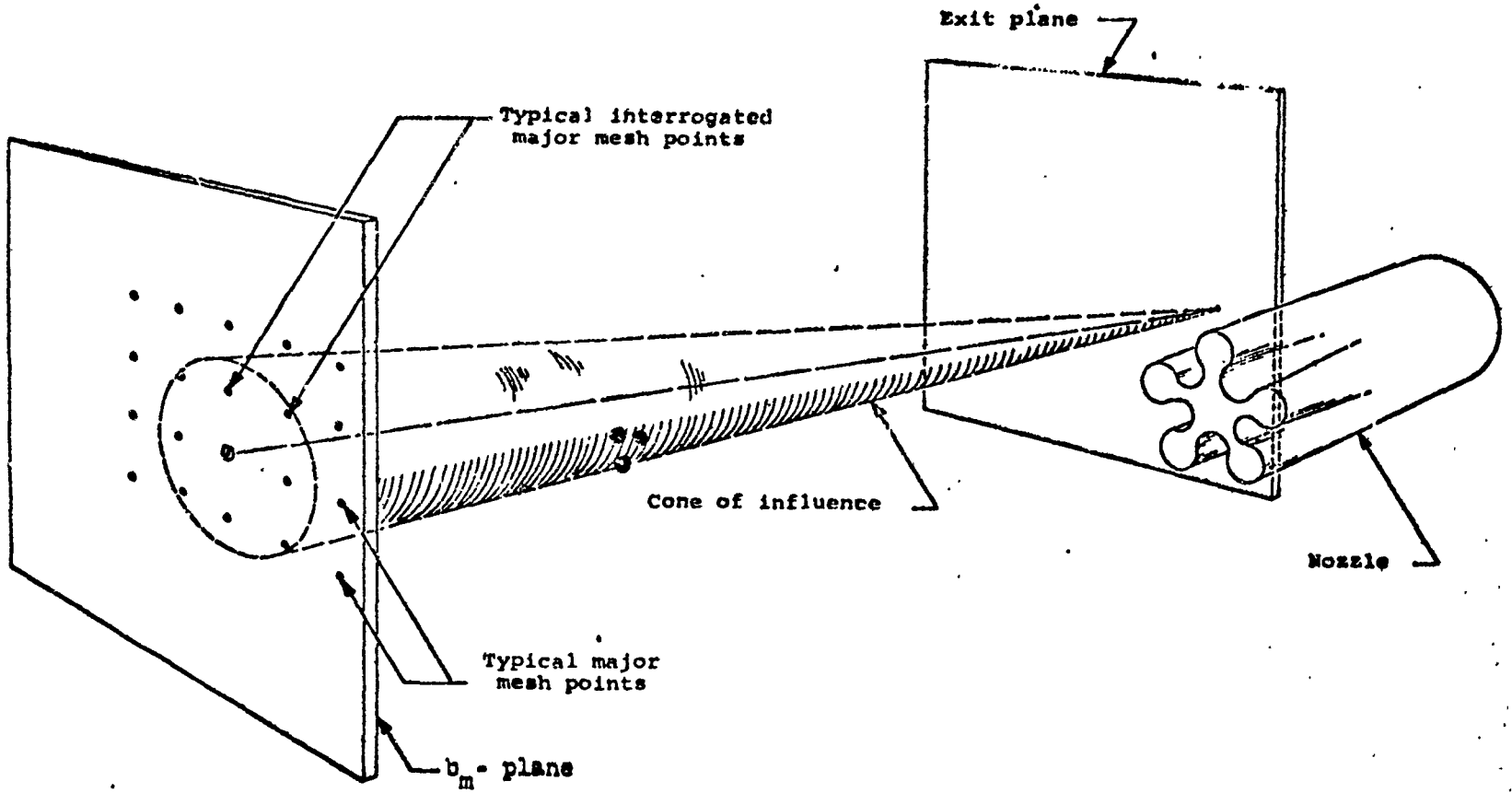

Figure 2.4 - Cone of Influence for b_m Plane

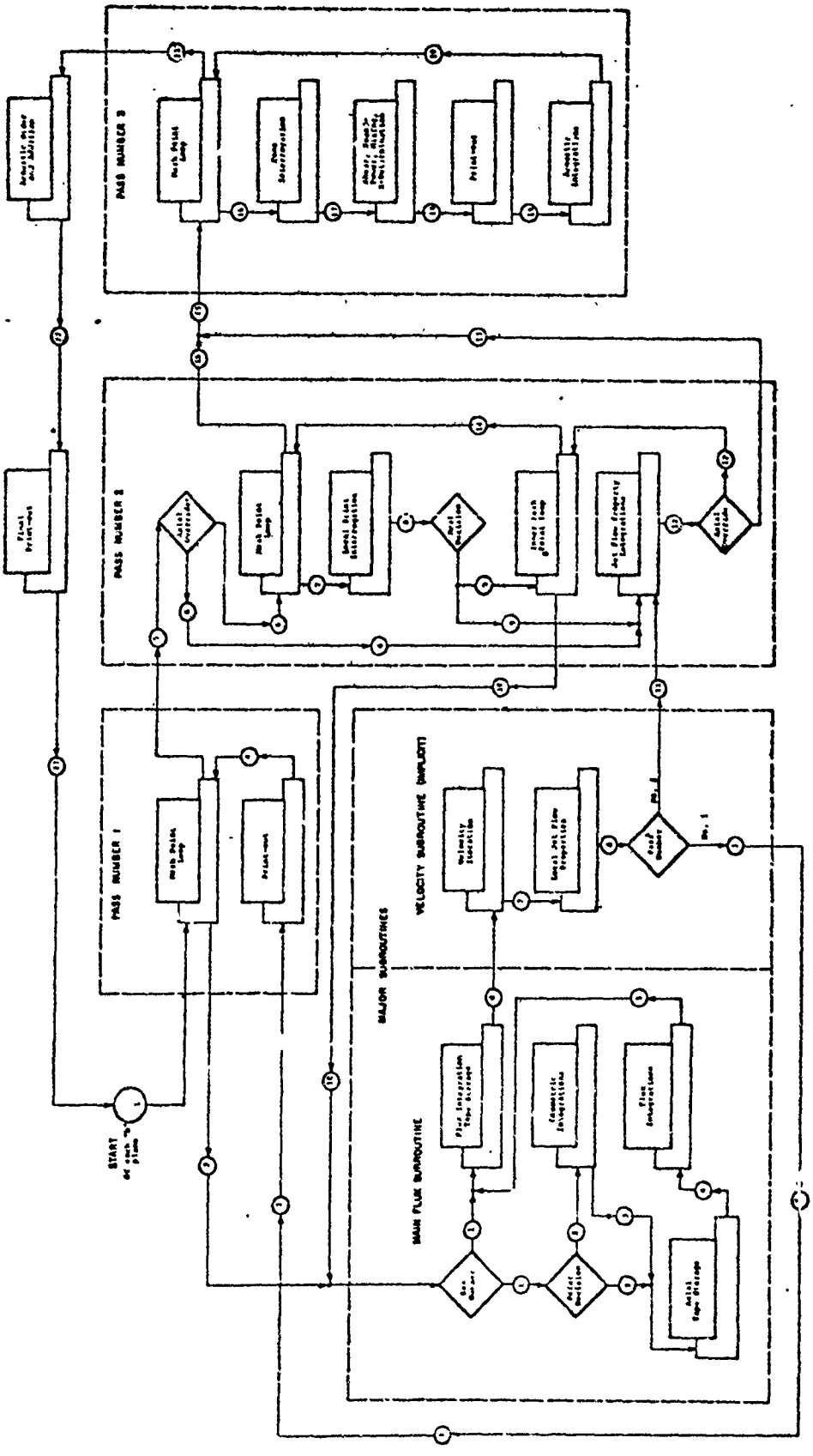

Figure 2.5 - Flow chart.

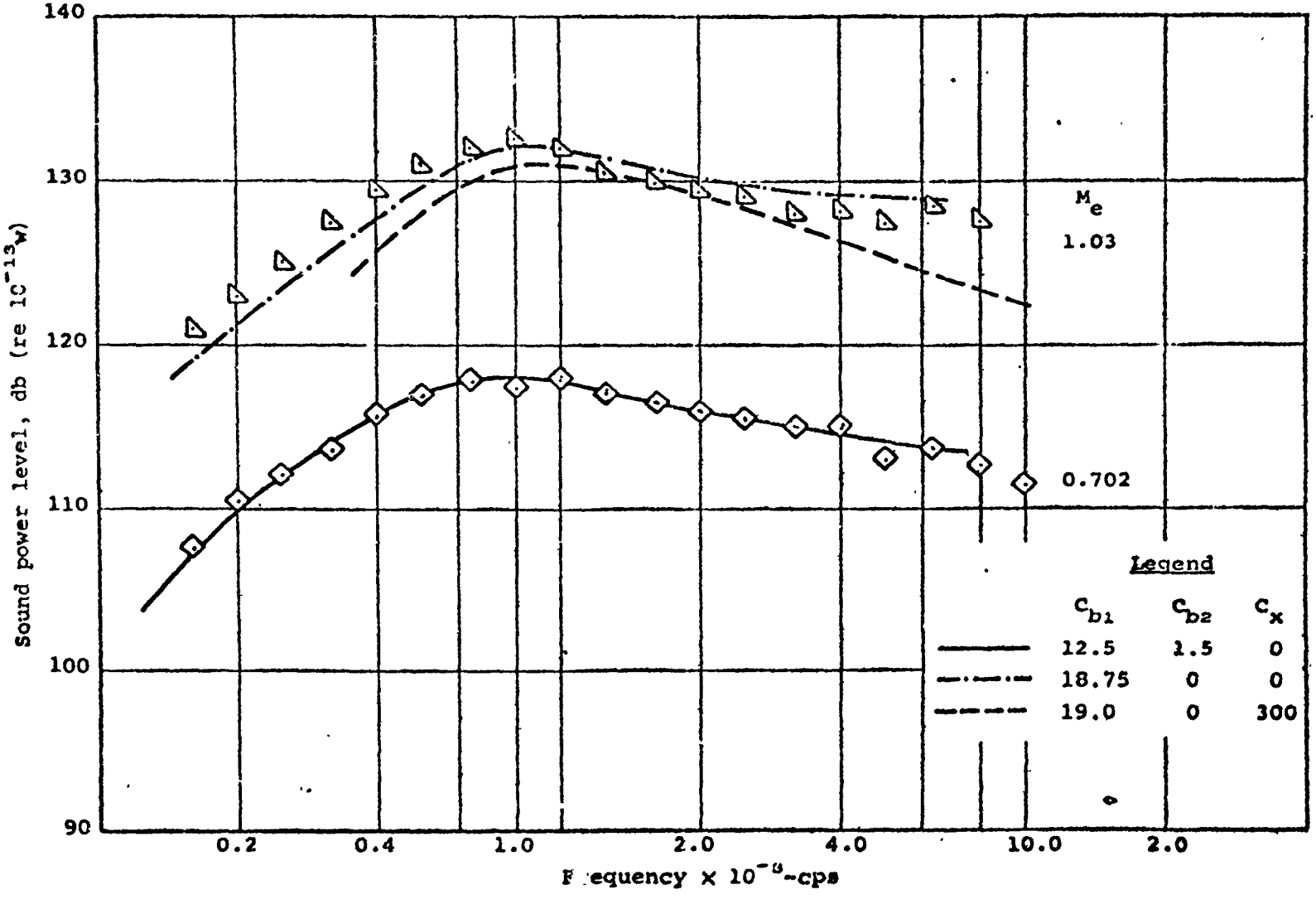

Figure 2.6 - Acoustic prediction - circular exit.

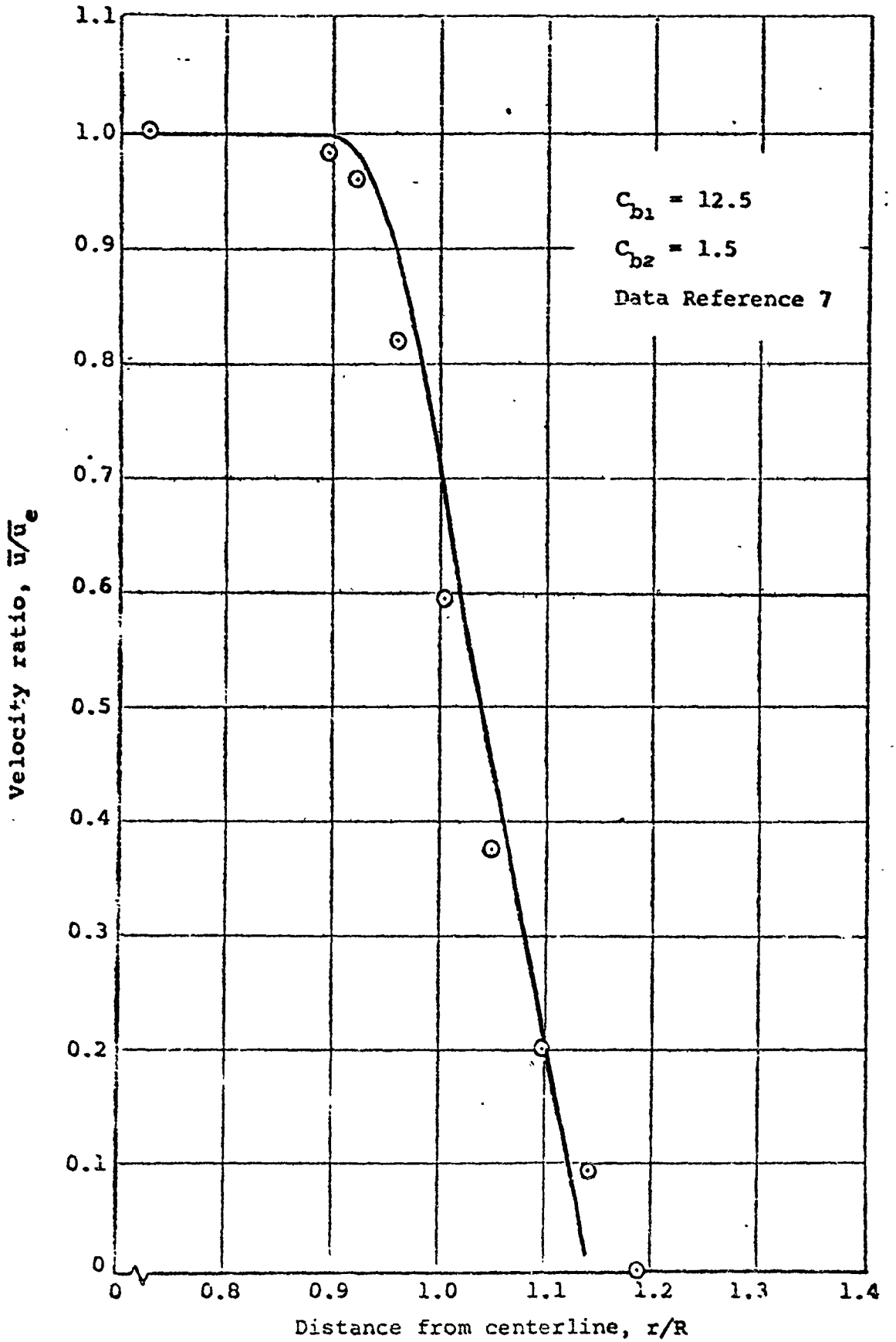

(a) $x/\bar{x} = 1.14$.

Figure 2.7 - Velocity profile comparison.

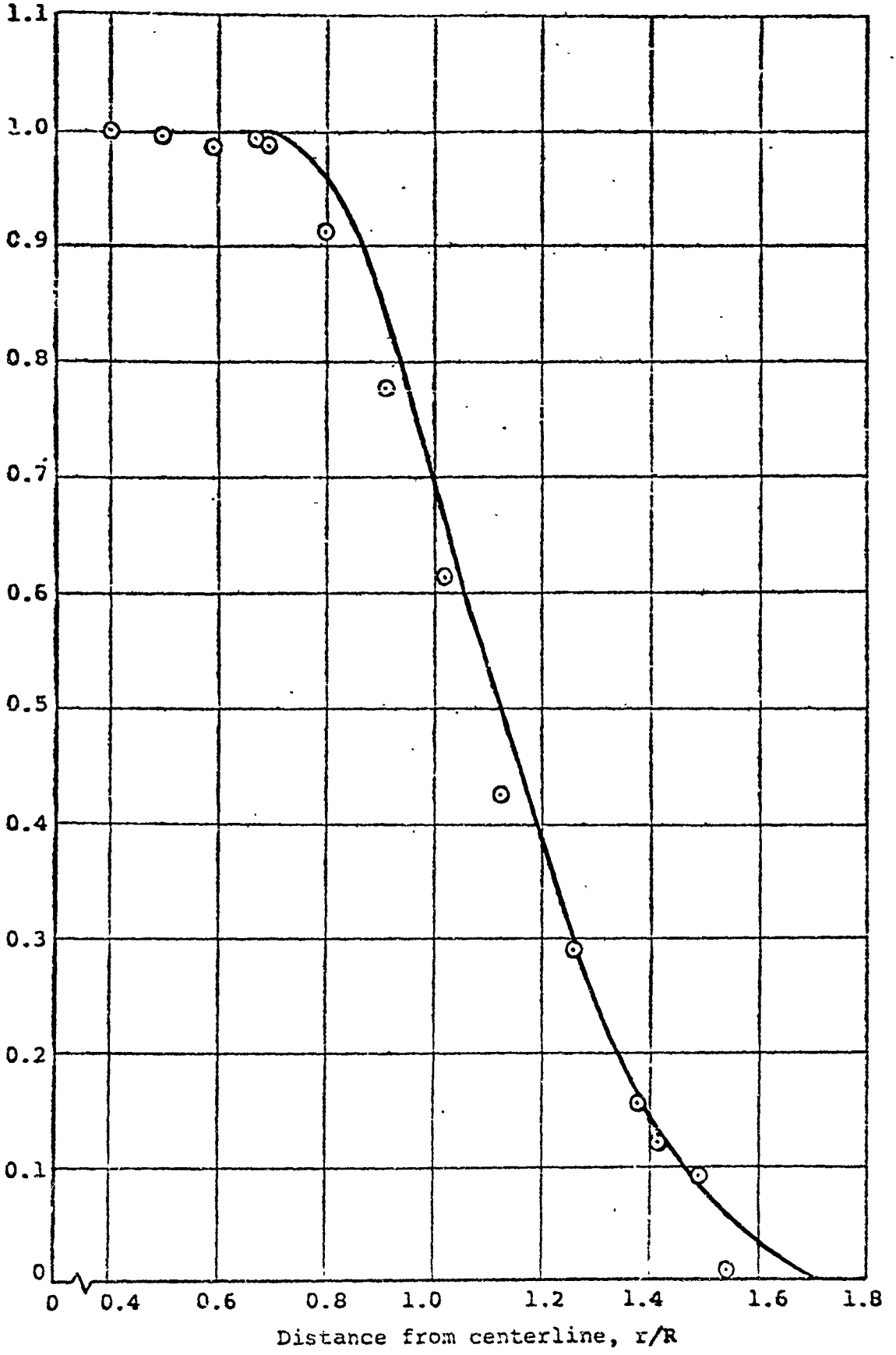

(b) $x/R = 4.58$.

Figure 2.7 - Continued.

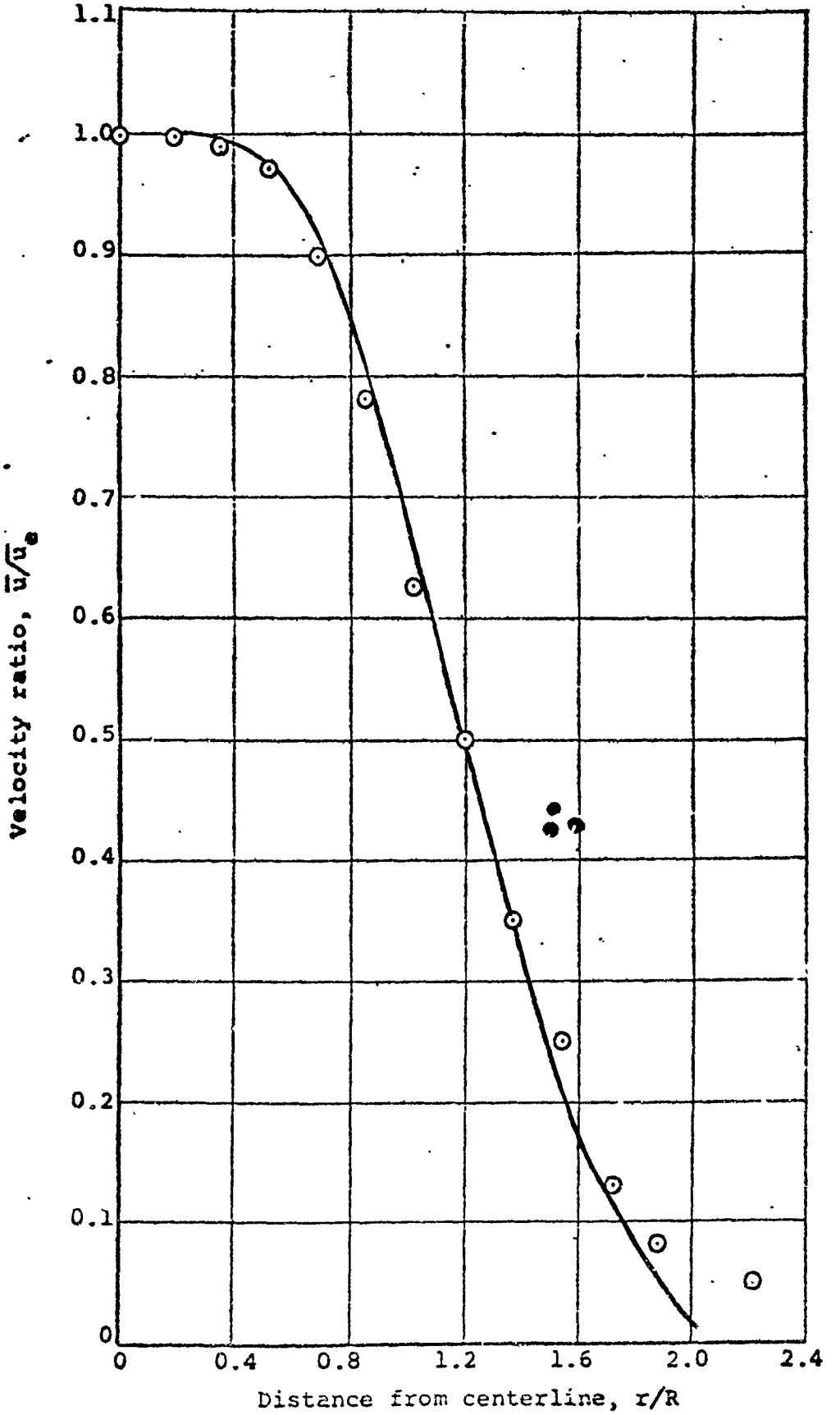

(c) x/R = 8.0.

Figure 2.7 - Continued.

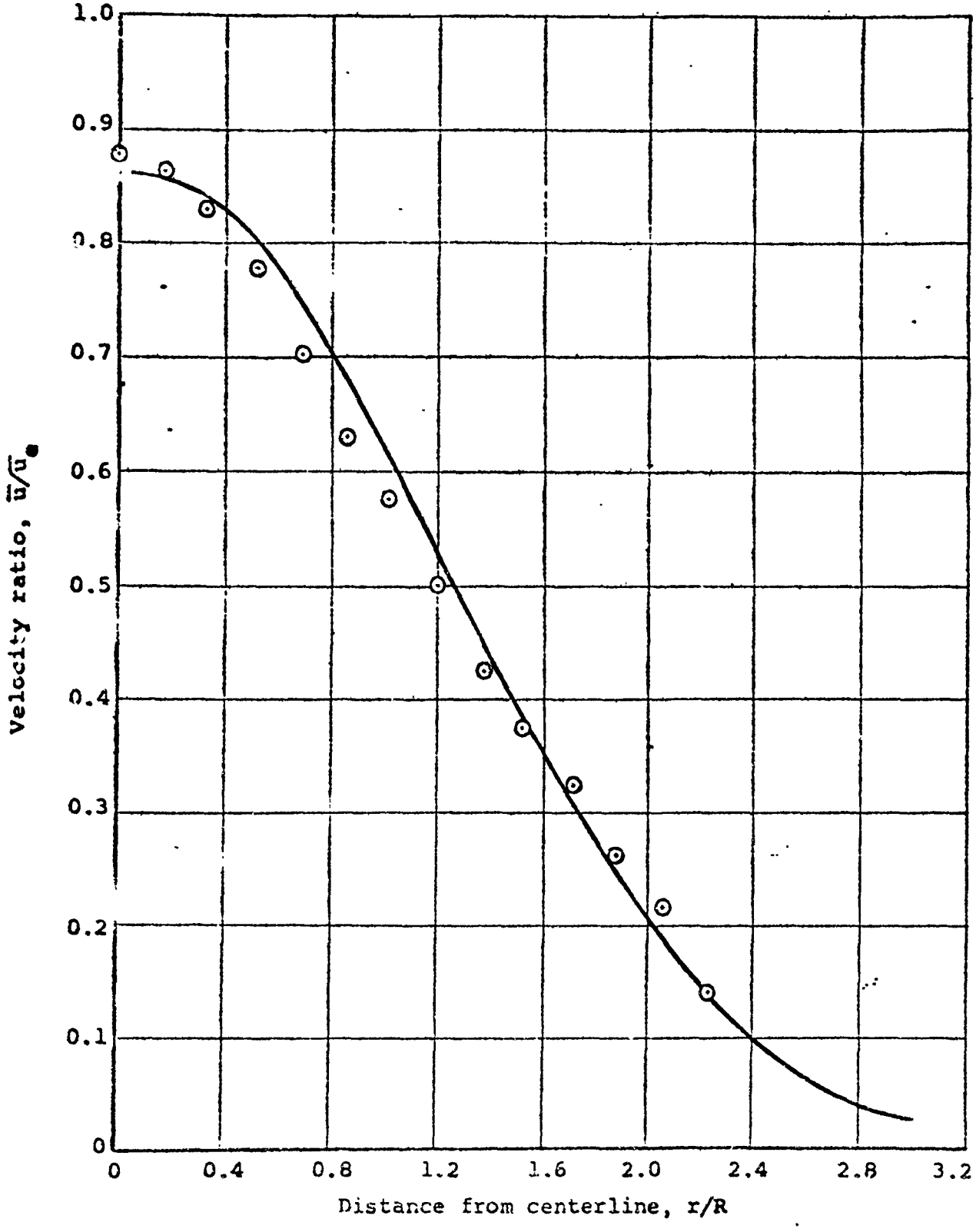

(d) x/R = 16.0.

Figure 2.7 - Continued.

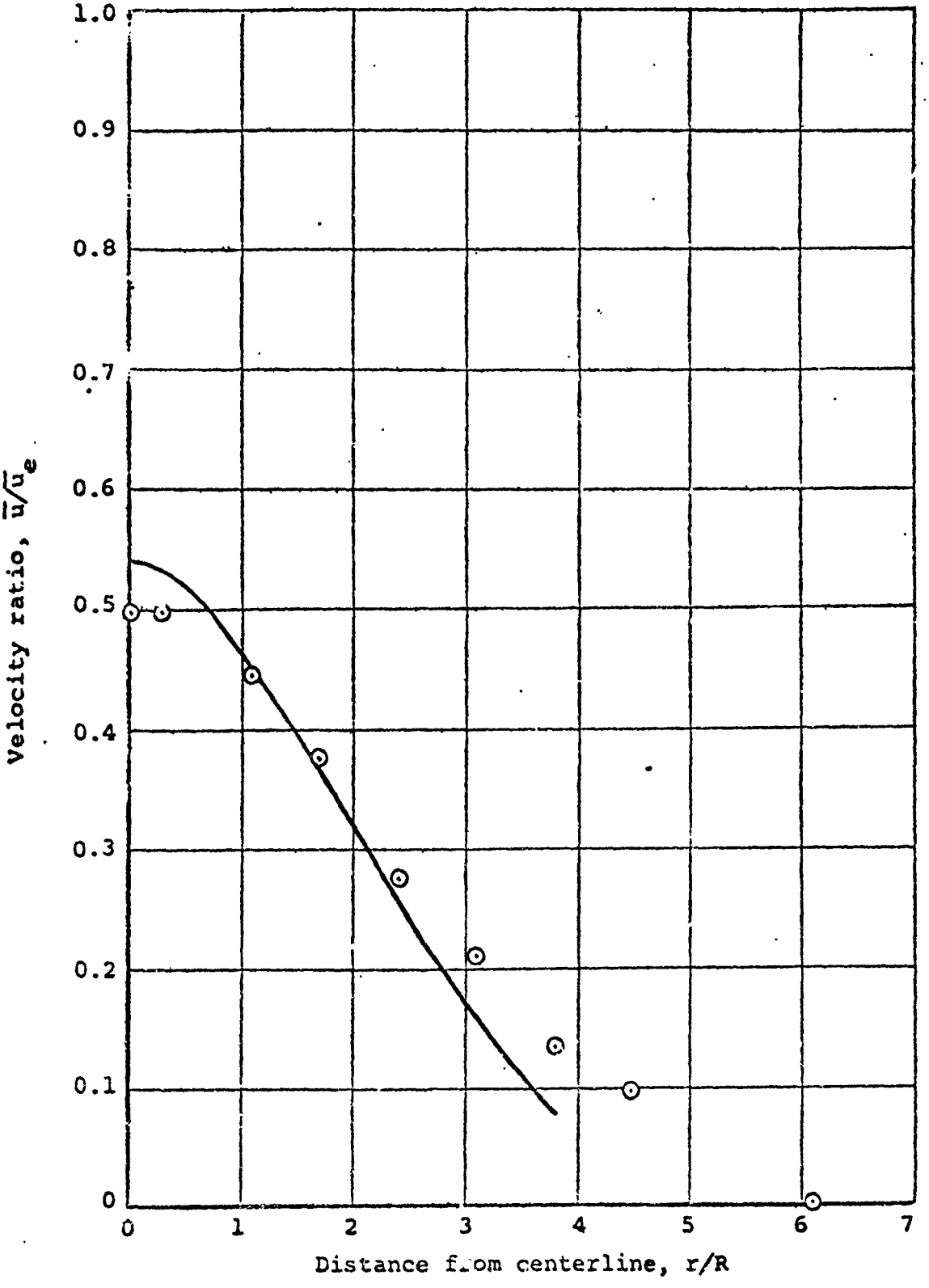

(e) x/R = 32.0.

Figure 2.7 - Concluded.

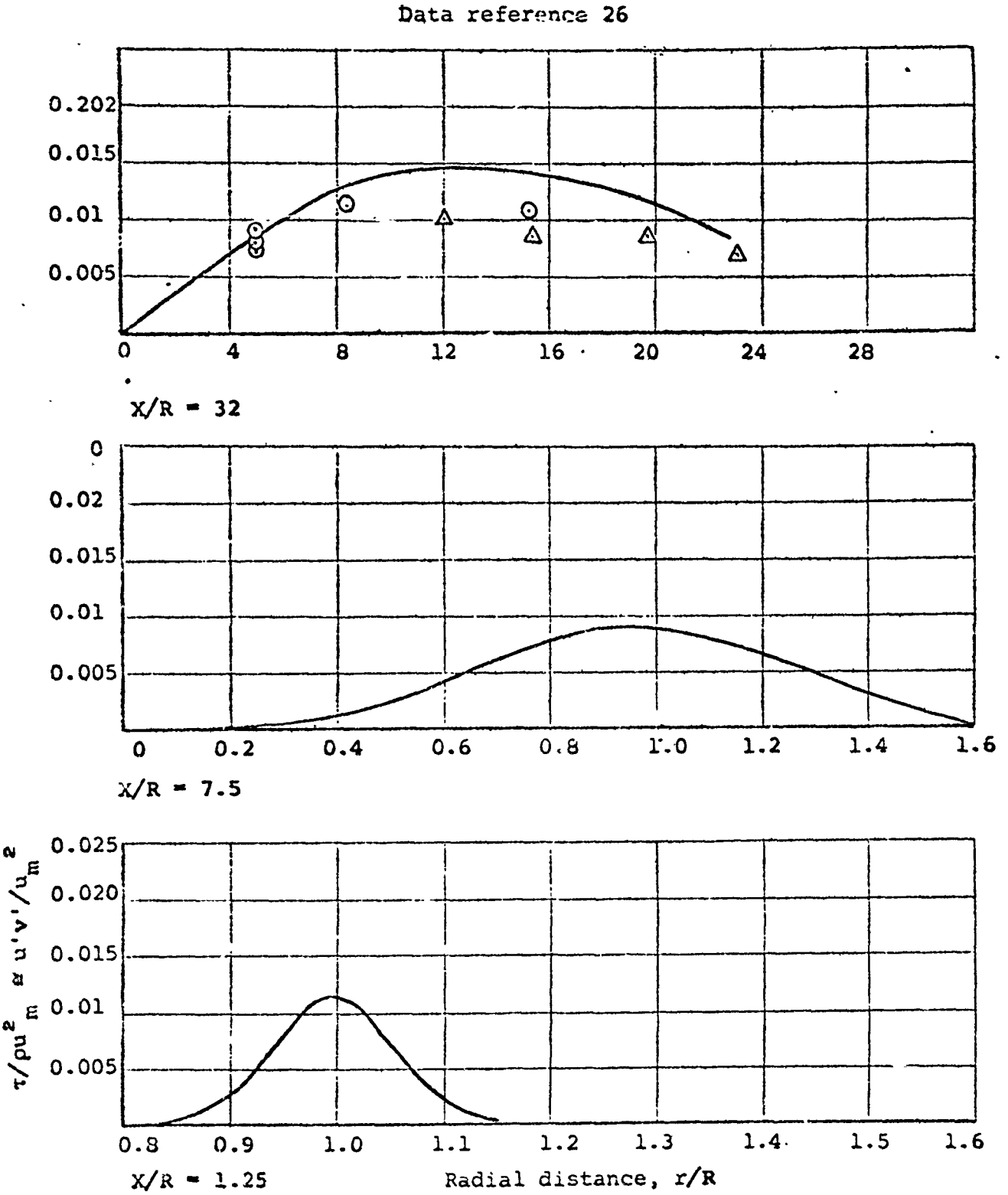

Figure 2.8 - Shear stress prediction.

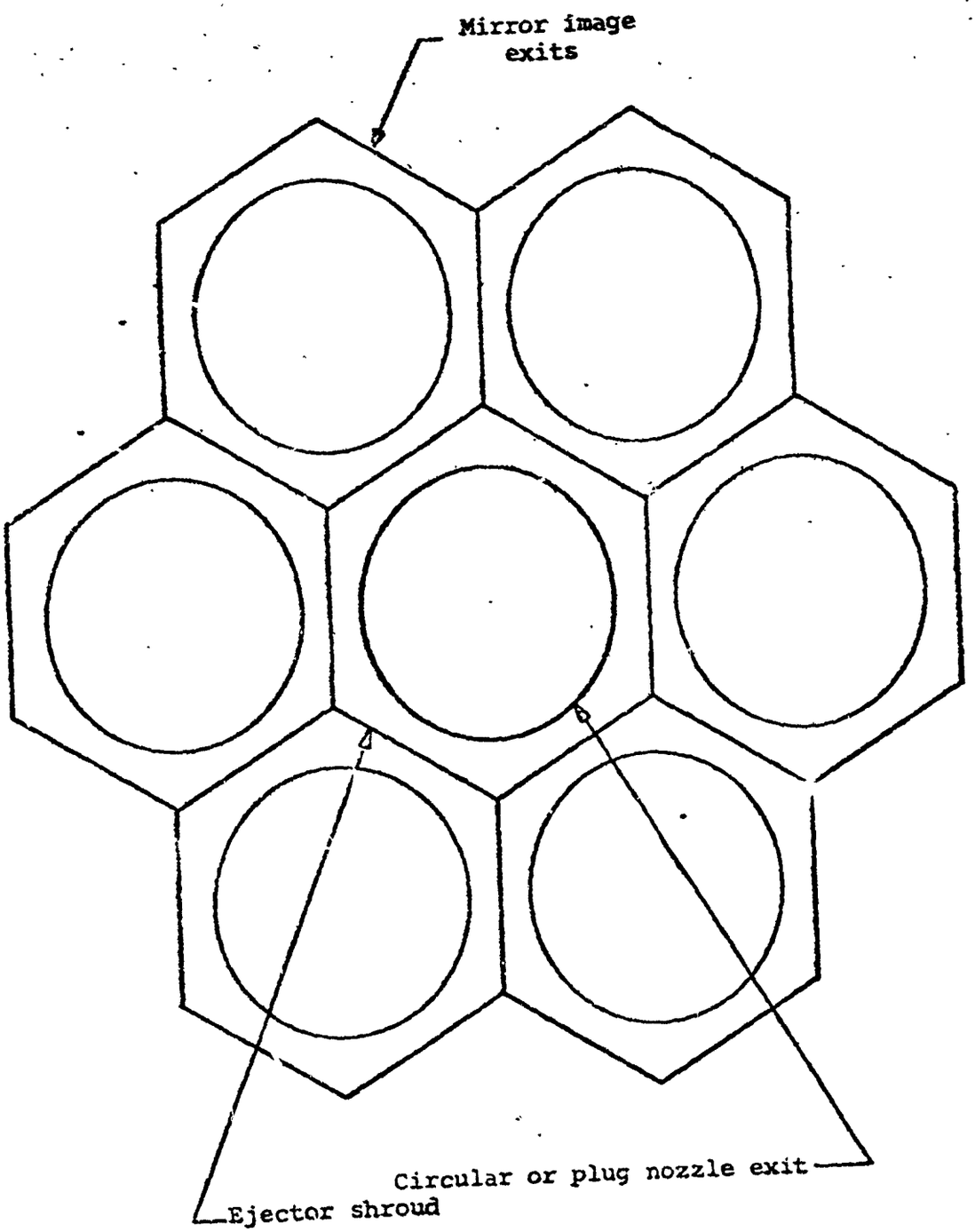

Figure 2.9 - Hexagonal ejector approximation.

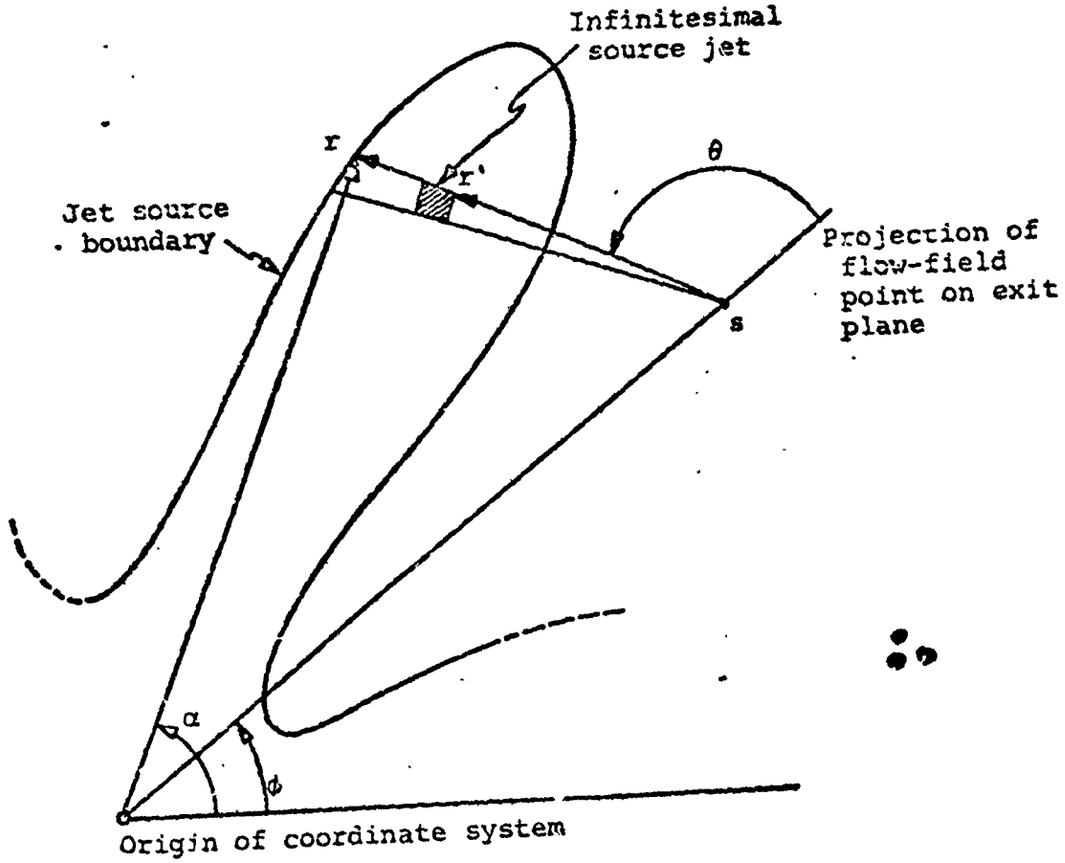

Figure 2.10 - Flux integration coordinate nomenclature.

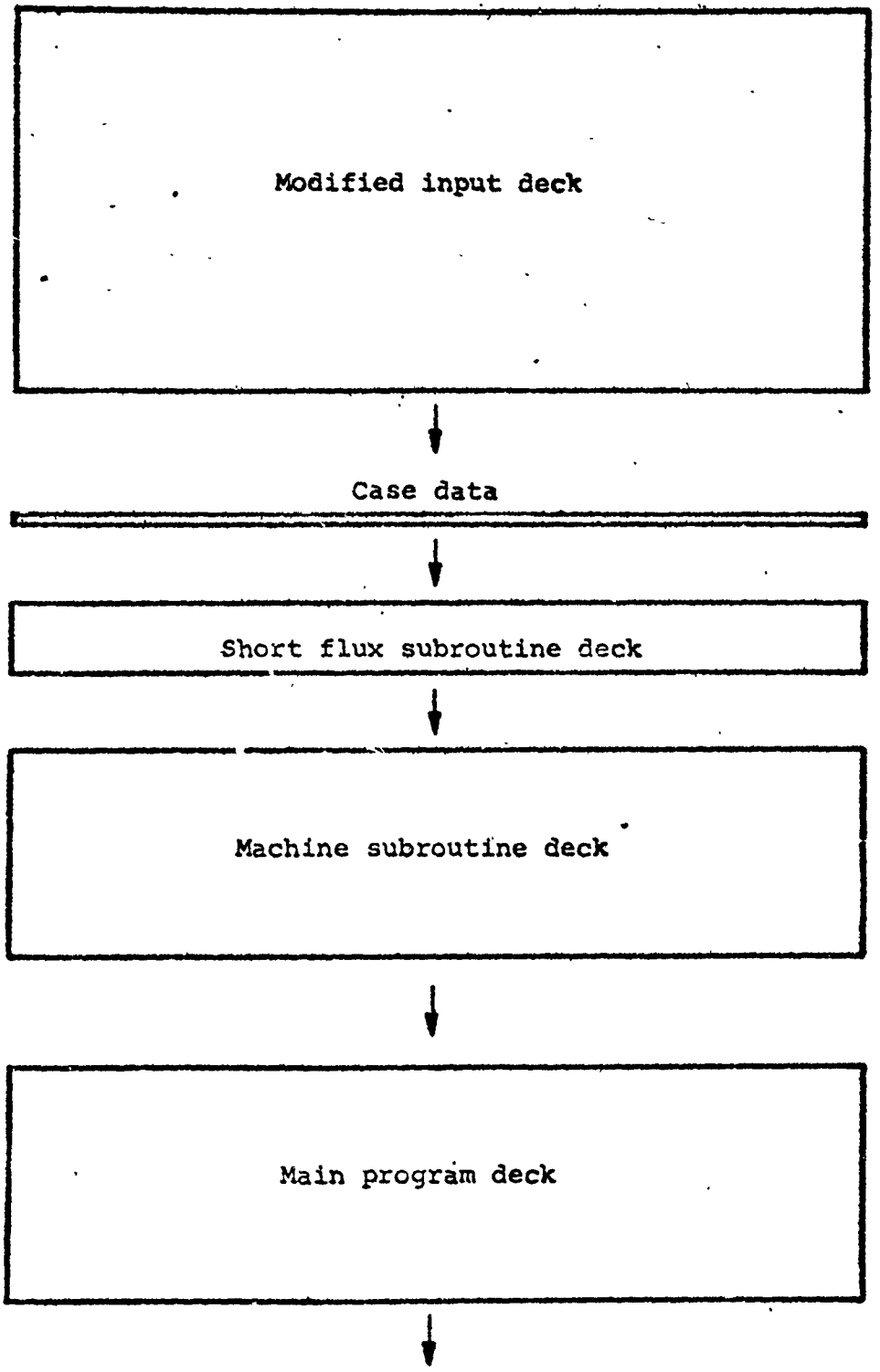

Figure 2.11 - Loading sequence for circular exit program.

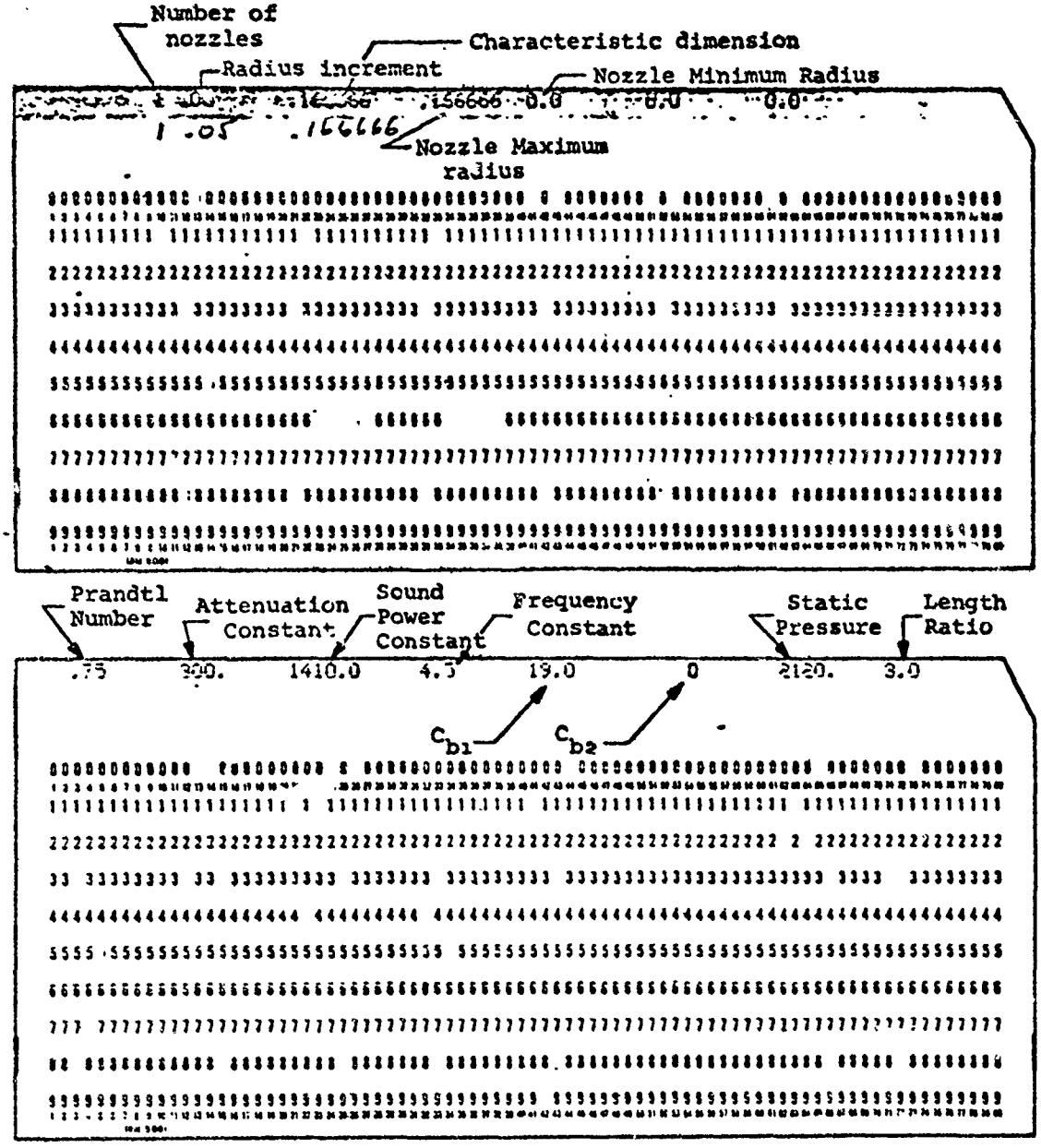

Figure 2.12a - Typical input.

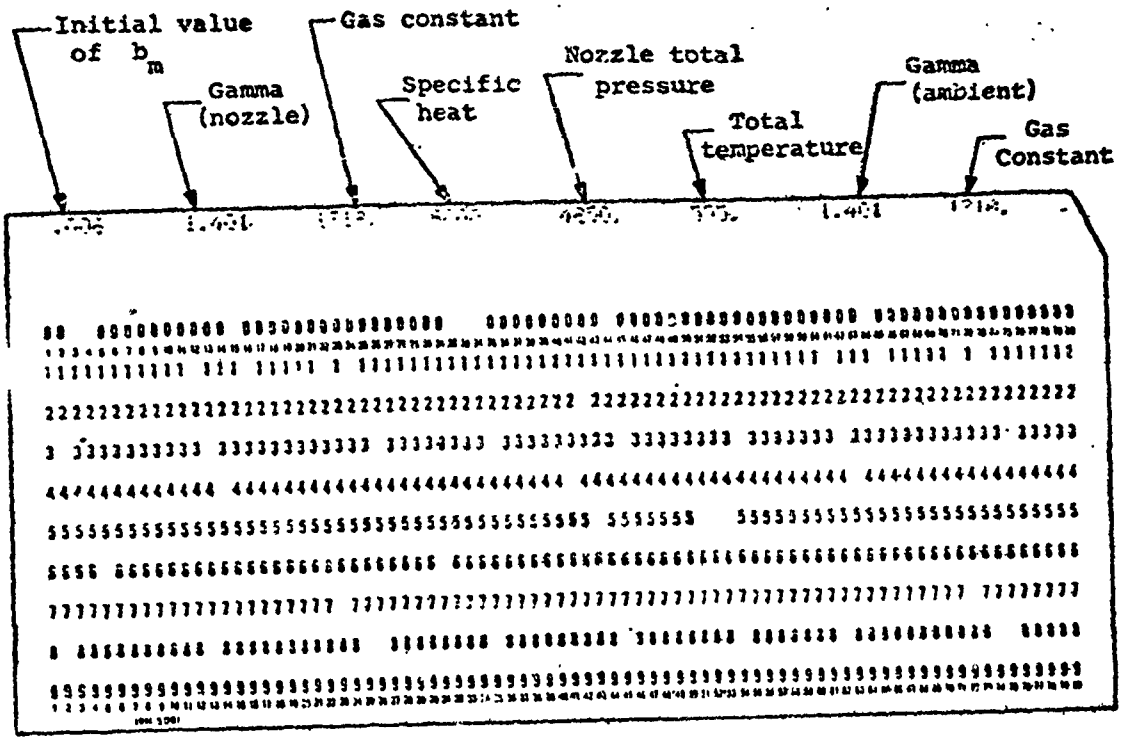

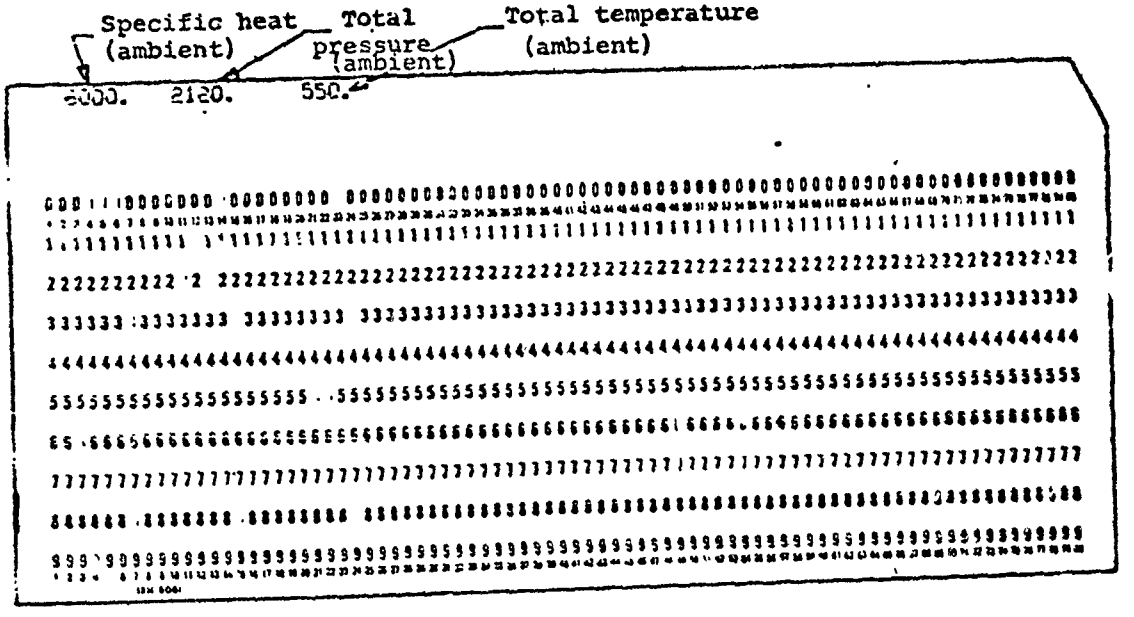

Figure 2.12b - Typical input. (Concluded)

Figure 2.13 - Typical Output

Distance Ratio	Radius Ratio	Velocity Ratio	Shear Ratio	Enthalpy Flux	Mach Number	Momentum Flux	Shear Flux
45.1204	0.0452	0.0000	0.0000	1.000	0.0000	0.0000	0.0000
.0500	.2690	.0510	17.4339	.9920	0	0	
45.1204	-.0122	.0409	0.0000				

	Frequency	Sound Power
1	1.250E+02	0.000E-00
2	1.574E+02	0.000E-00
3	1.984E+02	0.000E-00
4	2.499E+02	1.281E-01
5	3.149E+02	2.896E-01
6	3.968E+02	0.000E-00
7	4.999E+02	5.445E-01
8	6.299E+02	8.029E-01
9	7.937E+02	0.000E-00
10	9.999E+02	8.989E-01
11	1.259E+03	8.248E-01
12	1.587E+03	7.191E-01
13	1.999E+03	6.402E-01
14	2.519E+03	5.794E-01
15	3.174E+03	5.332E-01
16	3.999E+03	0.000E-00
17	5.039E+03	5.984E-01
18	6.349E+03	4.734E-01
19	7.999E+03	4.394E-01
20	1.007E+04	4.044E-01
21	1.269E+04	3.727E-01
22	1.599E+04	3.616E-01
23	2.015E+04	3.807E-01
24	2.539E+04	4.152E-01

	Frequency	Sound Power	DB
1	1.250E+02	0.000E-00	0.0000
2	1.574E+02	4.912E-02	116.8336
3	1.984E+02	0.000E-00	0.0000
4	2.499E+02	1.281E-01	120.9943
5	3.149E+02	2.896E-01	124.5344
6	3.968E+02	0.000E-00	0.0000
7	4.999E+02	5.445E-01	127.2737
8	6.299E+02	8.029E-01	128.9594

3.0 Investigation of the Effects of Flow Temperature and Pressure on Jet Noise Generation and Suppression

3.1 Introduction

In order to apply jet noise suppression concepts to afterburning engines, an understanding of jet noise generation and suppression at high flow temperatures must be developed beyond the present state-of-the-art. The validity of the correlation between free jet mean-flow velocity profiles and noise generation and suppression by heated jets has been demonstrated in Section 1 of this report, but the flow temperature range investigated does not extend to levels achieved by afterburners. This section describes the results of acoustical investigations, carried out in addition to the original scope of the research program, for the purpose of providing information on noise generation by high temperature jets, for both simple circular nozzles and suppressor configurations. The results of this study provide basic information on noise generation by high temperature jets, and give further insight to the problem of evaluating noise suppressor performance by means of cold flow scale model tests.

Experimental investigations have been carried out to evaluate the jet noise generated by a conical nozzle over a range of flow temperatures and pressure ratios, extending up to a temperature of 3300°R and pressure ratio 3.4. The jet noise spectra and overall sound power levels are presented, and the effect of jet density on noise generation is described. The results of the high temperature scale model conical nozzle tests, as well as concentric jet and full scale engine data have been used to establish an empirical relationship between nozzle energy flux and total sound power generated, applicable to concentric jet flows of unequal velocities and temperatures as well as to

conical nozzles at all pressure ratios and temperatures.

Scale model acoustical evaluations of suppressor-nozzle noise reduction performance at high temperatures have been accomplished, with results indicating that jet noise suppressor action is temperature as well as pressure ratio dependent. Data obtained indicates that noise reduction may be more difficult to achieve at high flow temperature, and that suppressor scale model evaluations must be carried out with heated flow or suitable substitute gas. Further experimental activity in the area of jet noise generation and suppression at flow temperatures in the afterburner range is recommended for the purpose of defining generalized temperature scaling laws applicable to all nozzle configurations.

3.2 Noise Generation by High Temperature Jets

Experimental investigations on noise generation by jets operating at temperatures up to 3300°R have been carried out utilizing a free-field acoustic test facility (Figure 3.1), described in Section 1.3.1 of this report. Tests were conducted with a conical nozzle 3.85 inches in diameter at the exit, operating at pressure ratios of 1.7, 2.0, 2.5, 3.0, and 3.4, varying the flow total temperature from 560°R to 3300°R for each pressure ratio condition. Sound pressure spectra were measured along a circular arc at 15 feet from the nozzle exit, and at various angles from the discharge direction. Sound power specrta were computed by integration of the sound pressures over the hemispherical radiation surface.

3.2.1 Instrumentation

The flow conditions which were controlled and monitored during the experimental investigation were total pressure and total temperature at the inlet to the nozzle. An 8 inch diameter flow section preceding the nozzle

inlet contained a static pressure tap and three IR vs IR-Rh thermocouples which were continuously monitored during the tests. The area ratio of approximately 4:1 from the measuring section to the nozzle throat provided an effective plenum upsream of the nozzle inlet.

Acoustic measurements were made using a Bruel and Kjaer type 4133 condenser microphone system which was calibrated by means of a B & K pistonphone. The microphone system frequency response was flat to 40 kcps, covering the entire frequency range of measurements without need of response correction. Microphone output was filtered through a B & K 1/3 octave spectrometer, over a range of band center frequencies from 200 to 32,000 cps. Graphic representation of the sound pressure spectra was obtained by recording spectrometer output with a B & K level recorder. Sound power spectra and overall PWL were computed from the pressure level spectra obtained at a distance of 15 feet from the nozzle and at angles of 20, 30, 40, 50, 60, 75, 90, 110, 130, and 150° from the flow direction.

3.2.2 Test Results

The measured total acoustic power levels and sound power spectra are presented in Figures 3.2 and 3.3a through 3.3d, for the range of nozzle flow conditions investigated. In Figure 3.2 the overall sound power levels are plotted against flow velocity for the purpose of comparison with the Lighthill eighth-power parameter: $k\rho_a^2 A U^8 c_o^{-5}$. The flow velocity used is a calculated value, assuming that the flow fully expands isentropicly from the measured total pressure to the ambient static pressure of 30 in. Hg. As would be expected, excellent agreement with the Lighthill equation is obtained at moderate pressure ratios (up to 2.0) and relatively low temperatures (up to

approximately 1700°R). The limits of applicability of the Lighthill parameter are clearly visible in the figure, and a flow temperature influence, apart from velocity, is apparent. Thus it is seen that for estimates of jet noise total power at high flow pressure ratio and/or temperature the Lighthill relationship is inadequate. Figure 3.2 shows that at low flow temperature (560°R) sound power generation increases as U^{20} over the range of pressure ratios from 2.0 to 3.4, while at a flow temperature of 3300°R the overall sound power is proportional to approximately U^6. Examination of the increase in sound power resulting from velocity increase due to flow temperature rise at constant pressure ratio shows that at a pressure ratio of 3.0 sound power increase is proportional to U^2 from 1100 to 3300°R.

This variation of the velocity exponent from 2 to 20 suggests that the Lighthill parameter might take the form: $k(\rho_j/\rho_a)^n A U^8 c_c^{-5}$. In Figure 3.4 the effect of jet density on sound power generation is shown. Over the entire range of flow conditions investigated the sound power is observed to increase in proportion to jet density squared, considering the data in a rather gross manner. A detailed observation, however, indicates that for a given flow temperature the sound power varies with $(\rho_j/\rho_a)^n$, where n is temperature dependent. The magnitude of this temperature dependence is demonstrated by the substantial change in slope of the sound power vs jet density curve, progressing from temperature of 560 to 3300°R. The jet density ratio exponent n is plotted as a function of flow total temperature in Figure 3.5. Values of n vary from +12 to -6, and it is observed that the relationship between n and flow temperature is approximately: $n \propto T_o^{-3}$. For low pressure ratio jet flow at moderate temperatures the flow density effect on jet noise generation is negligible. However, the results of the investigations described herein

extend knowledge of the behavior of jet noise generation to a broader range of flow conditions, including high temperature and high pressure ratio flow which is likely to be experienced in advanced propulsion systems.

3.3 Correlation of Jet Noise with Nozzle Energy Flux

Results of the scale model investigations on noise generation by simple circular jets operating at temperatures up to 3300°R have been used to establish a general empirical relationship between total acoustic power and jet stream power.

Figure 3.6 shows normalized power level, $(PWL - 10Log_{10}A)$, plotted as a function of nozzle total energy flux. The scale model conical nozzle data presented is that described in Section 3.2, and turbojet engine noise data is included to demonstrate the generality of the relationship. For simple conical nozzles the energy flux, ϵ, is given by:

$$\epsilon = h_t(W/A) \qquad (1)$$

where h_t is the flow total enthalpy per pound of fluid.

A tentative method for including noise generation by concentric flows in this correlation has also been developed, and three concentric flow examples are included in Figure 3.6. A table of nozzle flow conditions is also given in the figure. The dual stream concentric flow nozzle utilized in obtaining the noise data is shown in Figure 3.7. Flow parameter variations tested included a heated high velocity outer flow with cold inner flow, and a case with nearly equal flow velocities but with substantial temperature difference between the two streams. The confirmation of the validity of the correlation for concentric flow requires additional experimental investigation, but results obtained thus far are extremely encouraging. The correlation developed is as follows:

Let: A = flow area, ft^2

h_t = total enthalpy, Btu/lb

h = static enthalpy, Btu/lb

W = weight flow, lb/sec

N = stream number

K = relative velocity correction factor

U = flow velocity, ft/sec

$U^2/2gJ$ = flow kinetic energy, Btu/lb

E_t = stream total power, Btu/sec

ϵ = energy flux, Btu/ft^2sec

The stream number, N, is defined by the following sketch of typical concentric nozzles:

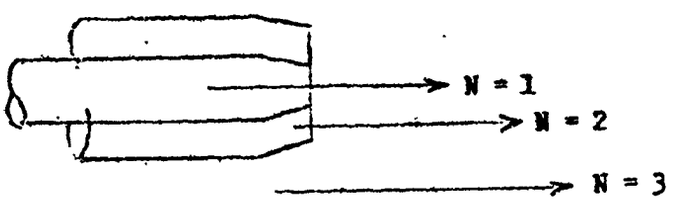

For each stream (N = 1, 2, - - -)

$$h_{tN} = h_N + (U_N^2/2gJ)K \tag{2}$$

where

$$K = (U_N - U_{N+1})^2/U_N^2 \tag{3}$$

Now, the total stream power is

$$E_t = \sum_N h_{tN}W_N \tag{4}$$

and

$$\epsilon = E_t/\sum_N A_N \tag{5}$$

By proper substitution:

$$\epsilon = \frac{\sum_N \left[h_{tN} - (1 - K)U_N^2/2gJ\right] W_N}{\sum_N A_N} \tag{6}$$

For a single stream, Eq. (6) reduces to the simple form of Eq. (1). The significance of Eq. (6) is that for consideration of concentric flows it is necessary to sum the energy flux for each of the jets. The inner jet flux is defined herein as the relative flux with respect to the surrounding jet; thus the inner flux is based upon the static enthalpy plus the relative velocity head.

The efficiency of conversion of jet stream power to acoustical power is seen in Figure 3.6 to be uniquely related to nozzle energy flux. Good correlation between model and full scale engine data has been demonstrated, thus indicating that the nozzle energy flux parameter is quite general and valid in application to the problem of jet noise estimation.

3.4 Effects of Flow Temperature on Jet Noise Suppressor Action

The value of cold flow scale model investigations in the development of jet noise suppressors is well recognized, both from the standpoint of time requirements and hardware expense and complexity. Up to the present time, jet noise suppressor investigations have been carried out under the assumption that noise reduction achieved in cold flow tests can be directly related to expected full scale suppressor noise reduction by Strouhal number scaling. Furthermore, experience has shown that jet noise suppressors in general perform poorly at low pressure ratios, with noise reduction performance (compared to an equal area conical nozzle) improving as pressure ratio increases. In order to apply scale model techniques to the development of a suppressor for afterburning turbojet engines, it was deemed necessary to investigate the effects of high temperature flow on suppressor performance in order to determine the validity of scaling laws and the Mach number effect on suppression.

Scale model suppressor noise investigations were carried out utilizing the nozzles shown in Figures 3.8, 3.9, and 3.10. These suppressor nozzles are of approximately the same flow area as the conical nozzle described previously in this section, and are described in detail in section 1 of this report. Measurements of total acoustic power were made in the same manner as for the conical nozzle, though over a somewhat more limited range of flow pressure ratio and temperature.

Comparisons of total acoustic power generation have been made for the suppressors and conical nozzle. For convenience, the conical nozzle data is replotted in terms of PWL vs pressure ratio, for various temperatures, in Figure 3.11. Figure 3.12 presents corresponding data for the three suppressor models: (1) 8-lobe, (2) 19-tube, and (3) 18-segment with plug. In order to determine the effect of flow temperature on suppression of jet noise, the data of Figures 3.11 and 3.12 has been cross plotted in Figure 3.13, which shows overall PWL as a function of flow temperature for the four nozzles operating at three pressure ratios: 1.8, 2.4, and 3.0. It can be readily observed that for each of the suppressor nozzles the noise reduction (the difference between the conical nozzle and suppressor nozzle curves) at constant pressure ratio is temperature dependent. Furthermore, this temperature dependence appears to be different for each suppressor. Note that at pressure ratio 1.8 little noise reduction is shown for cold flow, and that as temperature is increased the suppression capability increases and then finally declines. At flow temperatures near 1000°F, only slight Mach number (pressure ratio) effect is observed, and for pressure ratio 2.4 little temperature effect is evidenced. It is fortuitous that turbojet engine suppressor development up to the present time has been for engines operating at pressure ratios near 2.4 and temperatures near 1000°F,

since noise reduction at pressure ratio 2.4 shows little temperature dependence. However, at low pressure ratio (1.8) cold flow test results would not provide a satisfactory estimate of sound power reduction experienced at increased temperatures.

While no general means of correlating suppressor performance for all types of suppressors, for various temperatures and pressures, has been developed, the results of the investigation have several important implications. First, evidence has been presented to show that jet noise reduction is not simply pressure ratio dependent for a fixed configuration. Furthermore, the variation in noise reduction performance as a function of flow temperature for different suppressor configurations indicates that model suppressor evaluation must be ultimately performed experimentally at flow temperatures and pressures representing full scale conditions. Finally, the need for further research into normalization of suppressor performance for temperature and pressure effects is emphasized.

3.5 Conclusions and Recommendations

Results of scale model experimental investigations on noise generation by jets from conical and suppressor nozzles have been presented for flow temperatures ranging up to 3300°R. The following important conclusions are summarized:

1) Noise generation by conical jets is not adequately described by the Lighthill equation except for low pressure ratio and moderate temperature flow.

2) A temperature dependent flow density effect on noise generation by conical jets has been found to occur. Total sound power varies with $(\rho_j/\rho_a)^n$, where n is temperature dependent.

3) An empirical relationship between sound power and nozzle energy flux has been developed for conical nozzles, including concentric flows, for the

range of pressure ratios from 1.4 to 3.4, and temperatures up to 3300°R.

4) Jet noise suppressor acoustical performance is temperature as well as pressure ratio dependent, so that scale model suppressor development must include final experimental evaluation under flow conditions representing full scale engine temperature as well as pressure ratio.

It is recommended that further research effort be directed toward extending the generality of the energy flux concept to complex nozzle designs, including further verification of applicability to concentric flows. Jet noise suppression research should be continued for the purpose of developing general laws for scaling temperature and pressure ratio effects on noise reduction performance

SYMBOLS:

A - Nozzle throat area, ft^2

c_o - Ambient sonic velocity

E_t - Jet stream total power, Btu/sec.

h - Static enthalpy, Btu/lb.

h_t - Total enthalpy, Btu/lb.

k - Constant in Lighthill parameter; relative velocity correction factor in energy flux correlation.

n - Density ratio exponent

N - Stream number for concentric jet flow

P - Static or ambient pressure

P_o - Total pressure

PWL - Sound power level, db re 10^{-13} Watts

T_o - Total temperature

U - Flow velocity, or fully expanded flow velocity for supercritical pressure ratio

W - Weight flow, lb/sec.

ϵ - Energy flux, Btu/ft^2 sec.

ρ_a - Ambient air density

ρ_j - Jet static density

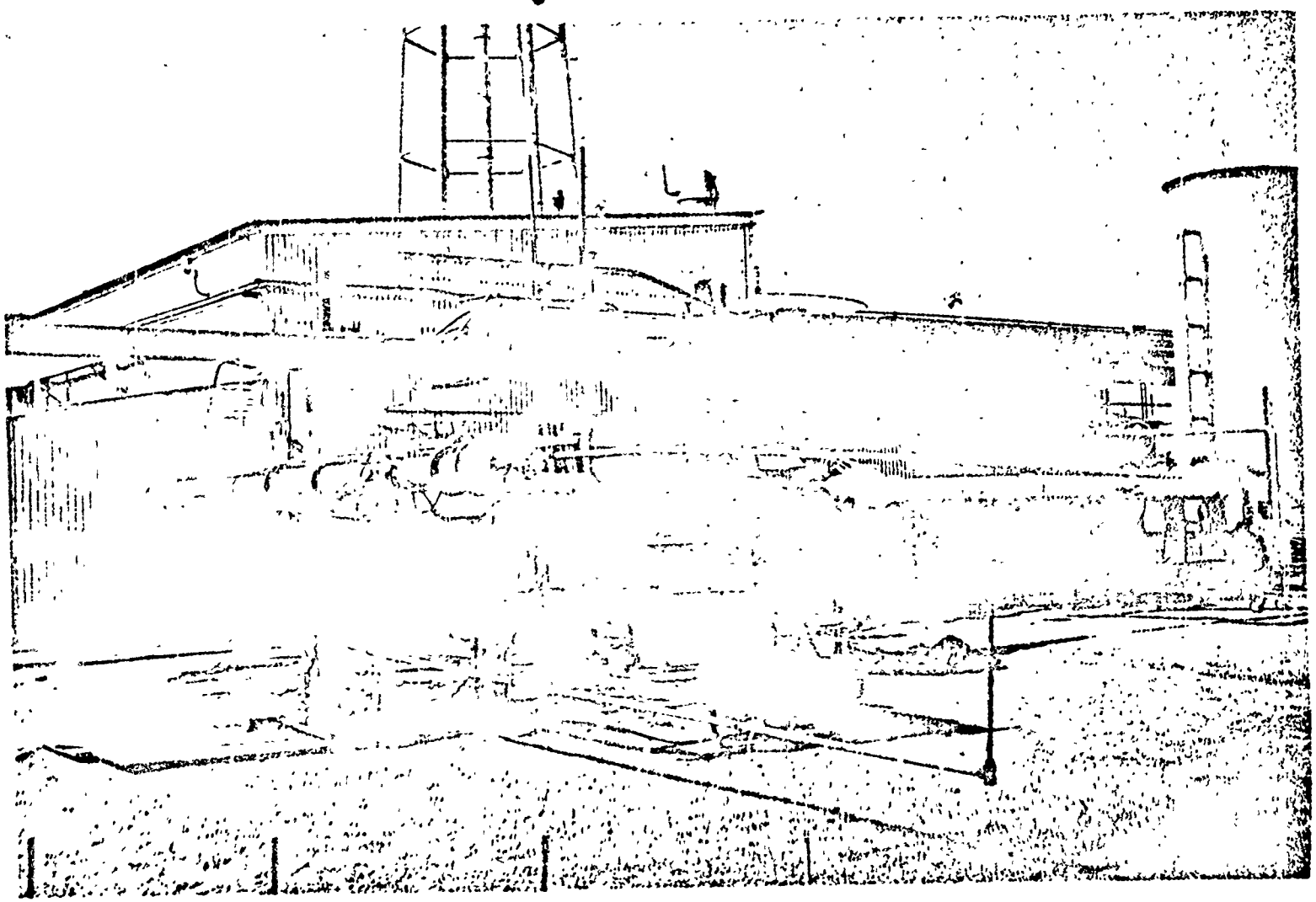

Figure 3.1 High Temperature Test Facility for Jet Noise Evaluation

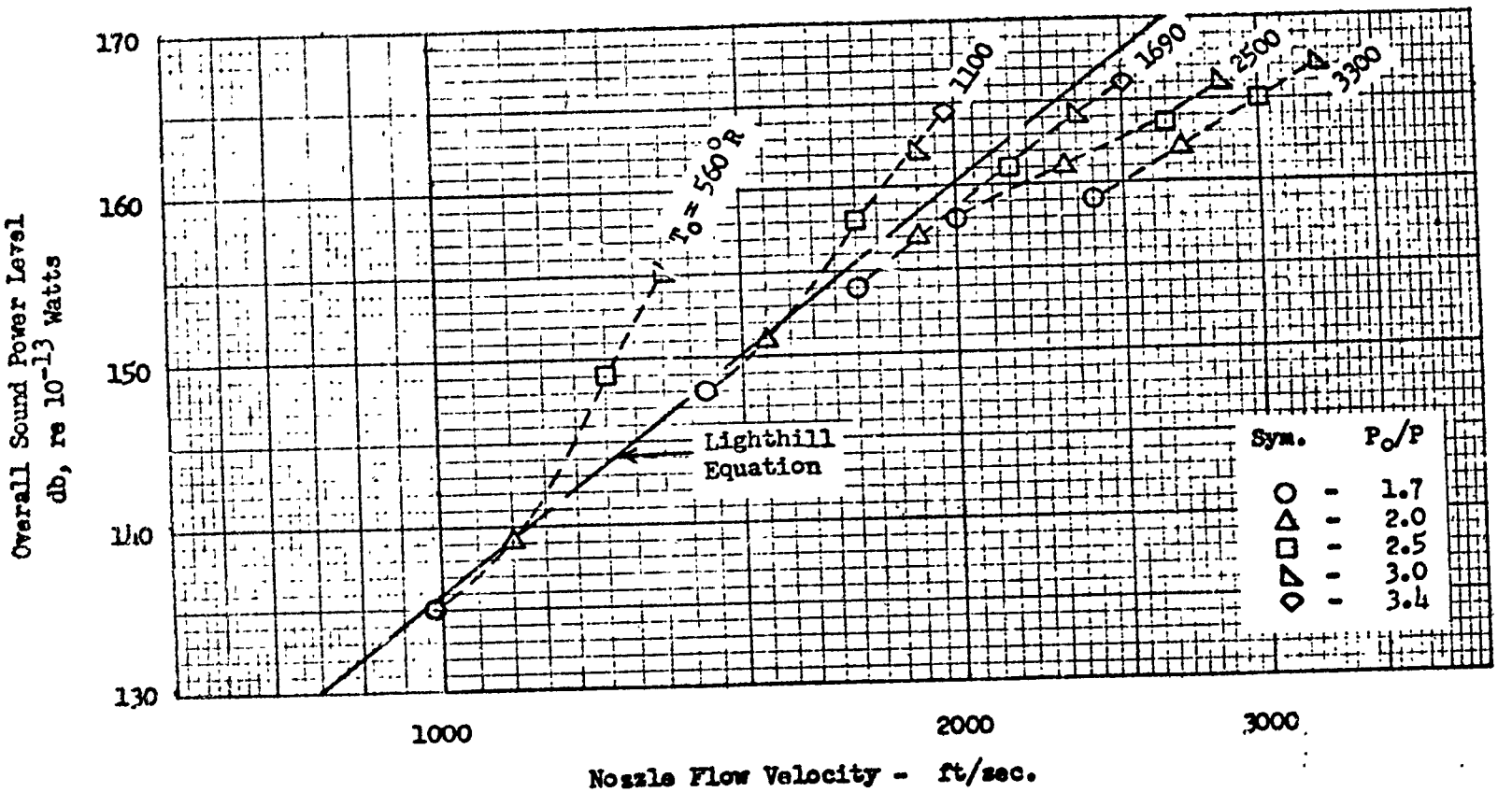

Figure 3.2 - Total Acoustic Power Generated by Scale Model Conical Nozzle (Dia. = 3.85 in.) as Compared to Levels Predicted by Lighthill Parameter.

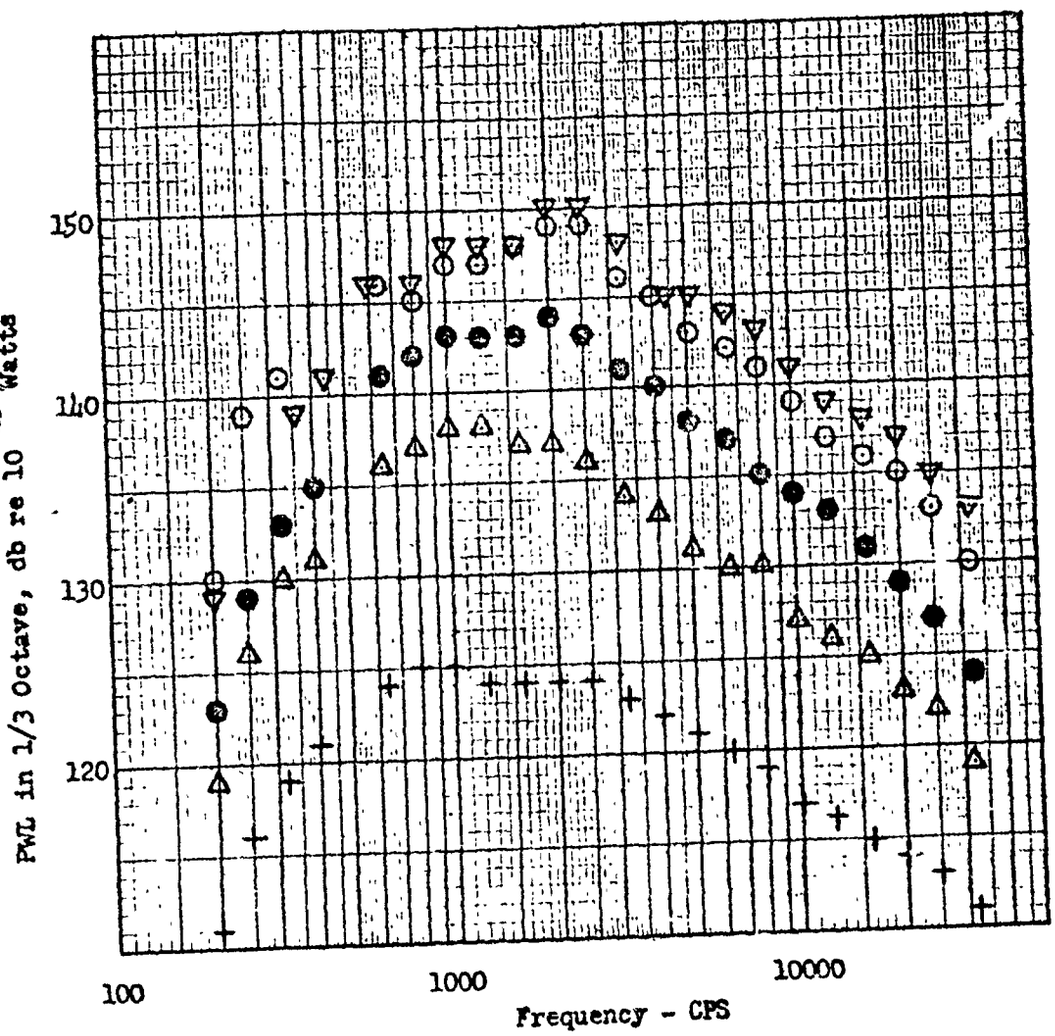

Figure 3.3a - Conical Nozzle Sound Power Spectra
Nozzle Diameter 3.85"

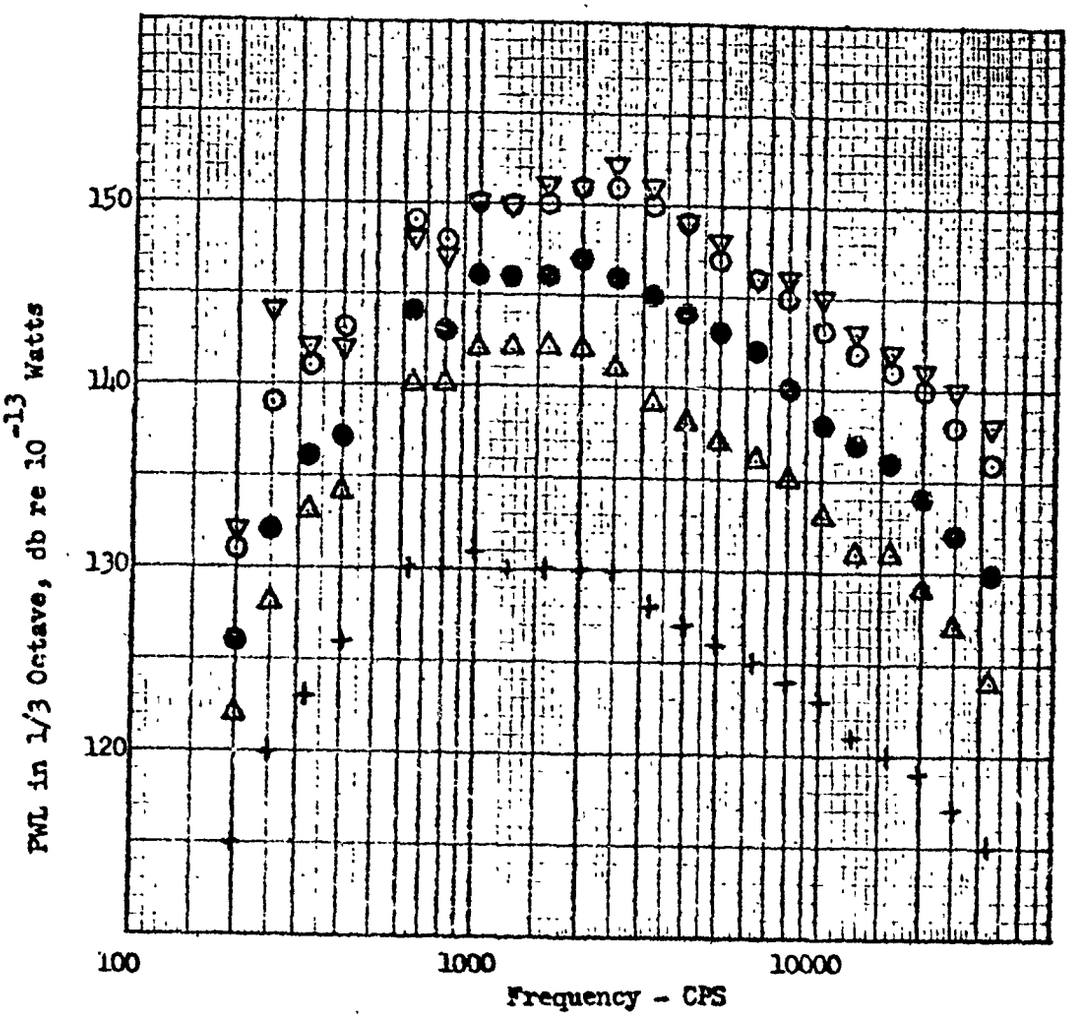

Figure 3.3b - Conical Nozzle Sound Power Spectra
Nozzle Diameter = 3.85"

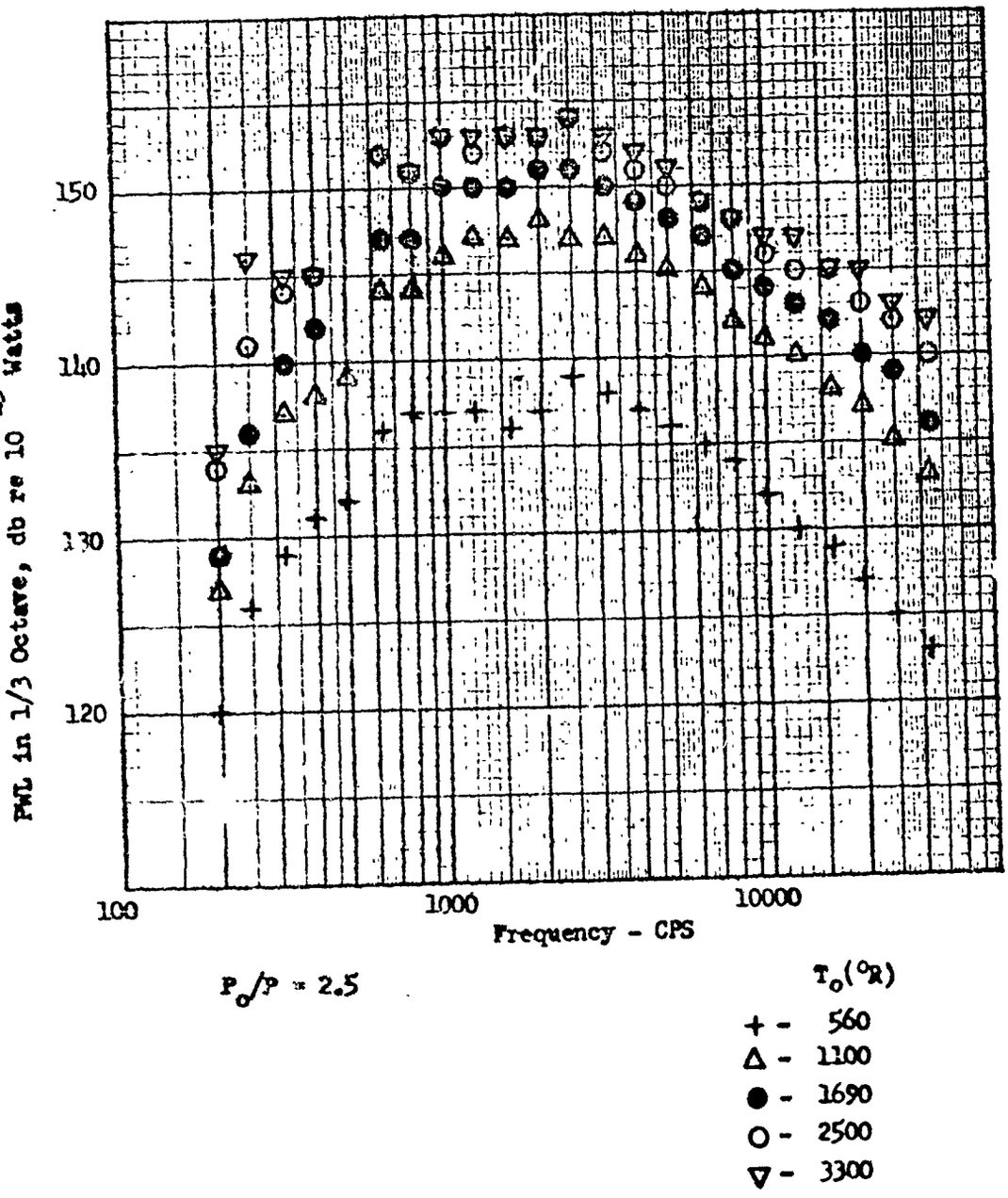

Figure 3.3c - Conical Nozzle Sound Power Spectra
Nozzle Diameter = 3.85"

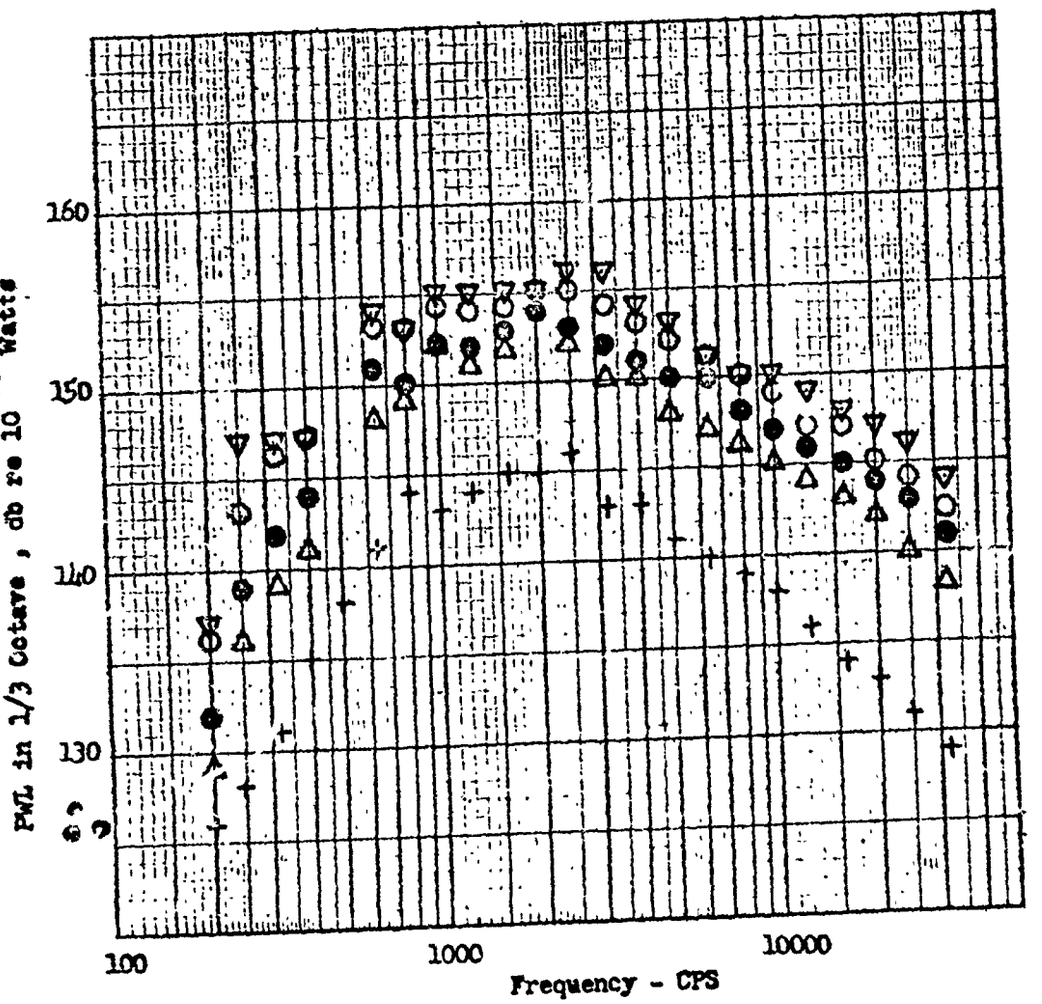

Figure 3.3d - Conical Nozzle Sound Power Spectra
Nozzle Diameter = 3.85"

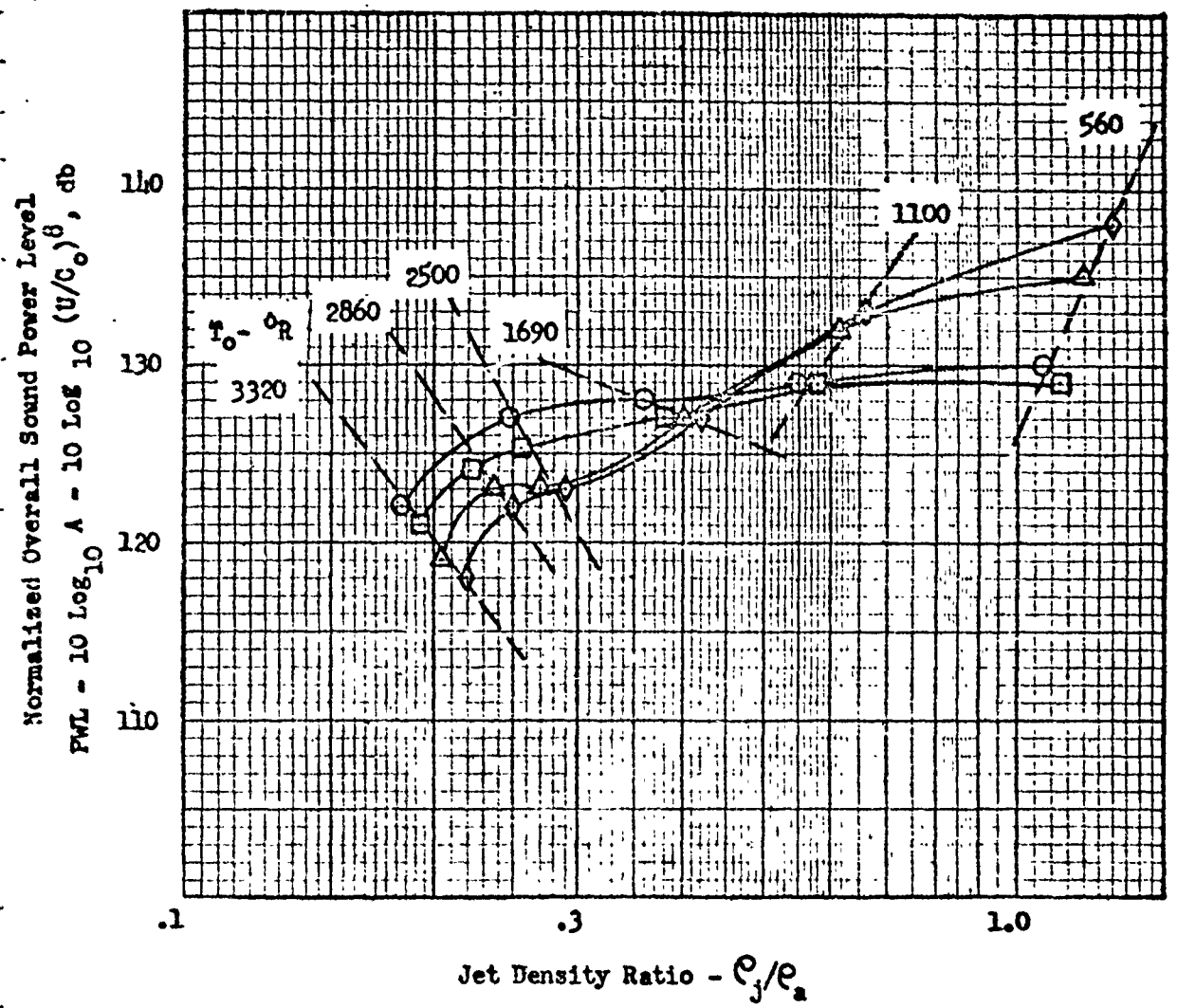

Figure 3.4 - Effect of Jet Density on Sound Power Generation.

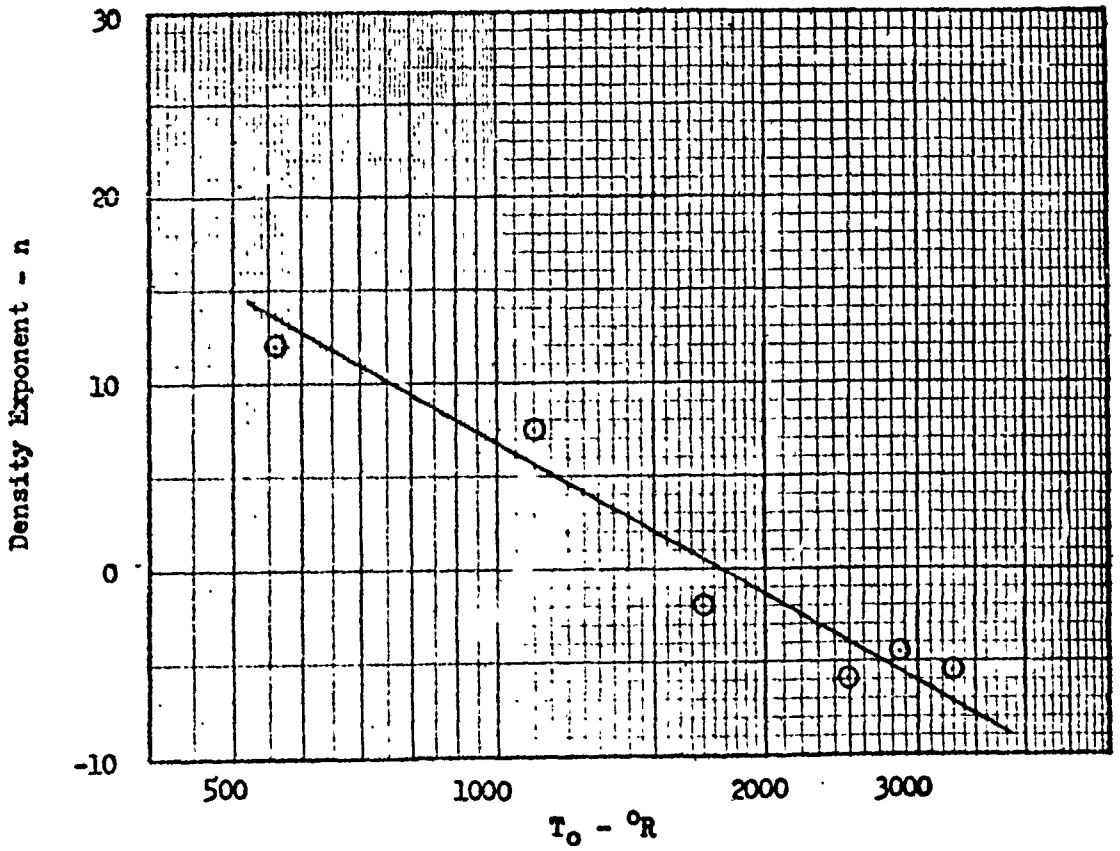

$$PWL = 10\ Log_{10}\ A + 10\ Log_{10}\ (U/C_o)^8 + 10\ Log\ (\rho_j/\rho_a)^n + K(T)$$

Figure 3.5 - Effect of Jet Total Temperature on Density Exponent n.

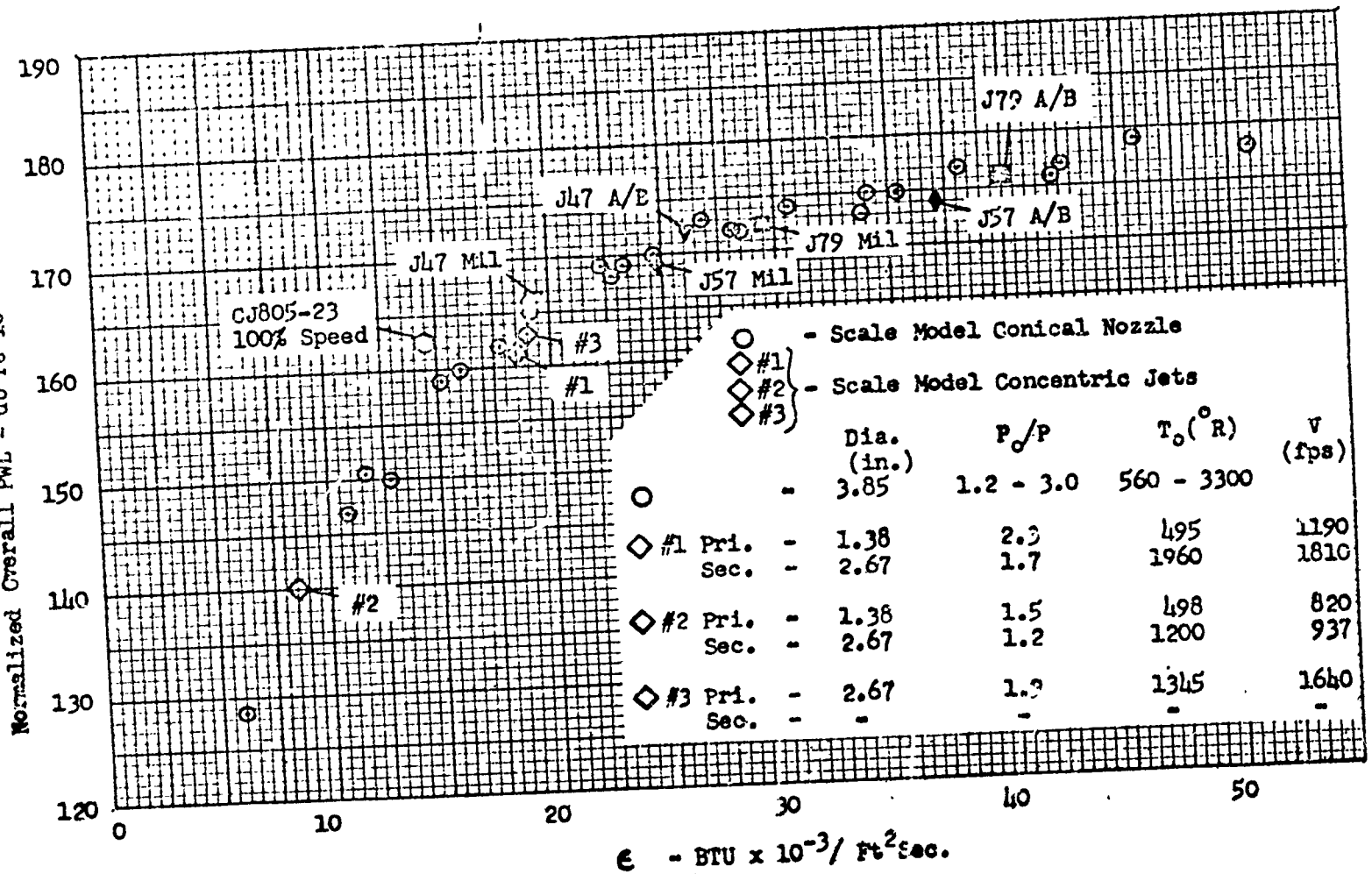

Figure 3.6 - Correlation of Jet Noise Total Acoustic Power with Nozzle Energy Flux.

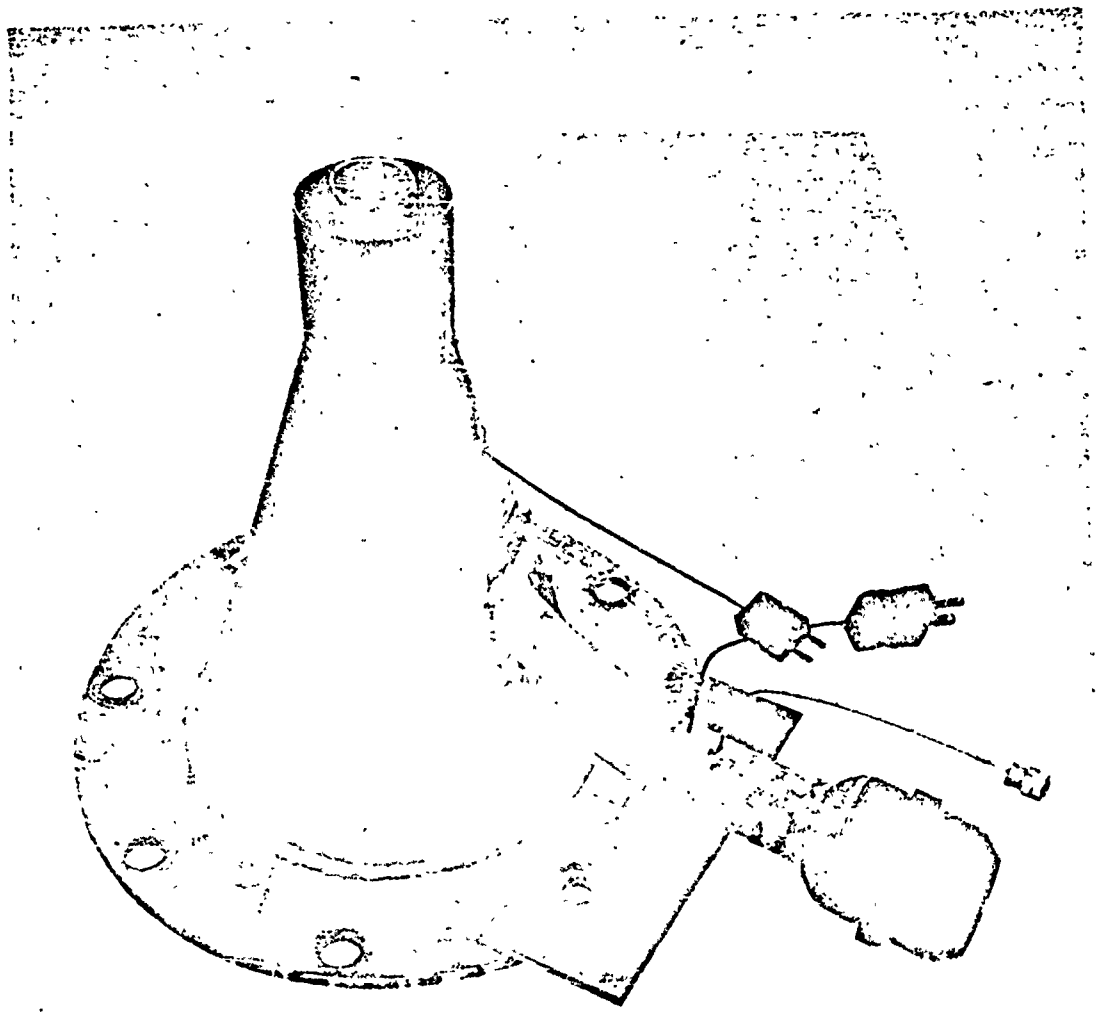

Figure 3.7 Concentric Flow Nozzle

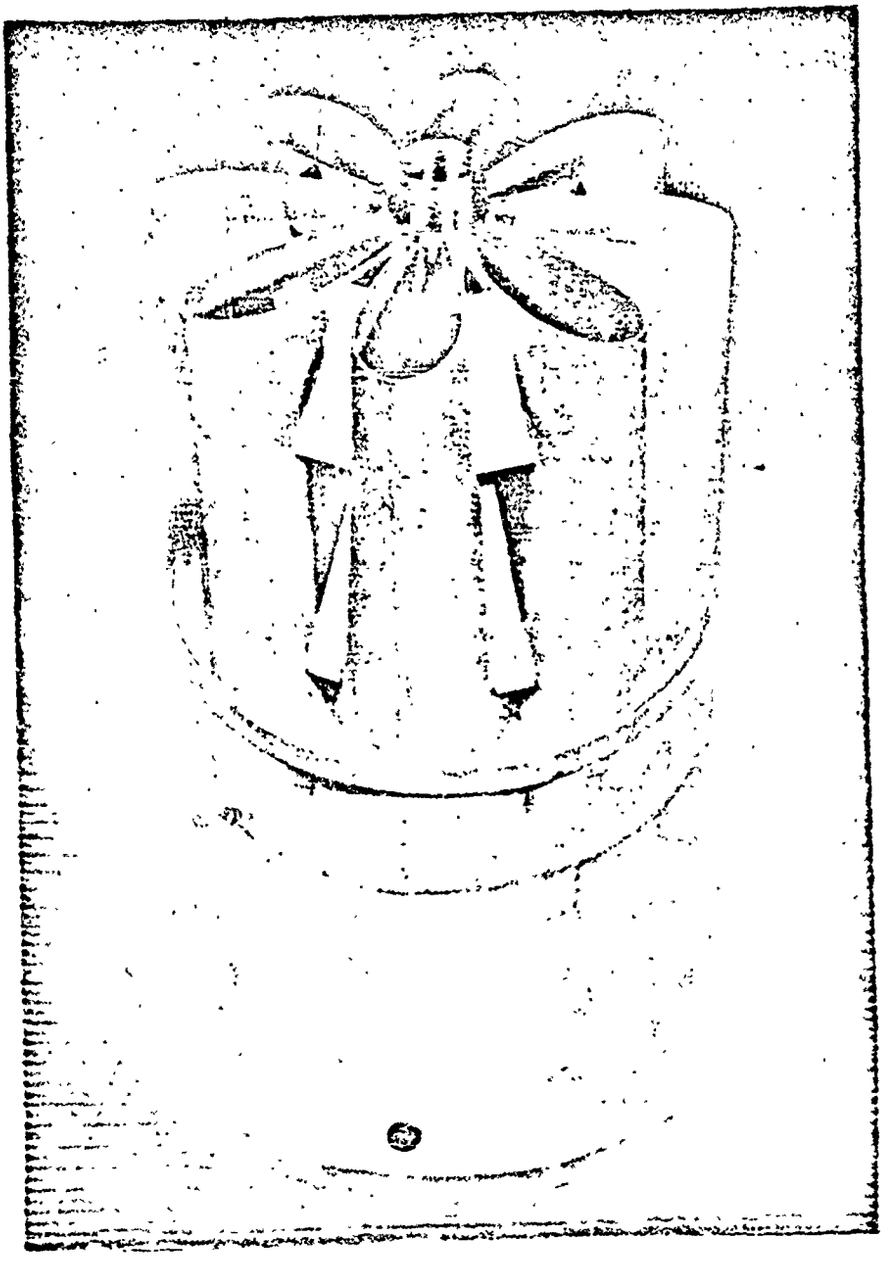

Figure 3.8 Eight Lobe Nozzle (298)

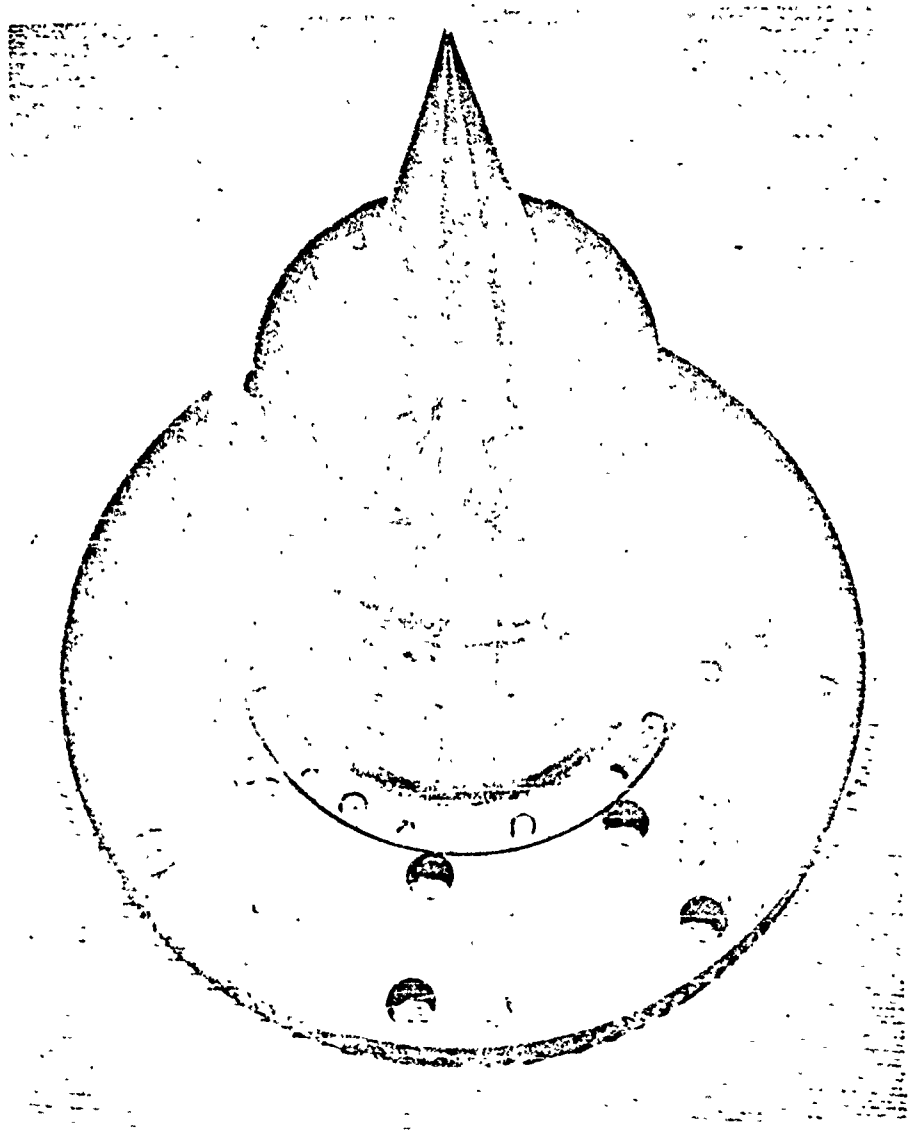

Figure 3.9 18 Segment Nozzle

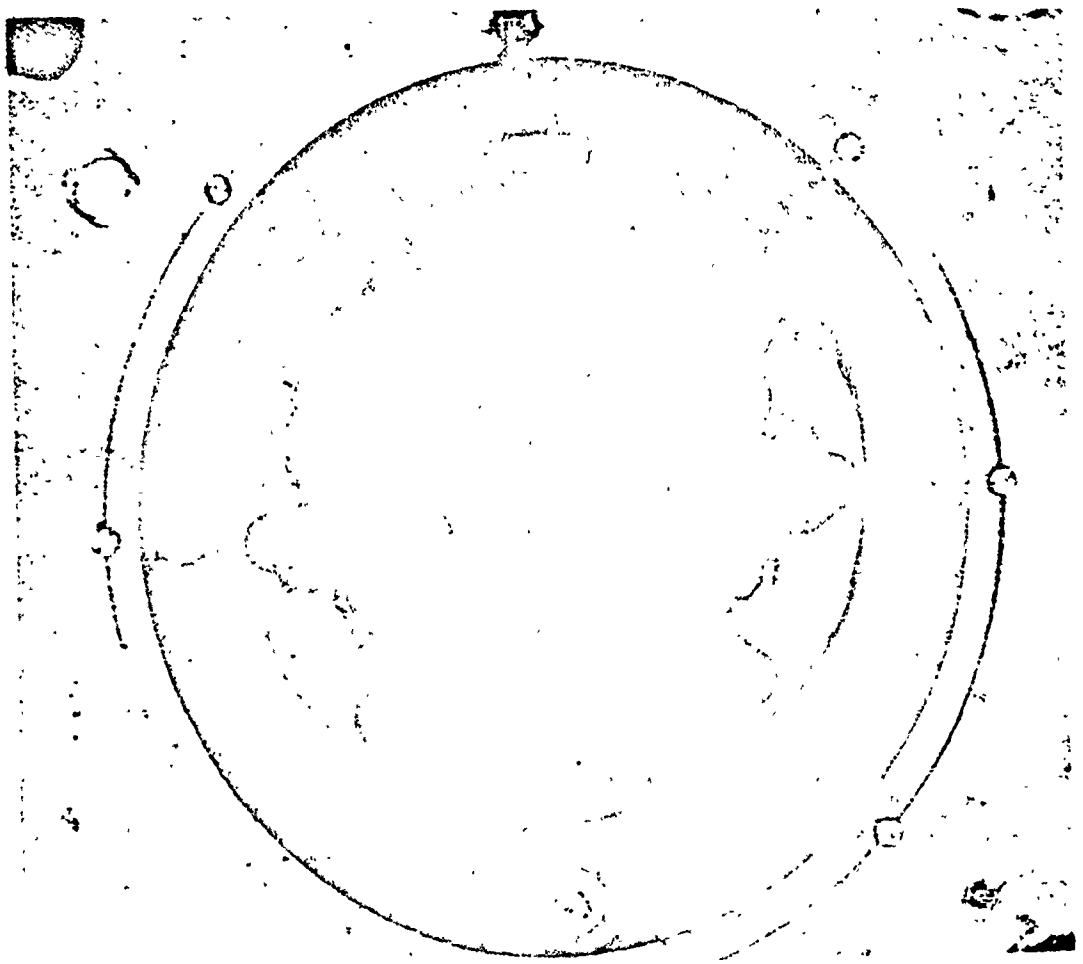

Figure 3.10 19 Tube Nozzle

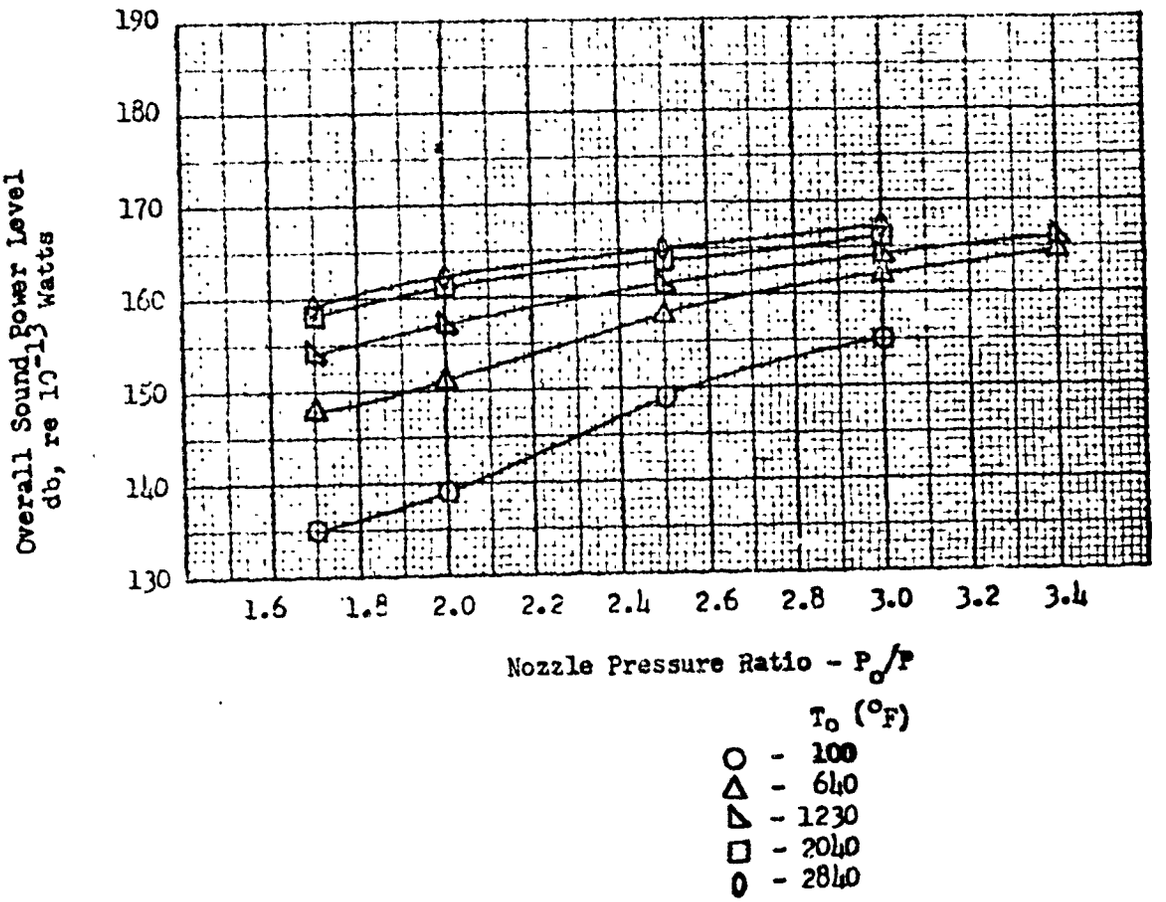

Figure 3.11- Conical Nozzle Jet Noise Generation.

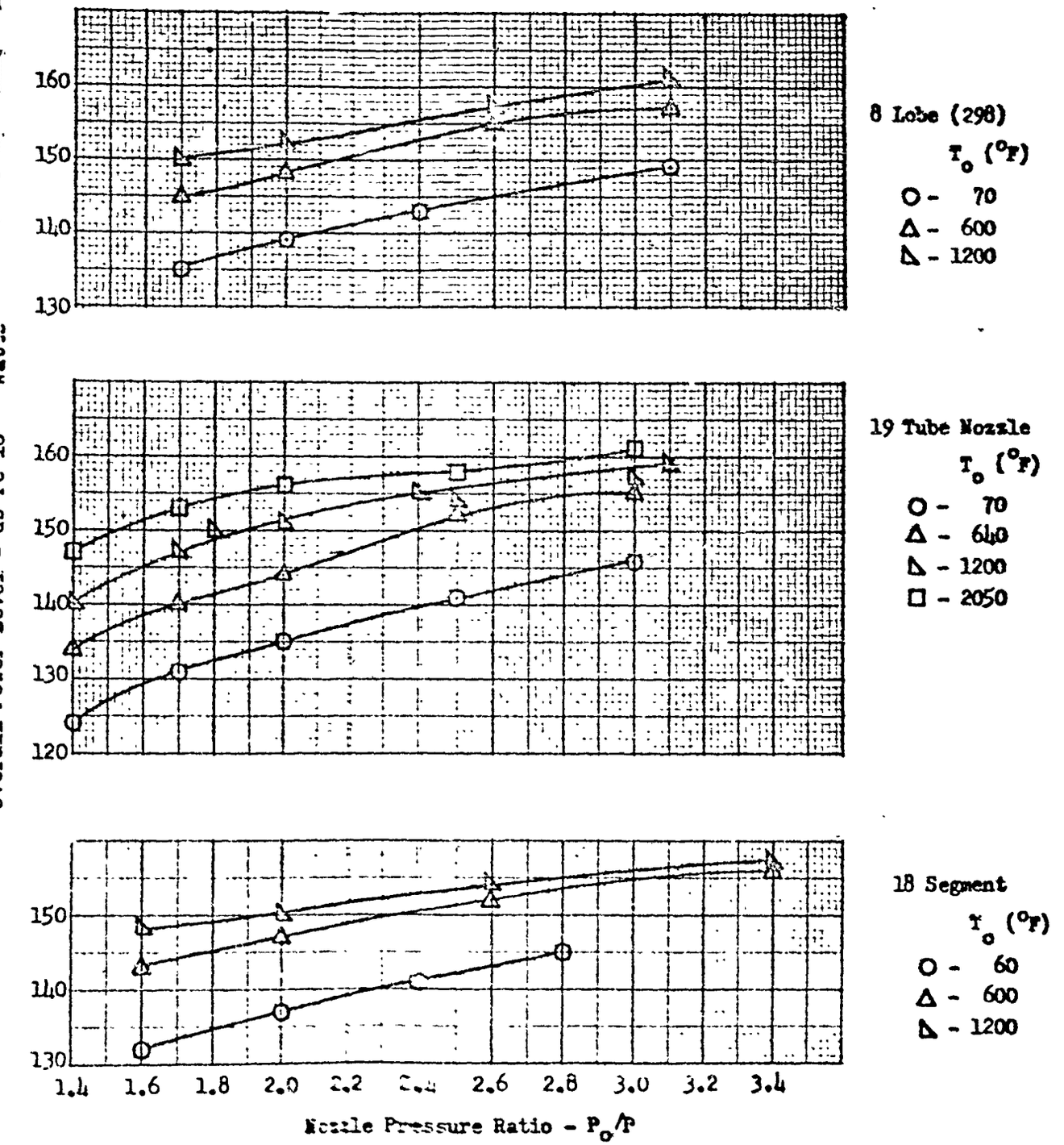

Figure 3.12 - Suppressor Nozzle Jet Noise Generation.

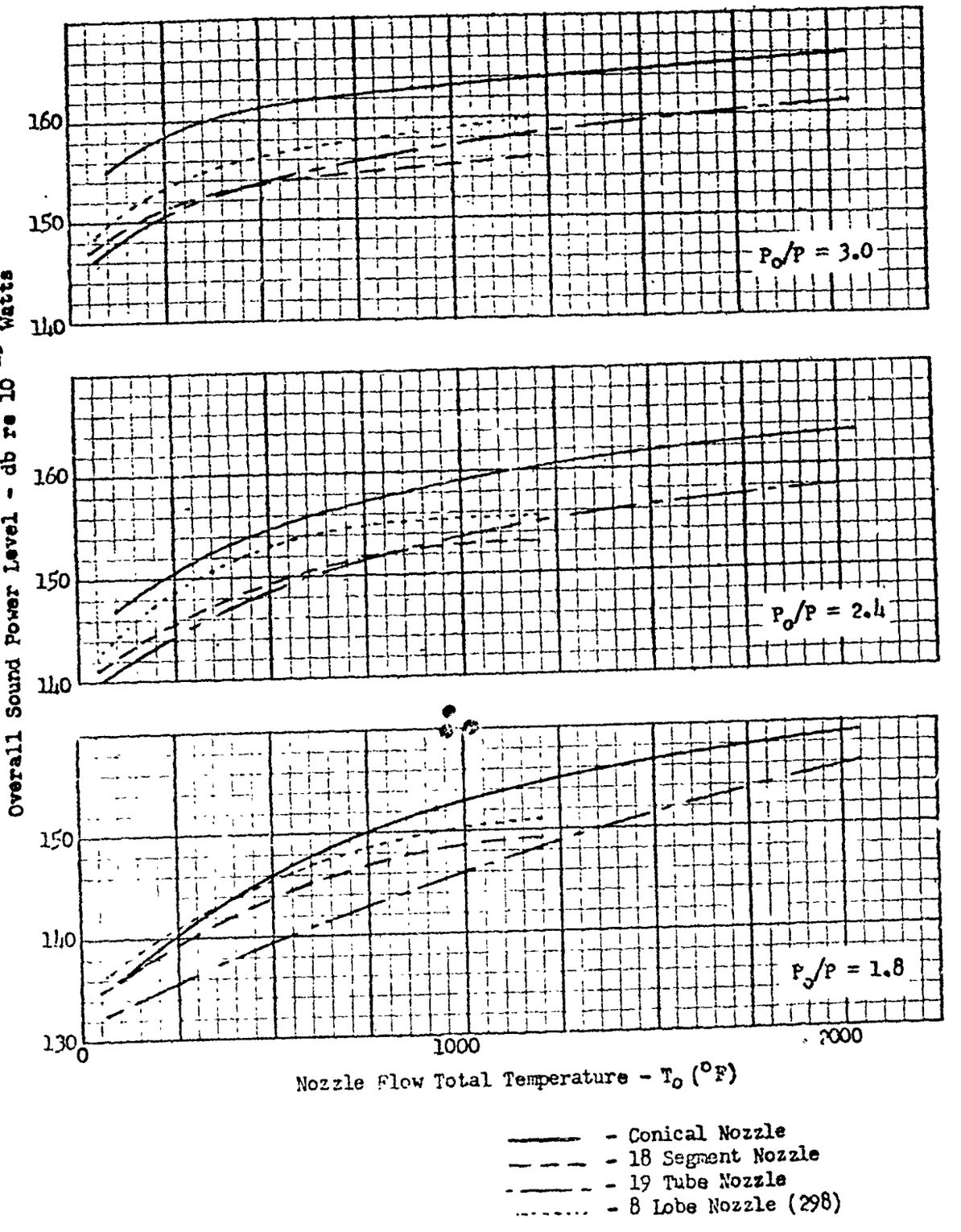

Figure 3.13 - Effect of Flow Temperature and Pressure Ratio on Suppressor Acoustic Performance.

4.0 EXPERIMENTAL STUDY ON TRANSMISSION AND DISSIPATION OF SOUND THROUGH A TURBULENT JET WAKE

4.1 Introduction

A major assumption of the jet noise suppression theory relating the aerodynamic and acoustic properties of jet flow is that all of the stream-generated noise radiates, without significant loss, into the far field. For complex suppressor-nozzle designs, the validity of this assumption can be questioned, since sound sources associated with the inner flow elements are surrounded by high velocity, turbulent flow. There exists some experimental evidence that acoustic energy is dissipated in the highly turbulent jet mixing region. In Reference 1, jet noise data is presented showing that sound levels measured in the far field of a rectangular array of nozzles is higher when the measuring location is oriented along the long side of the multiple tube configuration as compared to the short end of the array (Figure 4.1). This effect, referred to as shielding, indicates that perhaps the sound generated by innermost elements of a suppressor is unable to propagate through the turbulent regions created by surrounding suppressor elements. Although theoretical justification for significant absorption of audio frequency sound in a jet wake is lacking, it is important that the possibility be investigated since positive evidence of sound dissipation would require modification of the correlation between acoustic and aerodynamic properties of the jet wake. Furthermore, absorption of acoustic energy in the jet wake could explain in part the increase in noise reduction by a suppressor as pressure ratio is increased.

Experiments have been conducted in an effort to determine whether or not dissipation of sound does occur, or whether the noise reduction effect

referred to as shielding is a directivity rather than power level change effect.

4.2 Experimental Procedure

The determination of the magnitude of sound energy absorption in turbulent flow, as related to jet noise suppression, requires that the power level of a source be determined after propagation through a turbulent jet wake compared to the source power level in the absence of the turbulent jet. Ideally, a discrete frequency sound source, which could easily be distinguished from broad-band jet noise, could be located within a jet wake, and sound power level change could be determined in a reverberant room for various jet velocities. However, the problem of locating such a sound source within a jet wake without altering its acoustic output is quite difficult.

An alternative method for evaluating sound absorption by the jet wake involves placement of the sound source outside the jet boundary while positioning the acoustic pickup within the wake. While this scheme eliminates the source variation problem mentioned above, it presents the difficult problem of extracting the pure tone source signal from the jet noise and jet pressure fluctuations especially for high Mach flow. Even more difficult would be the evaluation of convective effects on the sound propagating through the jet flow. Since the sound path through the wake would depend on flow velocity, comparison of levels measured with and without flow would be exceedingly difficult.

In a third possible approach to the experimental investigation, the high intensity pure tone sound source can be located outside the jet wake, and a survey of sound pressure level is made by traversing a microphone along the jet boundary, but not in the flow, on the opposite side of the wake. Free

field acoustic environment is required, and effects of changing sound path length due to convection of the signal in the jet flow can be minimized by locating the sound source sufficiently far from the jet wake. Because of the decreasing flow velocity in the jet in the downstream axial direction, a focusing of the sound propagating through the flow would occur as described schematically in Figure 4.2. The sound waves entering the wake in the high flow velocity region near the nozzle exit are convected further downstream than waves entering in the lower velocity regions of the jet, thus forming the shadow zone near the nozzle exit and somewhat focusing the rays at a downstream location. In order to evaluate the possibility of sound dissipation, the intensity of the transmitted sound must be measured over a suitably long region of the jet so that a valid average sound pressure can be determined, considering both the shadow zone and region of apparent amplification.

Experimental investigations were conducted following the three previously described procedures, but concentrating on the first and third methods. The second scheme, with the sound pickup within the jet wake, presented considerable difficulty in extracting the pure tone sound from the jet pressure fluctuation and thus it was abandoned.

The acoustic signal for which attenuation effects were to be evaluated was produced by a Hartman generator (Figure 4.3). The device consists of a 3/8 inch diameter convergent nozzle which discharges at pressure ratio of 4.5 into a 1/2 inch diameter cavity. The generator produces a high intensity discrete tone. The frequency of the whistle is a function of the cavity depth which can be varied by a piston in the cavity. The acoustic power level produced is on the order of 150 db (re 10^{-13} watts) over a frequency range of 1200 to 9000 cps.

Experiments on the dissipation of sound with the source within the jet were carried out using the apparatus shown in Figure 4.4. The Hartman generator was located in a cylinder within an annular jet so that the jet flow would not affect its acoustic output. Measurements of reverberation sound pressure level were made in a reverberant room, for various source frequencies and nozzle pressure ratios. Average pure tone sound levels were determined by slowly moving the microphone within the room and reading its output, separated from jet noise by means of a narrow band filter, with an acoustic integrator (Ref. 2). Static pressure was measured within the Hartman generator enclosure, and the maximum variation from ambient was 2.5" H_2O at nozzle pressure ratio $P/P_0 = 2.2$. This small change in pressure could not affect the whistle performance. Results of the investigation are shown in Figure 4.5, where reverberation sound pressure level for the whistle tone is plotted against nozzle pressure ratio for various pure tone frequencies. A small decrease in sound level is observed as the jet flow begins, but this reduction does not appear to increase as flow pressure ratio is raised. If the sound energy is dissipated in the turbulent flow, then the more turbulent higher pressure ratio flow should provide increased noise reduction. Since this is not the case, a plausible explanation for the slight decrease in sound pressure level is that the supply pressure to the Hartman generator decreases slightly as nozzle airflow is initiated. Since rather small supply pressure variation can affect the whistle output, this is believed to be the source of the noise reduction. In the succeeding experiment, supply pressure was monitored much more closely so as to preclude such an occurrence.

Further experiments were conducted to determine if sound in the audible frequency range is attenuated during propagation through the turbulent flow exhausting from a nozzle. As in the previously described work, a high intensity, pure tone sound source (Hartman Generator) provided the acoustic signal, and a 3-1/2 inch diameter conical nozzle was utilized to create the turbulent wake. The experimental set up was as shown in Figure 4.6. The sound source was located 4-1/2 nozzle diameters downstream of the nozzle exit, and several diameters to the side of the stream. On the opposite side of the jet wake a microphone was traversed over a distance of approximately 4 nozzle diameters. Thus, by positioning the turbulent flow between sound source and acoustic pickup its effect on the acoustic signal could be determined. In order to measure only the direct sound and eliminate reverberation, the Acoustics Laboratory anechoic room was utilized. The room is capable of handling the airflow from the 3-1/2 inch diameter nozzle operating at pressure ratio up to 2.4. To test whether attenuation through the stream could be measured in this facility, a mechanical sound barrier 6" in diameter was positioned between sound source and microphone in the approximate location of the jet wake. The attenuation measured using the mechanical barrier in place of the jet wake was 13 db; sufficient to indicate that reflected and refracted sound is at a level low enough so as not to obscure attenuation through the stream, which might be of lesser magnitude.

Source frequencies of 2.5, 5.0, and 9.0 kcps were used, and nozzle pressure ratios up to 2.4 were tested. So as to obtain a usable signal to noise ratio, a Panoramic Sonic Analyzer with 25 cps filter band width was used as a signal filter for the microphone output.

A plot of sound pressure level along the microphone traverse path, for three nozzle pressure ratios, is shown in Figure 4.7. Note that "shielding" occurs in the region near the nozzle exit, and amplification is experienced further downstream due to convection of the signal in the jet wake. Results indicate that the peak amplitude measured is independent of flow velocity, but that the flow has a pronounced influence on directivity. Thus, if dissipation of sound does occur, it is insignificant in magnitude in the audible frequency range. The results indicate that the "shielding" of noise from one jet by the flow from another as reported by other researches is a directivity effect, and that the decrease in noise experienced at one position is accompanied by an increase where the sound is convected downstream.

4.3 Conclusions

The results of the experiments described indicate that little, if any, sound is absorbed by the turbulent jet wake, in agreement with the work in Ref. 3. Thus, no modification of the correlation of aerodynamic and acoustic jet properties is required from this consideration.

The shielding effect of a jet wake has been shown to be a result of directivity rather than sound power change. The problem of measuring the sound power of a jet in the presence of a shielding wake, requiring exceedingly precise acoustical measurements, has been bypassed by substitution of a pure tone sound source for the jet noise source.

REFERENCES

1. Greatrex, F.B., "Noise Suppressors for Avon and Conway Engines", ASME PP 59AJ49, 1959.

2. Lee, R., et al, "First Biannual Progress Report - Program of Research on Noise Suppression", General Electric Company, Flight Propulsion Laboratory Dept., Report No. R60FPD49. Prepared for Bureau of Aeronautics, Dept. of Navy, under Contract NOas 59-6160 C, Jan. 1960.

3. Miller, E.A., "Some Experimental and Theoretical Results Relating to the Production of Noise by Turbulence and the Scattering of Sound by Turbulence or Single Vortices". Second Symposium - Naval Hydrodynamics - ONR/ACR-38, Aug. 1958.

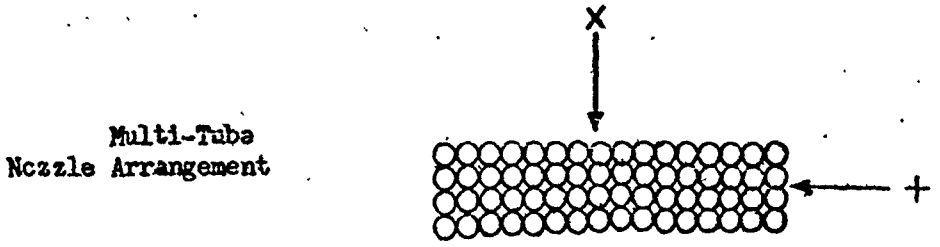

Symbols Indicate
Measuring Direction

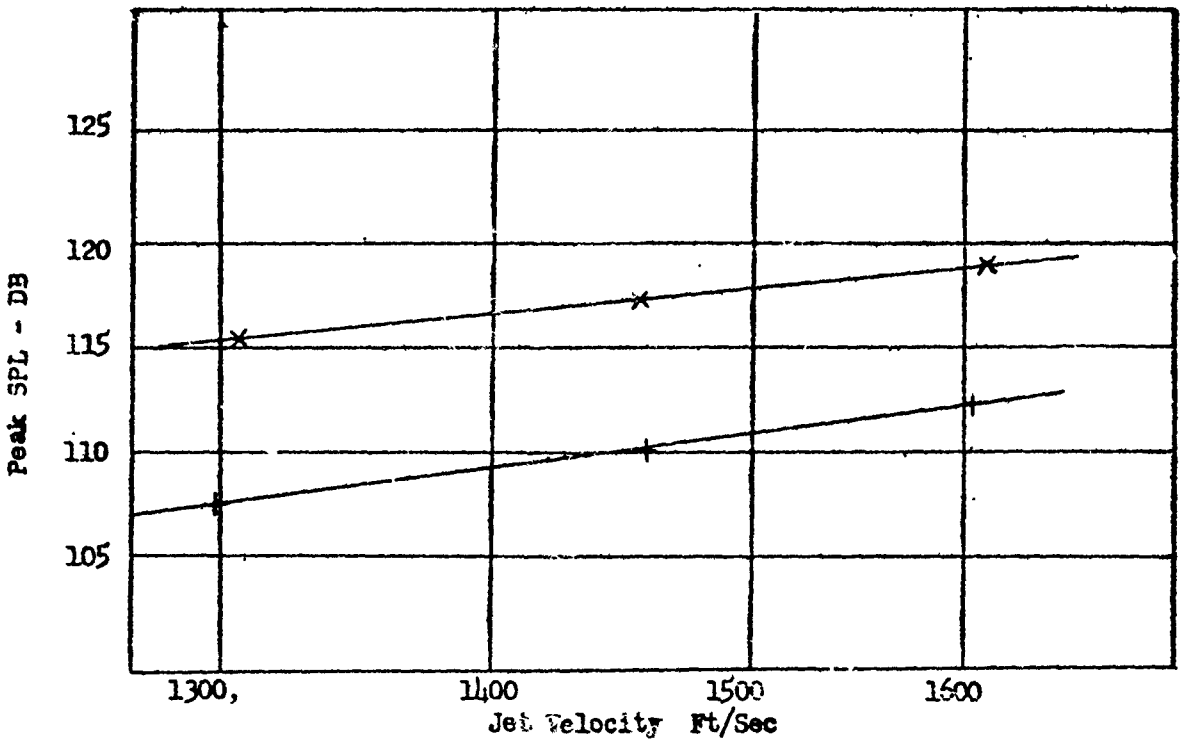

Figure 4.1 - Shielding of Jet Noise by Multi-Tube Nozzle Arrangement.

From Ref. 1

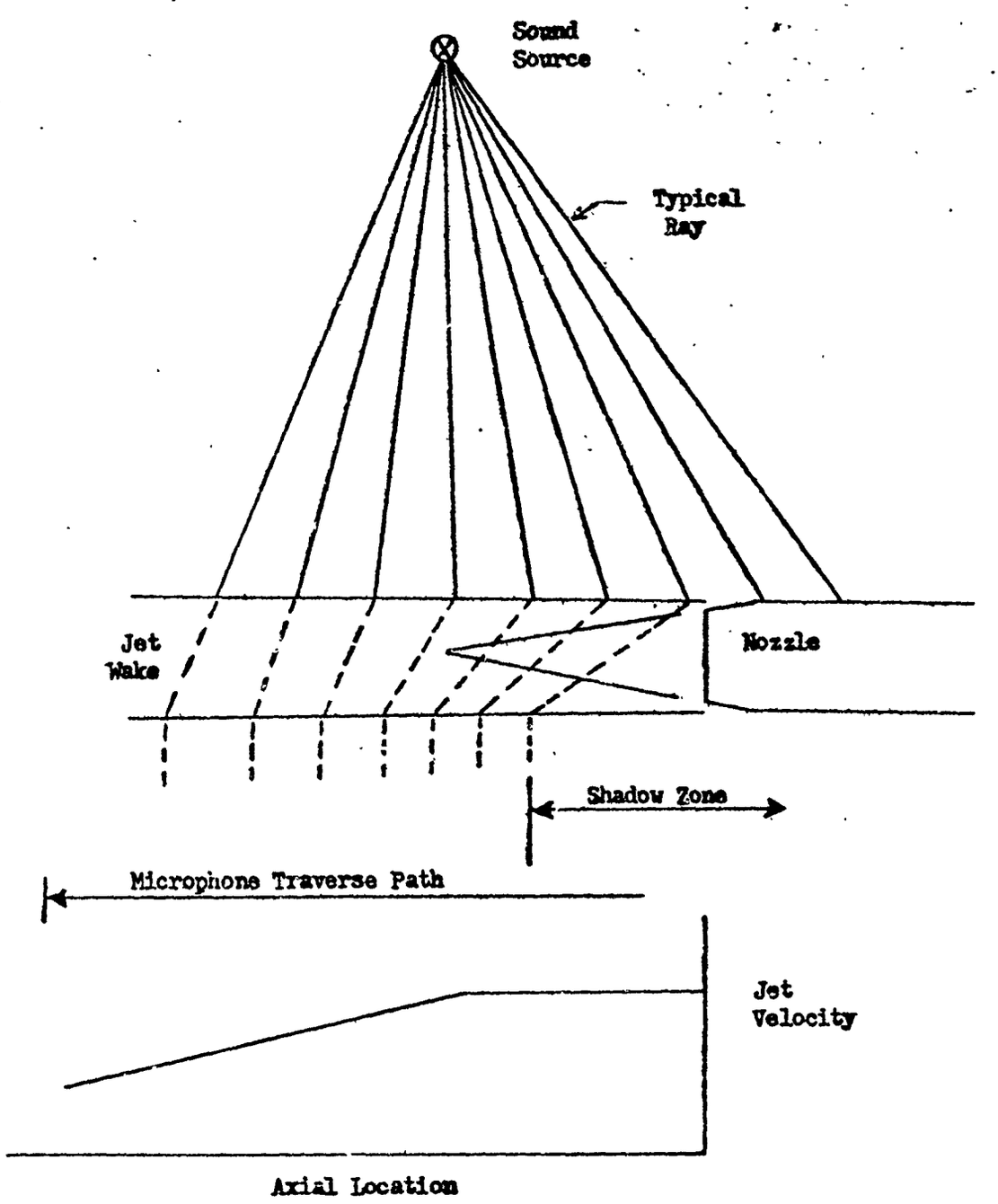

Figure 4.2 - Schematic Description of Focusing of Sound by a Jet Wake.

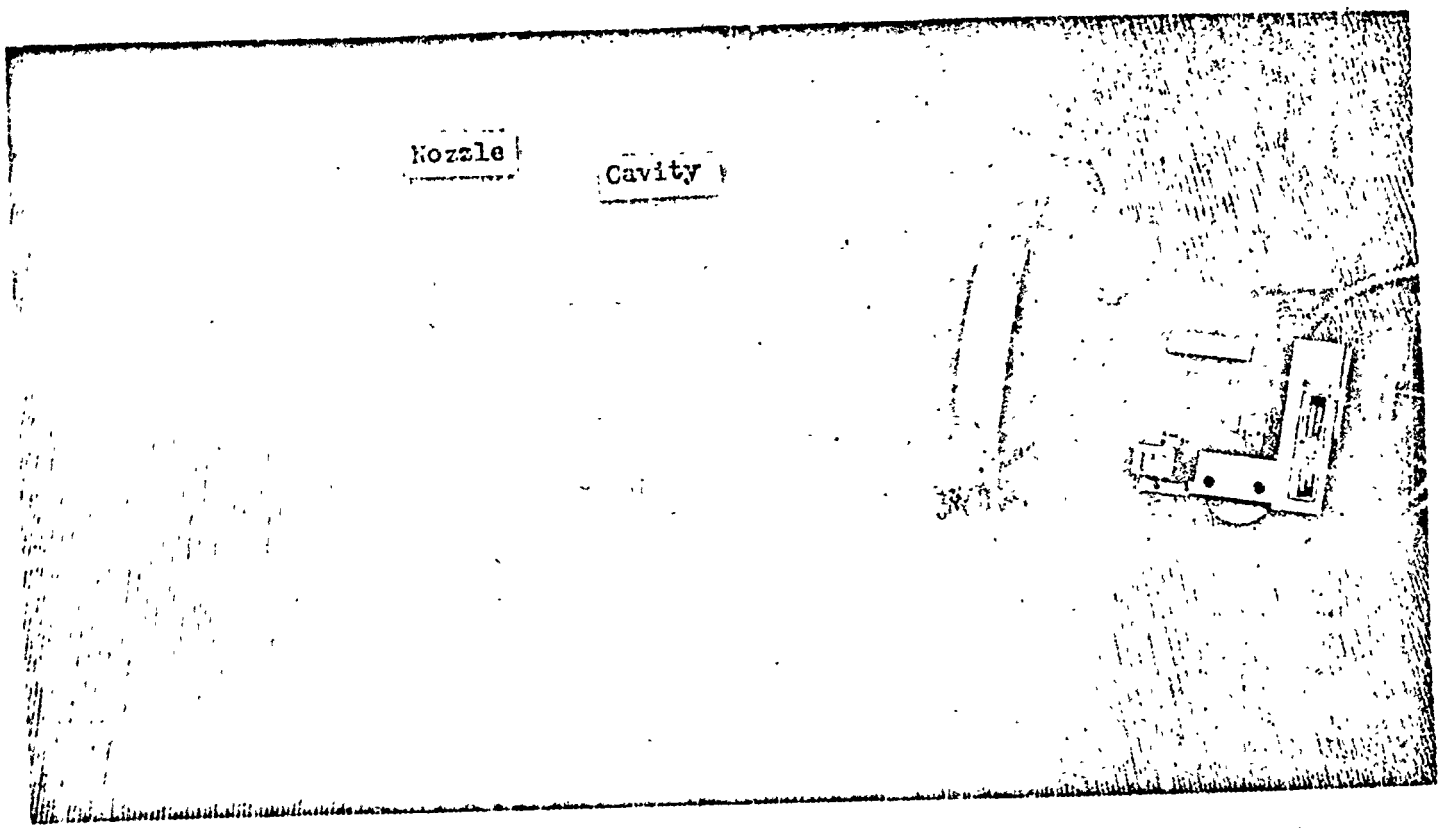

Figure 4.3 - Hartman Generator Noise Source

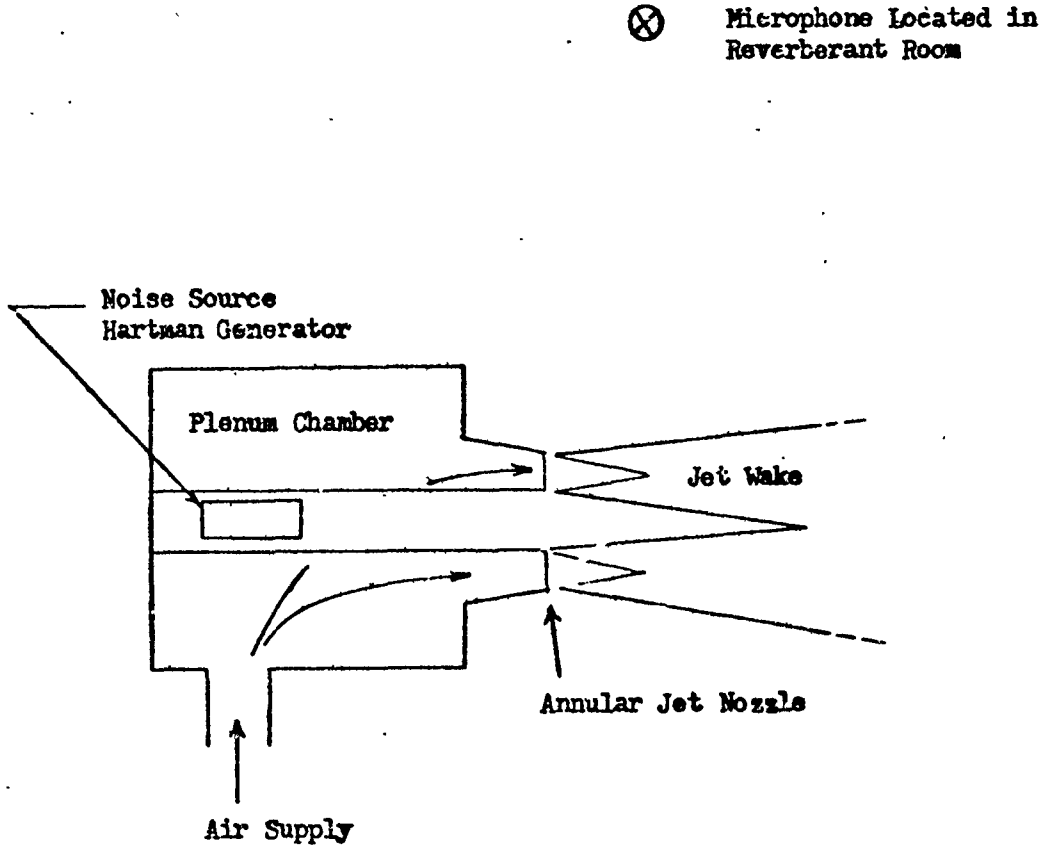

Figure 4.4 - Experimental Arrangement for Test of Dissipation of Sound through Turbulent Flow; Sound Source Located within Jet Wake.

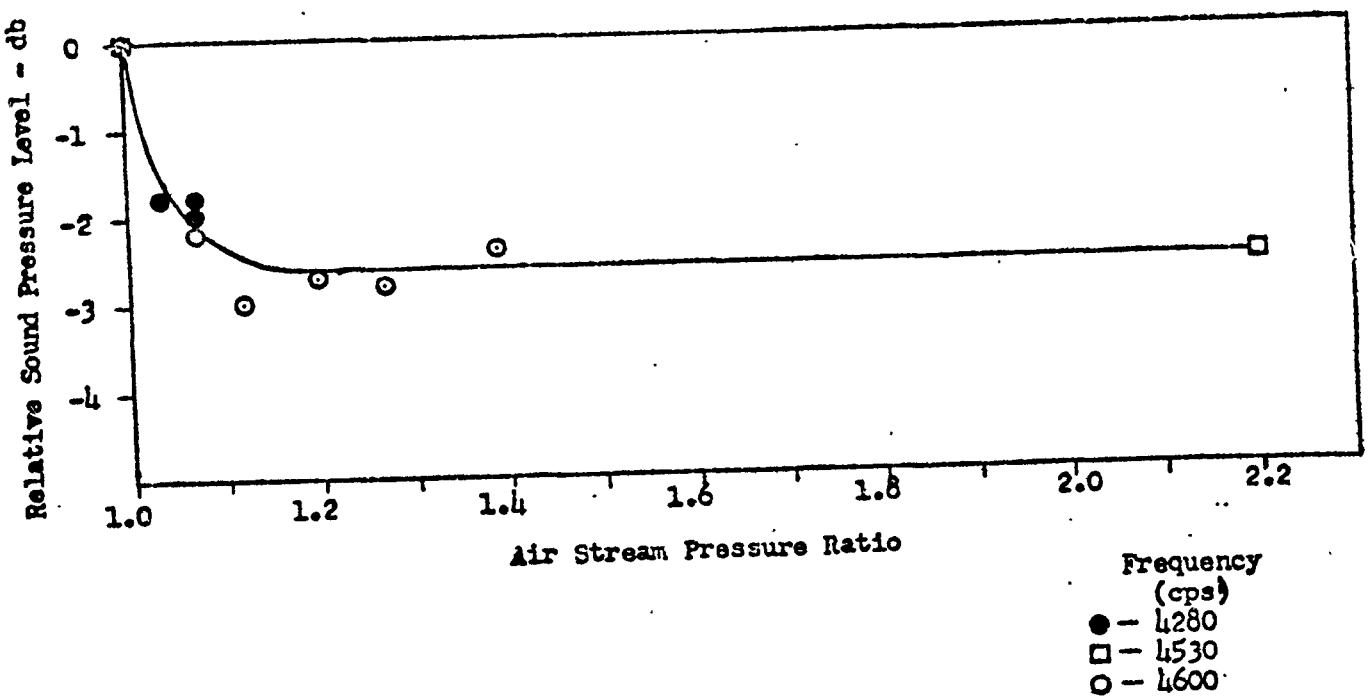

Figure 4.5 -- Sound Dissipation Test Results for Noise Source within Jet Stream

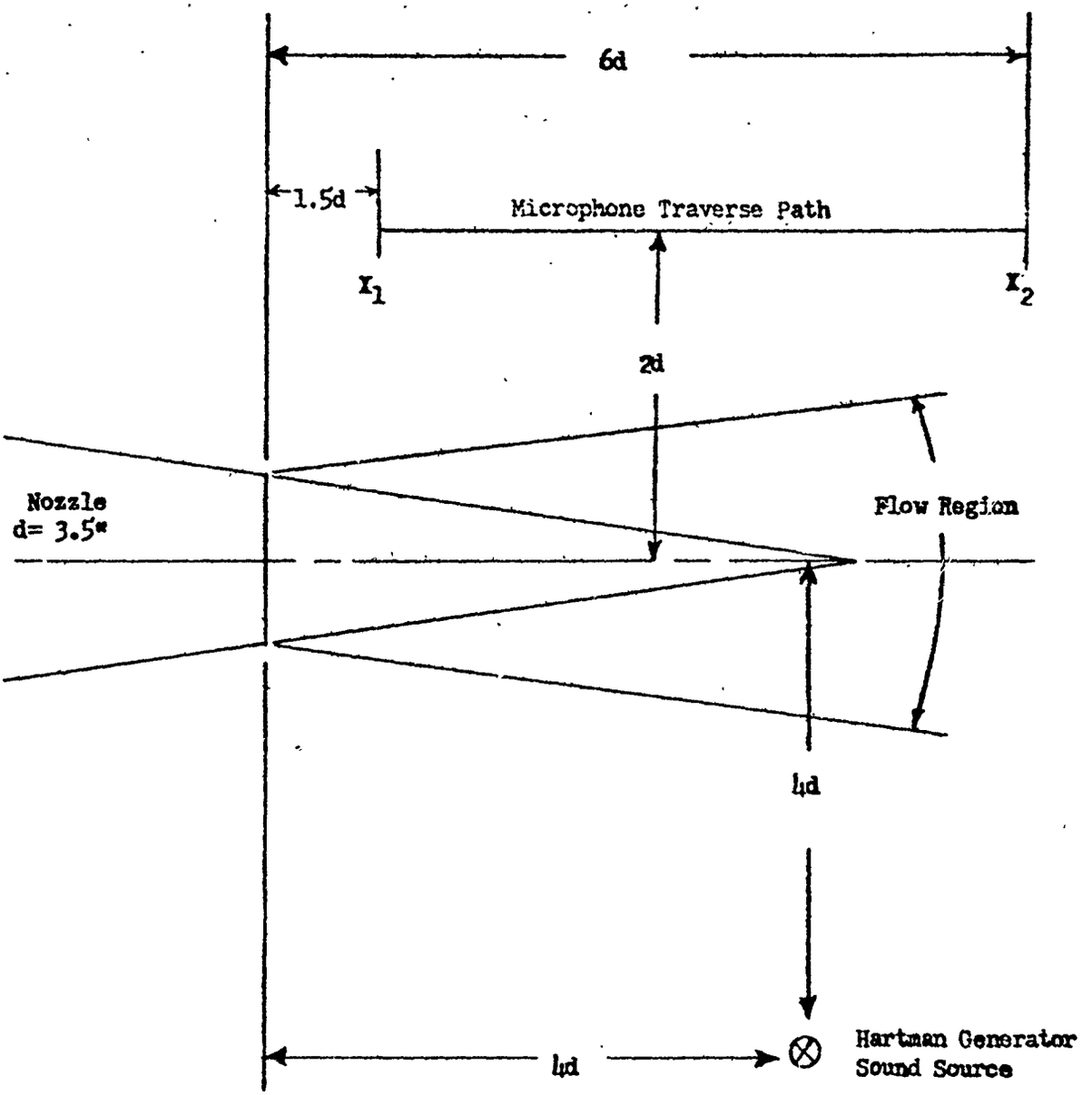

Figure 4.6 - Experimental Arrangement for Test of Dissipation of Sound through Turbulent Flow.

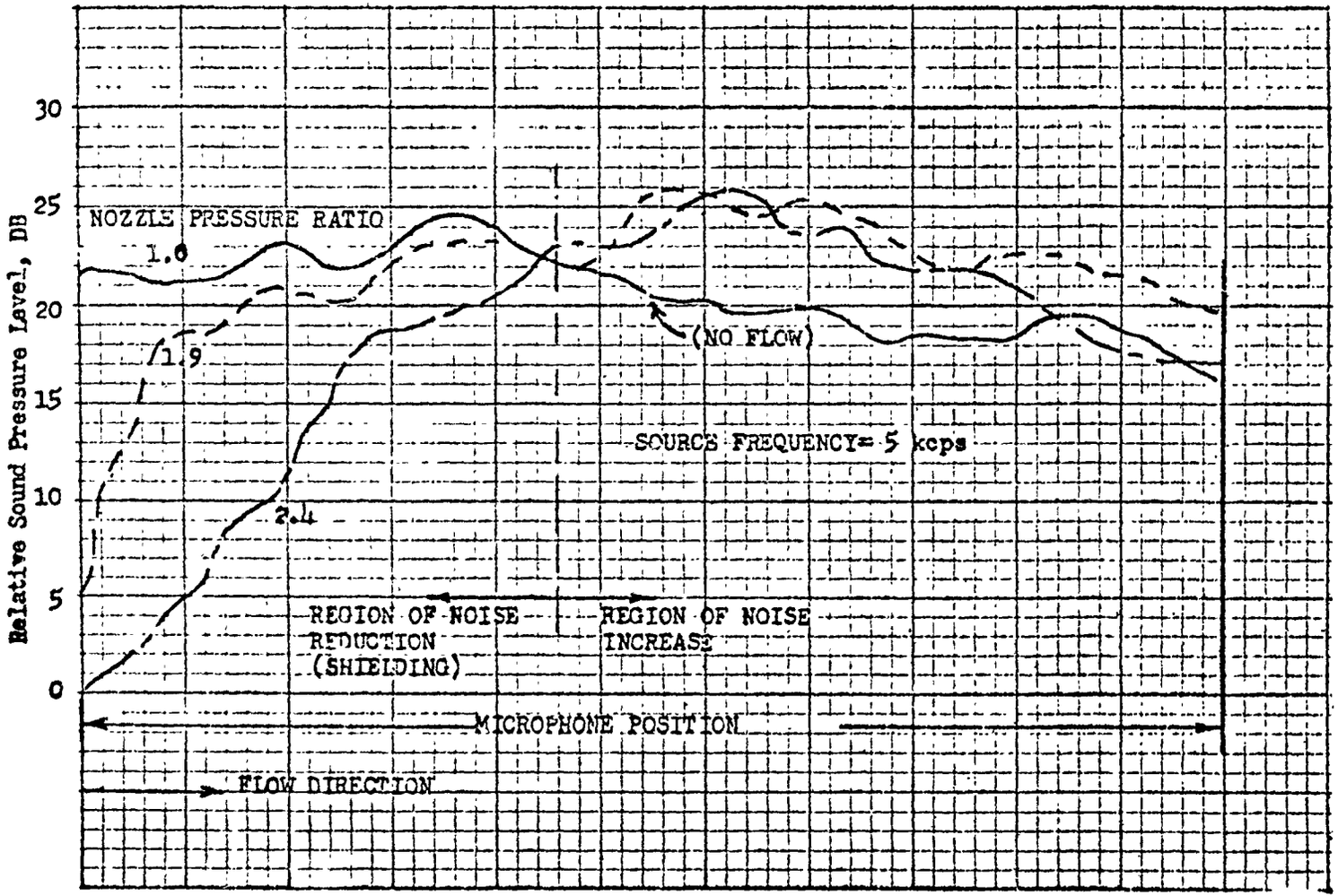

See Fig. 4.6

Figure 4.7 - Effect of Flow Velocity on Amplitude and Directionality of Sound Propagating Through Jet Wake.

5.0 AN EVALUATION OF SELECTIVE WATER INJECTION AS A JET NOISE SUPPRESSION TECHNIQUE.

5.1 Introduction

Conventional techniques for jet noise suppression basically rely on subdivision of the main nozzle flow into a number of separate streams in such a manner as to produce favorable jet mixing through interaction of the elemental jets. The velocity profile theory indicates that the sound power generated by a free jet depends only on the mean-flow velocity distribution in the mixing region of the wake. If indeed the noise generated at a given axial location along the jet is primarily dependent on the velocity profile at that position and sufficiently independent of past history or the flow and the means employed to achieve the velocity distribution, then a mixer-type suppressor could effectively be replaced by another scheme which would alter the mean-flow velocity profiles without first subdividing the main jet. By injecting water sprays into a heated jet, the temperature and velocity of the flow can be lowered in selected regions of the wake, altering the velocity profiles. While it is known that spraying large quantities of water into the jet wake will reduce the sound power, generated (Ref. 1) the quantity of water required is such that this means of suppression cannot be considered as practical for in-flight use. However, by proper utilization of limited water flow, it is possible to alter the mean-flow velocity profiles rather than accomplish a gross velocity reduction for the entire jet. It is the suppression effect of this means of water injection which has been investigated and is reported here in fulfillment of the proposal work statement (Ref. 2).

The objective of the investigation was to determine feasibility of the selective water injection concept for jet noise suppression. As previously stated, the noise reduction achieved by non-uniform introduction of water sprays should be greater than reduction by thorough mixing and evaporation of the water in the jet wake, if the scheme is to be successful. Thus, as a standard for comparison, a theoretical calculation of overall power level reduction was made for a jet with completely mixed and evaporated water. The results are shown in Figure 5.1, and are based on the assumption that acoustic power depends on the eighth power of the flow velocity. The change in flow velocity was determined from heat balance calculation for the air and water mixture.

5.2 Experimental Procedure

The experimental approach adopted was to measure noise reduction for a heated jet with water injection as compared to an unsuppressed jet. Rather than make a complete survey of the sound field for sound power determination, it was decided to measure the more significant acoustic parameter of sound pressure level reduction at the angle of maximum jet noise radiation (40° from the jet axis). On the basis of noise directivity studies reported in References 3 and 4, it is seen that the one point sound pressure spectrum measurement at the angle of maximum noise can be used to estimate the sound power level spectrum.

The noise measurement system consisted of a Bruel and Kjaer type 4133 microphone (with flat frequency response to 40 kcps) located 15 feet from the jet nozzle at an angle of 40° from the jet axis. Microphone output was frequency

analyzed by means of a Bruel and Kjaer spectrometer, and recorded on a B & K level recorder.

The test facility used was an outdoor free field test stand, with no significant reflecting surfaces except the ground, and capable of continuous heated flow. The test nozzle employed was a 4 inch diameter convergent design, and is shown with water spray tube configurations in Figure 5.2. Flow pressure and temperature were measured, as well as water and air mass flow. The airflow measurements were used to monitor the effective nozzle area, thus providing a rough indication of water evaporation upstream of the nozzle exit. A number of spray tube configurations were employed, with water inlet locations at two diameters upstream of the nozzle exit for initial tests and twelve diameters upstream for subsequent runs. The tubes were immersed radially into the airstream, and were equally spaced around the circumference of the air duct.

Eight tubes, with an orifice 0.050 inches dia. in the end of each, were used in the configuration with tube location 2 diameters upstream. Immersion depths of 0 (tube ends flush with nozzle wall), 2 inches, and alternate tubes at 0 and 1 inch were tested. Water flow was varied from 0 to 3.5 gallons/minute for airflow conditions of: (a) nozzle pressure ratio = 1.8, total temperature = 1400°F, and (b) pressure ratio = 2.7, total temperature = 1240°F. Sound pressure level reduction at the position 15 feet from the nozzle and at an angle of 40° from the jet axis was determined by comparing runs with and without water flow for a fixed airflow condition and spray tube geometry.

For the tests with water injection at 12 nozzle diameters upstream of the exit, 6 tubes were used. Water was introduced through a single 1/8" diameter hole in the end of each tube, and in an alternate scheme water was sprayed through 8 holes 0.045" dia. located along the length of each tube. Water flow rates up to 27% of the airflow (by weight) were achieved for flow temperatures up to 1340°F and over a range of pressure ratios from 1.35 to 2.15.

5.3 Discussion of Results

Initial investigations of noise reduction by means of selective water injection, utilizing the spray tubes located 2 diameters upstream of the nozzle exit, indicated that little evaporation of water occurred in the flow region near the nozzle exit. Even at the maximum water flow rate (13% of the airflow) only 4 db sound pressure level reduction was achieved, as shown in Figure 5.3.

Based on the theoretical curves in Figure 5.1, for complete mixing of the water with the heated airstream, a 6 db sound power level reduction would be expected. While it appears that this amount of suppression at the source might be obtainable in practice by complete mixing of water and air, the configuration tested did not achieve noise reduction as intended by alteration of flow velocity profiles. No change in airflow occurred as water flow was increased, indicating that only a limited amount of evaporation could have taken place in the nozzle, since formation of steam would effectively decrease the flow area available for the heated air.

Examination of the sound pressure reduction spectra (Figure 5.3) reveals that at the highest pressure ratio the noise reduction was shifted to a lower

frequency. This is explained by consideration of the increased jet velocity, since the water droplets were transported further downstream (toward the location of lower frequency sound source) before evaporation and resultant cooling and deceleration of the flow.

In order to achieve more complete vaporization of the water injected into the flow, further tests were conducted using the spray tubes located 12 nozzle diameters upstream of the exit. Comparison of suppression for the two spray tube designs (one hole in the end of each tube compared to 8 smaller holes spaced along the tube) showed no significant difference between the coarse and fine sprays. Rather, noise reduction was found to depend essentially on water/air ratio for a given airstream pressure and temperature. Overall sound pressure level reduction as a function of water/air ratio is shown in Figure 5.4, and it is apparent that suppression is a linear function of water/air ratio over the range tested. Comparing the curves for equal pressure ratios but varying temperatures it is evident that noise reducti increases as the flow temperature rises, and a maximum reduction is achieved, after which the additional temperature rise adversely affects suppression. Interpolated data from Figure 5.4 for water/air ratio of 15% is replotted in Figure 5.5 to indicate the effects of water residence time in the airstream (flow velocity effect). It is the combined effects of increase in flow temperature causing: 1) more rapid vaporization of water, 2) decreasing droplet residence time, and 3) providing less noise reduction capability (as shown in Figure 5.1) which cause the maximization of suppression noted in Figure 5.4.

The calculation adverse effect of temperature results from the fact that for a given water air ratio the flow temperature change accompanying complete mixing and evaporation is essentially independent of initial temperature and thus, percentage-wise, the cooling effect decreases with increase in initial temperature.

The effects of water injection on the jet noise sound pressure level spectrum are shown in Figure 5.6. Reduction is achieved over a wide range of frequencies, and it is significant that even at low pressure ratio suppression is accomplished in the high frequency region (for the test results shown, the sound pressure level spectrum peak occurs at 1250 cps).

5.4 Conclusions

Results of the selective water injection investigation indicate that the desired alteration of jet mixing cannot be achieved by this means in order to affect noise reduction. Although the mean-flow velocity profiles can be altered through use of selective sprays, the jet mixing is not greatly influenced and the suppression accomplished is less than would be possible through uniform mixing of water and air.

The adverse effect of high temperature and flow velocity on noise reduction capability of water injection and the large water/air ratios required indicate that this scheme might not be practical for application to existing aircraft and engines.

Effects on nozzle aerodynamic performance have not been measured, but losses would be small if water evaporation and resultant cooling of the flow

occurs primarily external to the nozzle, as is indicated by test results.

Jet noise suppression by means of water injection is unusual in that high frequency noise reduction can be achieved, and furthermore, suppression can be accomplished for low pressure ratio flow.

REFERENCES

1. Kurbjun, M. C., "Limited Investigation of Noise Suppression by Injection of Water Into Exhaust of Afterburning Jet Engine", NACA RM L57L05, Feb. 1958.

2. "A Proposal for Jet Noise Suppression Research and System Studies", General Electric Company, Flight Propulsion Division, P 61-86, 1961.

3. Lee, R., et. al., "Research Investigation of the Generation and Suppression of Jet Noise", General Electric Company, Flight Propulsion Division, Prepared under Bureau of Naval Weapons Contract No. NOas 59-6160-c, Jan. 1961.

4. Lee, R. and Semrau, W. R., "Method for Predicting the Overall Directivity Patterns of Suppressor Nozzles", General Electric Company, R58AGT947, 1958.

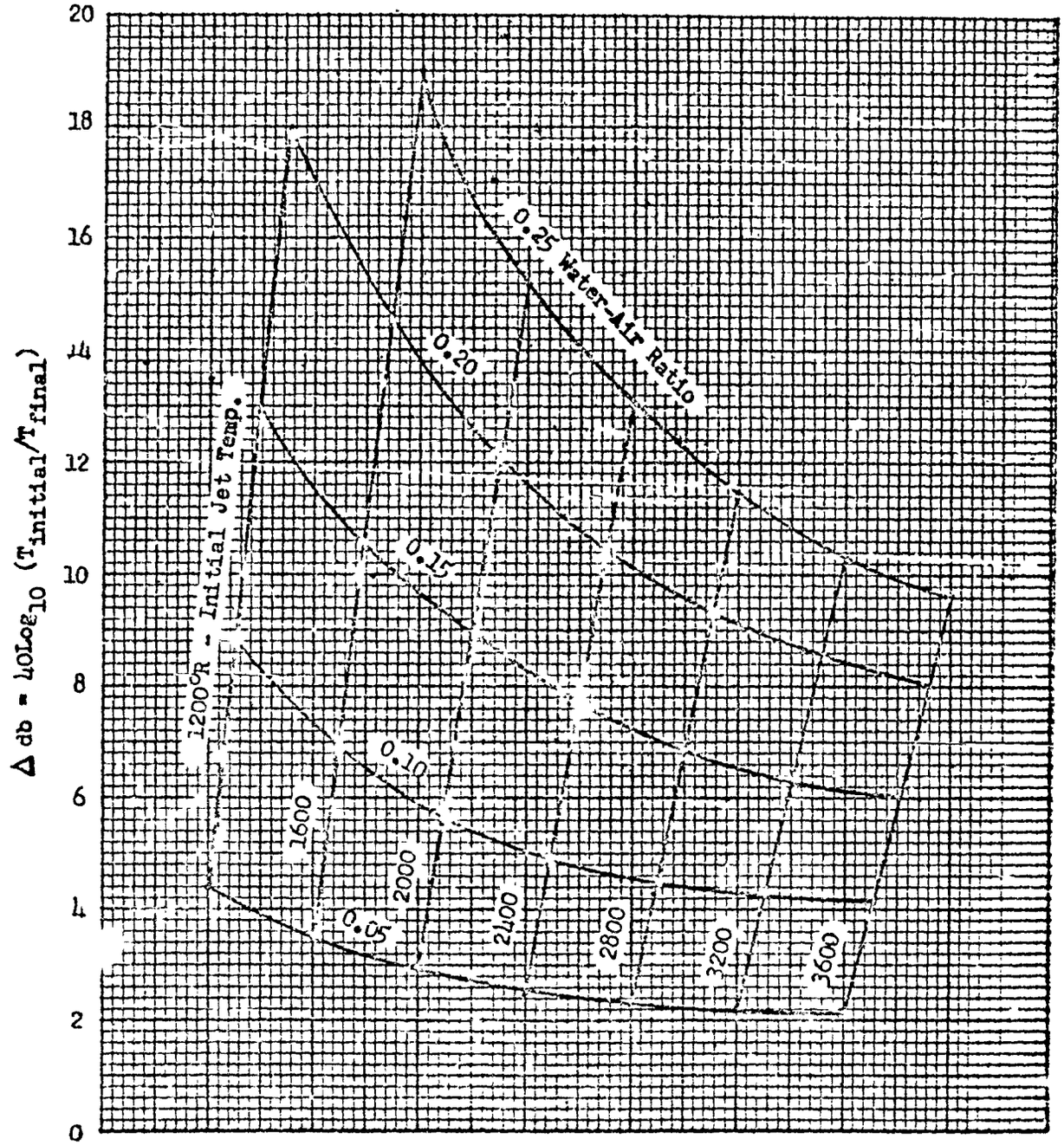

Figure 5.1 - Calculated Reduction of Sound Power Level for Complete Evaporation and Mixing of Water with Jet Exhaust.

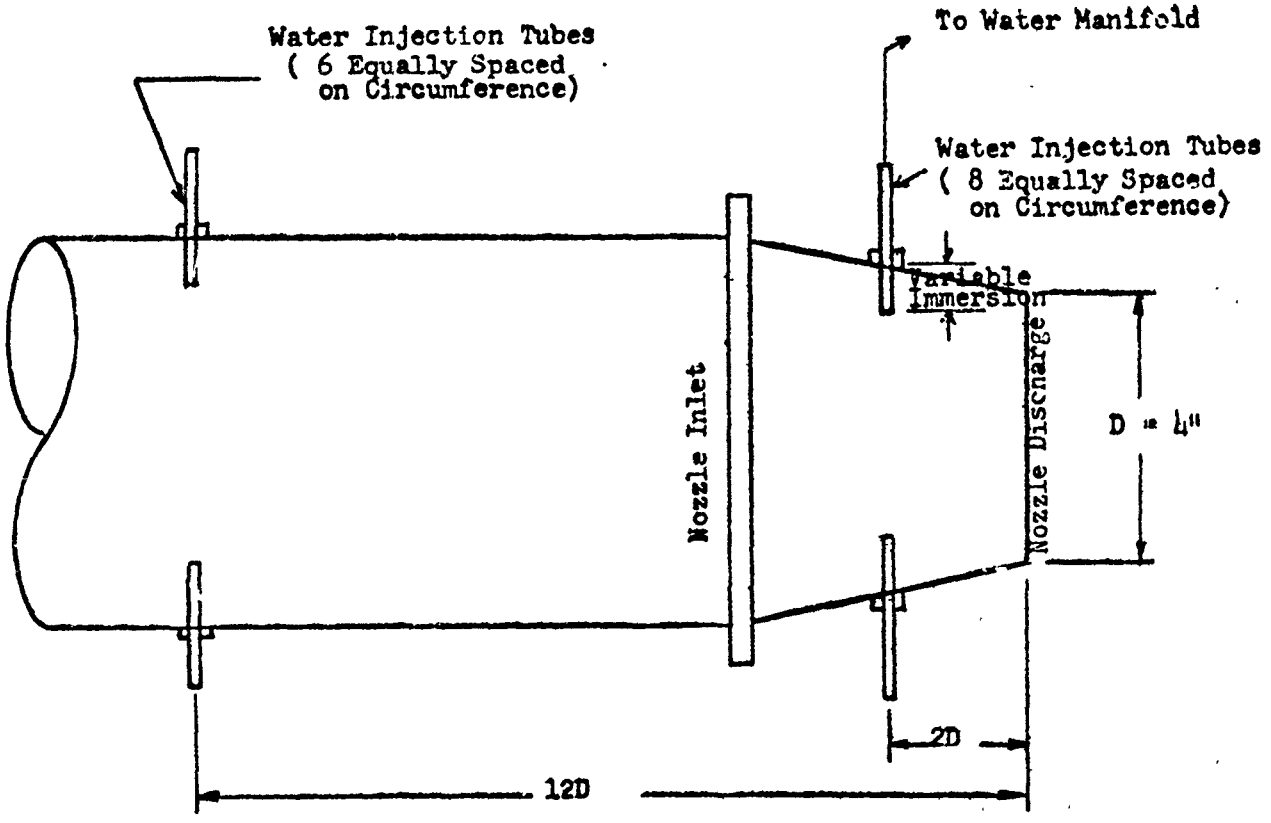

Figure 5.2 - Schematic of Water Injection Nozzle

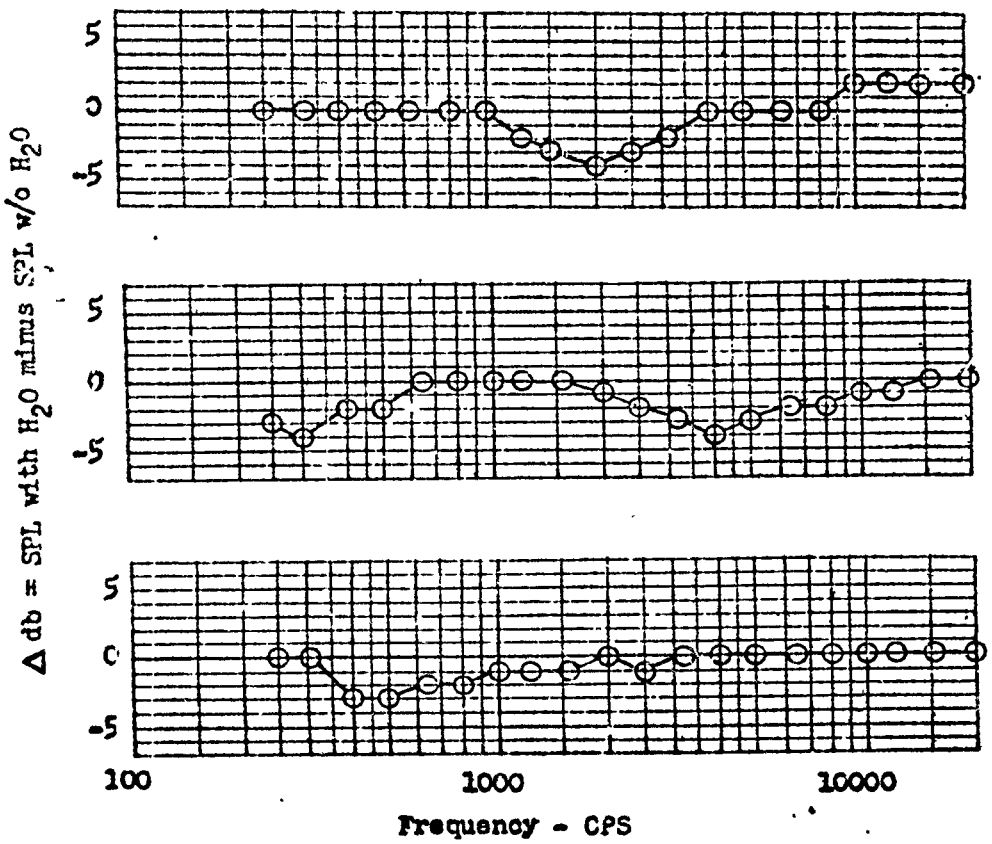

Pressure Ratio	Temp.	Tube Immersion	Water/Air Ratio
1.8	1860°R	2"	10.3%
1.8	1860°R	0", 1" (alternately 4 each)	13.2%
2.7	1700°R	2"	6.6%

Note: Spray tubes located 2 dia. upstream of nozzle exit.

Figure 5.3 - Sound Pressure Level Reduction of Water Injection Nozzle Measured at 40° from Jet Axis.

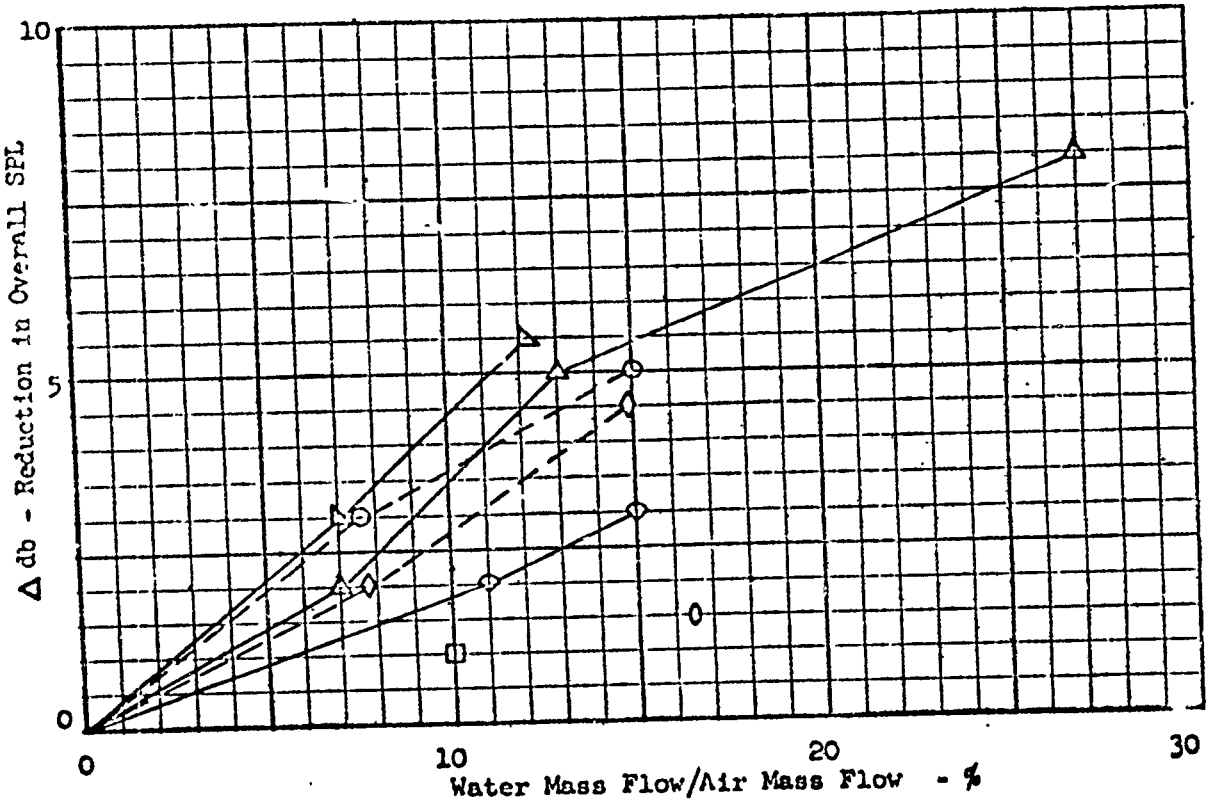

Symbol	V (ft/sec)	P_o/P	T_o (°F)
◇	2060	2.15	1340
◇	2010	2.15	1250
△	1720	2.15	800
○	1530	1.8	800
□	990	1.8	65
△	1300	1.35	1250
○	720	1.35	65

Figure 5.4 - Water Injection Nozzle Overall Sound Pressure Level Reduction at Angle of Maximum Noise (40° from Jet Axis)

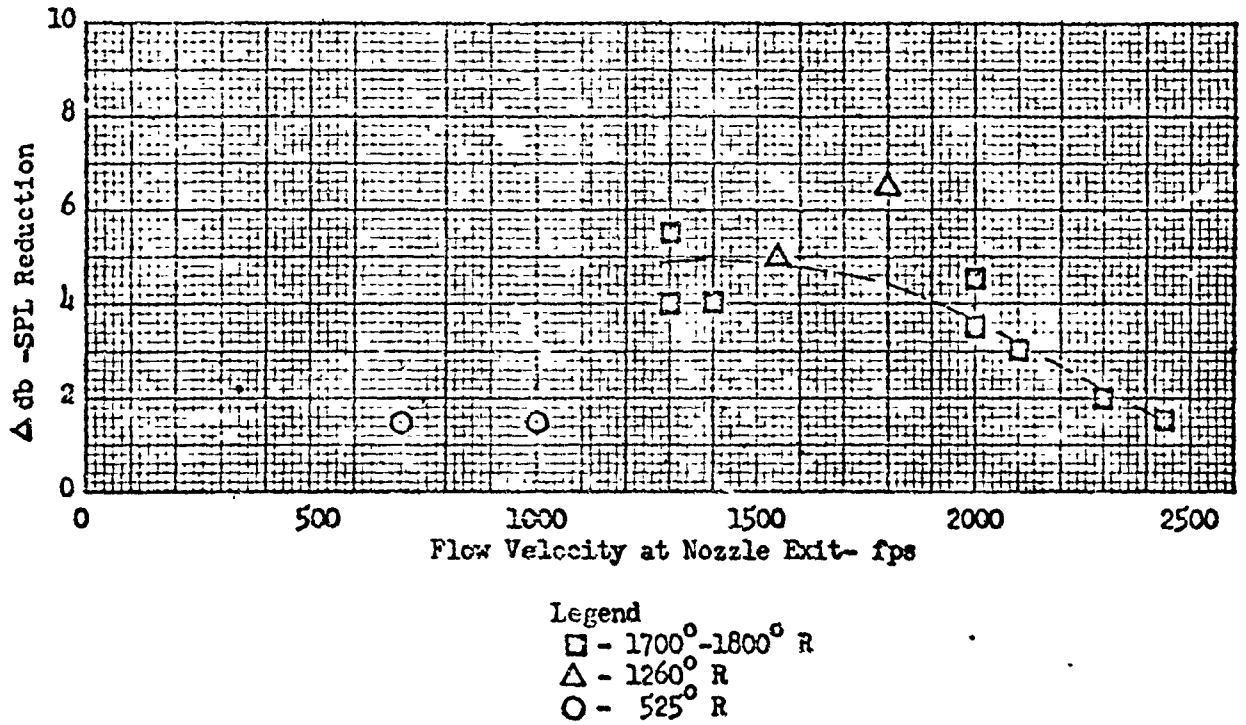

Figure 5.5 - Water Injection Nozzle Overall SPL Reduction at Angle of Maximum Noise

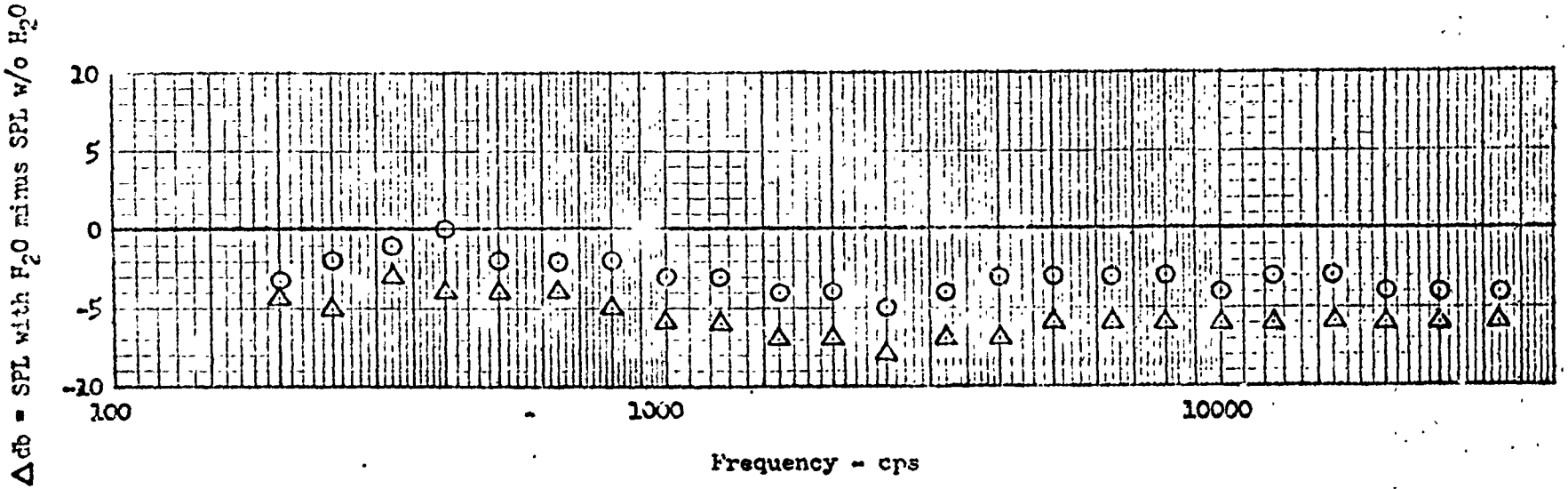

Nozzle Pressure Ratio - 1.83
Gas Temperature - 800°F

Tubes Located 12 Dia. Upstream

Legend
Water/Air Ratio
○ - 7.2 %
△ - 15.2 %

Figure 5.6 - Water Injection Nozzle Noise Reduction at Angle of Maximum Noise